# Hierarchical control scheme for multi-terminal high voltage direct current power networks

Miguel Jimenez-Carrizosa Jimenez Carrizosa

UNIVERSITÉ PARIS SUD

Comprendre le monde, construire l'avenir®

L2S

STITS ECOLE DOCTORALE

# Université Paris-Sud

École Doctorale Sciences et Technologies de l'Information, des Télécommunications et des Systèmes (ED STITS)

Laboratoire des signaux et systèmes

Disciplines :
Génie électrique
Génie informatique, automatique et traitement du signal

## Thèse de doctorat

Soutenue le 10 Avril 2015 par


# Miguel Jiménez Carrizosa


# Hierarchical control scheme for multi-terminal high voltage direct current power networks

## (Commande hiérarchique de réseaux multi-terminaux à courant continu et haute tension)

| | | |
|---|---|---|
| **Directrice de thèse :** | Mme. Françoise Lamnabhi-Lagarrigue | Directrice de Recherche, CNRS-LSS. |
| **Co-encadrant de thèse :** | M. Gilney Damm | Maître de conférences, HDR, LSS. |
| **Co-encadrant de thèse :** | M. Abdelkrim Benchaib | Ingéneur de recherche, HDR, ALSTOM. |

**Composition du jury :**

| | | |
|---|---|---|
| Président : | M. Jean-Luc Thomas | Professeur, HDR, CNAM. |
| Rapporteurs : | M. Séddik Bacha | Professeur, Université de Grenoble. |
| | M. Aleksandar Stanković | Professeur, TUFTS University. |
| Examinateurs: | M. Fernando Dorado Navas | Professeur, Universidad de Sevilla. |
| | M. Adrià Junyent Ferré | Lecturer, Imperial College London. |
| Invité : | M. Stéphan Lelaidier | R&D Vice-Président, ALSTOM GRID. |

*A todos aquellos que se alegran de mis éxitos y sufren con mis fracasos.*

# Acknowledges

I would like to express my gratitude to Françoise Lamnabhi-Lagarrigue for agreeing to be my thesis director, to Gilney Damm for being my advisor and for all the reviews that he has done in this work, and to Abdelkrim Benchaib for being the person which trusted in me and encouraged me to carry out this thesis.

Also, I would like to emphasize professors Pedro Alou and Fernando Dorado for their invaluable help and wise advices.

Finally, I would like to highlight the work done by professor Amir Arzandé in the test bench development, and the the help and the consent of professor Jean-Claude Vannier. Without their help it would not be possible.

# Abstract

This thesis focuses on the hierarchical control for a multi-terminal high voltage direct current (MT-HVDC) grid suitable for the integration of large scale renewable energy sources.

The proposed control scheme is composed of 4 layers, from the low local control at the power converters in the time scale of units of ms; through distributed droop control (primary control) applied in several terminals in the scale of unit of seconds; and then to communication based Model Predictive Control (MPC) that assures the load flow and the steady state voltage/power plan for the whole system, manage large scale storage and include weather forecast (secondary control); finally reaching the higher level controller that is mostly based on optimization techniques, where economic aspects are considered in the same time as longer timespan weather forecast (tertiary control).

Concerning the converters' level, special emphasis is placed on DC/DC bidirectional converters. The main task of these devices is to link several DC grids with different voltages, in analogous form as the use of transformers for AC grids. In this thesis, three different topologies are studied in depth: two phases dual active bridge (DAB), the three phases DAB, and the use of the Modular Multilevel Converter (MMC) technology as DC/DC converter. For each topology a specific non-linear control is presented and discussed. In addition, the DC/DC converter can provide other important services as its use as a direct current circuit breaker (DC-CB), which is a capital device for the future development of MT-HVDC networks. This is possible thanks to DC-DC converters studied here include an AC stage, and therefore there exist instants in which the current passes through zero, and consequently we can open the switches when a fault occurs in the network in a safer way. Several operation strategies are studied for these topologies used as DC-CB.

With respect to primary control, which is the responsible to maintain the DC voltage control of the grid, we have studied several control philosophies: master/slave, voltage margin control and droop control. Finally we have chosen to use droop control, among other reasons, because the communication between nodes is not required. Two different approaches have been studied for the droop control. Firstly, we have considered that dynamics of converters (AC/DC) are negligible (too fast compared to the network), and in a second step, based on these first results, we have studied the dynamics of droop control coupled to the AC/DC converters. Voltage source converters (VSC) are used as AC/DC converters in this approach.

Relative to the secondary control, its main goal is to schedule power transfer between the network nodes providing voltage and power references to local and primary controllers, providing steady state response to distur-

bances and managing power reserves. In this part we have proposed a new approach to solve the power flow problem (non-linear equations) based on the contraction mapping theorem, which gives the possibility to use more than one bus for the power balance (slack bus) instead of the classic approach based on the Newton-Raphson (NR) method. In addition with the method proposed in this thesis the unique existence of solution is guarantee when some feasible constraints are fulfilled.

Secondary control plays a very important role in practical applications, in particular when including time varying power sources, as renewable ones. In such cases, it is interesting to consider storage devices in order to improve the stability and the efficiency of the whole system. Due to the sample time of secondary control is on the order of minutes, it is also possible to consider different kinds of forecast (weather, load,..) and to achieve additional control objectives, based on managing storage reserves. All these characteristics encourage the use of a model predictive control (MPC) approach to design this task. In this context, several possibilities of optimization objective were considered, like to minimize transmission losses or to avoid power network congestions.

The main task of tertiary control is to manage the load flow of the whole HVDC grid in order to achieve economical optimization, especially relevant with the presence of storage devices. This control level provides power references to the secondary controller. In this thesis we were able to maximize the economic profit of the system by acting on the spot market, and by optimizing the use of storage devices. The MPC approach is again used in this level, but acting in a higher time scale, and in a complementary way of the secondary objectives.

With the aim of implementing the hierarchical control philosophy explained in this thesis, we have built an experimental test bench. This platform has 4 terminals interconnected via a DC grid, and connected to the main AC grid through VSC power converters. This DC grid can work at a maximum of 400 V, and with a maximum allowed current of 15 A. The local VSC converters are controlled by the dSPACE® software package. Also, in this network a supervisor PC (secondary controller) is included, which communicates with each dSPACE® software of each VSC through a National Instruments CompactRIO® programmable automation controller, which combines embedded real-time and FPGA technology, thought a local area network (internet).

# Symbols and abbreviations

### Symbols

| | |
|---|---|
| $D$ | *Duty cycle.* |
| $E_s^k$ | *Energy at instant k in storage s.* |
| $<i>$ | *Current average value.* |
| $J$ | *Cost function.* |
| $N_p$ | *Prediction horizon.* |
| $P_i^k$ | *Active power at instant k in node i.* |
| $T$ | *Sample time.* |
| $Q$ | *Reactive power.* |
| $u_i^k$ | *DC Voltage at instant k in node i.* |
| $[u^k]$ | *Vector of DC voltages at instant k.* |
| $\mathcal{V}$ | *Lyapunov function.* |
| $Y$ | *Admittance matrix.* |
| $\phi$ | *Phase shift ratio.* |
| $\mu_i$ | *Storage efficiency.* |

### Abbreviations

| | |
|---|---|
| CPM | *Conventional phase shift modulation.* |
| CSC | *Current source converters.* |
| DAB | *Dual active bridge.* |
| DHB | *Dual half bridge.* |
| DC-CB | *Direct current circuit breaker.* |
| FDNR | *Fast decoupled Newton-Rapshon method.* |
| HVDC | *High voltage direct current.* |
| IGBT | *Insulated-gate bipolar transistor.* |
| MMC | *Modular multilevel converter.* |
| MPC | *Model predictive control.* |
| MT-HVDC | *Multi terminal high voltage direct current.* |
| NR | *Newton-Raphson method.* |
| OPF | *Optimal power flow.* |
| QNR | *Quasi Newton-Rapshon method.* |
| PLL | *Phase lock loop.* |
| PWM | *Pulse width modulation.* |
| SRC | *Series resonant converter.* |
| SVM | *Space vector modulation.* |
| VSC | *Voltage source converter.* |
| ZCS | *Zero current switching.* |
| ZVS | *Zero voltage switching.* |

# Contents


**1 Introduction** **21**

1.1 State of the art. . . . . 21

1.1.1 Local controllers. . . . . 23

1.1.2 Primary controllers. . . . . 24

1.1.3 Secondary controllers. . . . . 24

1.1.4 Tertiary controllers . . . . . 26

**2 DC/DC bidectional converter** **27**

2.1 Chapter introduction. . . . . 27

2.2 Two phases DAB. . . . . 28

2.2.1 Modulations. . . . . 28

2.2.2 Modulation discussion. . . . . 38

2.2.3 System Modeling. . . . . 39

2.2.4 Dynamics of the real system. . . . . 41

2.2.5 Verification of differential equation. . . . . 44

2.2.6 Non-linear control design for DAB system. . . . . 46

2.2.7 Verification of non-linear control. . . . . 47

2.3 Robustness . . . . . 49

2.4 Three phases DAB. . . . . 50

2.4.1 PWM Modulation. . . . . 50

2.4.2 System modelling . . . . . 52

2.4.3 Control objective. . . . . 54

2.4.4 Bilinear system stability and control law. . . . . 55

2.4.5 Nonlinear system stability and control law. . . . . 57

2.4.6 Simulations for the three phases DAB. . . . . 60

2.5 DC/DC converter with MMC technology. . . . . 63

2.5.1 System modelling. . . . . 64

2.5.2 Stability. . . . . 70

2.5.3 Control. . . . . 76

2.5.4 Sinusoidal signal generation. . . . . 77

2.5.5 Harmonics study. . . . . 79

2.5.6 Power transport explanation. . . . . 81

2.5.7 Simulations. . . . . 81

2.6 Use as DC circuit-breaker. . . . . 85

2.6.1 DC circuit breaker based on DAB topology. . . . . 86

2.6.2 Simulations for a single converter. . . . . 86

2.6.3 DC circuit breaker based on MMC topology. . . . . 90

2.7 Conclusions. . . . . 94

**3 Primary control** **97**
3.1 Chapter introduction. . . . . 97
3.2 DC voltage control strategies. . . . . 98
3.3 Droop control with VSC as current sources. . . . . 101
3.3.1 Multi-Terminal HVDC grid . . . . . 101
3.3.2 Stability of droop control neglecting VSC dynamic . . 104
3.3.3 Simulations. . . . . 109
3.4 Droop control and VSC dynamics together. . . . . 113
3.4.1 Singular perturbation. Brief explanation. . . . . 118
3.4.2 Whole control . . . . . 119
3.4.3 System stability . . . . . 119
3.4.4 Simulations. . . . . 121
3.5 Conclusions . . . . . 123

**4 Secondary control** **125**
4.1 Chapter introduction. . . . . 125
4.2 DC power flow. . . . . 126
4.2.1 Definitions and basic relations. . . . . 126
4.2.2 Basic properties. . . . . 128
4.2.3 Main properties. . . . . 130
4.2.4 Application example. Six nodes system. . . . . 138
4.3 Secondary control with MPC. . . . . 143
4.3.1 Model predictive control strategy. . . . . 144
4.3.2 HVDC network. . . . . 146
4.3.3 Formulation of the problem. . . . . 147
4.3.4 Advantages. . . . . 149
4.3.5 Existence of solutions. . . . . 149
4.3.6 Existence of solutions in $\mathbb{R}^3$. . . . . 149
4.3.7 Existence of solutions in $\mathbb{R}^n$. . . . . 153
4.4 Application case: a six-terminal system. . . . . 154
4.4.1 Losses comparative. . . . . 159
4.5 Conclusions. . . . . 159

**5 Tertiary control** **161**
5.1 Chapter introduction. . . . . 161
5.2 Tertiary control. MPC Power formulation. . . . . 162
5.2.1 Optimization context. . . . . 162
5.2.2 Simulations for a seven-terminal system. . . . . 164
5.3 Tertiary control. MPC Volatge formulation. . . . . 167
5.3.1 Simulations. . . . . 169
5.4 Conclusions. . . . . 172

**6 Experimental test bench** **173**
6.1 Chapter introduction. . . . 173
6.2 Test bench explanation. . . . 173
6.2.1 Transformer. . . . 175
6.2.2 Current Sensor. . . . 176
6.2.3 VSC . . . . 176
6.2.4 dSPACE® software and hardware. . . . 177
6.2.5 Local Controller. . . . 178
6.2.6 Primary Controller. . . . 179
6.2.7 Secondary controller. . . . 180
6.2.8 cRIO® hardware. . . . 180
6.2.9 Hierarchical control. . . . 181
6.3 Results. . . . 182
6.3.1 Voltage control of a node with variable load. . . . 182
6.3.2 Three nodes grid. Experimental results with master/slave philosophy. . . . 184
6.3.3 Four node grid. Experimental results with droop control philosophy. . . . 186
6.4 Conclusions. . . . 189

**7 Conclusions and further work** **191**
7.1 Conclusions. . . . 191
7.2 Main results. . . . 193
7.3 Further work. . . . 193

**8 French summary** **197**

**A New AC power flow** **207**
A.1 Definitions and basic relations. . . . 207
A.1.1 Basic properties. . . . 211
A.2 Main property. . . . 213

**B Annex B** **217**

# List of Tables


1.1 Philosophy control. . . . . 22

2.1 Advantages and drawbacks of each DC/DC topology. . . . . 27
2.2 Values of $V_a$ in two phases DAB. . . . . 30
2.3 Values of $V_b$ in two phases DAB. . . . . 30
2.4 Values of $V_L$ in two phases DAB. . . . . 31
2.5 Parameters for triangular modulation configurations. . . . . 35
2.6 Obtained values for triangular modulation configurations. . . 36
2.7 State of the switches ($\phi_{15} > 0$). . . . . 40
2.8 Verification of differential equation. Simulation values. . . . 45
2.9 Simulation values. . . . . 47
2.10 Robustnesses simulation values. . . . . 49
2.11 Simulation values. . . . . 61
2.12 Harmonic amplitudes . . . . . 80
2.13 Simulation parameter values . . . . . 82
2.14 Simulation results. . . . . 83
2.15 Simulation values when short-circuit appears. DAB converter. 87
2.16 Two phases MMC converter. Simulation values when short-circuit appears. . . . . 94

3.1 Parameters Values. . . . . 111
3.2 Simulation parameter values. AC side. . . . . 121
3.3 Simulation parameter values. DC side. . . . . 121

4.1 Simulation values. . . . . 139
4.2 Power flow result. Example 1. . . . . 140
4.3 Power flow result. Example 2. . . . . 140
4.4 Power flow result. Example 3. . . . . 140
4.5 Power flow result. Example 4. . . . . 141
4.6 Simulation parameter values. . . . . 155
4.7 Losses comparative. . . . . 159

5.1 Simulation parameters. Power formulation. . . . . 165
5.2 Line distances. . . . . 166
5.3 Incomes. . . . . 167
5.4 Simulation parameters. Power formulation. . . . . 170
5.5 Incomes. . . . . 171

6.1 Test bench parameters. . . . . 176
6.2 Test bench parameters. . . . . 182

# List of Figures


1.1 Example of DC multi-terminal grid. . . . . 21
1.2 DC multi-terminal grid with an hierarchical control. . . . . 22

2.1 Structure of two phases dual active bridge. . . . . 28
2.2 Schematic form of two phases DAB. . . . . 30
2.3 Modulation variables. . . . . 31
2.4 Different layouts. . . . . 32
2.5 CPM modulation. . . . . 34
2.6 Triangular modulation. . . . . 36
2.7 Trapezoidal modulation. . . . . 37
2.8 Transmitted current for trapezoidal and triangular modulation. 38
2.9 Two phases DAB. Simplified circuit. . . . . 40
2.10 Voltages and currents for the two phases DAB circuit ($\phi_{15} > 0$). . . 41
2.11 Voltage and current in first moments for two phases DAB with CPM. 42
2.12 Sequence of even terms. . . . . 44
2.13 Two phases DAB SIMULINK® file. . . . . 45
2.14 Comparison between DAB SIMULINK file (mean value $i_1$) and the dynamic average model for $\phi_{15}$=0.15. . . . . 45
2.15 Current $_{<}i_{1>}$ response when the system is controlled. . . . . 48
2.16 Current response in real situation. . . . . 48
2.17 $\phi_{15}$ response in real situation for two phases DAB converter . . . . 49
2.18 Current average value in left side of single DAB cell under unbalance situation. . . . . 50
2.19 Three phases Dual Active Bridge. . . . . 51
2.20 PWM modulation. . . . . 51
2.21 Three phases DAB average model. . . . . 52
2.22 $i_{Lq}$ behavior (bilinear control). . . . . 61
2.23 a) $u_{C1}$ b) $u_{C2}$ behavior (bilinear control). . . . . 62
2.24 $i_{Ld}$ behavior (bilinear control). . . . . 62
2.25 a) $i_{Ld}$ b) $i_{Lq}$ behaviour (nonlinear control). . . . . 62
2.26 a) $u_{C1}$ b) $u_{C2}$ behavior (nonlinear control). . . . . 63
2.27 Multi DC/DC converter with $k$ phases based on MMC. . . . . 64
2.28 A single phase structure of the MMC. . . . . 65
2.29 Control scheme. . . . . 76
2.30 Sinusoidal signal generation. . . . . 78
2.31 Harmonic construction. . . . . 80
2.32 Multi DC/DC converter with $k$ phases based on MMC. . . . . 82
2.33 AC generated signal voltage. . . . . 83
2.34 a)Voltages for strategy 1 b)Voltages for strategy 2. . . . . 84

2.35 Phase currents. . . . . 84
2.36 Phase currents. Zoom. . . . . 84
2.37 Capacitors state of charge. . . . . 85
2.38 Line short-circuit model. . . . . 86
2.39 Current line and voltage in absorbing mode with over-voltage. . . . 87
2.40 a) Current line and voltage at node A in demanding mode without over-voltage. b) zoom. . . . . 88
2.41 Secondary side of DAB in short-circuit. . . . . 89
2.42 a) Current line and voltage at node A in demanding mode without over-voltage. b) Voltage capacitor zoom. . . . . 89
2.43 Current line and voltage at node A in injecting mode. . . . . 90
2.44 a) Half bridge b) Full bridge. . . . . 90
2.45 a) Half bridge short-circuit operation b) positive AC voltage c) negative AC voltage. . . . . 91
2.46 Negative AC voltage. Equivalent model. . . . . 92
2.47 a) Full bridge short-circuit operation b) positive AC voltage c) negative AC voltage. . . . . 92
2.48 SIMULINK® file. Short-circuit in MMC with full bridge cells. . . 93
2.49 a) AC current. Short-circuit in MMC with full bridge cells. b) Zoom. 93
2.50 DC current. Short-circuit in MMC with full bridge cells. . . . . 94
2.51 a) Capacitor voltage. Short-circuit in MMC with full bridge cells. b) Zoom. . . . . 94

3.1 Power/voltage characteristic for the master node in master/slave. . 98
3.2 Power/voltage characteristic for the slave nodes. . . . . 99
3.3 Current/voltage characteristic for the slave nodes. . . . . 99
3.4 Power/voltage characteristic for the voltage margin control. . . . . 100
3.5 Current/voltage characteristic for the voltage margin control. . . . 100
3.6 Droop control. . . . . 101
3.7 General configuration of a MT-HVDC network. . . . . 102
3.8 General benchmark. . . . . 109
3.9 Voltage results. Droop control neglecting VSC dynamics. . . . . 112
3.10 Power results. Droop control neglecting VSC dynamics. . . . . 112
3.11 Error. . . . . 113
3.12 Configuration of a VSC terminal node. . . . . 114
3.13 $\pi$-equivalent line circuit. . . . . 116
3.14 Simulation system . . . . . 121
3.15 Terminal node voltages. . . . . 122
3.16 Active power in terminal nodes. . . . . 122
3.17 $i_{q1}$ and $i_{q2}$ currents. . . . . 123
3.18 $i_{d3}$, $i_{q3}$, $i_{d4}$ and $i_{q4}$ currents. . . . . 123

4.1 Bipolar line. . . . . 127
4.2 General benchmark. . . . . 138

4.3 MPC strategy. Source . . . 145
4.4 MT-HVDC Grid with wind farms and storage devices. . . . . 146
4.5 Hyperbolic cylinder $S_1$. . . . . 151
4.6 Intersection of hyperbolic cylinders. . . . . 152
4.7 Current lines constraints. . . . . 153
4.8 Six-terminal simulation grid. . . . . 156
4.9 Wind power in production nodes for a typical week. . . . . 156
4.10 Consumption power for a typical week. . . . . 157
4.11 a) Power storage b) Energy storage. . . . . 157
4.12 Voltages in each node. . . . . 158
4.13 Currents thought the lines. . . . . 158
4.14 Losses comparison. . . . . 159

5.1 Seven-terminal simulation grid. . . . . 164
5.2 Energy prices. . . . . 165
5.3 Simulations results. Power formulation. Sub-system 1. . . . . 166
5.4 Simulations results. Power formulation. Sub-system 1. . . . . 166
5.5 Simulations results. Power formulation. Consumed power by AC grids. . . . . 167
5.6 Simulations results. Voltage formulation. DC voltage. . . . . 170
5.7 Simulations results. Voltage formulation. AC power. . . . . 171
5.8 Simulations results. Voltage formulation. Power lines. . . . . 171
5.9 Simulations results. Voltage formulation. Power lines. . . . . 172

6.1 Test bench network scheme. . . . . 174
6.2 Test bench network. . . . . 174
6.3 Transformer $\Delta/d$. . . . . 175
6.4 Current Sensor. . . . . 176
6.5 a) VSC scheme b) IGBT module. Source . . . . . 177
6.6 VSC. Real converter. . . . . 177
6.7 dSPACE 1104 controller card. . . . . 178
6.8 ControlDesk software file. . . . . 178
6.9 *Inner controller* . . . . . 179
6.10 *Outer controller* . . . . . 179
6.11 cRIO® . . . . . 181
6.12 LabView power flow file. . . . . 181
6.13 Whole hierarchical control. . . . . 181
6.14 A node with variable load. . . . . 183
6.15 DC Voltage result. Experimental test bench. Variable load. . . . . 183
6.16 DC Current result. Experimental test bench. Variable load. . . . . 183
6.17 AC voltage result. Experimental test bench. Variable load. . . . . 184
6.18 AC current result. Experimental test bench. Variable load. . . . . 184
6.19 Three nodes grid. Master/slave philosophy. . . . . 185
6.20 DC voltage node 1. Master/slave philosophy. . . . . 185

6.21 DC current node 2. Master/slave philosophy. . . . . 185
6.22 DC current node 3. Master/slave philosophy. . . . . 186
6.23 DC voltage node 2. Master/slave philosophy. . . . . 186
6.24 DC voltage node 3. Master/slave philosophy. . . . . 187
6.25 Four nodes grid. Droop control philosophy. . . . . 187
6.26 Voltage results. Experimental test bench. . . . . 188
6.27 Current results. Experimental test bench. . . . . 188

A.1 Bipolar line. . . . . 208

Chapter 1

# Introduction

## 1.1 State of the art.

The difficulty of satisfying the constant growth in worldwide energy demand is exacerbated by a number of well-known factors regarding the supply and use of conventional energy resources (oil, gas, coal, etc..): the inconvenient geographical location of many conventional energy production sites vis-à-vis the consumption centres, the continuous price inflation accompanying these resources and, of course, the fact that their use releases undesirable emissions into the atmosphere. These disadvantages are turning the world's attention towards renewable energy solutions. However, the inherent time varying ad intermittent nature of renewable energies are serious problems for classical AC networks. It is in this context where the community is seeking alternative solutions for the energy transport and distribution, where MT-HVDC grids (see figure 1.1) could play a key role in the future [1].

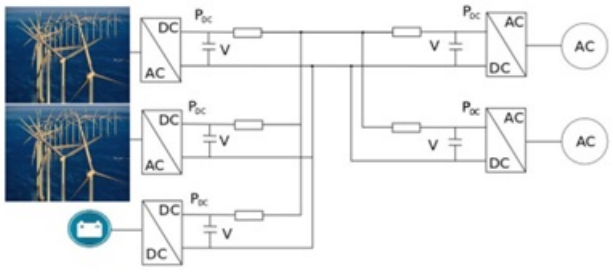


Figure 1.1: Example of DC multi-terminal grid.

In recent years the use of DC grids has grown significantly mainly due to their advantages over AC grids, such as the absence of reactive power, and therefore lower losses in power transmission, or the absence of skin effect in the cables [1, 2, 3, 4]. Due to these facts, DC grids favour the integration of renewable energy sources, especially wind offshore. Besides, current AC networks are reaching their limits and are becoming overloaded. As evidence thereof, the number of blackouts has been increased in the past years [5]. In addition, as DC networks can also be used to connect AC networks with different frequencies, the experience has revealed that blackouts are not propagated from one AC grid to the other through these DC bypass lines [6]. Finally, the recent development of power electronics,

and more specifically the development of converters for high voltage and high power applications, have generated a suitable framework for the development and study of MT-HVDC grids [1, 7]. However, the majority of operating DC grids only connect two nodes, in back to back mode operation, and the study of MT-HVDC networks is still an open field (see figure 1.2), mainly because it has not yet been developed and implemented with efficacy a DC-CB [8, 9].

Although MT-HVDC systems are technically feasible, they have not been widely accepted as a cost-effective transmission solution. There are only two HVDC installations which have operated as multi-terminal systems, but only for a limited time [10]. The first one is the HVDC Italy-Corsica-Sardinia [11] and the other one is the Quebec-New England MT-HVDC [12, 13]. These isolated applications highlight the fact that real exploitation of HVDC lines is not yet a mature technology.

All electrical system, DC or AC, requires the implantation of a control to ensure proper operation. Nevertheless, the control of MT-HVDC is still an open problem. The full control strategy must include all time scales involved in the system ranging from milliseconds to some hours [14]. This thesis address the control of MT-HVDC suitable for renewable energy integration, based on an hierarchical control strategy with the analogous philosophy that classical AC control which includes local, primary, secondary and tertiary controllers [15] as it is shown in table 1.1.

Table 1.1: Philosophy control.

| Control Level | AC | Thesis |
|---|---|---|
| Level 3 | Tertiary (+15 min) | Tertiary (+15 min) |
| Level 2 | Secondary (∼ min) | Secondary (∼ min) |
| Level 1 | Primary (∼ ms) | Primary (∼ s) |
| Level 0 | Local | Local (∼ ms) |

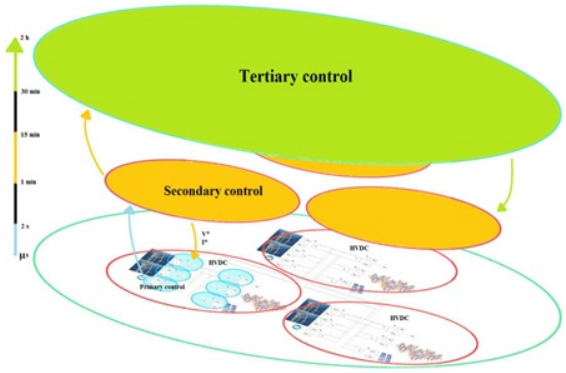


Figure 1.2: DC multi-terminal grid with an hierarchical control.

### 1.1.1 Local controllers.

In a MT-HVDC network connected to AC external grids, it is clear that bidirectional AC/DC converters are key elements to transmit the power in both directions. However the study of bidirectional DC/DC converters is also interesting, because they could apply to link different MT-HVDC networks with different voltage values.

In this thesis an entire chapter is devoted to study DC/DC converters (chapter 2), while the study of AC/DC converters is studied as complement of other tasks, see chapters 3 and 6. However, the applied control techniques to DC/DC converters could be valid for their adaptation to AC/DC ones, since the DC/DC converter is a device with DC/AC/DC steps.

#### AC/DC bidirectional converters.

Until development of VSC [1, 16, 17], CSC were used to carry out the inversion and rectification in HVDC systems. VSC converters use IGBTs and CSC use thyristors. VSC-HVDC systems present many advantages compared with CSC-HVDC systems. Some of them are: simultaneous control of active and reactive power, they create any phase angle or voltage magnitude (within certains limits), and they do not change voltage polarity when power direction is changed. Also CSC systems need communication between converters and in VSC systems it is not required [16].

However, more recently, a new topology is prevailing, the MMC [18]. The advantages of using MMC technology with respect to VSC technology are several: the resulting waveform has a very small harmonic content and it has reduced transient voltage stresses and hence lower high frequency noise [19]. Also it is able to operate at lower switching frequencies. Finally it has the ability to continue its operation under unbalance conditions [20].

#### DC/DC bidirectional converters.

A fundamental element for the development of MT-HVDC grids is the bidirectional DC/DC converter, the equivalent to the transformer for AC grids, which principal mission is to link networks with different voltages. Besides the DC/DC converter can provide other services, such as the use of itself as DC-CB and also to regulate the power flow in the grid [9].

A line of research for the DC/DC bidirectional converters suitable for MT-HVDC was discussed in sections 2.2 and 2.4, which are based on the topology DAB. Nevertheless, and although it has optimal performances and advantages over other topologies, particularly alongside SRC and DHB, the main drawback is that it uses an internal transformer at high frequency [21, 22], which increases significantly the cost of this device. Other authors suggest to link two MMC by the alternative side in order to connect two networks with different DC voltages, as proposed [23]. This structure provides

the advantage that the internal transformer is avoided, and consequently the costs are decreased, and also it offers all the advantages given by the use of MMC technology explained before.

### 1.1.2 Primary controllers.

As in DC systems there is no frequency, from the point of view of safety and reliability of operation, the correct operation of a MT-HVDC system requires a proper coordination of voltage-power or voltage-current regulations.

The primary control operates in a time range of a few seconds. It is responsible to maintain the voltage of the grid. In DC systems, there are some suitable candidates for primary control: master/slave, voltage margin control and droop control [24, 25].

In master/slave strategy there is one node responsible for maintaining the voltage level of the entire network (master), while the others are responsible for controlling the absorption or insertion of power, by means of adapting its DC voltage values (slaves). The master node must be able to absorb or provide sufficient active power to achieve a power balance in the DC system [26]. An outage of this converter cannot be tolerated because it will entail the losing the DC voltage control, which is a great drawback. Other important inconvenience is that, suboptimal operation points could be achieved with this strategy [27].

The voltage margin control philosophy can be summarized in that it is the same as previous but the master node is changing along the time when it reaches its limits [25]. Consequently, it passes the responsibility to maintaining the voltage of the grid to other terminal. Although it is a safer strategy than previous one, it also entails risks because for a given instant there is only one node which is accountable to maintain the grid voltage. On the other hand, suboptimal operation points could also be achieved with this strategy [27].

Finally, droop control is decentralized, and it employs the droop mechanism to regulate the DC voltage adapting the power injections or absorptions in nodes. in this strategy there are several nodes responsible of the grid voltage at same instant. For this reason we have opted to use droop control philosophy, and also because the communication between nodes is not required.

### 1.1.3 Secondary controllers.

In electrical networks with real load and generation, the main task of the secondary level is to carry out the power flow, which is crucial for the proper functioning of the system. The main goal of a power flow study is to obtain voltage and power informations for each bus in the grid in steady state.

However it may perform other types of analysis, such as short-circuit fault analysis, stability studies, unit commitment or economic dispatch.

In AC power systems, power flow problem is defined by non-linear and non-convex equations. In HVDC systems where there is no reactive power involved, the power flow problem is less complex but still retains its non-linear characteristic. There are several different methods to solve non-linear system of equations. The most popular is the well known NR method [15]. With this method the solutions can be easily obtained trough the equations' linearization. An important disadvantage is that the convergence of the method is not always guaranteed. Furthermore, in the case of power systems a slack bus is usually considered. This fact entails risks for the proper modelling of the system, such as the loss of the slack bus (for example a communication lost), that would cause the loss of the reference and consequently the abandon of the equilibrium because the method is not applicable. In this thesis, it is proposed a new algorithm to calculate the power flow such that this risk disappears, because more than one node can be used as voltage reference.

More recently, some authors have proposed other solutions to solve the problem. For example in [28] a multi-terminal DC power flow with a conventional AC power flow has been proposed. Or in [29] a steady-state multi-terminal DC model for power flow programs has been developed which allows to include converter limits as well as different converter topologies. However, both methods are based on the iterative resolution of the NR method until to find a solution which is smaller than a given error. Others authors have solved the problem applying new techniques as in [30] where the problem is solved by genetic algorithm that is an evolutionary-based heuristic algorithm.

The new method proposed in this thesis to solve the power flow problem is based on the well-known contraction mapping theorem is explained. The contraction mapping theorem is also known as Banach fixed-point theorem [31]. For a network with $n$ nodes, if we know the power in $k$ nodes ($0 < k < n$) and the voltages in the other $n - k$ nodes, the system of equations can have multiple solutions, but only one in which the voltages of all nodes are close to the nominal voltage value of the network, when this one is sufficiently high. The method exposed here always leads to this solution, and few iterations are necessary to achieve it.

On the other hand, if ability to store energy comes into play, this power flow could be optimized. In [32] an optimal power flow problem for MT-HVDC systems with predictive control tools is shown. It uses a geometrical techniques in order to guarantee the existence of solutions. Other authors like [33], proposed an optimal power flow in order to minimize the losses in a multi-terminal HVDC grid. They considered the network state at each sample time for which they formulated an optimization problem regarding the transmission losses.

However, in practical applications of variable energy power sources, it is interesting considering storage devices in order to improve the stability and the efficiency of the whole system [34]. In [35] an economic and environmental dispatch problem for a smart grid composed of multiple sources of generation systems (both conventional and renewable), consuming nodes and storage systems are proposed using the energy hub formulation. Their formulation, including weather forecasts to optimally operate the storage systems, was stated under the model predictive control approach, MPC, resulting in a mixed integer quadratic optimization problem.

This thesis also presents a power flow strategy for multi-terminal HVDC grids in which transmission losses are minimized (see section 4.3). The proposed optimization problem yields a solution where the voltage values in network nodes minimizes the transmission losses and will also account for all the constraints taken into consideration as it will be presented in section 4.3.3. This formulation results in a quadratic convex objective function but with non convex constraints. The existence of the solution for this problem is also discussed in sections 4.3.5 and 4.3.7. Distribution losses are minimized for the whole network. This gives as a result a control strategy being able to deal with the whole system and its inherent constraints giving the framework for a multi-objective optimization control. Energy is mainly generated via renewable energy sources and there are nodes in the network with the possibility to store energy. This energy is generated taking into account real weather conditions in order to make the best scheduling of the system in a realistic approach. An optimization scheme is proposed in which all these elements are included as well as real operation constraints.

### 1.1.4 Tertiary controllers

The tertiary control is responsible for organising the electrical power scheduling from the economic point of view.

The electricity market is based on a set of negotiations between the producers and operators in order to obtain a final price for the produced energy. It is divided in the day-ahead (day D-1) and intra-day markets (day D) [36]. The day-ahead market is a marginal market where price for each hour results from the balance between supply and demand. Every day the operators receive bids from producers for the electricity price of next day. Subsequently, the operator communicates the energy prices (purchase and sale) in a public platform for the following day (day D-1). At the day D, several intra-day markets are carried out in order to allow buyers and sellers to adjust their bids due to the new and better available forecasts. In this thesis we have used the final price (day D) derived of all negotiations to carry out the power scheduling via MPC techniques.

Chapter 2

# DC/DC bidectional converter

## 2.1 Chapter introduction.

The DC/DC converter is a key element for the development of MT-HVDC systems. It must be bidirectional in order to guarantee the power flow in both directions. The main task of this device is to link several DC grids with different voltages, in analogous form as transformers for AC grids. However, the DC/DC converter can provide other services as for example the use of it as a DC-CB, which is a capital device for the future development of MT-HVDC networks.

There are several topologies for DC/DC bidirectional converters, but only few for HVDC applications. This is because the internal devices must support high voltages and high currents. In [37] a discussion between several topologies valid for HVDC applications is presented. In table 2.1 some advantages and disadvantages of the most common topologies for these type of applications are short listed.

Table 2.1: Advantages and drawbacks of each DC/DC topology.

| | Advantages | Drawbacks |
|---|---|---|
| MMC | Internal transformer is avoid<br>Soft switching<br>Less harmonics | Hundreds of semiconductors<br>Complex control<br>Expensive technology |
| DAB | Electrical Insulation<br>Soft switching<br>Resonant inductance into transformer<br>Less reactive power | Soft switching may be lost at light load<br>Complex control<br>High ripple current in $C_2$<br>Large inductance leakage<br>Transformer saturation |
| SRC | Electrical Insulation<br>Soft switching<br>Sinusoidal currents<br>Inductance leakage is not a problem | Large resonant inductor<br>High-voltage resonant capacitors<br>Variable frequency control |
| DHB | Electrical Insulation<br>Soft switching<br>Use less devices | More reactive power<br>MOSFETs voltage limitation<br>High current through the transformer<br>Complex control algorithm |

In this chapter, three different topologies are studied in depth: DAB with two phases (section 2.2), the three phases DAB (section 2.4) and the use of the MMC technology as DC/DC converter (section 2.5). For each

topology a specific non-linear control is presented and discussed. In this sense, a non-linear control based on Lyapunov theory is applied to the two phases DAB (see [38, 39, 40]). For the three phases DAB a control based on the bilinear systems control theory is developed (see [41, 42, 43, 44]), as well as a control based on Lyapunov theory where the zero dynamics of the system has been studied in depth [45]. Finally for the DC/DC converter with MMC technology a control based in switching systems control theory is developed [46].

In addition, a study of the dynamic behaviour of these converters as DC-CB when a short-circuit appears is shown in this chapter.

## 2.2 Two phases DAB.

The two phases dual active bridge is comprised of two full bridge converters connected each one to a side of the transformer, which will provide galvanic insulation (necessary to protect against unforeseen circumstances) [47]. This topology can enable a ZCS in both sides of the converter. An inductance L, which is used as a component of energy transfer, is placed in series with the transformer. The scheme of this structure is shown in figure 2.1.

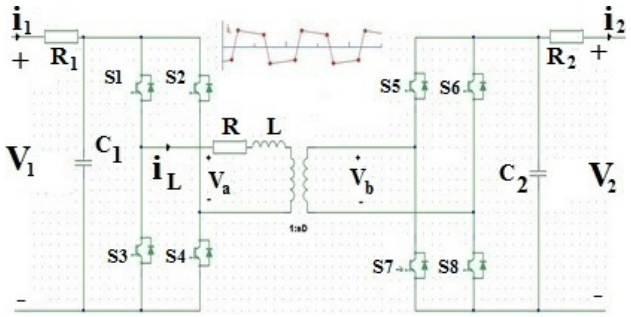


Figure 2.1: Structure of two phases dual active bridge.

For HVDC applications, medium frequency transformer is used [21, 48]. It provides insulation and the step up/down of the different voltage levels. This transformer is based on a single magnetic core with windings in both legs. Using this type of transformer the ratio weight/volume could be improved. It works at frequencies around 10/20 kHz [21]. For this type of converter SiC-JFETs can be used [49, 50, 51, 52]. However, the study of these devices, semiconductors and the internal transformers, is not within the objectives of this thesis.

### 2.2.1 Modulations.

The term modulation refers to the strategy to switch on/off for the semiconductors in the converter. For the eight semiconductors which exist in

the two phases DAB, all possible switching combinations can be generalized in a compact manner by means of a set of variables. Thus, if we define a general rule for the behaviour of semiconductors, all possible modulations will be a particular case of this general rule. In order to define it, we will state some hypotheses that will help us to synthesize the rule.

*Hypothesis:*

1) We will considerer that in each switching cycle, one semiconductor changes its state only once. That means, in a cycle we can not turn on and turn off each semiconductor several times. Thus, PWM technique is not considered in concordance with this idea.

2) There are some combinations which are not possible, since the sources would be short-circuited. According to the numbering for semiconductors showed in figure 2.1, the combinations that would produce this phenomenon are: when semiconductors $S1$ and $S3$ are on at the same instant, the same for the pairs $S2$ and $S4$, $S5$ and $S7$, and finally for $S6$ and $S8$. Any of these four combinations will produce a short-circuit, and therefore they must be avoided. In the same way, it can never happen that both semiconductor of these pairs will be simultaneously open, since in that case there will be an open circuit.

3) We will take into account that the change of state from on to off, or vice versa, is instantaneous.

4) For simplicity, the transformer is omitted in figure 2.1. We have considered that the circuit is seen from the transformer primary side.

5) We will consider that capacitors $C_1$ and $C_2$ from figure 2.1 are charged at $V_1$ and $V_2$ respectively.

From hypothesis 2, we conclude that semiconductor $S1$ is conducting when the $S3$ is open and vice versa. The same criteria is applied to other pairs of semiconductors. Consequently, for the pairs $S1 - S3$, $S2 - S4$, $S5 - S7$ and $S6 - S8$ the behaviour of elements are complementary between them.

The circuit of figure 2.1 can be summarized in figure 2.2, where the variables $V_a$ and $V_b$ are the voltages in the terminals of the inductance $L$. The total resistances of the system are summarized in $R$, which could be neglected with respect to $L$. According to the criterion of signs, it is clear that $V_L = V_a - V_b$. In tables 2.2 and 2.3 the values of $V_a$ and $V_b$ according to the state of semiconductor devices are shown respectively.

Supposing that the resistance is negligible and the voltage applied at each interval is constant, the waveform of the current through the inductance in an interval can be approximated by a line determined by:

$$initial \quad value \quad + \frac{V_L}{L} \cdot \tau_d = \quad final \quad value \tag{2.1}$$

where $V_L$ is the voltage applied in the inductance, and $\tau_d$ is the duration of this interval.

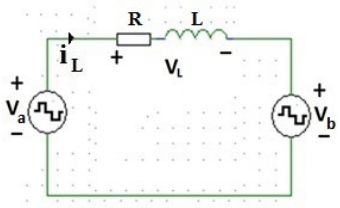


Figure 2.2: Schematic form of two phases DAB.

Table 2.2: Values of $V_a$ in two phases DAB.

| Semiconductor | | | | |
|---|---|---|---|---|
| 1 | on | on | off | off |
| 2 | on | off | on | off |
| 3 | off | off | on | on |
| 4 | off | on | off | on |
| $V_a$ | 0 | $V_1$ | -$V_1$ | 0 |

Tables 2.2 and 2.3 show that the voltages in the terminals of the inductance can reach 3 different values, the positive value of the corresponding source, the negative or zero. In consequence, 9 different voltage values may appear in the terminals of the inductance (see table 2.4). We also observe that different combinations for semiconductors achieve the same voltage in the inductance.

Table 2.3: Values of $V_b$ in two phases DAB.

| Semiconductor | | | | |
|---|---|---|---|---|
| 5 | on | on | off | off |
| 6 | on | off | on | off |
| 7 | off | off | on | on |
| 8 | off | on | off | on |
| $V_b$ | 0 | $V_2$ | -$V_2$ | 0 |

According to explained above, we are able to define the parameters that will allow us to study the behaviour of the system in a comprehensive and global manner. These are shown in figure 2.3. $D_1$ is the *duty cycle* of the semiconductor $S1$ or in other words, the fraction of the period T where $S1$ is on, so $D_1 \cdot T$ is the time that S1 is conducting in each period. It should be noted that when $D_1$ is defined, the time while S3 is conducting is also specified. It has a complementary behaviour as explained before in the hypothesis. Hence, the behaviour of semiconductors $S1$ and $S3$ is completely defined. Besides, without loss of generality, we can considerer the instant when $S1$ begins to conduct in each cycle will as the reference. Proceeding

in similar way, $D_2$ is the *duty cycle* of $S2$. Also, $\phi_{12}$ (*phase shift ratio*) is the gap between the turn on of $S1$ (the reference) and $S2$. In this way, the behaviours of $S2$ and $S4$ are completely defined. Proceeding in analogously way, we can defined $D_5$, $D_6$, $\phi_{15}$ and $\phi_{56}$ (the gap between the turn on of $S1$ and $S5$, and the gap between $S5$ and $S6$ respectively). Thus, the behaviour of all semiconductor are completely defined. Therefore, we can chose as variables to study the global system the states of the semiconductors $S1$, $S2$, $S5$ and $S6$.

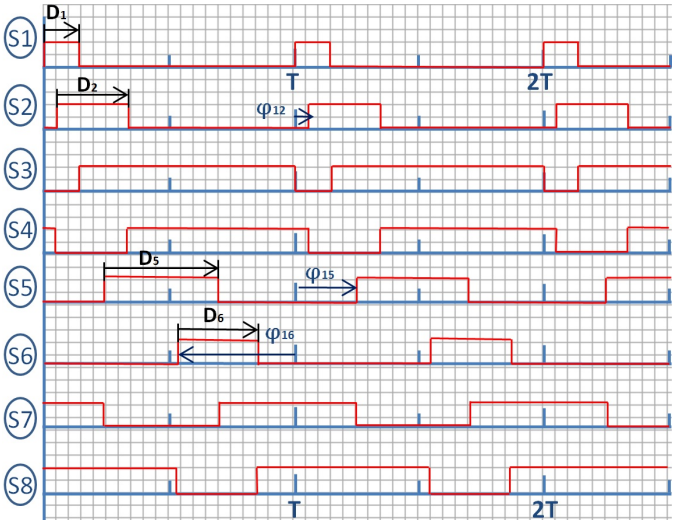


Figure 2.3: Modulation variables.

Table 2.4: Values of $V_L$ in two phases DAB.

| $V_L$ | Semiconductors *on* |
|---|---|
| $V_1 + V_2$ | 1 4 6 7 |
| $V_2$ | 1 2 6 7<br>3 4 6 7 |
| $V_1$ | 1 4 5 6<br>1 4 7 8 |
| $-V_1 + V_2$ | 2 3 6 7 |
| 0 | 1 2 5 6<br>1 2 7 8<br>3 4 5 6<br>3 4 7 8 |
| $V_1 - V_2$ | 1 4 5 8 |
| $-V_1$ | 2 3 5 6<br>2 3 7 8 |
| $-V_2$ | 1 2 5 8<br>3 4 5 8 |
| $-V_1 - V_2$ | 2 3 5 8 |

As such semiconductor can be on or off, there are 16 different configurations that are compatible with the assumptions exposed before (table 2.4). All variables explained above can be written as:

$$0 \leq D_i \leq 1, \qquad with \quad i = 1, 2, 5 \; or \; 6 \tag{2.2}$$

$$-0.5 \leq \phi_{ij} \leq 0.5, \qquad with \quad ij = 12, 15 \; or \; 56 \tag{2.3}$$

In figure 2.4 some of the multiple combinations in a cycle are shown. It is clear that in each cycle there are a maximum of eight different intervals. Besides, for each interval, one of the sixteen combinations shown in table 2.4 can appear. Also, we must take into account that the same combination for the semiconductors can not arise in the same cycle.

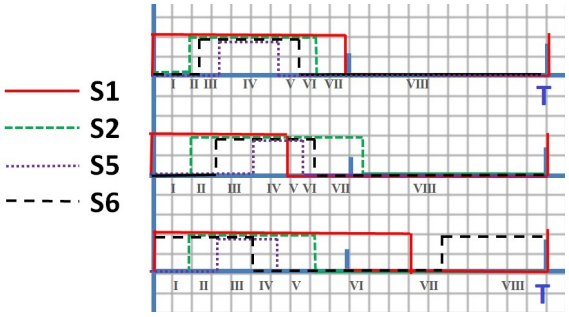


Figure 2.4: Different layouts.

As explained above, there are 16 different configuration for each of 8 intervals, but also the order of these intervals are important. Therefore, the possible combinations in each cycle are very high, and as the duration of each interval depends on the variables $D_i$ and $\phi_{ij}$, the waveform of the voltage in the inductance in each cycle can achieve multiple forms, and consequently the current across the inductance. It is also important to remark that different combinations can carry out the same average value of current through the inductance.

The numerous combinations will be reduced significantly if we impose that the mean value of the voltage through $L$ will be zero in each cycle (in steady state), moreover this fact is greatly desirable in order to avoid the saturation of the inductance and the internal transformer. To reach this, the following restriction must be fulfilled (note that they do not depend on $\phi_{ij}$):

$$V_1 \cdot (D_1 - D_2) = V_2 \cdot (D_5 - D_6) \tag{2.4}$$

Moreover, we must mention that to avoid the saturation of the inductance, it is sufficient but not necessary, that the mean values of $V_1$ and $V_2$ will be zero in each cycle. On the other hand, the average value of $V_1$ is zero in a cycle if, and only if, $D_1 = D_2$, and the average value of $V_2$ is zero if,

and only if, $D_5 = D_6$. In this way the number of variables is reduced and the number of possible combinations too.

Considering this explanation, we only need the variables $D_1$, $D_5$, $\phi_{12}$, $\phi_{15}$ and $\phi_{56}$. Moreover, with these variables, we can achieve all values for the average value of the currents $<i_1>$ and $<i_2>$ (currents through $R_1$ and $R_2$ in figure 2.2), so without loss of generality we can operate only with these variables. It is also important to point out that the values of $\phi_{ij}$ will only take influence in the transmitted power, but not in the saturation of the inductance, as explained above. In addition, and due to the symmetry of the problem, in some cases, different values of the variables produce the same current waveform in the inductance.

In the literature there are 3 types of modulations commonly used for two phases DAB structure, these are: rectangular (or conventional phase shift modulation, CPM), trapezoidal and triangular [53, 54]. In the next subsections, we will discuss each of these modulations, and the possible values for our variables defined above. we have to note that the most general modulation is trapezoidal, because the triangular and CPM modulations can be viewed as a special case of the trapezoidal one.

As our ultimate goal is to transmit the maximum energy, from the view of point of transported energy, the current waveforms $i_1$ and $i_2$ are important, and not the current through the inductance $i_L$, because its average value must be zero in order to avoid its saturation. We will see clearly in the next sections as the instantaneous value of currents $i_1$ and $i_2$, will be the same or the opposite than $i_L$, or even zero, depending the state of semiconductors as will be explain in next subsections.

### CPM modulation.

CPM occurs when $D_1 = D_5 = 0.5$, and $\phi_{12} = \phi_{56} = 0.5$, and consequently $\phi_{15}$ is the only variable which we can module (see figure 2.5). Remember that $-0.5 \leq \phi_{15} \leq 0.5$ .

### Calculation of parameters for CPM modulation.

The values for the peaks in the inductance current (in steady state) show in figure 2.5 can be calculate as follows:

$$-a + \frac{V_1 + V_2}{L} \cdot \phi_{15} \cdot T = b \tag{2.5}$$

$$b + \frac{V_1 - V_2}{L} \cdot (0.5 - \phi_{15}) \cdot T = a \tag{2.6}$$

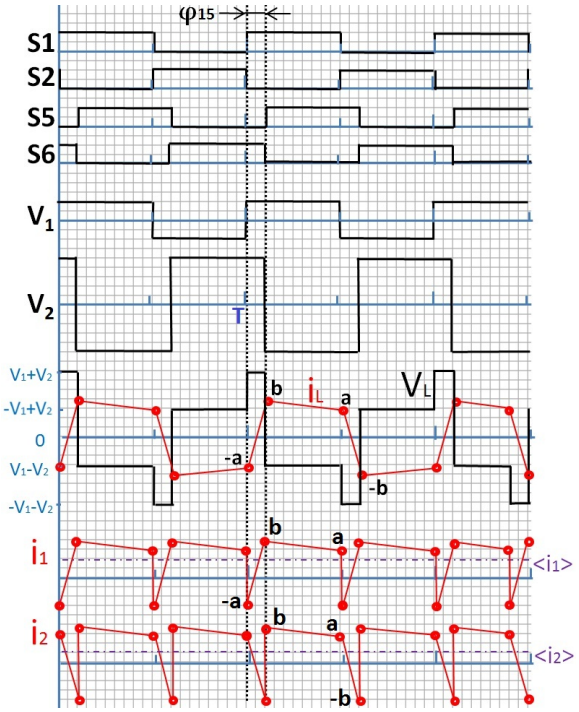


Figure 2.5: CPM modulation.

and consequently

$$a = \frac{T}{4L}[V_1 + (4 \cdot \phi_{15} - 1)V_2)] \tag{2.7}$$

$$b = \frac{T}{4L}[(4 \cdot \phi_{15} - 1)V_1 + V_2)] \tag{2.8}$$

From equations (2.7) and (2.8) we can remark that the peak values, $a$ and $b$, are maximum for values $|\phi_{15}| = 0.5$.

The mean value of current $_{<i_{1>}}$ in steady state is equal to:

$$_{<i_{1>}} = \frac{1}{T/2}\left[\frac{b-a}{2} \cdot \phi_{15} \cdot T + \frac{a+b}{2} \cdot (0.5 - \phi_{15}) \cdot T\right] = \frac{T}{L}\phi_{15}(1 - 2\phi_{15})V_2 \tag{2.9}$$

Proceeding in analogy with the current $_{<i_{2>}}$, we obtain:

$$_{<i_{2>}} = \frac{1}{T/2}\left[\frac{a-b}{2} \cdot \phi_{15} \cdot T + \frac{a+b}{2} \cdot (0.5 - \phi_{15}) \cdot T\right] = \frac{T}{L}\phi_{15}(1 - 2\phi_{15})V_1 \tag{2.10}$$

From equations (2.9) and (2.10), it is clear that $_{<i_{1>}}$ and $_{<i_{2>}}$ are maximum for $|\phi_{15}| = 0.25$, and they are zero for values $|\phi_{15}| = 0.5$ or $\phi_{15} = 0$. We can also observe as with only this variable, $\phi_{15}$, it is possible to achieve any

average value for the currents $i_1$ and $i_2$ between zero and their maximum values:

$$|_{<}i_{1>}| \leq V_2 \frac{T}{8L} \qquad |_{<}i_{2>}| \leq V_1 \frac{T}{8L} \tag{2.11}$$

**Triangular modulation.**

The goal of triangular modulation is to obtain a triangular waveform in the inductance current (figure 2.6). It is also common that in each cycle the current in the inductance will be zero for some intervals (dead band), this fact requires to tune the parameters correctly. If it is reached, then zero voltage switching, ZVS, is also possible to achieve, and therefore the losses will be lower. Usually the duration of this dead band interval is around %10 of the whole cycle [53].

In order to obtain a triangular waveform in the current through the inductance, it is clear that we need a positive slope during an interval and negative slope during the next interval, or vice-versa. So in principle, all combinations of voltage levels shown in table 2.4 are possible. However, if we want to respect the assumptions discussed above (see section 2.2.1), specially the one which restricts the switch on and off the semiconductor in one cycle and if we also want to obtain zero average value in the current inductance, not all voltage levels shown in table 2.4 are feasible, in fact they are reduced to 12 if there not exists a dead band or only 2 if it is included. In table 2.5 half of these possibilities are shown, and if we change the order of the intervals, we obtain the other half (in this case the current average value $_{<}i_{1>}$ has the opposite sign from table 2.6).

Table 2.5: Parameters for triangular modulation configurations.

| case | Slope | $D_1$ | $D_5$ | $\phi_{12}$ | $\phi_{15}$ | $\phi_{56}$ |
|---|---|---|---|---|---|---|
| 1 | $\uparrow V_1+V_2$<br>$\downarrow V_2$ | 0.5 | 0.5 | $\frac{V_2}{V_1+2V_2}\cdot\frac{T}{2}$ | $\frac{V_2}{V_1+2V_2}\cdot\frac{T}{2}$ | 0.5 |
| 2 | $\uparrow V_1+V_2$<br>$\downarrow V_1$ | 0.5 | 0.5 | 0.5 | $\frac{-V_1}{2V_1+V_2}\cdot\frac{T}{2}$ | $\frac{V_1}{2V_1+V_2}\cdot\frac{T}{2}$ |
| 3 | $\uparrow V_1+V_2$<br>$\downarrow V_2-V_1$ | 0.5 | 0.5 | 0.5 | $\frac{V_2-V_1}{2V_2}\cdot\frac{T}{2}$ | 0.5 |
| 4 | $\uparrow V_2$<br>$\downarrow V_1$ | 0.5 | 0.5 | $\frac{-V_1}{V_1+V_2}\cdot\frac{T}{2}$ | $\frac{-V_1}{V_1+V_2}\cdot\frac{T}{2}$ | $\frac{V_1}{V_1+V_2}\cdot\frac{T}{2}$ |
| 5 | $\uparrow V_2$<br>$\downarrow V_2-V_1$ | 0.5 | 0.5 | $\frac{V_2}{V_1+V_2}\cdot\frac{T}{2}$ | 0 | 0.5 |
| 6 | $\uparrow V_1$<br>$\downarrow V_2-V_1$ | 0.5 | 0.5 | 0.5 | 0 | $\frac{V_2-V_1}{V_2}\cdot\frac{T}{2}$ |
| 7 | $\uparrow V_2$ (dead<br>$\downarrow V_1$ band) | $1-\phi_{15}$ | $1-DB-2\phi_{15}$ | 0.5 | $-\frac{(1-DB)V_2}{2(V_1+V_2)}$ | 0.5 |

Table 2.6: Obtained values for triangular modulation configurations.

| case | $a$ | $<i_{1>}$ |
|---|---|---|
| 1 | $\frac{V_2(V_1+V_2)}{(V_1+2V_2)} \cdot \frac{T}{2L}$ | $\left(\frac{V_2}{V_1+2V_2}\right)^2 \cdot (V_1+V_2) \cdot \frac{T}{4L}$ |
| 2 | $\frac{V_1(V_1+V_2)}{(2V_1+V_2)} \cdot \frac{T}{2L}$ | $\frac{-V_1V_2}{(V_1+2V_2)^2} \cdot (V_1+V_2) \cdot \frac{T}{4L}$ |
| 3 | $\frac{V_2^2-V_1^2}{V_2} \cdot \frac{T}{4L}$ | $\frac{V_2^2-V_1^2}{V_2} \cdot \frac{T}{8L}$ |
| 4 | $\frac{V_1V_2}{V_1+V_2} \cdot \frac{T}{2L}$ | $\frac{-V_1V_2^2}{(V_1+V_2)^2} \cdot \frac{T}{4L}$ |
| 5 | $\frac{(V_2-V_1)V_2}{2V_2-V_1} \cdot \frac{T}{2L}$ | $\frac{V_2^2(V_2-V_1)}{(2V_2-V_1)^2} \cdot \frac{T}{4L}$ |
| 6 | $\frac{(V_2-V_1)V_1}{V_2} \cdot \frac{T}{2L}$ | $\frac{V_1(V_2-V_1)}{V_2} \cdot \frac{T}{4L}$ |
| 7 | $\frac{(1-DB)V_1V_2}{(V_1+V_2)} \cdot \frac{T}{2L}$ | $-\frac{(1-DB)^2V_1V_2^2}{(V_2+V_1)^2} \cdot \frac{T}{4L}$ |

In figure 2.6 are shown, as an example, the parameters for the cases 1 and 7.

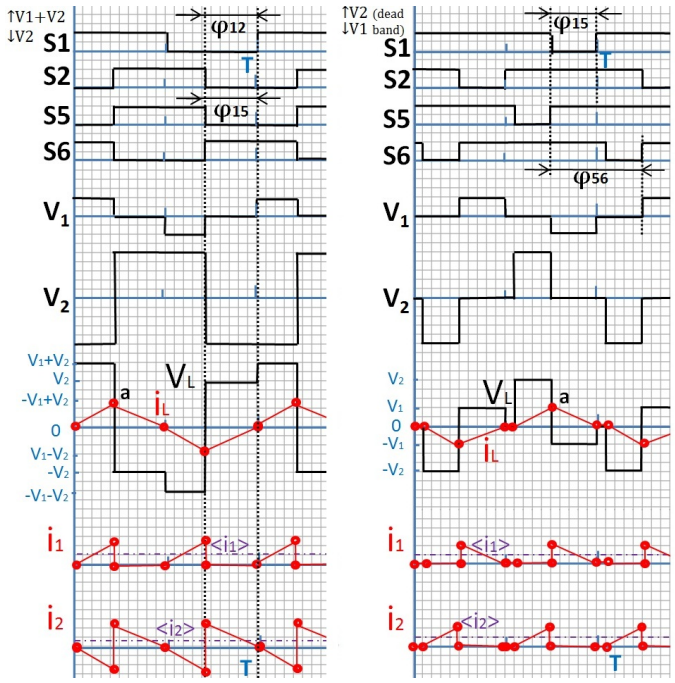


Figure 2.6: Triangular modulation.

### Trapezoidal modulation.

The trapezoidal modulation is the most general of the three. It is also common that in each half cycle a dead band (interval where the current is zero) exists, as occurs in triangular modulation. Consequently ZVS is possible too, and consequently the losses will be smaller.

With this type of modulation, we can achieve the maximum number of possible configurations respecting all the hypothesis. In total we can obtain 192 different waveform if dead band is not included. This number can be obtained as follows. Considering that there is no dead band in each half cycle, then there will be 3 different intervals. If we consider that in the first interval the slope is positive, then 4 possible configurations for semiconductors can be obtained. In the second interval, 7 different could be achieved (3 with positive slope plus 4 with negative slope). In this second interval the current still has positive value, otherwise we can not achieve trapezoidal form. In the third interval, and because we want that the current be zero at the end of the semi-cycle, the slope must be negative. In this case, it depends on the slopes used in the previous state. If in the second interval, it was positive, then we have 4 possibilities to come down, and if it is was negative, then we only have 3 possibilities. This reasoning gives us 96 possibilities if the slope in the first interval was positive. If we make the reasoning considering that in the first interval there is negative slope, we obtain the remain 96 possibilities. Besides the values obtained in this case for the average current will be the opposite to the obtained above.

In figure 2.7 one of the 192 possible configuration is shown.

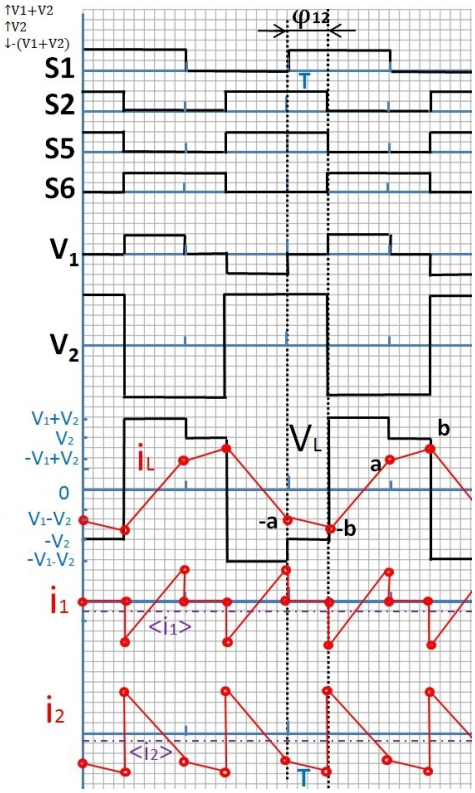


Figure 2.7: Trapezoidal modulation.

### 2.2.2 Modulation discussion.

We have presented each modulation in details in the above subsections. Now, we will compare them, and we will chose the most appropriate for our case. From the viewpoint of the maximum transmitted power, and for the same parameters ($V_1$, $V_2$, $R$, $L$ and $T$), the CPM modulation is whose can transmit more power. In order to ensure this, we make the following statement.

According to figure 2.8, the triangular modulation will produce always more power than the trapezoidal one, because the dashed area (trapezoidal) will be always smaller than the triangular one. Thus, and although the trapezoidal modulation has many more possible configurations, we can always choose a triangular modulation that gives us a larger area, which means more average current value, and consequently our converter can transmit more power.

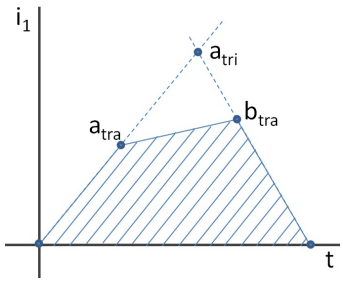


Figure 2.8: Transmitted current for trapezoidal and triangular modulation.

Therefore, to know the modulation which provides higher power, we have to compare the triangular and CPM modulations.

From table 2.6, and considering absolute values for the average currents of each case, it is clear that for the assumption $V_2 > V_1$:

$$|_{<i_1> \ case1}| > |_{<i_1> \ case2}| \tag{2.12}$$

$$|_{<i_1> \ case3}| > |_{<i_1> \ case6}| \tag{2.13}$$

$$|_{<i_1> \ case4}| > |_{<i_1> \ case7}| \tag{2.14}$$

Consequently, we have to compare the cases 1, 3, 4 and 5 of triangular modulation with the maximum value for the average current of CPM modulation of equation (2.9), which is $V_2 \cdot \frac{T}{8L}$, for $\phi_{15} = |0.25|$.

*CPM modulation vs Triangular modulation case 1:*

In this case we show as the maximum average current for CPM modulation is always higher than $|_{<i_1> \ case1}|$ for triangular modulation. From equation (2.9) and table 2.6:

$$V_2 \cdot \frac{T}{8L} > \left(\frac{V_2}{V_1 + 2V_2}\right)^2 \cdot (V_1 + V_2) \cdot \frac{T}{4L} \Leftrightarrow \frac{V_2}{2} > \left(\frac{V_2}{V_1 + 2V_2}\right)^2 \cdot (V_1 + V_2)$$

as $\left(\frac{V_2}{V_1+2V_2}\right)^2 < \frac{1}{4}$ and $V_1 + V_2 < 2V_2$, it is clear that:

$$\forall\ V_2 > V_1 > 0, \quad \frac{V_2}{2} > \left(\frac{V_2}{V_1+2V_2}\right)^2 \cdot (V_1+V_2) \tag{2.15}$$

*CPM modulation vs Triangular modulation case 3:*

$$V_2 \cdot \frac{T}{8L} > \frac{V_2^2 - V_1^2}{V_2} \cdot \frac{T}{8L} \Leftrightarrow V_2 > \frac{V_2^2 - V_1^2}{V_2}$$

it is clear that:

$$\forall\ V_2 > V_1 > 0, \quad V_2 > \frac{V_2^2 - V_1^2}{V_2} \tag{2.16}$$

*CPM modulation vs Triangular modulation case 4:*

$$V_2 \cdot \frac{T}{8L} > \frac{V_1 V_2^2}{(V_1+V_2)^2} \cdot \frac{T}{4L} \Leftrightarrow \frac{V_2}{2} > \frac{V_1 V_2^2}{(V_1+V_2)^2}$$

as $(V_1 + V_2)^2 > 2V_1V_2$ it is clear that:

$$\forall\ V_2 > V_1 > 0, \quad \frac{V_2}{2} > \frac{V_1 V_2^2}{(V_1+V_2)^2} \tag{2.17}$$

*CPM modulation vs Triangular modulation case 5:*

$$V_2 \cdot \frac{T}{8L} > \frac{V_2^2(V_2 - V_1)}{(2V_2 - V_1)^2} \cdot \frac{T}{4L} \Leftrightarrow \frac{1}{2} > \frac{V_2(V_2 - V_1)}{(2V_2 - V_1)^2} = \frac{V_2^2 - V_1V_2}{4(V_2^2 - V_1V_2) + V_1^2}$$

which is clearly smaller than 1/4, consequently:

$$\forall\ V_2 > V_1 > 0, \quad \frac{V_2}{2} > \frac{V_2^2(V_2 - V_1)}{(2V_2 - V_1)^2} \tag{2.18}$$

Therefore, it is clear that from the point of view of maximum power transport capacity the best modulation is the CPM. We will use it in the next sections in order to synthesize the control law for the two phases DAB.

### 2.2.3 System Modeling.

The two phases DAB system is inherently discontinuous and consequently not adapted for control algorithm synthesis, because it is based on power electronics. In this section a continuous average model is proposed in order to synthesise a control law [37, 55, 56].

In the modelling process, we will assume that the capacitors $C_1$ and $C_2$ are always precharged at the voltage levels $V_1$ and $V_2$ as have been discussed in the hypothesis made in section 2.2.1. Therefore, these capacitors can be considered as ideal voltage sources with internal resistances. If all

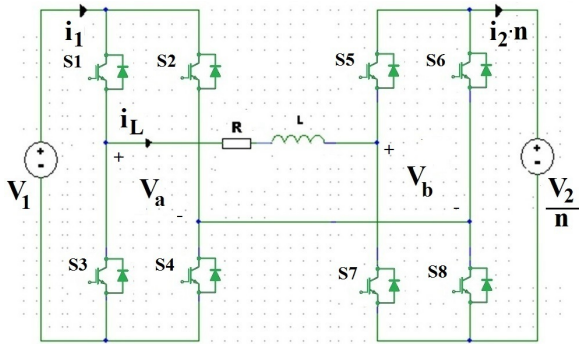


Figure 2.9: Two phases DAB. Simplified circuit.

parameters are seen from the primary side, we obtain the following simplified scheme as figure 2.9 shows, where all the resistances of the circuit are included in $R$.

In the previous section, 2.2.1, we have asserted that the best modulation for this topology , from the point of view of maximum transmitted power, is the CPM modulation, and the unique variable on which we can act was $\phi_{15}$. It represents the phase shift ratio between the voltages applied to the inductance $V_1$ and $V_2$. In order to have a bidirectional converter, the phase shift ratio $\phi_{15}$ is defined in the interval $0 < \phi_{15} < 0.5$ for power flowing from the left side to right side, and in the interval $-0.5 < \phi_{15} < 0$ for power flowing in the opposite direction. Consequently, the state of the switch components for the adopted strategy for case $\phi_{15} > 0$ is summed up in table 2.7, where "on" denotes the state when the switch is conducting and "off" denotes the state when the switch is open.

Table 2.7: State of the switches ($\phi_{15} > 0$).

| **Intervals** | **S1** | **S2** | **S3** | **S4** | **S5** | **S6** | **S7** | **S8** |
|---|---|---|---|---|---|---|---|---|
| $[0, \phi_{15} \cdot T]$ | on | off | off | on | off | on | on | off |
| $[\phi_{15} \cdot T, T/2]$ | on | off | off | on | on | off | off | on |
| $[T/2, (0.5 + \phi_{15}) \cdot T]$ | off | on | on | off | on | off | off | on |
| $[(0.5 + \phi_{15}) \cdot T, T]$ | off | on | on | off | off | on | on | off |

With the sequence given in table 2.7 ($\phi_{15} > 0$), the applied voltages $V_a$ and $V_b$, the current $i_L$ and voltage $V_L$ in the inductance and currents $i_1$ and $i_2$ with their average values $_<i_{1>}$ and $_<i_{2>}$ (discontinuous lines) are obtained for a few cycles in steady state in figure 2.10.

Figure 2.10 shows two interesting things. Firstly, for the phase shift ratio chosen in the interval $0 < \phi_{15} < 0.5$, the average values of currents $_<i_{1>}$ and $_<i_{2>}$ are positive, that means, the power is flowing from the source $V_1$ to $V_2$. Secondly, we can remark that the average values of voltage applied

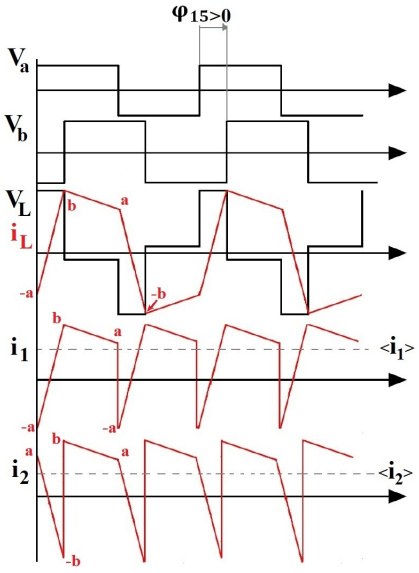


Figure 2.10: Voltages and currents for the two phases DAB circuit ($\phi_{15} > 0$).

to the inductance and the current through it are zero. These facts are in accordance with the explanation made in section 2.2.1. If we chose $\phi_{15}$ such that $-0.5 < \phi_{15} < 0$ the opposite effect appears in the system.

### 2.2.4 Dynamics of the real system.

In order to design the non-linear control (based in Lyapunov theory), a differential equation model that represents the real system is required. The control is performed on the mean value of current $i_1$, therefore all calculations will be indicated with respect to the current $<i_1>$.

In the next Lemma 1 we introduce one of the results of this chapter:

***Lemma* 1** *The differential equation which governs the system shown in figure 2.9 is:*

$$\frac{d}{dt} <i_1>(t) = -\frac{R}{L} \cdot <i_1>(t) + \frac{T \cdot R}{L^2} \cdot \phi_{15} \cdot (1 - 2|\phi_{15}|) \frac{V_2}{n} \tag{2.19}$$

*where $n$ is the transformer ratio.*

***Proof.-***

Now, we are going to proof Lemma 1 in the case $0 < \phi_{15} < 0.5$. The case of negative $\phi_{15}$ is analogous. In any case we have a similar circuit than in figure 2.2, that is, an RL circuit where the supply voltage is a stepped waveform. We have assumed that $V_1 < \frac{V_2}{n}$, but if we chose the opposite, we can reach the same result.

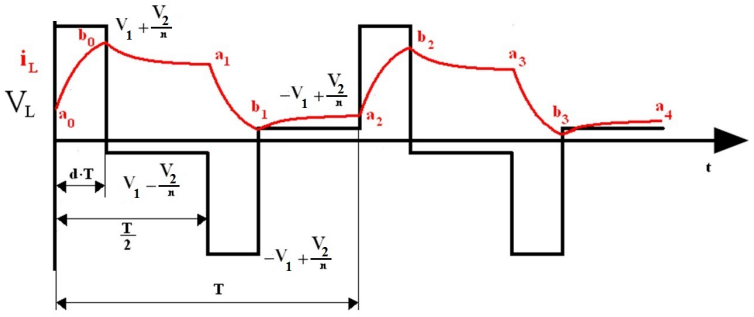


Figure 2.11: Voltage and current in first moments for two phases DAB with CPM.

In $[0, \phi_{15} \cdot T]$ the differential equation that governs the circuit is:

$$\frac{d}{dt} i_L(t) = -\frac{R}{L} \cdot i_L(t) + \frac{U}{L} \tag{2.20}$$

where $U = V_1 + \frac{V_2}{n}$. The solution of equation 2.20 is:

$$i_L(t) = -\frac{U}{R} + \left(a_0 - \frac{U}{R}\right) e^{-\frac{R}{L} \cdot t} = a_0 \cdot e^{-\frac{R}{L} \cdot t} + \left(1 - e^{-\frac{R}{L} \cdot t}\right) \cdot \frac{U}{R} \tag{2.21}$$

Consequently:

$$b_0 = i_L(\phi_{15} \cdot t) = a_0 \cdot e^{-\frac{R}{L} \phi_{15} \cdot t} + \left(1 - e^{-\frac{R}{L} \phi_{15} \cdot t}\right) \frac{V_1 + \frac{V_2}{n}}{R} \tag{2.22}$$

For $[\phi_{15} \cdot T, T/2]$ we proceed in the same way as above, but now taking into account that $U = V_1 - \frac{V_2}{n}$. We obtain:

$$i_L(t) = -\frac{U}{R} + \left(b_0 - \frac{U}{R}\right) e^{-\frac{R}{L} \cdot (t - \phi_{15} \cdot T)} = b_0 \cdot e^{-\frac{R}{L} \cdot (t - \phi_{15} \cdot T)} + \left(1 - e^{-\frac{R}{L} \cdot t}\right) \cdot \frac{U}{R} \tag{2.23}$$

And therefore:

$$a_1 = i_L(\frac{T}{2}) = b_0 \cdot e^{-\frac{R}{L}(\frac{1}{2} - \phi_{15})T} + \left(1 - e^{-\frac{R}{L}(\frac{1}{1} - \phi_{15})T}\right) \frac{V_1 - \frac{V_2}{n}}{R} \tag{2.24}$$

From equations (2.22) and (2.24), we can put $a_1$ in terms of $a_0$, because $b_0$ depends on $a_0$, the expression is:

$$a_1 = a_0 \cdot e^{-\frac{RT}{2L}} + \left(1 - e^{-\frac{RT}{2L}}\right) \frac{V_1}{R} - \left(1 - 2e^{-\frac{R}{L}(\frac{1}{2} - \phi_{15})T + e^{-\frac{RT}{2L}}}\right) \frac{V_2}{n \cdot R} \tag{2.25}$$

As in the second part of the period the differential equations which govern the system are equal but with opposite voltages applied, proceeding in a similar way we obtain $a_2$ in terms of $a_1$:

$$a_2 = a_1 \cdot e^{-\frac{RT}{2L}} - \left(1 - e^{-\frac{RT}{2L}}\right) \frac{V_1}{R} + \left(1 - 2e^{-\frac{R}{L}(\frac{1}{2} - \phi_{15})T + e^{-\frac{RT}{2L}}}\right) \frac{V_2}{n \cdot R} \tag{2.26}$$

Replacing equation (2.25) into (2.26):

$$a_2 + a_1 = (a_1 + a_0) \cdot e^{-\frac{RT}{2L}} \tag{2.27}$$

If we write equation (2.27) in general form, we achieve:

$$a_{n+2} + (1 - e^{-\frac{RT}{2L}})a_{n+1} - (e^{-\frac{RT}{2L}})a_n = 0 \tag{2.28}$$

Equation (2.28) is a homogeneous linear recurrent sequence with constant coefficients whose solution is:

$$a_n = Cte_1 \cdot (-1)^n + Cte_2 \cdot e^{-n\frac{RT}{2L}} \tag{2.29}$$

where the constants have the following values:

$$\begin{cases} Cte_1 = \frac{a_0 \cdot e^{-\frac{RT}{2L}} - a_1}{1 + e^{-\frac{RT}{2L}}} \\ Cte_2 = \frac{a_0 + a_1}{1 + e^{-\frac{RT}{2L}}} \end{cases} \tag{2.30}$$

The limit of the sub-sequences of even and odd terms are shown in equations (2.31) and (2.32) respectively:

$$\lim_{n \to +\infty} a_{2n} = Cte_1 = \frac{-\left[1 - e^{-\frac{RT}{2L}}\right] \frac{V_1}{R} + \left[1 - 2e^{-\frac{R}{L}(\frac{1}{2} - \phi_{15})T} + e^{-\frac{RT}{2L}}\right] \frac{V_2}{n \cdot R}}{1 + e^{-\frac{RT}{2L}}} \tag{2.31}$$

$$\lim_{n \to +\infty} a_{2n+1} = -Cte_1 = \frac{\left[1 - e^{-\frac{RT}{2L}}\right] \frac{V_1}{R} - \left[1 - 2e^{-\frac{R}{L}(\frac{1}{2} - \phi_{15})T} + e^{-\frac{RT}{2L}}\right] \frac{V_2}{n \cdot R}}{1 + e^{-\frac{RT}{2L}}} \tag{2.32}$$

It should be pointed out that the two expressions (2.31) and (2.32) are independent of the initial values. Note that in steady state the terms $a_{2n}$ and $a_{2n+2}$ have the same value, and the term $a_{2n+1}$ has the same value but opposite sign with respect to previous terms. For this reason, the average value of the current through the inductance is zero in each period in steady state.

The current dynamics in each period is expected to be the same that the dynamics obtained for the sequence of even terms shown in figure 2.12, because both have the same time constant. We will now verify this affirmation.

The time constant, $\tau$, is by definition the time to reach $\left(1 - \frac{1}{e}\right) \approx 0.63$ of the final value. If we proceed as follows:

$$(final\ value - a_0)\left(1 - \frac{1}{e}\right) = a_{2n} - a_0 \tag{2.33}$$

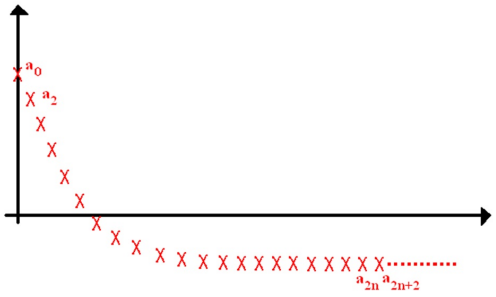


Figure 2.12: Sequence of even terms.

The final value is obtained by the next expression:

$$\lim_{n\to+\infty} a_{2n} = \frac{a_0 \cdot e^{-\frac{RT}{2L}} - a_1}{1 + e^{-\frac{RT}{2L}}} \tag{2.34}$$

We obtain that $n \cdot T = \frac{L}{R}$, where $n$ is the number of periods for which the time constant reaches $\tau = n \cdot T$. And consequently, the time constant for the average value of the current and the time constant for the sequence are the same, as we wished to prove.

As we know the time constant, and due to the system shown in figure 2.9 is a linear differential system of first order, we achieve:

$$\frac{d}{dt} <i_{1>}(t) = -\frac{<i_{1>}(t)}{\tau} + c \tag{2.35}$$

where $c$ is a constant to be calculated.

In equation (2.9), the average current in steady state was calculated. Applying this result to equation (2.35), we obtain:

$$c = \frac{T}{\tau \cdot L} \cdot \phi_{15} \cdot (1 - 2|\phi_{15}|)\frac{V_2}{n} = \frac{TR}{L^2} \cdot \phi_{15} \cdot (1 - 2|\phi_{15}|)\frac{V_2}{n} \tag{2.36}$$

Therefore, we have demonstrated that equation (2.35) is identical to equation (2.19), as we want to prove. □

### 2.2.5 Verification of differential equation.

With the purpose to verify that our model (differential equation) has similar behaviour than a real converter, we will use SIMULINK® environment. We have created a file, which is shown in figure 2.13. In order to simulate real semiconductors, we have chosen the blocks IGBT's of SIMULINK® library. The values of the simulation are shown in table 2.8.

In Figure 2.14 the solid plot corresponds to the real value of $i_1$ and the dashed plot is the output of our model corresponding to the differential

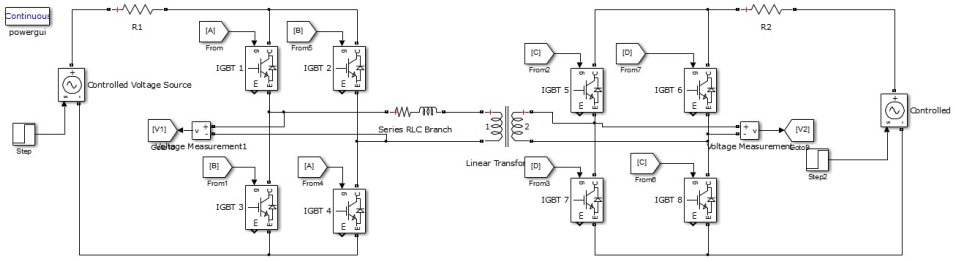


Figure 2.13: Two phases DAB SIMULINK® file.

Table 2.8: Verification of differential equation. Simulation values.

| | | |
|---|---|---|
| $\phi_{15}$ | Phase shift ratio | 0.15 |
| n | Transformer ratio | 100/11 |
| $R_{total}$ | Total resistance | 0.01Ω |
| $V_1$ | Voltage side 1 | 1000 V |
| $V_2$ | Voltage side 2 | 10000 V |
| L | Inductance | $6.875{\cdot}10^{-5}$H |
| T | Period | 1/20000 s |

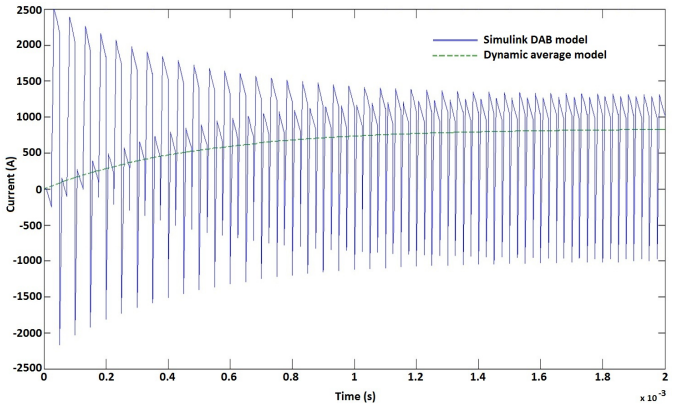


Figure 2.14: Comparison between DAB SIMULINK file (mean value $i_1$) and the dynamic average model for $\phi_{15}$=0.15.

equation (2.19). Figure 2.14 shows that the dynamic of the peaks of solid plot is the same as the dynamic of the dashed plot, thus the transient behaviour of the real current $i_1$ is the same that in the differential equation. In steady state the value of $_{<}i_{1>}$ is given by equation (2.9) which is the same as the steady state value in the differential equation (2.19), in consequence, we can conclude that our model given by equation (2.19) adjusts to the real case.

### 2.2.6 Non-linear control design for DAB system.

Since our system is non-linear, due to the presence of the absolute value, we have chosen Lyapunov theory to design the controller. This theory is a powerful and widely used tool to prove the stability of dynamical systems, especially nonlinear systems, see [38, 39, 40].

We consider the dynamic model shown in equation (2.37), which represents the average model of the two phases DAB converter.

$$\frac{d}{dt} <i_{1>}(t) = -\frac{R}{L} <i_{1>}(t) + \frac{TR}{L^2} \cdot \phi_{15} \cdot (1 - 2|\phi_{15}|)\frac{V_2}{n} \tag{2.37}$$

Our aim is to track the reference of the average current $<i_{1>ref}$ . If we defined the following Lyapunov energy function, which represents the necessary energy for the current to converge to its reference.

$$\mathcal{V}_{<i_{1>}} = \frac{1}{2}\left(<i_{1>} - <i_{1>ref}\right)^2 \tag{2.38}$$

Its time derivate is:

$$\dot{\mathcal{V}}_{<i_{1>}} = <\tilde{i}_{1>}\left(-\tfrac{R}{L} <i_{1>}(t) + \tfrac{TR}{L^2}\phi_{15}(1 - 2|\phi_{15}|)\tfrac{V_2}{n} - \tfrac{d}{dt} <i_{1>ref}\right) \tag{2.39}$$

where the $<\tilde{i}_{1>} = (<i_{1>} -< i_{1>ref})$ is the tracking error.

In order to achieve negative derivate of the Lyapunov function, we can chose:

$$-\tfrac{R}{L} <i_{1>}(t) + \tfrac{TR}{L^2}\phi_{15}(1 - 2|\phi_{15}|)\tfrac{V_2}{n} - \tfrac{d}{dt} <i_{1>ref} = -\alpha <\tilde{i}_{1>} - \beta sign(<\tilde{i}_{1>}) \tag{2.40}$$

with the positive tuning gain parameters $\alpha > 0$ and $\beta > 0$. The sign function is added to improve the robustness properties of the proposed control law, in analogous form as the proposed in sliding mode control theory [57]. Thereafter, the time derivative of the Lyapunov function becomes:

$$\dot{\mathcal{V}}_{<i_{1>}} = -\alpha \cdot <\tilde{i}_{1>}^{\,2} - \beta \cdot sign(<\tilde{i}_{1>}) \cdot <\tilde{i}_{1>} < 0, \quad \forall\ <i_{1>} \neq 0 \tag{2.41}$$

Equation (2.41) satisfies the stability condition, that is , $<i_{1>}$ is asymptotically stabilized towards its reference. Consequently, the following relation holds:

$$\phi_{15}(1 - 2|\phi_{15}|) = \tfrac{n \cdot L^2}{R \cdot T \cdot V_2}\left[-\alpha <\tilde{i}_{1>} - \beta sign(<\tilde{i}_{1>}) + \tfrac{d}{dt} <i_{1>ref} + \tfrac{R}{L} <i_{1>}\right] \tag{2.42}$$

Let consider the right hand side of equation (2.42) as:

$$K = \frac{n \cdot L^2}{RTV_2}\left[-\alpha \cdot <\tilde{i}_{1>} - \beta \cdot sign(<\tilde{i}_{1>}) + \frac{d}{dt} <i_{1>ref} + \frac{R}{L} <i_{1>}\right] \tag{2.43}$$

Developing equation (2.43), we obtain the general solution for the two cases, leading to the control law which is able to track the reference and to ensure the system stability:

$$\phi_{15}(1-2|\phi_{15}|) = \begin{cases} \phi_{15} - 2\phi_{15}^2, & for \ \ \phi_{15} \geq 0 \\ \phi_{15} + 2\phi_{15}^2, & for \ \ \phi_{15} \leq 0 \end{cases} \tag{2.44}$$

Depending on the sign of the phase shift ration $\phi_{15}$, two different solutions are possible.

$$\begin{cases} <i_{1>ref} \ > 0 \Rightarrow K > 0 \Rightarrow \phi_{15}^2 - 2\phi_{15} - K = 0 \Rightarrow \phi_{15} = \frac{1-\sqrt{1-8K}}{4} \\ <i_{1>ref} \ < 0 \Rightarrow K < 0 \Rightarrow \phi_{15}^2 + 2\phi_{15} - K = 0 \Rightarrow \phi_{15} = \frac{-1+\sqrt{1+8K}}{4} \end{cases} \tag{2.45}$$

The general solution for the two cases leads to the control driving the current to track its reference, and that assures system's stability. We obtain:

$$\phi_{15} = \frac{1-\sqrt{1-8K}}{4} \cdot S_1 + \frac{-1+\sqrt{1+8K}}{4} \cdot S_2 \tag{2.46}$$

where $S_1$ is 1 if the condition $K > 0$ is true, and 0 otherwise. Something similar could be explained for $S_2$ with the condition $K < 0$.

***Theorem* 1** *The converter described by (2.19) under control law (2.46) (with $\alpha$ and $\beta$ positive constants) is globally asymptotically stabilized to an equilibrium point given by its references.*

The proof of this theorem 1 is composed by the steps of the current subsection. □

### 2.2.7 Verification of non-linear control.

In order to verify the performance of the non-linear control exhibited in (2.46), simulations in SIMULINK® are carried out. The simulation parameters are gathered in Table 2.9.

Table 2.9: Simulation values.

| | | |
|---|---|---|
| $<i_{1>ref}$ | Current reference | 640 A |
| n | Transformer ratio | 100/11 |
| $R_{total}$ | Total resistance | 0.01Ω |
| $V_{in}$ | Input voltage | 1000 V |
| $V_{out}$ | Output voltage | 10000 V |
| L | Inductance | $6.875 \cdot 10^{-5}$H |
| T | Period | 1/20000 s |
| $\alpha$ | Positive tuning gain parameter | 2100 |
| $\beta$ | Positive tuning gain parameter | 0.001 |

Figure 2.15 is obtained after simulation, and it shows the current $<i_{1>}$ response when the system is controlled. We observe as the current tracks its reference in a proper way.

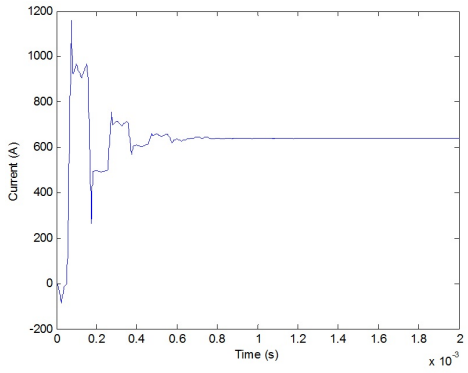


Figure 2.15: Current $<i_{1>}$ response when the system is controlled.

As the converter is bidirectional, it must be capable of change the power direction at any instant. In order to carry out this task, it is enough to change the current direction, because the voltages in each side remain constant. In figure 2.16 a variable current reference is proposed with the aim to show this phenomenon. This reference has three current levels. The first at 960 A ($\phi_{15} = 0.2$ in steady state), the second at -960 A ($\phi_{15} = -0.2$ in steady state) and the third at 500 A ($\phi_{15} = 0.073$ in steady state). It should be noted that depending on the current reference imposed the power transmitted will be higher or lower. With the reference values given in each interval the power transmitted are respectively 1 $MW, -1$ $MW$ and 0.5 $MW$, where we have considered the positive sense of power, when it goes from the left side to the right. Figure 2.16 shows that the system behaves well with respect to the different changes in the reference signal.

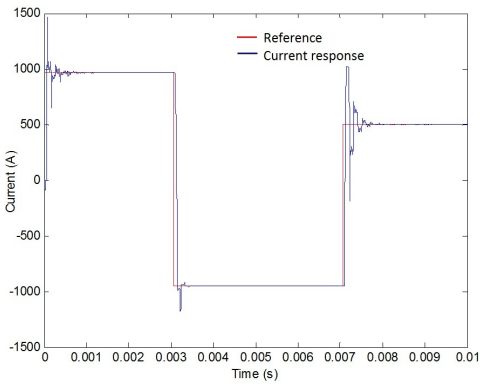


Figure 2.16: Current response in real situation.

The behaviour of the control variable, $\phi_{15}$, is shown in Figure 2.17.

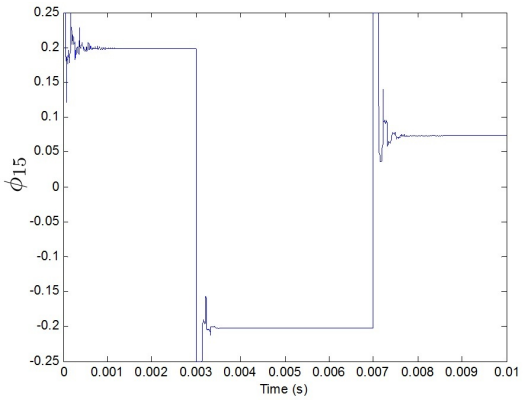


Figure 2.17: $\phi_{15}$ response in real situation for two phases DAB converter

Figure 2.17 shows that $\phi_{15}$ has a correct behaviour. We conclude that our control is valid for the bidirectional two phases DAB converter.

## 2.3 Robustness

In this section we explore the robustness of the control. This is a very meaningful aspect because all systems are subject to the effects of disturbances and uncertainties. For these reasons, it is important to analyse our controller submit to disturbances.

The disturbances will be the voltage variations in each side of the system, which we have considered constant when the controller was developed. A 20% of difference with respect to the nominal value is included in simulations. It is important to remark that in HVDC systems the maximum deviation from the nominal value are usually not greater than 10% [58]. To simulate the perturbations, random signals with sample time equals to 1 $ms$ has been considered in both sides. Data from this system is shown in table 2.10.

Table 2.10: Robustnesses simulation values.

| | | |
|---|---|---|
| n | Transformer ratio | 100/11 |
| $R_{total}$ | Total resistance | 0.01Ω |
| $V_{in}$ | Nominal input voltage | 1000 V |
| $V_{out}$ | Nominal output voltage | 12000 V |
| L | Inductance | $6.875{\cdot}10^{-5}$H |
| T | Period | 1/2000 s |

In view of figure 2.18, we can observe how despite there is a variation grater than 20% in the capacitor voltages, the designed control allows that

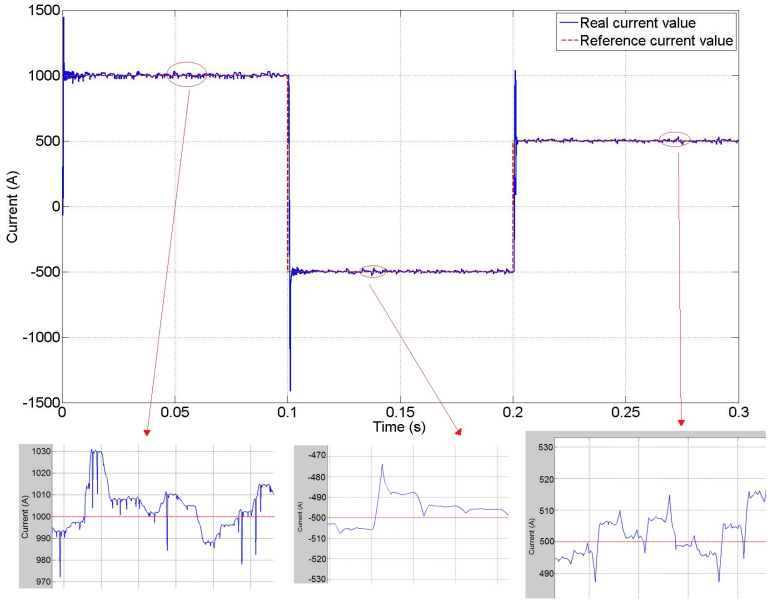


Figure 2.18: Current average value in left side of single DAB cell under unbalance situation.

the current follows its reference, and also one can remark that the real current does not exceed 10% of reference. Considering these simulations, we can affirm that our control is robust to disturbances.

## 2.4 Three phases DAB.

This section presents the modelling and control of the three phases DAB bidirectional converter [59]. As happens with the two phases one, the three phases DAB converter is composed of two full bridges, each one connected to one side of the transformer, as figure 2.19 shows. The transformer provides the galvanic insulation necessary to protect against unforeseen circumstances (see [47]). The inductances, which are used as an energy transfer device, are placed in series with the transformer.

### 2.4.1 PWM Modulation.

For this type of converter, we can also implement the same modulation philosophies shown in section 2.2.1. The study would be analogous to the already analysed. It is easily to realise that the best modulation for this case would be the same as before, that is, the CPM modulation. However, for the sake of extending the modulations investigated, we will study the PWM modulation for the three phases DAB case. It must be emphasized that using this technique creates higher switching losses, so its use for high

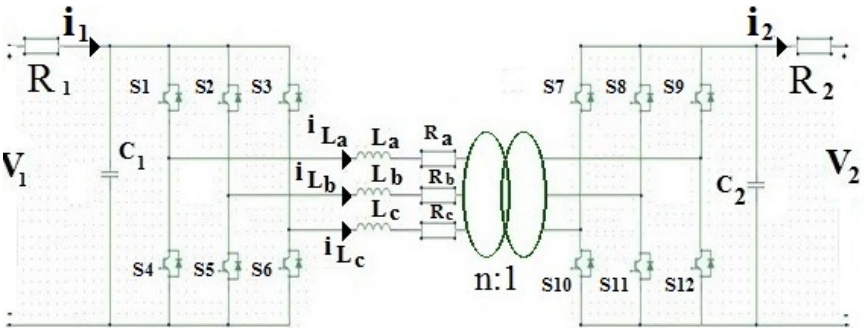


Figure 2.19: Three phases Dual Active Bridge.

voltage levels is not recommended.

PWM is a well known modulation technique [60, 61]. It is used in transmission applications to encode information, and it is also used to allow the control of the power supplied to electrical devices, especially to inertial loads such as motors. The typical construction of a PWM modulation is carried out by a comparator with two signals. One of the signals has typically a sawtooth wave form with a frequency much higher than the other one, which is the modulating signal, as figure 2.20 shows. The frequency at the output signal is generally equal to that of the sawtooth signal and the duty cycle is a function of the modulating signal.

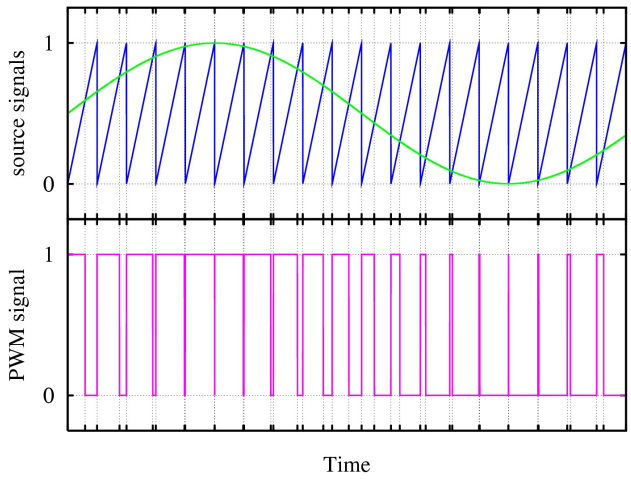


Figure 2.20: PWM modulation.

The space vector modulation SVM should be also mentioned, because it is an algorithm for the control of PWM [62]. There are various variations of SVM that result in different quality and computational requirements. One active area of development is in the reduction of total harmonic distortion (THD) created by the rapid switching inherent to these algorithms. How-

ever, SVM has not been studied in depth in this thesis.

### 2.4.2 System modelling

Thanks to PWM technique, and applying the well known Park's transformation (see [55, 63]), it is possible to obtain an averaged dynamic model from the system shown in figure 2.19 in the $dq$ frame, which is shown in figure 2.21. All devices are in the primary side of the transformer, where $n$ is the transformer ratio. This way of proceeding is standard, as for example is developed in [64].

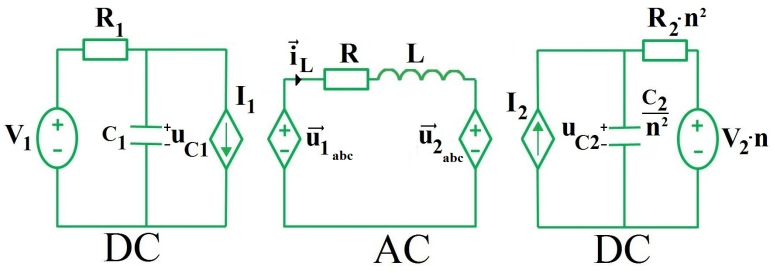


Figure 2.21: Three phases DAB average model.

The converter can then be modelled as in figure 2.21, where:

$$u_{1a} = u_{C1} \cdot m_1 cos \cdot (\omega t + \delta) \tag{2.47}$$

$$u_{2a} = u_{C2} \cdot m_2 cos \cdot (\omega t) \tag{2.48}$$

with $0 < m_1 < 1$, $0 < m_2 < 1$ and $\delta$ is the phase for AC left side. So using the $dq$ transformation, we obtain that:

$$\begin{cases} u_{1d} = \sqrt{\frac{3}{2}} u_{C1} m_{1d} & -1 < m_{1d} = m_1 cos(\delta) < 1 \\ u_{1q} = -\sqrt{\frac{3}{2}} u_{C1} m_{1q} & -1 < m_{1q} = m_1 sin(\delta) < 1 \\ u_{2d} = \sqrt{\frac{3}{2}} u_{C1} m_{2d} & 0 < m_{2d} = m_2 < 1 \\ u_{2q} = 0 \end{cases} \tag{2.49}$$

where $u_{1d}$ and $u_{1q}$, are the $dq$ voltage components of the three phases voltage system $u_{1a}, u_{1b}$, and $u_{1c}$ (AC left side), and the same for $u_{2d}$ and $u_{2q}$ (AC right side).

It should be noted that $u_{2q} = 0$, and this is due to our choice of the voltage phase in the right side of the converter was equal to zero. This is in concordance with the real behaviour of the system, because when we work in $dq$ frame, a phase lock loop (PLL) is necessary in order to generate a signal whose phase is related to the phase of an input signal (see [65]). Usually in electronic devices this technique is used to detect the frequency of the voltage and current and to detect the phase between them. So a voltage

reference is needed, and if we select voltage $u_2$ as reference, its phase is zero, and consequently $m_{2q} = 0$, and therefore $u_{2q} = 0$.

On the other hand, and taking into account the power equalities shown in equations (2.50) and (2.51):

$$u_{C1} I_1 = u_{1a} i_{La} + u_{1b} i_{Lb} + u_{1c} i_{Lc} \tag{2.50}$$

$$u_{C2} I_2 = u_{2a} i_{La} + u_{2b} i_{Lb} + u_{2c} i_{2c} \tag{2.51}$$

and carry out the Park's transformation we obtain that:

$$I_1 = \sqrt{\frac{3}{2}} \left( m_{1d} i_{Ld} + m_{1q} i_{Lq} \right) \tag{2.52}$$

$$I_2 = \sqrt{\frac{3}{2}} m_{2d} i_{Ld} \tag{2.53}$$

The system shown in figure 2.21 can then be described by:

$$\begin{cases} \frac{d}{dt} i_{Ld} = \frac{1}{L} \left( -R \cdot i_{Ld} + \omega \cdot L \cdot i_{Lq} + \sqrt{\frac{3}{2}} \left( m_{1d} \cdot u_{c1} - m_{2d} \cdot u_{c2} \right) \right) \\ \frac{d}{dt} i_{Lq} = \frac{1}{L} \left( -\omega \cdot L \cdot i_{Ld} - R \cdot i_{Lq} + \sqrt{\frac{3}{2}} m_{1q} \cdot u_{c1} \right) \\ \frac{d}{dt} u_{C1} = -\frac{1}{C_1} \left( \sqrt{\frac{3}{2}} \left( m_{1d} \cdot i_{Ld} + m_{1q} \cdot i_{Lq} \right) - \frac{V_1 - u_{C1}}{R_1} \right) \\ \frac{d}{dt} u_{C2} = \frac{n^2}{C_2} \left( \sqrt{\frac{3}{2}} m_{2d} i_{Ld} - \frac{u_{C2} - V_2 \cdot n}{R_2 \cdot n^2} \right) \end{cases} \tag{2.54}$$

where $i_{Ld}, i_{Lq}, u_{C1}, u_{C2}$ are the state variables, $m_{1d}, m_{2d}, m_{1q}$ are the control variables and $V_1, V_2$ are external variables.

The systems equations shown in (2.54) may be represented by:

$$\frac{d}{dt}\mathbf{x} = \mathbf{A}\mathbf{x} + \sum_{i=1}^{5} u_i \mathbf{B}_i \ \mathbf{x} + \mathbf{C}\mathbf{u} \tag{2.55}$$

where:

$$\mathbf{A} = \begin{bmatrix} -\frac{R}{L} & \omega & 0 & 0 \\ -\omega & -\frac{R}{L} & 0 & 0 \\ 0 & 0 & -\frac{1}{R_1 C_1} & 0 \\ 0 & 0 & 0 & -\frac{1}{R_2 C_2} \end{bmatrix}; \quad \mathbf{B}_1 = \sqrt{\frac{3}{2}} \begin{bmatrix} 0 & 0 & \frac{1}{L} & 0 \\ 0 & 0 & 0 & 0 \\ -\frac{1}{C_1} & 0 & 0 & 0 \\ 0 & 0 & 0 & 0 \end{bmatrix}$$

$$\mathbf{B}_2 = \sqrt{\frac{3}{2}} \begin{bmatrix} 0 & 0 & 0 & -\frac{1}{L} \\ 0 & 0 & 0 & 0 \\ 0 & 0 & 0 & 0 \\ \frac{n^2}{C_2} & 0 & 0 & 0 \end{bmatrix}; \quad \mathbf{B}_3 = \sqrt{\frac{3}{2}} \begin{bmatrix} 0 & 0 & 0 & 0 \\ 0 & 0 & \frac{1}{L} & 0 \\ 0 & -\frac{1}{C_1} & 0 & 0 \\ 0 & 0 & 0 & 0 \end{bmatrix}$$

$$\mathbf{B}_4 = \mathbf{B}_5 = \mathbf{0}$$

$$\mathbf{C} = \begin{bmatrix} 0 & 0 & 0 & 0 & 0 \\ 0 & 0 & 0 & 0 & 0 \\ 0 & 0 & 0 & \frac{1}{R_1 C_1} & 0 \\ 0 & 0 & 0 & 0 & \frac{n}{R_2 C_2} \end{bmatrix} \quad \mathbf{x} = \begin{bmatrix} i_{Ld} \\ i_{Lq} \\ u_{C1} \\ u_{C2} \end{bmatrix} \quad \mathbf{u} = \begin{bmatrix} m_{1d} \\ m_{2d} \\ m_{1q} \\ V_1 \\ V_2 \end{bmatrix}$$

Whatever the control objective, the average model of DC/DC converters via PWM have a structure of bilinear system. A system is called bilinear if it is described by linear differential equations in which the control inputs appear as coefficients. The study of bilinear systems began in the 60's as a gateway between the linear and nonlinear systems. A large amount of definitions and properties have been formulated until our days with respect to bilinear systems and their control, see: [41, 42, 43, 44, 66]. However there are not yet general results to study their stability and controllability as in the case of linear systems. There exists only global proofs in the case of $2^{nd}$ order bilinear systems (see [67, 68, 69, 70]). Due to this fact, it is very usual to treat bilinear systems as nonlinear systems and apply all the results of nonlinear control, since the theory of nonlinear control has global results on stability and controllability (see [45, 38]). In this section, both a bilinear controller and a nonlinear controller based on Lyapunov theory are designed and compared.

Two different control strategies are addressed in this section in order to achieve the overall control of the DC/DC converter: a bilinear systems' control based on *quadratic feedback control*, and a non-linear control based in Lyapunov theory. System's controllability and stability are studied, in particular by the analysis of *zero dynamics*, which corresponds to the dynamics describing the internal behaviour of the system when input and initial condition are chosen to achieve zero (or even constant manifold) output [45].

### 2.4.3 Control objective.

As shown in system equations (2.54), we have three variables on which we may act $(m_{1d}, m_{1q}, m_{2d})$ and four state variables, in principle we may only control three of these state variables, leaving a free behaviour in the other state variable. The control objective is then to assure that each state variable which could be controlled tracks its reference.

#### Under-actuation.

Since we may only arbitrarily control at most three state variables, we will now study whether these input variables we may control these three states. Controllability of general bilinear systems is still an open problem, there exist sufficient conditions for planar bilinear systems (scalar control) (see [67] [69]), but unfortunately there exits only partial criteria to assure con-

trollability of the systems for the case $n \geq 3$ (see [68]). Necessary conditions for bilinear controllability systems are shown in [42].

In our case the system is not fully actuated, so we can separate it into two parts, one actuated and one non-actuated. This separation will help us to study the controllability of the actuated part.

$$\dot{\mathbf{x}} = \begin{bmatrix} \dot{\mathbf{x}}_a \\ \dot{\mathbf{x}}_{na} \end{bmatrix} = \begin{bmatrix} \mathbf{A}_a & \mathbf{A}_{12} \\ \mathbf{A}_{21} & \mathbf{A}_{na} \end{bmatrix} \cdot \begin{bmatrix} \mathbf{x}_a \\ \mathbf{x}_{na} \end{bmatrix} + \left( \sum_{i=1}^{5} u_i \begin{bmatrix} \mathbf{B}_{i_a} & \mathbf{B}_{i_{12}} \\ \mathbf{B}_{i_{21}} & \mathbf{B}_{i_{na}} \end{bmatrix} \right) \begin{bmatrix} \mathbf{x}_a \\ \mathbf{x}_{na} \end{bmatrix} + \begin{bmatrix} \mathbf{C}_a \\ \mathbf{C}_{na} \end{bmatrix} \mathbf{u} \tag{2.56}$$

where $\mathbf{x}_a$ denotes the actuated states, $\mathbf{x}_{na}$ denotes the non-actuated state, $\mathbf{A}_a$ denotes the actuated part of matrix $\mathbf{A}$, $\mathbf{A}_{na}$ denotes the non-actuated part of $\mathbf{A}$ and the same reasoning for $\mathbf{B}$ and $\mathbf{C}$ .

Three variables $(m_{1d}, m_{1q}, m_{2d})$ are used for controlling three state variables, leaving the last free. The reasoning of the choice of the control variables is the following: since $i_{Lq}$ is closely linked with the reactive power consumed by the inductance in the AC step of the converter, and since this power decreases the transmitted active power, it is clearly a variable whose control is important and whose reference in most cases will be to make it as small as possible or even zero. Between the three state variables that remains ($i_{Ld}, u_{C1}$ and $u_{C2}$), we will always chose a voltage as variable to control in order to guarantee the voltage stability of the converter. As we have chosen $u_{C2}$ as phase reference for PLL, we will chose this variable as control objective, remaining the other two variables to pick one in order to complete the set. We will present results with both control objectives, that means, either we control the trio $(i_{Ld}, i_{Lq}, u_{C2}.)$ or the trio $(i_{Lq}, u_{C1}, u_{C2})$. In both cases we can easily verify the necessary conditions explained above (see [42]) for bilinear controllability systems.

### 2.4.4 Bilinear system stability and control law.

Bilinear systems' stability has been studied extensively over the past decades (see [42]). In [70] the stability of second order bilinear systems under certain conditions is proven. In [43] a *quadratic feedback control* $\mathbf{u(x)}$:

$$u_i = -\alpha[\mathbf{B}_i\mathbf{x} + \mathbf{c}_i]^T\mathbf{P}\mathbf{x} \tag{2.57}$$

with $i = 1, \cdots, m$ stabilizes the system presented in (2.54) in the origin, by means of the quadratic Lyapunov function, $\mathcal{V} = \mathbf{x}^T\mathbf{P}\mathbf{x}$. Where $\mathbf{P}$ is positive definite and $\alpha > 0$.

Indeed, if we derive the Lyapunov function, we obtain:

$$\dot{\mathcal{V}} = \mathbf{x}^T[\mathbf{P}\mathbf{A} + \mathbf{A}^T\mathbf{P}]\mathbf{x} - 2\alpha \sum_{i=1}^{m} \left[\mathbf{x}^T\mathbf{P}(\mathbf{B}_i\mathbf{x} + \mathbf{c}_i)\right]^2 \tag{2.58}$$

where it is assumed that:

$$\begin{bmatrix} (\mathbf{B}_1\mathbf{x}+\mathbf{c}_1)^T\mathbf{P}\mathbf{x} \\ \vdots \\ (\mathbf{B}_m\mathbf{x}+\mathbf{c}_m)^T\mathbf{P}\mathbf{x} \end{bmatrix} \neq \mathbf{0} \tag{2.59}$$

$\forall \mathbf{x}$ such that $\mathbf{x} \neq \mathbf{0}$ and $\mathbf{x}(\mathbf{P}\mathbf{A}+\mathbf{A}^T\mathbf{P})\mathbf{x} \leq 0$ in order to guarantee $\dot{V} \leq 0$.

Since our system is not fully actuated, and we have separated it in two parts, we may apply the control strategy presented in 2.4.4 to the controllable part. Applying the *quadratic feedback control* explained above we will only act over $i_{Lq}, u_{C1}$ and $u_{C2}$. Consequently, $\mathbf{x}_a = [i_{Lq}, u_{C1}, u_{C2}]$.

If $\bar{\mathbf{x}}_a$ is an equilibrium state of the controlled variables corresponding to an input $\bar{\mathbf{u}}$, making the change of variables $\mathbf{x}_a = \bar{\mathbf{x}}_a + \tilde{\mathbf{x}}_a$, and $\mathbf{u} = \bar{\mathbf{u}} + \tilde{\mathbf{u}}$, in order to achieve that the state variables track their references, and taking into consideration that $B(u,x) = (\sum_{i=1}^{m} u_i \mathbf{B}_i)\,\mathbf{x} = (\sum_{i=1}^{n} x_i \mathbf{H}_i)\,\mathbf{u}$, with a suited $H_i \in \mathbb{R}^{n\times m}$, we obtain that:

$$B(\mathbf{u},\mathbf{x}_a) = B(\bar{\mathbf{u}}+\tilde{\mathbf{u}}, \bar{\mathbf{x}}_a+\tilde{\mathbf{x}}_a) = B(\bar{\mathbf{u}},\bar{\mathbf{x}}_a) + B(\bar{\mathbf{u}},\tilde{\mathbf{x}}_a) + B(\tilde{\mathbf{u}},\bar{\mathbf{x}}_a) + B(\tilde{\mathbf{u}},\tilde{\mathbf{x}}_a) \tag{2.60}$$

and consequently from (2.56):

$$\dot{\tilde{\mathbf{x}}}_a = \tilde{\mathbf{A}}_a \cdot \tilde{\mathbf{x}}_a + B(\tilde{\mathbf{u}},\tilde{\mathbf{x}}_a) + B_{na}(\tilde{\mathbf{u}},\mathbf{x}_{na}) + \tilde{\mathbf{C}}_a \cdot \bar{\mathbf{u}} \tag{2.61}$$

where $B(\tilde{\mathbf{u}},\tilde{\mathbf{x}}_a)$ and $B_{na}(\tilde{\mathbf{u}},\mathbf{x}_{na}) \in \mathbb{R}^5 \to \mathbb{R}^3$ and:

$$\tilde{\mathbf{A}}_a = \left[\mathbf{A}_a + \sum_{i=1}^{m} \bar{u}_i \mathbf{B}_{ai}\right] \qquad \tilde{\mathbf{C}}_a = \left[\mathbf{C}_a + \sum_{i=1}^{n} x_{ai}\mathbf{H}_{ai}\right]. \tag{2.62}$$

Proceeding in analogous form showed above, we are going to prove that the following control (2.63) stabilizes the system (2.61) in the desired point given by the references, by means of the quadratic Lyapunov function, $\tilde{\mathcal{V}} = \tilde{\mathbf{x}}^T\tilde{\mathbf{P}}\tilde{\mathbf{x}}$.

$$\tilde{u}_i = -\alpha[\mathbf{B}_{ai}\tilde{\mathbf{x}}_a + \tilde{\mathbf{c}}_{ai} + \mathbf{b}_{nai}\mathbf{x}_{na}]^T\tilde{\mathbf{P}}\tilde{\mathbf{x}}_a \tag{2.63}$$

with $i = 1, \cdots, 3$ where $\tilde{\mathbf{c}}_{ai}$ are the columns of the matrix $\tilde{\mathbf{C}}_a$, $\mathbf{b}_{nai}$ are the columns of matrix $\mathbf{B}_{na}$, and $\tilde{\mathbf{P}}$ is a positive definite symmetric matrix of appropriate dimension (in this case the identity matrix of order 3).

***Theorem 2*** *The converter described by (2.54), with arbitrary initial conditions, under control law shown in (2.63), will exponentially tracks its references.*

***Proof.-***

System (2.61) can be rewritten as:

$$\dot{\tilde{\mathbf{x}}}_a = \tilde{\mathbf{A}}_a \cdot \tilde{\mathbf{x}_a} + \sum_{i=1}^{m} (\tilde{u}_i[\mathbf{B}_{ai}\tilde{\mathbf{x}}_a + \tilde{\mathbf{c}}_{ai} + \mathbf{b}_{nai}\mathbf{x}_{na}]) \tag{2.64}$$

and taking into account that given two column vectors $a$ and $b$, it is true that $a^T\tilde{P}b = b^T\tilde{P}a$ because $\tilde{P}$ is symmetric. Applying this property:

$$\dot{\tilde{\mathcal{V}}} = \tilde{\mathbf{x}}_a^T[\tilde{\mathbf{P}}\tilde{\mathbf{A}}_a + \tilde{\mathbf{A}}_a^T\tilde{\mathbf{P}}]\tilde{\mathbf{x}}_a - 2\alpha\sum_{i=1}^{m}\left[\tilde{\mathbf{x}}_a^T\tilde{\mathbf{P}}(\mathbf{B}_{ai}\tilde{\mathbf{x}}_a + \tilde{\mathbf{c}}_{ai} + \mathbf{b}_{nai}\mathbf{x}_{na})\right]^2 \quad (2.65)$$

and $\tilde{\mathbf{A}}_a$ in our case has the following form if we control the trio $i_{Ld}, i_{Lq}, u_{C2}$

$$\tilde{\mathbf{A}}_a = \begin{bmatrix} -\frac{R}{L} & \omega & -\frac{\bar{u}_2\sqrt{3}}{L\sqrt{2}} \\ -\omega & -\frac{1}{R_1C_1} & 0 \\ \frac{n^2\bar{u}_2\sqrt{3}}{C_2\sqrt{2}} & 0 & -\frac{1}{R_2C_2} \end{bmatrix} \quad (2.66)$$

which is Hurwitz $\forall\ \bar{u}_2 \in \mathbb{R}$. Or if we control the trio $i_{Lq}, u_{C1}, u_{C2}$ then $\tilde{\mathbf{A}}_a$ has the form:

$$\tilde{\mathbf{A}}_a = \begin{bmatrix} -\frac{R}{L} & \frac{\bar{u}_3\sqrt{3}}{L\sqrt{2}} & 0 \\ -\frac{\bar{u}_3\sqrt{3}}{C_1\sqrt{2}} & -\frac{1}{R_1C_1} & 0 \\ 0 & 0 & -\frac{1}{R_2C_2} \end{bmatrix} \quad (2.67)$$

which is Hurwitz $\forall\ \bar{u}_3 \in \mathbb{R}$. So the Lyapunov function $\dot{\tilde{\mathcal{V}}} < \lambda\tilde{\mathcal{V}}$, with $\lambda$ a positive constant, and consequently the control law shown in (2.63) stabilizes exponentially the system. (Note that for the other combinations of actuated variables its corresponding $\tilde{\mathbf{A}}_a$ are always Hurwitz).

Now remains to study what happens with the non-actuated variable. But in our case, due to it being a first order differential equation with a constant negative value in the coefficient of the state variable, and as we have controlled the remaining states, this free variable is also exponentially stable. □

### 2.4.5 Nonlinear system stability and control law.

As discussed above, bilinear systems are a class of nonlinear systems, but bilinear systems paradoxically have not global stability specified results. Therefore, they are commonly dealt with non-linear control techniques. In this section we will use Lyapunov theory to develop another controller to our system.

If we take a glance on system (2.54), we observe that the variable $i_{Lq}$ may be controlled through the control variable $m_{1q}$. Something similar happens with the variable $u_{C2}$, which may be controlled by $m_{2d}$. So it is clear that both variables can be controlled independently. With respect to the other variables, $i_{Ld}$ and $u_{C1}$, the same reasoning explained in 2.4.3 is valid, that means, we may only control one of them, and the other has a free behavior. In the section above we have shown a control for the trio $i_{Lq}, u_{C1}$ and $u_{C2}$. The present section will develop a controller for the trio $i_{Ld}, i_{Lq}$ and $u_{C2}$,

although one could have chosen the other trio. Let's start with the following equation:

$$\frac{d}{dt}i_{Lq} = -\omega \cdot i_{Ld} - \frac{R}{L} \cdot i_{Lq} + \frac{m_{1q}\sqrt{3}}{L\sqrt{2}} \cdot u_{c1} \tag{2.68}$$

Considering the following tracking error:

$$\tilde{i}_{Lq} = i_{Lq} - \bar{i}_{Lq} \tag{2.69}$$

with the associated Lyapunov function:

$$\mathcal{V}_{i_{Lq}} = \frac{1}{2}\left(i_{Lq} - \bar{i}_{Lq}\right)^2 \tag{2.70}$$

Its time derivate is:

$$\dot{\mathcal{V}}_{i_{Lq}} = \tilde{i}_{Lq} \cdot \left(-\omega \cdot i_{Ld} - \frac{R}{L} \cdot i_{Lq} + \frac{m_{1q}\sqrt{3}}{L\sqrt{2}} \cdot u_{c1} - \dot{\bar{i}}_{Lq}\right) \tag{2.71}$$

in order to achieve negative derivative of the Lyapunov function:

$$-\omega \cdot i_{Ld} - \frac{R}{L} \cdot i_{Lq} + \frac{m_{1q}\sqrt{3}}{L\sqrt{2}} \cdot u_{c1} - \dot{\bar{i}}_{Lq} = -\alpha_1 \cdot \tilde{i}_{Lq} \tag{2.72}$$

with $\alpha_1$ a positive constant. Therefore, the time derivative becomes:

$$\dot{\mathcal{V}}_{i_{Lq}} = -\alpha_1 \cdot \tilde{i}_{Lq}^2 \tag{2.73}$$

which applying the Lyapunov theory one can guarantee its exponential stability.

The control law for this variable becomes:

$$m_{1q} = \frac{L\sqrt{2}}{u_{C1}\sqrt{3}}\left(\omega \cdot i_{Ld} + \frac{R}{L} \cdot i_{Lq} + \dot{\bar{i}}_{Lq} - \alpha_1 \cdot \tilde{i}_{Lq}\right) \tag{2.74}$$

If we apply the same reasoning to the equation[1]:

$$\frac{d}{dt}u_{c2} = \frac{n^2}{C_2}\left(\sqrt{\frac{3}{2}}m_{2d} \cdot i_{Ld} - \frac{u_{C2} - V_2 \cdot n}{n^2 R_2}\right) \tag{2.75}$$

and considering the following tracking error,

$$\tilde{u}_{C2} = u_{C2} - \bar{u}_{C2} \tag{2.76}$$

with the associated Lyapunov function:

$$\mathcal{V}_{u_{C2}} = \frac{1}{2}\left(u_{C2} - \bar{u}_{C2}\right)^2 \tag{2.77}$$

[1]In the following it is important to remark that in practice the three states can never remain equal to zero, and therefore we are only considering the case of states limited into an operation region.

we obtain the following control law which guaranteed the stability of the variable $u_{C2}$, where $\alpha_2$ is a positive constant:

$$m_{2d} = \frac{C_2\sqrt{2}}{n^2 \cdot i_{Ld}\sqrt{3}} \left( \frac{u_{C2} - V_2 \cdot n}{R_2 C_2} - \dot{\bar{u}}_{C2} - \alpha_2 \tilde{u}_{C2} \right) \tag{2.78}$$

At this point, considering that $m_{1d}$ is the only variable that remains to be defined, we will use it to stabilize $i_{Ld}$ proceeding in analogous form to the following equation:

$$\frac{d}{dt} i_{Ld} = -\frac{R}{L} \cdot i_{Ld} + \omega \cdot i_{Lq} + \frac{m_{1d}\sqrt{3}}{L\sqrt{2}} \cdot u_{c1} - \frac{m_{2d}\sqrt{3}}{L\sqrt{2}} \cdot u_{c2} \tag{2.79}$$

and considering the following tracking error,

$$\tilde{i}_{Ld} = i_{Ld} - \bar{i}_{Ld} \tag{2.80}$$

with the associated Lyapunov function:

$$\mathcal{V}_{i_{Ld}} = \frac{1}{2} \left( i_{Ld} - \bar{i}_{Ld} \right)^2 \tag{2.81}$$

we obtain the following control law which guaranteed the stability of the variable $i_{Ld}$, where $\alpha_3$ is a positive constant:

$$m_{1d} = \frac{L\sqrt{2}}{u_{C1}\sqrt{3}} \left( \frac{R}{L} i_{Ld} - \omega \cdot i_{Lq} + \frac{m_{2d}\sqrt{3}}{L\sqrt{2}} u_{C2} + \dot{\bar{i}}_{Ld} - \alpha_3 \tilde{i}_{Ld} \right) \tag{2.82}$$

Now we will study the behavior of the free state in order to verify if and where it converges. To carry out this task, we will apply the well known theory of zero dynamics (see [45] and [71]). To analyze it, we first divide the state variables (considering the error variables) in two parts:

$$\begin{aligned} \eta &= u_{C1} \\ \xi &= [\tilde{i}_{Ld}, \tilde{i}_{Lq}, \tilde{u}_{C2}]^t \end{aligned} \tag{2.83}$$

So the whole system may be considered as in the normal form:

$$\begin{aligned} \dot{\eta} &= f_1(\eta, \xi, u) \\ \dot{\xi} &= f_2(\eta, \xi, u) \end{aligned} \tag{2.84}$$

with

$$u = f_3(\eta, \xi) \tag{2.85}$$

given the equations (2.74), (2.78) and (2.82).

So given $u$ such that $\xi \to \bar{\xi}$ ($\bar{\xi}$ could be zero or not) then the behaviour of the system (2.84) is governed by the differential equation:

$$\dot{\eta} = f_1(\eta, \bar{\xi}, \bar{u}) \tag{2.86}$$

If we apply this result to system (2.54), the behavior of the free variable $u_{C1} = \eta$ could be written as:

$$\dot{u}_{C1} = \frac{k_1}{u_{C1}} + k_2 \cdot u_{C1} + k_3 \tag{2.87}$$

where,

$$k_1 = -\frac{1}{C_1}\left(R\left(\bar{i}_{Ld}^2 + \bar{i}_{Lq}^2\right) + \frac{1}{n^2}\left(\frac{\bar{u}_{C2} - V_2 \cdot n}{R_2}\right)\bar{u}_{C2}\right) \tag{2.88}$$

$$k_2 = -\frac{1}{C_1 R_1} \tag{2.89}$$

$$k_3 = \frac{V_1}{C_1 R_1} \tag{2.90}$$

If we study the behaviour of equation (2.87), calling:

$$f(u_{C1}) = \frac{k_1}{u_{C1}} + k_2 \cdot u_{C1} + k_3 \tag{2.91}$$

and taking into account that in steady state by energy balance it is always true that:

$$\frac{\bar{u}_{C1} - V_1}{R_1}\bar{u}_{C1} = R\left(\bar{i}_{Ld}^2 + \bar{i}_{Lq}^2\right) + \frac{1}{n^2}\left(\frac{\bar{u}_{C2} - V_2 \cdot n}{R_2}\right)\bar{u}_{C2} \tag{2.92}$$

then the derivate of $f$ is always negative and consequently equation (2.87) is exponentially stable, thereforethe whole system is stabilized by the control law $u = f_3(\eta, \xi)$ given by equations (2.74), (2.78) and (2.82). We could obtain an analogous result, if we had chosen $u_{C1}$ instead of $i_{Ld}$ proceeding in a similar form.

***Theorem* 3** *The converter described by (2.54) under control laws (2.74), (2.78) and (2.82) (with $\alpha_1$, $\alpha_2$ and $\alpha_3$ positive constants) is exponentially stabilized to an equilibrium point given by its references.*

***Proof.-***

The proof of theorem 2 is composed by the steps of the current subsection. □

### 2.4.6 Simulations for the three phases DAB.

The controllers studied in the previous sections are tested in MATLAB-SIMULINK®.

Table 2.11: Simulation values.

| | | |
|---|---|---|
| n | Transformer ratio | 11/100 |
| $R_{total-i}$ | Total resistance branch $i$ | 0.022 Ω |
| $R_1$ | Resistance source 1 | 0.001 Ω |
| $R_2$ | Resistance source 2 | 0.1 Ω |
| $V_1$ | Input voltage | 1000 V |
| $V_2$ | Output voltage | 10000 V |
| $L_i$ | Inductance branch $i$ | 0.01 H |
| $C_1$ | Input capacitor | 1 mF |
| $C_2$ | Output capacitor | 20 $\mu$ F |
| $f$ | Switching frequency | 1000 Hz |

**Bilinear control simulations.**

In this section it is shown the simulations of control for the trio $i_{Lq}, u_{C1}$ and $u_{C2}$. The parameter values of the simulated example are presented in table 2.11.

In figure 2.22 the behaviour of $i_{Lq}$ is shown. We observe as the variable tracks its references (100 A until 0.4 $s$ and 85 A for the rest) satisfactorily.

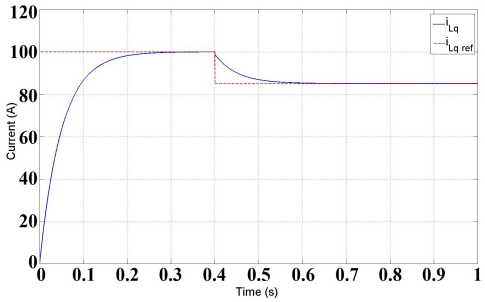


Figure 2.22: $i_{Lq}$ behavior (bilinear control).

In figure 2.23 the behaviour of $u_{C1}$ and $u_{C2}$ are shown. We observe as the $u_{C1}$ tracks its reference (990 V until 0.5 $s$ and 980 V for the rest) in an appropriate way, where the voltage has a small oscillation band, caused by the size of the capacitors. For $u_{C2}$, we observe as the variable tracks its references (10015 V until 0.8 $s$ and 10005 V for the remaining) satisfactorily. Observing figure 2.23 it is clear that the power direction flows from left side to right side of the converter, therefore $i_{Ld}$, the free variable, must be positive. This is in according with the simulations shows in figure 2.24

**Non-linear control simulations.**

In this section it is shown the simulations for the control of the trio $i_{Ld}, i_{Lq}$ and $u_{C2}$, leaving $u_{C1}$ as free variable. The parameter values are the same

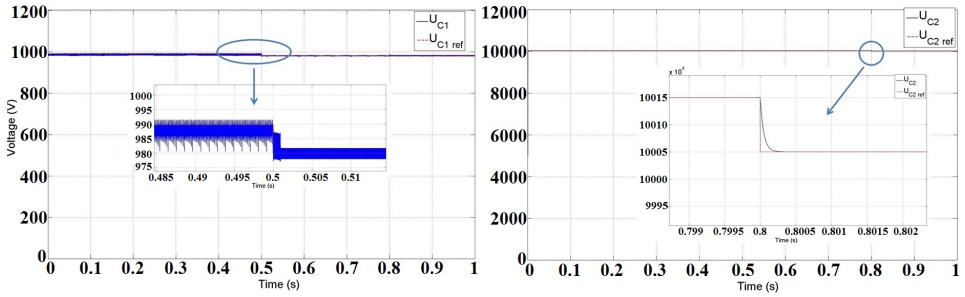


Figure 2.23: a) $u_{C1}$ b) $u_{C2}$ behavior (bilinear control).

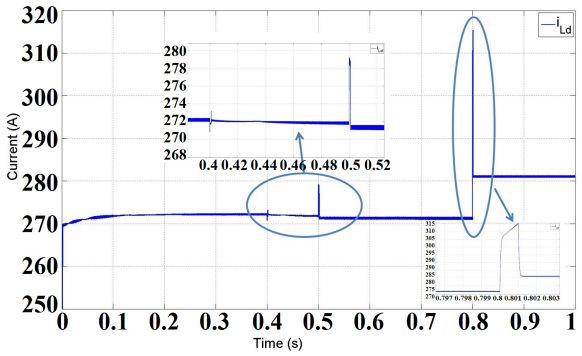


Figure 2.24: $i_{Ld}$ behavior (bilinear control).

as above (see table 2.11).

In figure 2.25 the behavior of $i_{Ld}$ and $i_{Lq}$ are shown. We observe as in figure 2.25a the variable tracks its references satisfactorily (-200 A until 0.8 $s$ and -250 A for the remaining). In figure 2.25b the variable tracks its references satisfactorily (-15 A until 1.2 $s$ and -45 A for the rest).

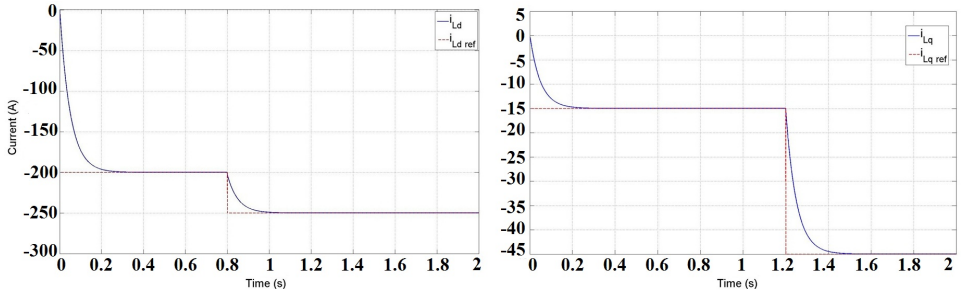


Figure 2.25: a) $i_{Ld}$ b) $i_{Lq}$ behaviour (nonlinear control).

In figure 2.26b the behavior of $u_{C2}$ is shown. We observe as the variable tracks its references (9990 V until 1.6 $s$ and 9995 V for the remaining) satisfactorily. We observe that due to the current has negative value and

the voltage in capacitor $C_2$ is less than $V_2$= 10000 V, the power direction flows from right side to left side of the converter. Therefore, $u_{C1}$ (figure 2.26a), the free variable, must be greater than $V_1$=1000 V. We can check it showing figure 2.26a.

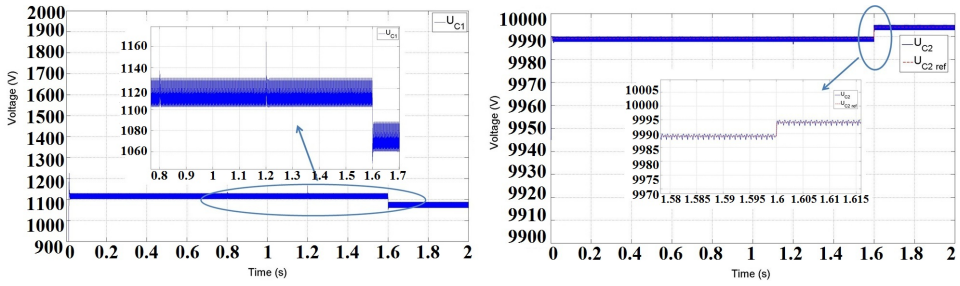


Figure 2.26: a) $u_{C1}$ b) $u_{C2}$ behavior (nonlinear control).

## 2.5 DC/DC converter with MMC technology.

This section presents the modelling and control of a DC/DC bidirectional converter with $n$ terminals suitable for high voltage and power applications in MT-HVDC. The proposed converter topology is based on Modular Multilevel Converter (MMC). Furthermore, a model based controller is designed and a mathematical proof is given in order to guarantee the global stability of the non-linear system by means of switching control theory. In addition, a study on how to improve the generated harmonics is shown.

One line of research for the DC/DC bidirectional converters for MT-HVDC was discussed in sections 2.2 and 2.4, which are based on the topology DAB. Nevertheless, and although it has optimal performances and advantages over other topologies, particularly alongside Series Resonant Converter (SRC) and Dual half Bridge (DHB), the main drawback is that it uses an internal transformer at high frequency [21, 22], which increases significantly the cost of this device. Other authors suggest to link two MMC by the alternative side in order to connect two networks with different DC voltages, as proposed [23]. This structure provides the advantage that the internal transformer is avoided, and consequently the costs are decreased, and also it offers all the advantages given by the use of MMC technology explained above.

The main idea proposed in this section is to implement a DC/DC bidirectional converter which operates with several terminals (a number of DC networks, in general $n$) using MMC converters (with $k$ phases) as shows figure 2.27. Consequently the DC/DC converter explain here could address the fucntion of the *hub* (or common connection point) which carries out the union between several grids with different voltages[72, 73, 74].

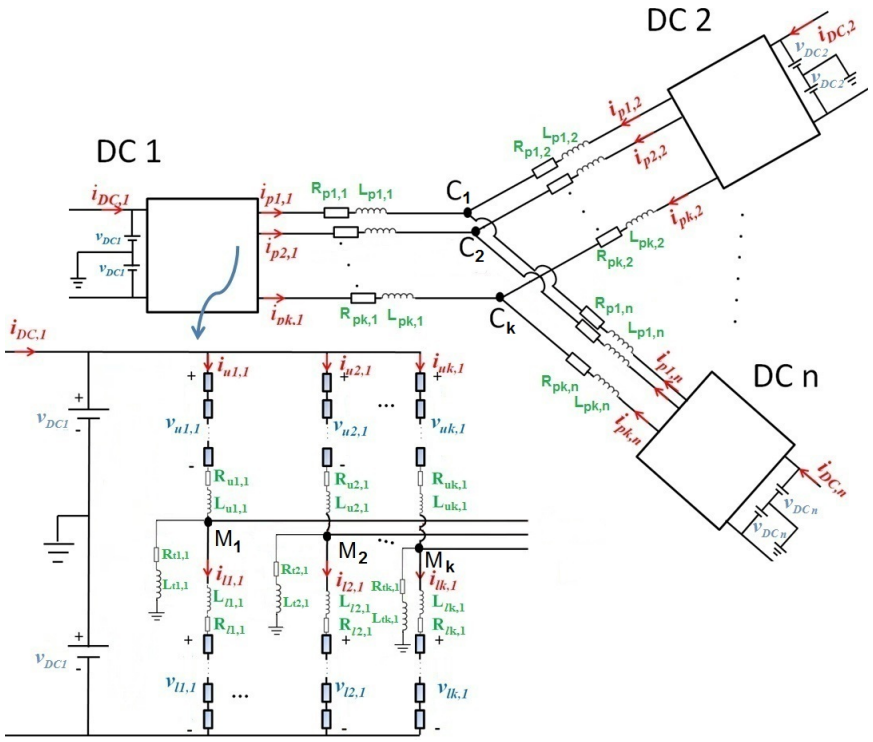


Figure 2.27: Multi DC/DC converter with $k$ phases based on MMC.

### 2.5.1 System modelling.

A single phase structure of the MMC is shown in figure 2.28. Each phase is divided in two arms, the upper and the lower. Each arm is composed by $N$ sub-modules (hundreds in HVDC applications) which usually could have two different forms (see [23]): the half bridge, constituted by two switches (IGBT and diode), or the full bridge, formed by four switches as figure 2.28 shows. The use of full bridges is specially interesting when a fault appears, because controlling them, we can impose the appropriate polarity of voltage during fault events in order to block the fault current [75] (see section 2.6.3). However, for the purpose of this explanation is sufficient to consider half bridges. On the other hand, it is important to point out that it is necessary an inductance in the arm, $L_{u,l}$, in order to compensate the voltages imbalances between the upper and lower arms and the DC voltage. Finally, $R_t$ and $L_t$ are the resistances and inductances respectively, which links the arms with the earth, as figure 2.28 shows, see [75].

#### Sub-module Operation.

According to [76, 77], the semiconductors of each sub-module (half bridge) show in figure 2.28 can be switched in three different ways:

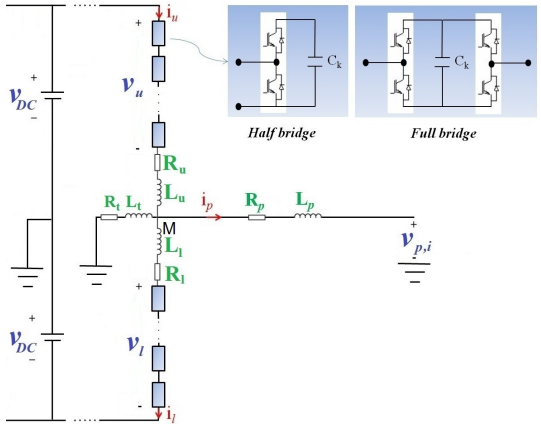


Figure 2.28: A single phase structure of the MMC.

a) *Inserted*: $S_1$ is *off* and $S_2$ is *on*, then the capacitor is charged or discharged according to the current direction.

b) *By-passed*: $S_1$ *on* and $S_2$ *off*, then the capacitor voltage remains constant.

c) *Bloqued*: $S_1$ and $S_2$ *off*, then the capacitor may charge through the diode of $S_2$, but it cannot discharge.

In this thesis we only consider the states *inserted* and *by-passed*.

**DC/DC multi-terminal converter model based on MMC. System modelling.**

In figure 2.27 a DC/DC converter with $n$ terminals and $k$ phases based on MMC is shown. With the aim of building its model, we will start writing the system equations. Regarding figure 2.27, it is true that:

$$\begin{cases} V_{DC1} = R_{u1,1}\cdot i_{u1,1} + L_{u1,1}\cdot \dot{i}_{u1,1} + v_{u1,1} + R_{t1,1}\cdot i_{t1,1} + L_{t1,1}\cdot \dot{i}_{t1,1} \\ V_{DC1} = R_{l1,1}\cdot i_{l1,1} + L_{l1,1}\cdot \dot{i}_{l1,1} + v_{l1,1} - R_{t1,1}\cdot i_{t1,1} - L_{t1,1}\cdot \dot{i}_{t1,1} \\ \vdots \\ V_{DC1} = R_{lk,1}\cdot i_{lk,1} + L_{lk,1}\cdot \dot{i}_{lk,1} + v_{lk,1} - R_{tk,1}\cdot i_{tk,1} - L_{tk,1}\cdot \dot{i}_{tk,1} \\ \vdots \\ V_{DCn} = R_{lk,n}\cdot i_{lk,n} + L_{lk,n}\cdot \dot{i}_{lk,n} + v_{lk,n} - R_{tk,n}\cdot i_{tk,n} - L_{tk,n}\cdot \dot{i}_{tk,n} \end{cases} \tag{2.93}$$

Also we can achieve, that:

$$\begin{cases} R_{t1,1}\cdot i_{t1,1} + L_{t1,1}\cdot \dot{i}_{t1,1} = R_{p1,1}\cdot i_{p1,1} + L_{p1,1}\cdot \dot{i}_{p1,1} - \\ -R_{p1,2}\cdot i_{p1,2} - L_{p1,2}\cdot \dot{i}_{p1,2} + R_{t1,2}\cdot i_{t1,2} + L_{t1,2}\cdot \dot{i}_{t1,2} \\ \vdots \\ R_{tk,n-1}\cdot i_{tk,n-1} + L_{tk,n-1}\cdot \dot{i}_{tk,n-1} = R_{pk,n-1}\cdot i_{pk,n-1} + \\ +L_{pk,n-1}\cdot \dot{i}_{pk,n-1} - R_{pk,n}\cdot i_{pk,n} - L_{pk,n}\cdot \dot{i}_{pk,n} + \\ +R_{tk,n}\cdot i_{tk,n} + L_{tk,n}\cdot \dot{i}_{tk,n} \end{cases} \tag{2.94}$$

In each middle point of the arms, point M in figure 2.27, it is also true by means of Kirchhoff's law that:

$$\begin{cases} i_{u1,1} = i_{l1,1} + i_{p1,1} + i_{t1,1} \\ \vdots \\ i_{uk,1} = i_{lk,1} + i_{pk,1} + i_{tk,1} \\ \vdots \\ i_{uk,n} = i_{lk,n} + i_{pk,n} + i_{tk,n} \end{cases} \tag{2.95}$$

If we proceed in analogous form, for the connecting points C shown in figure 2.27, we obtain:

$$\begin{cases} i_{p1,1} + i_{p1,2} + \ldots + i_{p1,n} = 0 \\ \vdots \\ i_{pk,1} + i_{pk,2} + \ldots + i_{pk,n} = 0 \end{cases} \tag{2.96}$$

From equations (2.95) and (2.96), it is clear that the order of the state variable will be reduced. At this point, we will use as state variables all the currents in the upper and lower arms, in total $2nk$ variables, and $k(n-1)$ state variables for the currents in each AC phase.

In concordance with [76, 77], and considering the total energy stored in the arms, the dynamics of $v_{i,j}$ and could be expressed as:

$$\begin{cases} \dot{v}_{u1,1} = \frac{N_{u1,1} \cdot n_{u1,1}}{\mathcal{C}_{u1,1}} \cdot i_{u1,1} \\ \dot{v}_{l1,1} = \frac{N_{l1,1} \cdot n_{l1,1}}{\mathcal{C}_{l1,1}} \cdot i_{l1,1} \\ \vdots \\ \dot{v}_{lk,1} = \frac{N_{lk,1} \cdot n_{lk,1}}{\mathcal{C}_{lk,1}} \cdot i_{lk,1} \\ \vdots \\ \dot{v}_{lk,n} = \frac{N_{lk,n} \cdot n_{lk,n}}{\mathcal{C}_{lk,n}} \cdot i_{lk,n} \end{cases} \tag{2.97}$$

where $n_{uj,s}$ and $n_{lj,s}$ are the index number for the upper and lower arm respectively ($0 < n_{u,l} \leq 1$), $\mathcal{C}_{uj,s}$ and $\mathcal{C}_{lj,s}$ are the upper and lower sub-module capacitance respectively for each capacitor in the arms, and $N_{uj,s}$ and $N_{lj,s}$ are the number of sub-modules for the upper and lower in the $j^{th}$ leg of the $s^{th}$ terminal. It is important to remark that the product $N_{uj,s} \cdot n_{uj,s} \in \mathbb{N}$ (the same in the lower arms).

In order to achieve an optimal performance all modules must have the same number of sub-modules. Henceforth, we will consider that $N_s$ sub-modules exist in each arm with the same capacitance $\mathcal{C}_s$ for the terminal $s^{th}$. In this conditions, and for the proper operation of the converter, the sum of the sub-modules in state on between the upper and lower arms in each leg must be always constant. Consequently, the sum of the upper and lower index number must be always equals to one for all legs.

From equations (2.93) to (2.97), the multi-terminal converter dynamics with $k$ arms and $n$ terminals could be expressed, in a first instance, by the following non linear system.

$$\Lambda \dot{x} = \Gamma(u)x + B \tag{2.98}$$

where $x \in \mathbb{R}^{k(5n-1)}$.

$$x = [\overbrace{.., v_{ui,j}, v_{li,j}, ..}^{2nk}, \overbrace{.., i_{ui,j}, i_{li,j}, ..}^{2nk}, \overbrace{i_{p1.1}, .., i_{pk,1}, .., i_{pk,n-1}}^{k(n-1)}]^T \tag{2.99}$$

In $B \in \mathbb{R}^{k(5n-1)}$ are the external excitations of the system, which are the DC voltage sources:

$$B = [\overbrace{.., 0, ..}^{2nk}, \overbrace{.., V_{DC,i}, V_{DC,i}, ..}^{2nk}, \overbrace{.., 0, ..}^{k(n-1)}]^T \tag{2.100}$$

In $u \in \mathbb{R}^{2nk}$ are the control variables:

$$u = [n_{u1,1}, n_{l1,1}, ..., n_{uk,n}, n_{lk,n}]^T \tag{2.101}$$

which are always positive and bounded.

The matrix $\Lambda \in \mathbb{R}^{k(5n-1)\times k(5n-1)}$ has the following form:

$$\Lambda = \begin{bmatrix} \Lambda_{11} & \Lambda_{12} \\ \Lambda_{21} & \Lambda_{22} \end{bmatrix} = \begin{bmatrix} \mathbf{I}_{2nk} & \mathbf{0} \\ \mathbf{0} & \Lambda_{22} \end{bmatrix} \tag{2.102}$$

where $\Lambda_{11} \in \mathbb{R}^{2nk\times 2nk}$ is equal to the identity matrix of same dimensions, $\Lambda_{12} \in \mathbb{R}^{2nk\times k(3n-1)}$ and $\Lambda_{21} = \Lambda_{12}^T$ are null. Matrix $\Lambda_{22} \in \mathbb{R}^{k(3n-1)\times k(3n-1)}$ is defined as:

$$\Lambda_{22} = \begin{bmatrix} \Lambda_{22}^a & \Lambda_{22}^b \\ (\Lambda_{22}^b)^T & \Lambda_{22}^c \end{bmatrix} \tag{2.103}$$

where matrix $\Lambda_{22}^a \in \mathbb{R}^{2nk\times 2nk}$ is:

$$\Lambda_{22}^a = \begin{bmatrix} L_{u1,1}+L_{t1,1} & -L_{t1,1} & .. & 0 & 0 \\ -L_{t1,1} & L_{l1,1}+L_{t1,1} & .. & 0 & 0 \\ \vdots & \vdots & \ddots & \vdots & \vdots \\ 0 & 0 & .. & L_{uk,n}+L_{tk,n} & -L_{tk,n} \\ 0 & 0 & .. & -L_{tk,n} & L_{lk,n}+L_{tk,n} \end{bmatrix} \tag{2.104}$$

and matrix $\Lambda_{22}^c \in \mathbb{R}^{k(n-1)\times k(n-1)}$ is:

$$\Lambda_{22}^c = \begin{bmatrix} \Sigma_1 & S & .. & S & S \\ S & \Sigma_2 & .. & S & S \\ \vdots & \vdots & \ddots & \vdots & \vdots \\ \vdots & \vdots & \vdots & \ddots & \vdots \\ S & S & .. & S & \Sigma_{n-1} \end{bmatrix} \tag{2.105}$$

where:

$$\Sigma_s = diag(\sigma_1^s, .., \sigma_k^s) \in \mathbb{R}^{k\times k} \ , \ \forall s \in \{1, .., n-1\} \tag{2.106}$$

with $\sigma_i^s = L_{ti,s} + L_{pi,s} + L_{ti,n} + L_{pi,n} \ \forall i \in \{1, 2, .., k\}$, and the index $n$ refers to the terminal $n$. We must note that in the system of equations (2.96), the phase currents of terminal $n$ can be cleared as function of the phase current of the others.

The terms $S$ of matrix shown in equation (2.105) are defined as:

$$S = diag(.., L_{ti,n} + L_{pi,n}, ..) \in \mathbb{R}^{k\times k} \tag{2.107}$$

Matrix $\Lambda_{22}^b \in \mathbb{R}^{2nk\times k(n-1)}$ is shown in equation (2.108).

$$\Lambda_{22}^b = \begin{bmatrix}
-L_{t1,1} & 0 & .. & 0 & 0 & .. & 0 & .. & 0 & .. & 0 \\
L_{t1,1} & 0 & .. & 0 & 0 & .. & 0 & .. & 0 & .. & 0 \\
0 & -L_{t2,1} & .. & 0 & 0 & .. & 0 & .. & 0 & .. & 0 \\
0 & L_{t2,1} & .. & 0 & 0 & .. & 0 & .. & 0 & .. & 0 \\
\vdots & \vdots & \ddots & \vdots & \vdots & & \vdots & & \vdots & & \vdots \\
\vdots & \vdots & \ddots & \vdots & \vdots & .. & \vdots & .. & \vdots & .. & \vdots \\
0 & 0 & .. & -L_{tk,1} & 0 & .. & 0 & .. & 0 & .. & 0 \\
0 & 0 & .. & L_{tk,1} & 0 & .. & 0 & .. & 0 & .. & 0 \\
0 & 0 & .. & 0 & -L_{t1,2} & .. & 0 & .. & 0 & .. & 0 \\
0 & 0 & .. & 0 & L_{t1,2} & .. & 0 & .. & 0 & .. & 0 \\
\vdots & \vdots & \vdots & \vdots & \vdots & \ddots & \vdots & \vdots & \vdots & & \vdots \\
\vdots & \vdots & \vdots & \vdots & \vdots & & \ddots & \vdots & \vdots & .. & \vdots \\
0 & 0 & .. & 0 & 0 & .. & -L_{tk,2} & .. & 0 & .. & 0 \\
0 & 0 & .. & 0 & 0 & .. & L_{tk,2} & .. & 0 & .. & 0 \\
\vdots & \vdots & \vdots & \vdots & \vdots & & \vdots & \vdots & \vdots & & \vdots \\
\vdots & \vdots & \vdots & \vdots & \vdots & .. & \vdots & \vdots & \vdots & .. & \vdots \\
0 & 0 & .. & 0 & 0 & .. & 0 & .. & -L_{t1,n-1} & .. & 0 \\
0 & 0 & .. & 0 & 0 & .. & 0 & .. & L_{t1,n-1} & .. & 0 \\
\vdots & \vdots & & \vdots & \vdots & & \vdots & & \vdots & \ddots & \vdots \\
\vdots & \vdots & .. & \vdots & \vdots & .. & \vdots & .. & \vdots & & \vdots \\
0 & 0 & .. & 0 & 0 & .. & 0 & .. & 0 & .. & -L_{tk,n-1} \\
0 & 0 & .. & 0 & 0 & .. & 0 & .. & 0 & .. & L_{tk,n-1} \\
L_{t1,n} & 0 & .. & 0 & L_{t1,n} & .. & 0 & .. & L_{t1,n} & .. & 0 \\
-L_{t1,n} & 0 & .. & 0 & -L_{t1,n} & .. & 0 & .. & -L_{t1,n} & .. & 0 \\
\vdots & \vdots & \vdots & \vdots & \vdots & \vdots & \vdots & \vdots & \vdots & \vdots & \vdots \\
\vdots & \vdots & \vdots & \vdots & \vdots & \vdots & \vdots & \vdots & \vdots & \vdots & \vdots \\
0 & 0 & .. & L_{tk,n} & 0 & .. & L_{tk,n} & .. & 0 & .. & L_{tk,n} \\
0 & 0 & .. & -L_{tk,n} & 0 & .. & -L_{tk,n} & .. & 0 & .. & -L_{tk,n}
\end{bmatrix} \tag{2.108}$$

On the other hand, the matrix $\Gamma(u) \in \mathbb{R}^{k(5n-1)\times k(5n-1)}$ has the following form:

$$\Gamma(u) = \begin{bmatrix} \Gamma_{11} & \Gamma_{12}(u) \\ \Gamma_{21} & \Gamma_{22} \end{bmatrix} \tag{2.109}$$

where $\Gamma_{11} \in \mathbb{R}^{2nk\times 2nk}$ is null, $\Gamma_{21}$ could be defined as:

$$\Gamma_{21} = \begin{bmatrix} -I_{2nk} \\ \mathbf{0} \end{bmatrix} \in \mathbb{R}^{k(3n-1)\times 2nk} \tag{2.110}$$

where $I_{2nk}$ is the identity matrix of dimension $2nk$, and $\mathbf{0}$ is a null matrix with $k(n-1)$ rows and $2nk$ columns.

Matrix $\Gamma_{12}(u)$ is defined as:

$$\Gamma_{12}(u) = -U(u) \cdot C^{-1} \cdot \Gamma_{21}^{T} \in \mathbb{R}^{2nk \times k(3n-1)} \tag{2.111}$$

where $U(u) \in \mathbb{R}^{2nk \times 2nk}$ is a diagonal matrix which includes the control variables defined in (2.112), and $C \in \mathbb{R}^{2nk \times 2nk}$, defined in (2.113), is a diagonal matrix which includes the capacitance of each sub-module.

$$U(u) = diag\left[N_{u1,1} \cdot n_{u1,1}, N_{l1,1} \cdot n_{l1,1}, .., N_{lk,n} \cdot n_{lk,n}\right] \tag{2.112}$$

$$C = diag\left[\mathcal{C}_{u1,1}, \mathcal{C}_{l1,1}, .., \mathcal{C}_{lk,n}\right] \tag{2.113}$$

And finally, matrix $\Gamma_{22} \in \mathbb{R}^{k(3n-1) \times k(3n-1)}$ is equal to $-\Lambda_{22}$ by changing only the coefficients of the inductances by the respective resistances.

***Remark* 1** *Matrix $\Lambda$ define in equation (2.102) is symmetric and invertible. Consequently $\Lambda^{-1}$ is symmetric too. As will be demonstrated in section 2.5.2 it is positive definite.*

It is possible to write the system (2.98) in the following classic form:

$$\dot{x} = A(u)x + \mathcal{B} \tag{2.114}$$

where $A(u) \in \mathbb{R}^{k(5n-1) \times k(5n-1)}$ is:

$$A(u) = \Lambda^{-1} \cdot \Gamma(u) = \begin{bmatrix} \mathbf{0} & \Gamma_{12}(u) \\ \Lambda_{22}^{-1} \cdot \Gamma_{21} & \Lambda_{22}^{-1} \cdot \Gamma_{22} \end{bmatrix} = \begin{bmatrix} \mathbf{0} & A_{12}(u) \\ A_{21} & A_{22} \end{bmatrix} \tag{2.115}$$

$$\mathcal{B} = \Lambda^{-1} \cdot B \in \mathbb{R}^{k(5n-1)} \tag{2.116}$$

At this point, it is important to realize that the system is not linear, since the input $u$ is multiplied by the state $x$, but if we apply the theory of switching systems [46], we can transform the same problem in another which will be composed of a finite number of linear systems, as many as possible combinations between the control variables could appear. From equation (2.115), we can note as all of these possible linear system, which appear variating the input $u$, have always the same equilibrium point. This fact should not surprise us, moreover from the point of view of physics is consistent. Basically, the change in the control variables is the same as if we change the total capacity of each module. Due the structure of the system, where inductances are placed in series with the capacitors in the upper and lower arms, in steady state the current through these arms will be zero whatever the combination of control variables $u$, and therefore the voltage drop in the capacitor will always be the same. From the point of view of switched control theory the fact that all systems have the same equilibrium point, is very important in order to prove the global stability of the system and to find a global Lyapunov function, as will be explained in section 2.5.2.

Another important remark is that, in this study we have not used the commonly called circulating current, which is habitually used in the literature for MMC applications [75, 76, 78]. Operation with this virtual variable, which is the supposed current that is passing through the mesh which includes upper and lower arm of the same leg. This fact is only true if the resistances and inductances are exactly the same, and it is very difficult to be true in real applications. Besides, it is more natural to work with the state variables chosen here.

### 2.5.2 Stability.

Firstly, it is straightforward to verify that matrix $\Lambda$ shown in (2.102) is invertible. Moreover we are going to prove that it is positive definite. We proceed as follows, equation (2.102) could be rewritten as:

$$\Lambda = \begin{bmatrix} I_{2nk\times 2nk} & \mathbf{0} \\ \mathbf{0} & \Lambda_{2,2} \end{bmatrix} = \begin{bmatrix} I_{2nk\times 2nk} & \mathbf{0} & \mathbf{0} \\ \mathbf{0} & \Lambda^a_{2,2} & \Lambda^b_{2,2} \\ \mathbf{0} & (\Lambda^b_{2,2})^T & \Lambda^c_{2,2} \end{bmatrix} \tag{2.117}$$

therefore, it is clear that if, and only if $\Lambda_{2,2}$ , defined in equation (2.103), is positive definite then matrix $\Lambda$ is positive definite also.

The next Lemma 2 and Lemma 3 will give us sufficient conditions for achieve that matrix $\Lambda_{22}$ will be positive definite.

***Lemma 2*** *Let $n, l \in \mathbb{N}^*$, $A_{11} \in \mathbb{R}^{n\times n}$, $A_{12} \in \mathbb{R}^{n\times l}$, $A_{21} \in \mathbb{R}^{l\times n}$, $A_{22} \in \mathbb{R}^{l\times l}$ and*

$$A = \begin{bmatrix} A_{11} & A_{12} \\ A_{21} & A_{22} \end{bmatrix} \in \mathbb{R}^{(n+l)\times(n+l)}, \tag{2.118}$$

*$A$ is positive definite if, and only if, $A_{22} - A_{21}\cdot A_{11}^{-1}\cdot A_{12}$ is positive definite and $A_{11}$ is positive definite (or equivalently, if, and only if $A_{22}$ is positive definite and $A_{11} - A_{12}\cdot A_{22}^{-1}\cdot A_{21}$ is positive definite).*

***Proof.-***

$\forall x \neq 0 \in \mathbb{R}^{n+l}$, with $x^T = [x_1^T \; x_2^T]$ where $x_1 \in \mathbb{R}^n$ and $x_2 \in \mathbb{R}^l$, it holds that:

As $x^TAx = x_1^TA_{11}x_1 + x_1^TA_{12}x_2 + x_2^TA_{21}x_1 + x_2^TA_{22}x_2$, then if $A$ is positive definite, then $A_{11}$ and $A_{22}$ are positive definite, because, if:

$$x_1 \neq 0 = x_2, \quad x_1^TA_{11}x_1 = x^TAx > 0 \tag{2.119}$$

$$x_1 = 0 \neq x_2, \quad x_2^TA_{22}x_2 = x^TAx > 0 \tag{2.120}$$

On the other hand, it is also true that:

$$x^TAx = (x_1^T + x_2^TA_{21}A_{11}^{-1})A_{11}(x_1 + A_{11}^{-1}A_{12}x_2) + x_2^T(A_{22} - A_{21}A_{11}^{-1}A_{12})x_2 \tag{2.121}$$

then if $A$ is positive definite, then $A_{22} - A_{21}A_{11}^{-1}A_{12}$ is positive definite, because:

If $x_2 \neq 0$ and $x_1 = -A_{11}^{-1}A_{22}x_2$, then it is clear that:

$$x_2^T(A_{22} - A_{21}A_{11}^{-1}A_{12})x_2 = x^T Ax > 0 \tag{2.122}$$

Besides, from (2.121) we can conclude that if matrices $A_{11}$ and $A_{22} - A_{21} \cdot A_{11}^{-1} \cdot A_{12}$ are positive definite, $A$ is also positive definite, because:

$$x_2 \neq 0, \quad x^T(A_{22} - A_{21}A_{11}^{-1}A_{12})x > 0 \tag{2.123}$$

$$x_1 \neq 0 = x_2, \quad x^T Ax = x_1^T A_{11}x_1 > 0 \tag{2.124}$$

□

***Lemma 3*** *Let $n, k \in \mathbb{N}^*$, let $A \in \mathbb{R}^{(nk)\times(nk)}$ be a matrix defined as follows:*

$$A = \begin{bmatrix} A_1 & B & .. & B \\ B & A_2 & .. & B \\ \vdots & \vdots & \ddots & \vdots \\ B & B & .. & A_n \end{bmatrix} \tag{2.125}$$

where $A_i \in \mathbb{R}^{k\times k}$ is defined as $A_i = diag(\alpha_i^1, .., \alpha_i^k)\ \forall\ i \in \{1, ..n\}$ and $B \in \mathbb{R}^{k\times k}$ is defined as $B = diag(\beta^1, .., \beta^k)$.

If $\forall i \in \{1, ..n\}$, and $\forall j \in \{1, ..k\}$, $\alpha_i^j > \beta^j \geq 0$ then $A$ is positive definite.

***Proof.-***

If we define matrix: $C_i = A_i - B$, as $\forall i \in \{1, ..n\}$, and $\forall j \in \{1, ..k\}$, $\alpha_i^j > \beta^j \geq 0$, then matrix: $C_i$ is positive definite. Therefore, matrix $A$ shown in (2.125) could be rewrite as:

$$A = \begin{bmatrix} C_1 & 0 & .. & 0 \\ 0 & C_2 & .. & 0 \\ \vdots & \vdots & \ddots & \vdots \\ 0 & 0 & .. & C_n \end{bmatrix} + \begin{bmatrix} B & B & .. & B \\ B & B & .. & B \\ \vdots & \vdots & \ddots & \vdots \\ B & B & .. & B \end{bmatrix} \tag{2.126}$$

but the first matrix is clearly positive definite, and second matrix is positive semi-definite because, $\forall x_i \in \mathbb{R}^k$, with $i \in \{1, ..n\}$, then:

$$[x_1^T\ x_2^T\ ..\ x_k^T] \begin{bmatrix} B & B & .. & B \\ B & B & .. & B \\ \vdots & \vdots & \ddots & \vdots \\ B & B & .. & B \end{bmatrix} \begin{bmatrix} x_1 \\ x_2 \\ \vdots \\ x_k \end{bmatrix} =$$

$$= (x_1^T + x_2^T + ... + x_k^T) \cdot B \cdot (x_1^T + x_2 + ... + x_k) \geq 0 \tag{2.127}$$

Consequently, matrix $A$ is equal to the sum of a definite positive matrix, and a semi-definite positive matrix, therefore, it is always definite positive.□

Consequently, applying Lemma 2, we can assert that $\Lambda_{22}$ is positive definite if, and only if, $\Lambda^a_{22}$ and $\Lambda^c_{22} - (\Lambda^b_{22})^T \cdot (\Lambda^a_{22})^{-1} \cdot \Lambda^b_{22}$ are positive definite.

Matrix $\Lambda^a_{22}$ is defined in equation (2.104). It is composed by blocks $2 \times 2$, which are easily demonstrable that they have two positive eigenvalues, due to theirs leading principal minors are all positive.

$$\Lambda^a_{22} = diag(B_{11}, .., B_{ij}, .., B_{kn}) \tag{2.128}$$

where:

$$B_{ij} = \begin{bmatrix} L_{ui,j} + L_{ti,j} & -L_{ti,j} \\ -L_{ti,j} & L_{li,j} + L_{ti,j} \end{bmatrix} \forall\ i \in \{1, .., k\},\ \forall\ j \in \{1, .., n\} \tag{2.129}$$

the leading principal minor of order 1, is clearly positive, and the leading principal minor of order 2 (its determinant) is:

$$L_{ui,j} \cdot L_{li,j} + L_{ui,j} \cdot L_{ti,j} + L_{li,j} \cdot L_{ti,j} > 0 \tag{2.130}$$

therefore, matrix $\Lambda^a_{2,2}$ is positive definite.

Besides:

$$(\Lambda^a_{22})^{-1} = diag\left(B^{-1}_{11}, .., B^{-1}_{ij}, .., B^{-1}_{kn}\right) = diag(M_1, .., M_n) \tag{2.131}$$

where $\forall\ j \in \{1, .., n\}$, $M_j = diag(B^{-1}_{1j}, .., B^{-1}_{1j})$, with:

$$B^{-1}_{ij} = \frac{1}{L_{ui,j}L_{ti,j} + (L_{ui,j} + L_{ti,j})L_{ti,j}} \begin{bmatrix} L_{li,j} + L_{ti,j} & L_{ti,j} \\ L_{ti,j} & L_{ui,j} + L_{ti,j} \end{bmatrix} \tag{2.132}$$

On the other hand, $\Lambda^b_{22}$ is defined in equation (2.108), which could be redefined as:

$$\Lambda^b_{22} = \begin{bmatrix} T_1 & 0 & .. & 0 & 0 \\ 0 & T_2 & .. & 0 & 0 \\ \vdots & \vdots & \ddots & \vdots & \vdots \\ 0 & 0 & .. & 0 & T_{n-1} \\ -T_n & -T_n & .. & -T_n & -T_n \end{bmatrix} \tag{2.133}$$

with:

$$T_j = \begin{bmatrix} -L_{t1,j} & 0 & .. & 0 \\ L_{t1,j} & 0 & .. & 0 \\ 0 & -L_{t2,j} & .. & 0 \\ 0 & L_{t2,j} & .. & 0 \\ \vdots & \vdots & \ddots & \vdots \\ 0 & 0 & .. & -L_{tk,j} \\ 0 & 0 & .. & L_{tk,j} \end{bmatrix} \tag{2.134}$$

Therefore, we can write:

$$(\Lambda_{22}^b)^T \cdot (\Lambda_{22}^a)^{-1} \cdot \Lambda_{22}^b =$$

$$= \begin{bmatrix} T_1^T & 0 & .. & 0 & -T_n^T \\ 0 & T_2^T & .. & 0 & -T_n^T \\ \vdots & \vdots & \ddots & \vdots & \vdots \\ 0 & 0 & .. & 0 & -T_n^T \\ 0 & 0 & .. & T_{n-1}^T & -T_n^T \end{bmatrix} \begin{bmatrix} M_1 & 0 & .. & 0 \\ 0 & M_2 & .. & 0 \\ \vdots & \vdots & \ddots & \vdots \\ 0 & 0 & .. & M_n \end{bmatrix} \begin{bmatrix} T_1 & 0 & .. & 0 & 0 \\ 0 & T_2 & .. & 0 & 0 \\ \vdots & \vdots & \ddots & \vdots & \vdots \\ 0 & 0 & .. & 0 & T_{n-1} \\ -T_n & -T_n & .. & -T_n & -T_n \end{bmatrix}$$

$$= \begin{bmatrix} T_1^T M_1 T_1 + T_n^T M_n T_n & T_n^T M_n T_n & .. & T_n^T M_n T_n \\ T_n^T M_n T_n & T_2^T M_2 T_2 + T_n^T M_n T_n & .. & T_n^T M_n T_n \\ \vdots & \vdots & \ddots & \vdots \\ T_n^T M_n T_n & T_n^T M_n T_n & .. & T_{n-1}^T M_{n-1} T_{n-1} + T_n^T M_n T_n \end{bmatrix} =$$

$$= \begin{bmatrix} H_1 + H_n & H_n & .. & H_n \\ H_n & H_2 + H_n & .. & H_n \\ \vdots & \vdots & \ddots & \vdots \\ H_n & H_n & .. & H_{n-1} H_n \end{bmatrix} \tag{2.135}$$

where $H_j = T_j^T M_j T_j \ \forall \ j \in \{1, .., n\}$, and taking into account equations (2.132) and (2.134), we can write:

$$H_j = \begin{bmatrix} \frac{(L_{u1,j}+L_{l1,j})L_{t1,j}^2}{L_{u1,j}L_{l1,j}+(L_{u1,j}+L_{l1,j})L_{t1,j}} & .. & 0 \\ \vdots & \ddots & \vdots \\ 0 & .. & \frac{(L_{uk,j}+L_{lk,j})L_{tk,j}^2}{L_{uk,j}L_{lk,j}+(L_{uk,j}+L_{lk,j})L_{tk,j}} \end{bmatrix} \tag{2.136}$$

Moreover $\forall \ i \in \{1, .., k\}$ and $\forall \ j \in \{1, .., n\}$, it is always true that:

$$0 \leq \frac{(L_{ui,j} + L_{li,j})L_{ti,j}^2}{L_{ui,j}L_{li,j} + (L_{ui,j} + L_{li,j})L_{ti,j}} \leq L_{ti,j} \tag{2.137}$$

From equation (2.105), is is true that:

$$\Lambda_{22}^c - (\Lambda_{22}^b)^T \cdot (\Lambda_{22}^a)^{-1} \cdot \Lambda_{22}^b =$$

$$= \begin{bmatrix} \Sigma_1 - H_1 - H_n & S - H_n & .. & S - H_n \\ S - H_n & \Sigma_2 - H_2 - H_n & .. & S - H_n \\ \vdots & \vdots & \ddots & \vdots \\ S - H_n & S - H_n & .. & \Sigma_{n-1} - H_{n-1} - H_n \end{bmatrix} \tag{2.138}$$

where $S - H_n$ is a diagonal matrix whose elements are:

$$\beta_i = L_{ti,n} + L_{p-i,n} - \frac{(L_{ui,j} + L_{li,j})L_{ti,j}^2}{L_{ui,j}L_{li,j} + (L_{ui,j} + L_{li,j})L_{ti,j}} \geq L_{pi,n} \tag{2.139}$$

and matrix $\Sigma_j - H_j - H_n$ is also diagonal, where their elements are:

$$L_{ti,j} + L_{pi,j} + L_{ti,n} + L_{pi,n} - \frac{(L_{ui,j}+L_{li,j})L_{ti,j}^2}{L_{ui,j}L_{li,j}+(L_{ui,j}+L_{li,j})L_{ti,j}} - \frac{(L_{ui,n}+L_{li,n})L_{ti,n}^2}{L_{ui,n}L_{li,n}+(L_{ui,n}+L_{li,n})L_{ti,n}} > \beta_i \tag{2.140}$$

and therefore, matrix $\Lambda_{22}^c - (\Lambda_{22}^b)^T \cdot (\Lambda_{22}^a)^{-1} \cdot \Lambda_{22}^b$ fulfils with the hypothesis of Lemma 3 and consequently, matrix $\Lambda$ will be always positive definite.

**Equilibrium points.**

Now we study the form of the equilibrium points, and we will see for any different input $u$ all the systems have the same equilibrium point (which is an invariant set, see [38]), as discussed before.

In the equilibrium $(x^*)$, if we define:

$$x^* = [\overbrace{.., v^*_{ui,j}, v^*_{li,j}, ..}^{2nk}, \overbrace{.., i^*_{ui,j}, i^*_{li,j}, ..}^{2nk}, \overbrace{i^*_{p1.1}, .., i^*_{pk,1}, .., i^*_{pk,n-1}}^{k(n-1)}]^T = [\overbrace{x^*_v}^{2nk}, \overbrace{x^*_i}^{2nk}, \overbrace{x^*_{ip}}^{k(n-1)}]^T$$

from systems (2.98) and (2.115), and for any bounded input $u \neq 0$, it is clear that:

$$\begin{cases} -\Lambda_{22}^{-1} \cdot \Gamma_{22} \begin{bmatrix} x^*_i \\ x^*_{ip} \end{bmatrix} + \Lambda_{22}^{-1} \cdot \begin{bmatrix} I \\ \mathbf{0} \end{bmatrix} \cdot x^*_v - \Lambda_{22}^{-1} \cdot \begin{bmatrix} V \\ \mathbf{0} \end{bmatrix} = \mathbf{0} \\ U(u) \cdot C^{-1} \cdot x^*_i = \mathbf{0} \end{cases} \tag{2.141}$$

where $V = [.., V_{DCi}, V_{DCi}, ..]^T \in \mathbb{R}^{2nk}$ in concordance with equation (2.100).

From (2.141) as $\exists \left(U(u)\right))^{-1}$ if $u \neq 0$, then $x^*_i = 0$, and consequently:

$$-\Gamma_{22} \begin{bmatrix} \mathbf{0} \\ x^*_{ip} \end{bmatrix} + \begin{bmatrix} x^*_v \\ \mathbf{0} \end{bmatrix} = \begin{bmatrix} V \\ \mathbf{0} \end{bmatrix} \tag{2.142}$$

and, in analogous form as (2.103), if we define

$$\Gamma_{22} = \begin{bmatrix} \Gamma^a_{22} & \Gamma^b_{22} \\ (\Gamma^b_{22})^T & \Gamma^c_{22} \end{bmatrix} \tag{2.143}$$

then:

$$\Gamma^c_{22} \cdot x^*_{ip} = \mathbf{0} \Rightarrow x^*_{ip} = \mathbf{0} \tag{2.144}$$

and therefore,

$$x^*_v = V \tag{2.145}$$

Summarizing, for the system (2.98) and for any input $u$ all the equilibrium points have always the form:

$$\begin{cases} x^*_v = V \\ x^*_i = \mathbf{0} \\ x^*_{ip} = \mathbf{0} \end{cases} \tag{2.146}$$

**Stability.**

The follow theorem 4 summarizes the stability proposed for of this MMC converter for a general case with $k$ phases and $n$ terminals.

***Theorem* 4** *The converter described by (2.98) is globally exponentially stable for any bounded control variable defined in (2.101).*

***Proof.-***

With the same reasoning as for $\Lambda$, we can prove that $\Gamma(u)$ is always negative definite for any $u$ bounded, since the elements of $\Gamma_{22}$ have opposite sign than the $\Lambda_{22}$ ones.

All possible systems that can exist, which are derived from all possible combinations for the control variables $u$, have the same point of equilibrium as has been shown above. Consequently, if we find a global Lyapunov function for all of them, the theorem will be prove.

The matrix $A(u)$ of the system (2.98) could be rewritten as:

$$A(u) = \Lambda^{-1} \cdot \Gamma(u) = \begin{bmatrix} \mathbf{0} & -C^{-1} \cdot U(u) \cdot \Gamma_{21}^T \\ \Lambda_{22}^{-1} \cdot \Gamma_{21} & \Lambda_{22}^{-1} \cdot \Gamma_{22} \end{bmatrix} \tag{2.147}$$

where $\Lambda_{22}^{-1}$ could be defined as:

$$\Lambda_{22}^{-1} = \begin{bmatrix} \mathcal{M}^a & \mathcal{M}^b \\ (\mathcal{M}^b)^T & \mathcal{M}^c \end{bmatrix} \tag{2.148}$$

where $\mathcal{M}^a$ and $\mathcal{M}^c$ are symmetric and positive definite matrices.

If we suppose that the equilibrium point of system (2.98) could be rewritten as:

$$x^* = -A(u)^{-1} \cdot \mathcal{B} \tag{2.149}$$

and if we define, $\tilde{x} = x - x^*$, then the system (2.98) becomes to:

$$\dot{\tilde{x}} = A(u) \cdot \tilde{x} \tag{2.150}$$

If we consider the Lyapunov function:

$$\tilde{\mathcal{V}} = \tilde{x}^T P \tilde{x} \tag{2.151}$$

is clearly a positive definite function since $P$

$$P = \begin{bmatrix} U^{-1} \cdot C & \epsilon I & \mathbf{0} \\ \epsilon I & \Lambda_{22}^a & \Lambda_{22}^b \\ \mathbf{0} & (\Lambda_{22}^b)^T & \Lambda_{22}^c \end{bmatrix} \tag{2.152}$$

is positive definite by means of Lemma 2 and Lemma 3. Therefore, $\tilde{\mathcal{V}}$ is always positive $\forall\ \tilde{x} \neq 0$. The parameter $\epsilon$ is chosen as $\epsilon^2 < \lambda_0 \mathcal{C}_0 / u_m$, where

$\lambda_0 = min(\sigma(\Lambda_{22}))$ [2], $\mathcal{C}_0$ is the minimum value of sub-module capacitors, and $u_m$ is the maximum value of the control variable $u$.

On the other hand:

$$PA + A^T P = \begin{bmatrix} -2\epsilon\mathcal{M}^a & \epsilon[\mathcal{M}^a \ \mathcal{M}^b]\Gamma_{22} \\ \epsilon\Gamma_{22}\begin{bmatrix} \mathcal{M}^a \\ (\mathcal{M}^b)^T \end{bmatrix} & 2\left(\Gamma_{22} + \epsilon\begin{bmatrix} U\cdot C^{-1} & \mathbf{0} \\ \mathbf{0} & \mathbf{0} \end{bmatrix}\right) \end{bmatrix} \tag{2.153}$$

and applying Lemma 2 it holds that $\exists\delta > 0$ such that if $0 < \epsilon < \delta$ the matrix $AP + P^T A$ shown in (2.153) is negative definite, and consequently the time derivate of Lyapunov function defined in (2.151) is always negative. Consequently, for any control variable $u$, the Lypaunov function defined in (2.151) is positive definite and its time derivate is always negative definite. This means that the the system defined in (2.98) is asymptotically stable. □

### 2.5.3 Control.

Theorem 4 shows that the system is asymptotically stable for any bounded control input $u$.

As we want to control the power flow between $n$ terminals, our state variables will be controlled by the control variables $u$ given in equation 2.101. The proposed control is shown in figure 2.29.

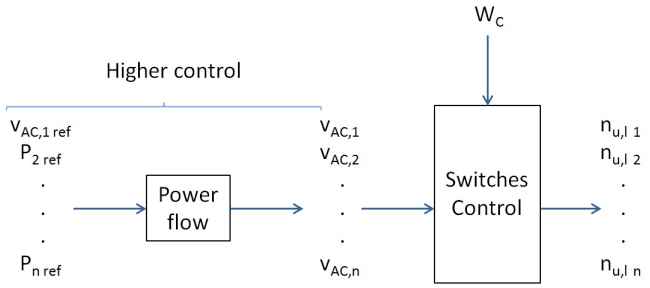


Figure 2.29: Control scheme.

The idea of the proposed control is explained as follows. We have supposed that a higher-level controller gives the references for the converter. A terminal (for example terminal 1) will take care to create the appropriate internal converter AC voltage signal to track the AC voltage reference, by means of the suitable values for $n_{u1}$ and $n_{l1}$ respectively (they will have influence over the amplitude of the signal). The remaining terminals will entrust to create the appropriate signals for the AC voltage references given by a periodic calculation of power flow, which guarantees the power equilibrium. This philosophy is called, master/slave because only one node controls

[2] $\sigma(A)$ is the spectrum of A.

the AC voltage. The power flow is solved by the higher controller thanks to the well known NR method, for example (see [15]), or also could be solve by other methods as proposed in this thesis (see sections 4.2 and annex A) in which more than one node could impose the voltages [79, 80].

Depending on the state of charge of the capacitors in each sub-module, multiple strategies may be employed, as proposes [81]. We have adopted a strategy in order that, according to the state of charge of each capacitor ($W_C$) and insertion indices ($n_u$ and $n_l$), capacitors are used as uniform as possible in order to distribute theirs efforts. The most important is that the total module voltage remains constant, and this is possible thanks to state of charge of capacitors are close between them.

On the other hand, henceforth we will consider that the number of sub-modules will be the same, $N$, in all arms of the converter, and also that each sub-modules will have the same capacitor value $\mathcal{C}$.

### 2.5.4 Sinusoidal signal generation.

Before explaining how we will generate the corresponding sinusoidal signals at each terminal, it is necessary to clarify that since $n$ terminals are internally connected in AC, and with the purpose to avoid unnecessary losses, all signals generated at each terminal will have the same frequency and also between equivalent phases of each terminal the generated voltage will be in phase. Thanks to these considerations the control over the IGBTs is simple to implement. Also, it should be mentioned that between upper and lower arms of each phase, the capacitors have a complementary behaviour. That is, if for example in the upper arm $k$ capacitors are connected, in the lower arm $N-k$ are disconnected, as figure 2.30 shows. Consequently, insertion indices in each arm will be dependent. This is one of the multiple solutions that we could use to govern the IGBTs, but as it provides a balanced actuation form and also due to its simplicity, is a convenient solution.

After this brief explanation, we are ready to explain the sinusoidal generated voltage signal between phases in each terminal. If the capacitors are gradually connect in sequence, a sinusoidal voltage will appear between two phases as shows figure 2.30. It is considered that the signals for the first arm are used as reference for the other arms of the same terminal. In figure 2.30 appears the parameter $m$, which is defined as the phase difference between the pulse control signals of the capacitors in one arm (it is noteworthy that duty cycle in each signal is always 50 %). This value depends on the number of sub-modules per arm. On the other way, the parameter $\mu$ is the phase difference between the control signal for different arms and it depends on the number of arms in each terminal.

In this way, and from the viewpoint of control, only one insertion index value is required by terminal in order to govern the converter. In equations (2.154) and (2.155) both parameters are defined, where $T$ is the period of

the sinusoidal signals, $N$ is the number of sub-modules per arm, and $k$ is is the number of phases per terminal.

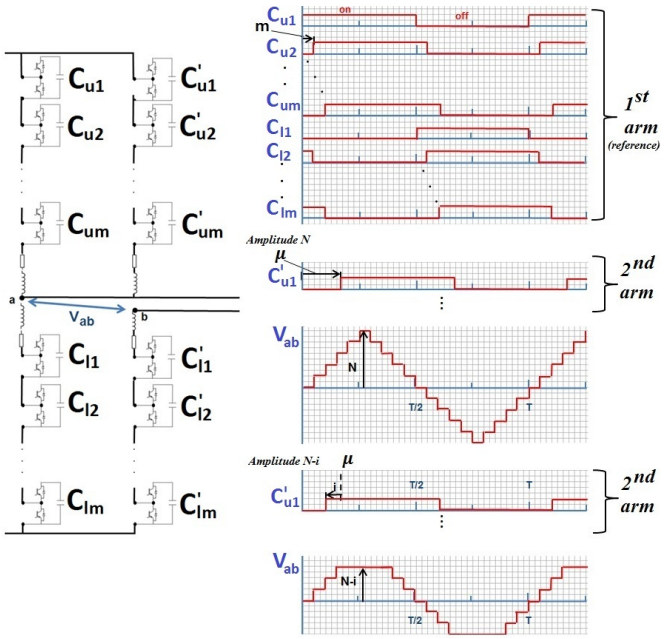


Figure 2.30: Sinusoidal signal generation.

$$m \in \mathbb{R}, \quad 0 \leq m \leq \frac{T}{2} \quad s.t \quad m = \frac{T/4}{N} \tag{2.154}$$

$$\mu \in \mathbb{R}, \quad 0 \leq \mu \leq \frac{T}{2} \quad s.t \quad \mu = \frac{T}{k} \tag{2.155}$$

If we want to obtain a phase voltage ($V_{ab}$) with an amplitude equal to $N - i$, where $i \in \mathbb{N}$, then we have to advance the pulse signal for the corresponding arm $i$ intervals of length $m$ with respect to value $\mu$, which corresponds for a phase voltage ($V_{ab}$) with an amplitude equals to $N$, as figure 2.30 shows. In this way, we achieve that all capacitors will be always used the same amount of time. Also, we can remark that in the phase voltage appears a *landing* whose length is equal to $(i + 1)m$, but the value for the first harmonic of this signal is always displaced the value $\mu$ with respect to the reference. In consequence, the obtained phase voltages at each terminal are uniformly separated according to the number of arms that there exists, as shown equation (2.156):

$$V_{ab} = 2 \cdot n_j \cdot V_{DC,j} \cdot sin(\omega \cdot t + \frac{2\pi}{k}) \tag{2.156}$$

where $n_j$ is the insertion index and $2 \cdot V_{DC,j}$ is the total bipolar DC voltage of the grid $j$.

The obtained voltage has not a pure sinusoidal form, but if we consider sufficient sub-modules, it can be approximated by a sine. When the number of sub-modules is not big enough, it is interesting to study the harmonics of the created signals, in order to improve the behaviour of the converter. In subsection 2.5.5 a discussion in order to improve the harmonics is presented.

**Balancing.**

Although all capacitors are connected the same amount of time, it is also important the order of the connection in each cycle, since the instantaneous currents are not the same for each interval of each cycle. Therefore, depending on the state of charge of each capacitor ($W_C$), the sequence will vary in each cycle. The less charged capacitor will be connected in the first interval, and the more charged in the last interval of each cycle. Thanks to this procedure, we can achieve that all capacitors are kept always charged with close values between them.

### 2.5.5 Harmonics study.

The problem of the harmonics for AC systems causes many disadvantages, including lower quality of the signal and therefore greater losses. In addition, for electronic devices, due to their discontinue nature the problem is increased. Therefore it is interesting to study them, especially if the number of modules is not very high.

In this section, a comparison between two control philosophies for the switches is shown. The first one considers that their *turn on* have a constant separation (variable $m$ defined above). In the second, the *turn on* is governed by a law in order to achieve that the first harmonic of the generated signal will have unity amplitude and the amplitude of the high order harmonics will be small. The idea is as follows, if we consider that we have $N$ sub-modules, then we have $N$ steps. If we define $a_1$ as the time necessary to achieve the value $1/N$ of the amplitude of the sine as shows figure 2.31, we can chose $d_1$ in order to obtain that the area enclose by the sine function between 0 and $a_1$ (the green area in figure 2.31), will be the same as the area of rectangle with sides $a_1 - d_1$ and $1/N$ (the hatched area in figure 2.31). Proceeding in analogous form, we can obtain the general terms as show equations (2.157) and (2.158).

$$\begin{cases} sin\left(\frac{2\pi}{T}\cdot a_1\right) = \frac{1}{N} \Rightarrow a_1 = \frac{T}{2\pi} arcsin\left(\frac{1}{N}\right) \\ sin\left(\frac{2\pi}{T}\cdot a_2\right) = \frac{2}{N} \Rightarrow a_2 = \frac{T}{2\pi} arcsin\left(\frac{2}{N}\right) \\ \vdots \\ sin\left(\frac{2\pi}{T}\cdot a_N\right) = \frac{N}{N} \Rightarrow a_N = \frac{T}{2\pi} arcsin\left(\frac{N}{N}\right) = \frac{T}{4} \end{cases} \tag{2.157}$$

$$\begin{cases} \int_0^{a_1} sin\left(\frac{2\pi}{T}\cdot t\right)dt = \frac{a_1-d_1}{N} \Rightarrow \\ d_1 = \frac{T}{2\pi}\cdot\left[arcsin\left(\frac{1}{N}\right) - \left(N-\sqrt{N^2-1}\right)\right] \\ \int_{a_1}^{a_2} sin\left(\frac{2\pi}{T}\cdot t\right)dt = \frac{d_2-a_1}{N} + 2\cdot\frac{a_2-d_2}{N} \Rightarrow \\ d_2 = \frac{T}{2\pi}\cdot\left[2\cdot arcsin\left(\frac{2}{N}\right) - arcsin\left(\frac{1}{N}\right) - \left(\sqrt{N^2-1}-\sqrt{N^2-4}\right)\right] \\ \vdots \\ d_p = \frac{T}{2\pi}\left[p\cdot arcsin\left(\frac{p}{N}\right) - (p-1)arcsin\left(\frac{p-1}{N}\right) - \left(\sqrt{N^2-(p-1)^2}-\sqrt{N^2-p^2}\right)\right] \end{cases} \quad (2.158)$$

where we have taken into account that:

$$cos\left(\frac{2\pi}{T}\cdot a_p\right) = \sqrt{1-\frac{p^2}{N^2}} \quad \forall p \quad 1 \le p \le N \quad (2.159)$$

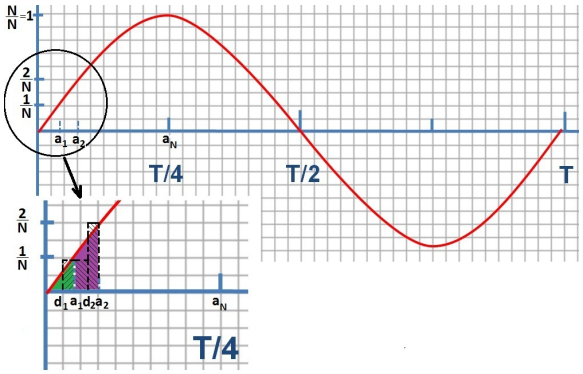


Figure 2.31: Harmonic construction.

In table 2.12 we can observe the different harmonics of both philosophies for $N = 5$.

Table 2.12: Harmonic amplitudes

| | Mode 1 | Mode 2 |
|---|---|---|
| Harmonic of order 1 | 0.82 | 1 |
| Harmonic of order 3 | 0.093 | 0.008 |
| Harmonic of order 5 | 0.036 | 0.009 |
| Harmonic of order 7 | 0.020 | 0.004 |
| Harmonic of order 9 | 0.014 | 0.005 |
| Harmonic of order 11 | 0.012 | 0.016 |
| Harmonic of order 13 | 0.011 | 0.020 |
| Harmonic of order 15 | 0.012 | 0.007 |

Another important consideration is that with both philosophies the duty cycle for each switch is always 50%. Therefore, all capacitors are connected the same amount of time, and thanks also to balance technique explained

above, we will ensure that all capacitors will be charged to the desired values, and thereby correct system operation is guaranteed.

### 2.5.6 Power transport explanation.

The power transfer between terminals could be explained as follows. Due to all voltages at each terminal between equivalent phases are in phase and have the same frequency, then the power direction in each terminal will depend on the amplitude of voltages, or equivalently, the insertion indices. Therefore the power goes from the higher voltage values to lower voltages.

However, another important explanation is required. In order to energy flows in all directions for all terminals, it is very important the relation between the different values of the DC voltage in each external network as well as the number of sub-modules.

If we assume that the system is well balanced in steady-state, the voltage in each capacitor of each sub-module will be as shown in equation (2.160):

$$u_{C,ul,i} = 2\frac{V_{DC,i}}{N} \tag{2.160}$$

so depending on the insertion index and the values of the voltage in each capacitor, it could be possible to transmit power in any direction, it is even possible to transmit power from networks with smaller DC voltage to other networks with higher DC values. In fact, the relationship that must be satisfied to transmit power from terminal $i^{th}$ to $j^{th}$ is shown in equation (2.161). The key issue is the amplitude of the AC internal generated signals.

$$u_{C,ul,i} \cdot n_i = 2\frac{V_{DC,i} \cdot n_i}{N} > 2\frac{V_{DC,j} \cdot n_j}{N} \tag{2.161}$$

It is important to remark that, the best performance is obtained when the relationship between the different DC voltages of each network are closer between them, because the losses are smaller.

On the other hand as the internal AC circuit is a star-shaped circuit, where the common points are the C points shown in figure 2.27. Consequently, in these points C, the value of the voltage (alternative) is the arithmetic average of the values of voltage (alternative) in each terminal, obviously if the elements of each phase, resistances and inductances, are equal.

### 2.5.7 Simulations.

A three terminal converter with two phases based in MMC technology is tested in order to verify the proper operation of the theorem 4 by means of controls shown in (2.101 and 2.156) as shown in figure 2.32.

The values of simulation are shown in table 2.13.

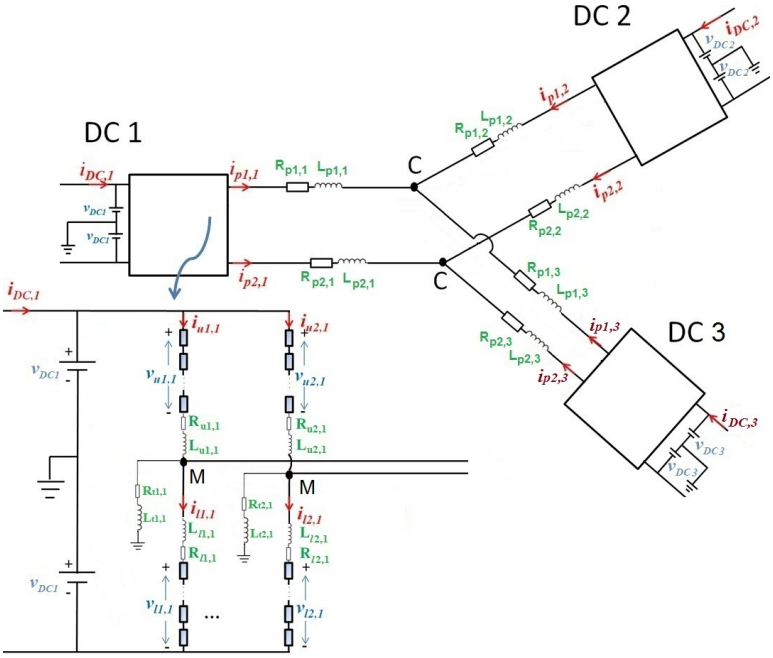


Figure 2.32: Multi DC/DC converter with $k$ phases based on MMC.

Table 2.13: Simulation parameter values

| | | |
|---|---|---|
| $V_{DC,1}$ | Voltage DC grid 1 | ±2.5 kV |
| $V_{DC,2}$ | Voltage DC grid 2 | ±3.125 kV |
| $V_{DC,3}$ | Voltage DC grid 3 | ±3.75 kV |
| $R_{p,1}$ | Resistance phase 1 | 0.1 Ω |
| $R_{p,2}$ | Resistance phase 2 | 0.1 Ω |
| $R_{p,3}$ | Resistance phase 3 | 0.1 Ω |
| $L_{p,1}$ | Inductance phase 1 | 0.01 H |
| $L_{p,2}$ | Inductance phase 2 | 0.01 H |
| $L_{p,3}$ | Inductance phase 3 | 0.01 H |
| MMC parameters | | |
| $R_1$ | Resistance arm 1 | 0.1 Ω |
| $R_2$ | Resistance arm 2 | 0.1 Ω |
| $L_1$ | Inductance arm 1 | 0.01 H |
| $L_2$ | Inductance arm 2 | 0.01 H |
| $\mathcal{C}_{total}$ | Total module capacitance | 0.01 F |
| $N$ | Number of sub-modules per arm | 5 |
| $f$ | AC signals frequency | 100 Hz |

In figure 2.33 we observe the generated AC voltages in each terminal for the corresponding insertion index.

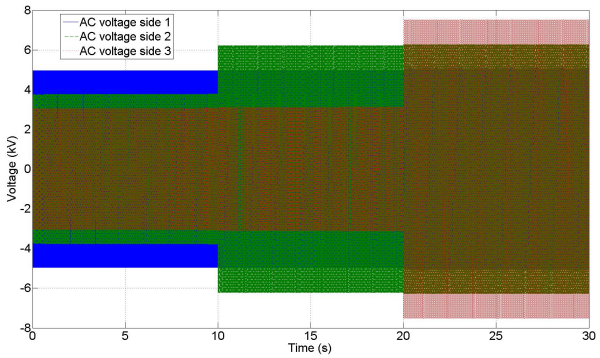


Figure 2.33: AC generated signal voltage.

In table 2.14 the obtained results are summarized. We can observe as during interval $0 \leq t \leq 10$, terminal 1 provides energy to terminals 2 and 3. In interval $10 \leq t \leq 20$, the first and the second one supply the energy to terminal 3, and finally during $20 \leq t \leq 30$, as the voltage in the point C is equals to voltage in node 2, the terminal 3 provides the energy only to the terminal 1, and the terminal 2 does not absorb or supply energy.

Table 2.14: Simulation results.

| | | $0 \leq t \leq 10$ | $10 \leq t \leq 20$ | $20 \leq t \leq 30$ |
|---|---|---|---|---|
| Terminal 1 | Insertion index | 1 | 1 | 1 |
| | AC voltage (peak) | 5 $kV$ | 5 $kV$ | 5 $kV$ |
| Terminal 2 | Insertion index | 0.6 | 1 | 1 |
| | AC voltage (peak) | 3.75 $kV$ | 6.25 $kV$ | 6.25 $kV$ |
| Terminal 3 | Insertion index | 0.4 | 0.4 | 1 |
| | AC voltage (peak) | 3 $kV$ | 3 $kV$ | 7.5 $kV$ |

In figure 2.34 we observe with more precision the generated voltages with both strategies explained in 2.5.5. We observe in it, as with strategy 2 the signals have a form more similar to a sine than with strategy 1.

In figure 2.35 the phase currents for terminal 1 are shown. We can observe as they have alternative form, which provides the capability to cut off the current when a problem appears (both DC or AC side) in each phase of the converter. Thus when a fault occurs it can isolate the bad side of the converter using the converter itself as DC circuit breaker, as it will be explained in section 2.6. In 2.36 we observe with more precision the current

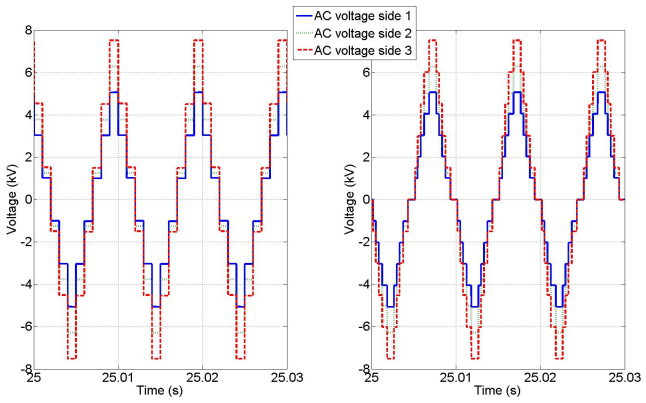


Figure 2.34: a)Voltages for strategy 1 b)Voltages for strategy 2.

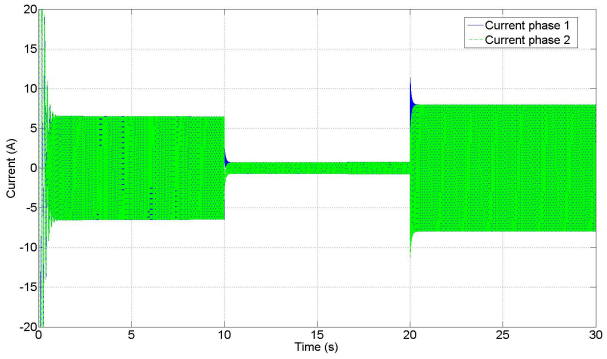


Figure 2.35: Phase currents.

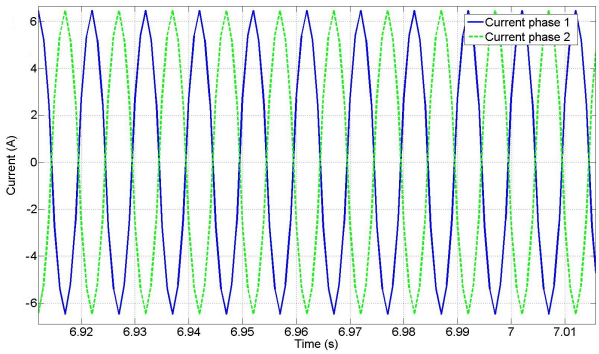


Figure 2.36: Phase currents. Zoom.

through the phases. In this figure we can observe that as there are only two phases, the phase difference between them is $\pi/2$.

Finally in figure 2.37, we observe as all capacitors for each terminal remains always with the same voltage according to the strategy adopted. In accordance with equation (2.160) we can remark that the voltages for each capacitor are 1 $kV$, 1.25 and 1.5 $kV$ respectively for each terminal.

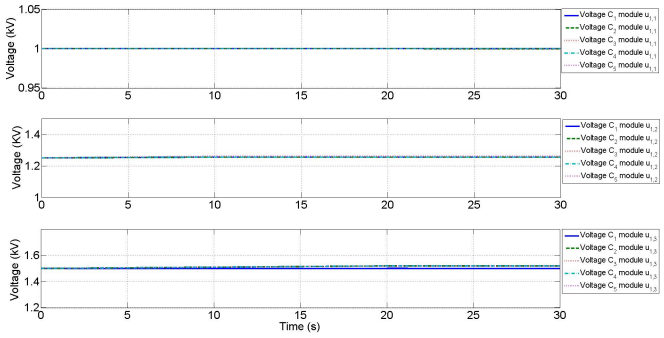


Figure 2.37: Capacitors state of charge.

## 2.6 Use as DC circuit-breaker.

DC lines have long been used to transmit power, in particular from large hydroelectric dams to cities, but only in *back to back* mode because it was not safe to connect more than two DC lines into a large-scale grid, due to the fact that there does not exist yet a device capable of cutting high DC current. This is why research efforts are currently focused on the development of DC-CB in order to implement MT-HVDC systems. This is possible thanks to the DC-DC converters studied in this chapter include an AC stage, and therefore there exist instants in which the current passes through zero, and consequently we can open the switches when a fault occurs in the network in a safer way.

What is proposed in this section 2.6 is a new concept, which try to take advantage of the DC/DC converter, employing the internal alternative state of the current and the zero crossing of it. This fact presents some advantages with respect to other DC-CB proposed in the literature. For example in [82, 83], the current is cut off with non zero values, in [84] a combination of electrical and mechanical devices is suggested, where a lightning rod is placed with the purpose to dissipate the excess energy in the system when a short circuit occurs.

From the point of view of security and reliability in a network, any protection system, AC or DC, must have the following properties according with [85, 86]: it should detect every fault, it must be selective and fast enough to interrupt faults before they may damage the equipments. And also, after the fault clearance, it must be capable to leave in secure state

operation the remain part of the system. These general principles have consequences on each element of the detection and action chain. Therefore, it is clear that they also determine the MT-HVDC grid behaviour. For instance, if we desire that each DC line will be cleared when a fault occurs, therefore put two DC-CB in each side of the line could be a solution in order to isolate each line.

It is true that if we introduce many DC/DC converters in the system the total cost is increased, but instead we gain in safety. However, this discussion is beyond the scope of this thesis.

### 2.6.1 DC circuit breaker based on DAB topology.

From the operating point of view, the actuation mode philosophy will be the same when the converter is working as DC-CD for the two phases or three phases DAB. For this reason, in this section we only work with the two phases DAB [9].

### 2.6.2 Simulations for a single converter.

Firstly we study the influence of the short-circuit for a single two phases DAB. It is clear that the converter has two possible behaviours: injecting power mode or absorbing power mode. Both events will be discussed separately. From the point of view of the DC/DC converter, the worst case is when the converter is absorbing energy and the short-circuit appears in the other side of the line (inductive), because in this case there is more energy fed into the system, and it is more difficult is its dissipation.

The main idea of this section is that as we can control the current in the converter, then we could drive gradually it to zero and thus dissipate the fault in a more optimal way. This study was carry out using the software SIMetrix/SIMPLIS®. For a single converter shown in figure 2.38, their values are in table 2.15.

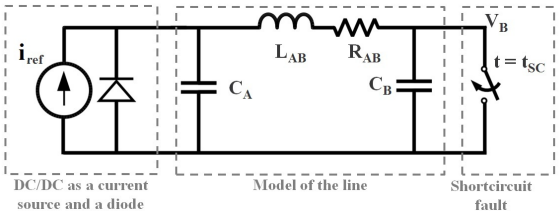


Figure 2.38: Line short-circuit model.

Table 2.15: Simulation values when short-circuit appears. DAB converter.

| | | |
|---|---|---|
| $V$ | Nominal voltage | 1000 V |
| $R_{AB}$ | Cable resistance | 0.0121 Ω/km |
| $L_{AB}$ | Cable inductance | 0.121 H/km |
| $C_{AB}$ | Cable capacitance | $1 \cdot 10^{-6}$ F/km |
| $l_{line-AB}$ | Length line AB | 160 km |
| $f_S$ | Switching frequency | 2000 Hz |
| $\tau_{line}$ | Time constant of the line | 40 s |

### Absorbing power mode

This is the worst case because the diodes are not conducting due to the direction of the current, and therefore any current passes through them, and it passes through the capacitors. In this situation we propose studying three different actuation modes in order to react when a short-circuit fault appears.

1) When fault is detected, set current reference to zero immediately.

When short-circuit fault occurs, and if $i_{ref}$ is set to 0 immediately, the current stored in the inductor can only flow through the capacitor $C_A$, and consequently it causes an over-voltage (around 120 kV) as figure 2.39 shows . We can also appreciate as the current varies much faster than the time constant of the line.

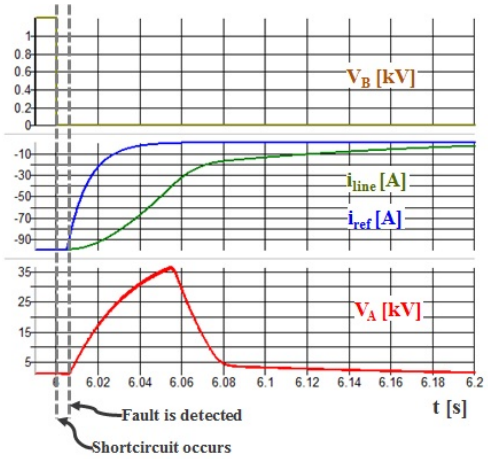


Figure 2.39: Current line and voltage in absorbing mode with over-voltage.

The advantages of this method are that we can open the line in 200 $ms$ (for this data), the energy can be recycled and the normal operation control of the semiconductors does not vary when the fault appears. However a drawback is that the output capacitor must be oversized.

2) When fault is detected, slowly take current reference to zero with the time constant of the line.

The idea with this philosophy is that as we know the current line dynamic (in the worst case), we could apply a reference with this dynamic as shows figure 2.40a. It is clear that when the converter is consuming power and a short-circuit fault occurs, if $i_{ref}$ is reduced to 0 with a slow slew rate, the voltage in $C_A$ does not rise. Also we can observe that the power is dissipated in 40 $s$. In the figure 2.40b a zoom for the first instants of the short-circuit is shown. We observe as the voltage in $C_A$ discharges automatically in approx $1ms$. This is because, just after the short-circuit occurs as $V_A > V_B = 0$, and $i_{line}$ increases by taking current from $C_A$, discharging it.

The advantages of this method are: the normal operation control of the semiconductors does not vary when the fault appears and there is not over voltage in the capacitor, since it does not resonate with the line. However two important drawbacks appear: we need 40 $s$ to open the line and the line energy is lost during the transient in the line resistances. From the point of view of the safety of a electrical system 40 $s$ is an unacceptable value.

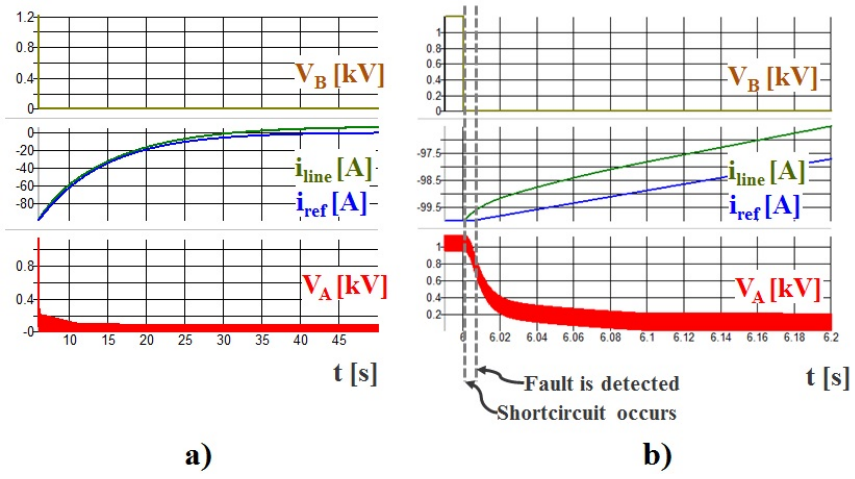


Figure 2.40: a) Current line and voltage at node A in demanding mode without over-voltage. b) zoom.

3) When fault is detected, put the secondary in short-circuit.

Another possible solution is to short-circuited the part of DAB nearest to fault, as figure 2.41 shows.

The advantage of this philosophy is that control is not necessary. However we need 40 $s$ to open the line and the line energy is lost during the transient in the line resistances as happens in the previous case, and also, the short-circuit causes a current surge in the output capacitor as figure 2.42b shows.

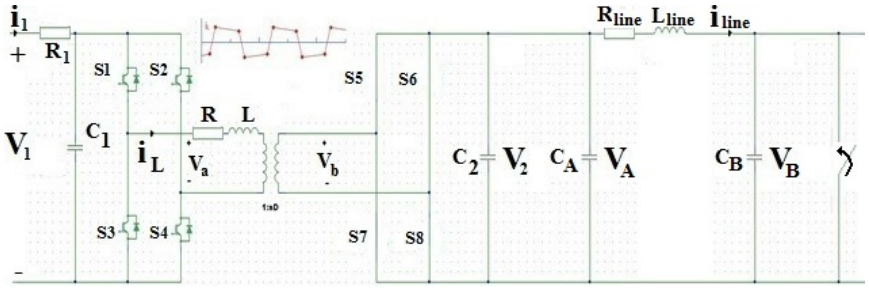


Figure 2.41: Secondary side of DAB in short-circuit.

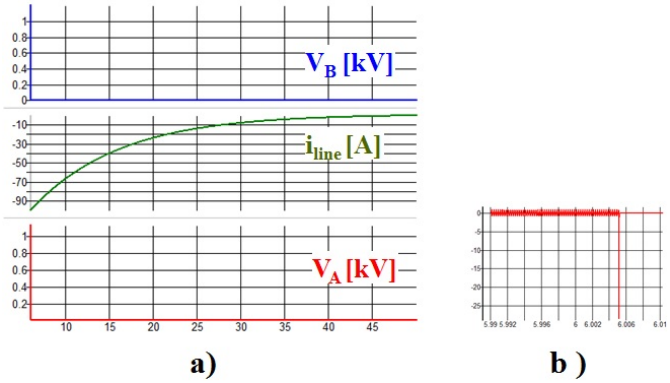


Figure 2.42: a) Current line and voltage at node A in demanding mode without over-voltage. b) Voltage capacitor zoom.

In conclusion the best philosophy from the electrical safety point of view is the first, that is, when fault is detected, set current reference to zero immediately.

### Injecting power mode.

This functioning mode should not produce important damages in the devices, due to the diodes of the IGBTs are conducting, and they are able to withstand high currents. However we have studied the behaviour of this mode of operation.

When the converter is producing power and a short-circuit fault occurs, if $i_{ref}$ (the current converter reference) is set to 0 immediately, the current stored in the inductor flows through the diodes of the switches and dissipates in 40 $s$, as shown figure 2.43. Note that over-voltage does not appears in voltage $V_A$, and this is because there exist diodes in the converter (it is required to size them correctly, in a way that they could support that current).

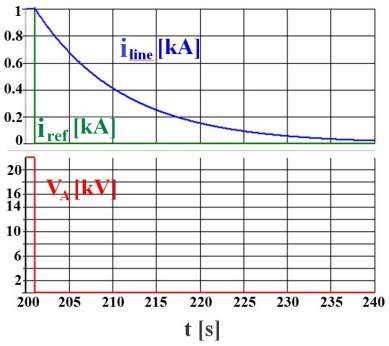


Figure 2.43: Current line and voltage at node A in injecting mode.

### 2.6.3 DC circuit breaker based on MMC topology.

With the same principle than the DAB but with a different idea, we will operate the MMC. Since in this topology there are hundreds of sub-modules in series (see figure 2.28), and as each sub-module is composed of capacitors and IGBTs (with their respective diodes), then the energy, which appears when a short-circuit happens, could be distribute among those sub-modules. This is because diodes are capable of supporting high currents. Evidently, we have supposed that short-circuit appears in the DC side, because if it arises in the AC side, there exits mature technical solutions for these kind of problems.

Considering the above explanation, it is clear that the key elements are the sub-modules. Typically there are two different types: the half bridge and the full bridge as figures 2.44a and 2.44b show. In this section,the two approaches will be studied and analysed.

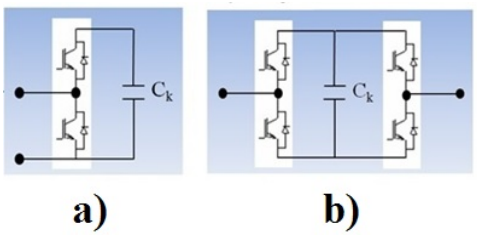


Figure 2.44: a) Half bridge b) Full bridge.

#### DC circuit breaker based on MMC topology with half bridge cells.

In a first approach we will assume that the short-circuit occurs close to the converter, always in the DC side. Therefore the effect of the energy stored in the DC line may be neglected.

In this situation the local current sensors of the converter detect that there exits a high variation in the current due to short-circuit and the control orders to open all the switches as figure 2.45a shows. We have only shown two phases for the MMC converter because the phenomena for the others pairs will be the same. Two different situation can arise: positive AC voltage polarity or negative.

When the short-circuit appears, if the polarity of the AC grid is positive, then the upper arm of phase A and the lower arm of phase B are short-circuited as figure 2.45b shows. When the AC voltage is negative, as the capacitors are charged each one at the total voltage of the DC grid divided by the total number of sub-modules per arm, see equation (2.160), and the sum of all of them is higher than the peak value of the AC voltage, then the capacitors in the upper and lower arms are connected as figure 2.45c shows. Consequently we can see this phenomenon as all capacitors are connected in series as figure 2.46 shows. As the total voltage of the capacitors is higher than the AC peak voltage, then the current can not circulate and the short-circuit is mitigate. On the other hand, it is import to realize that the diodes impede the discharge of the capacitors.

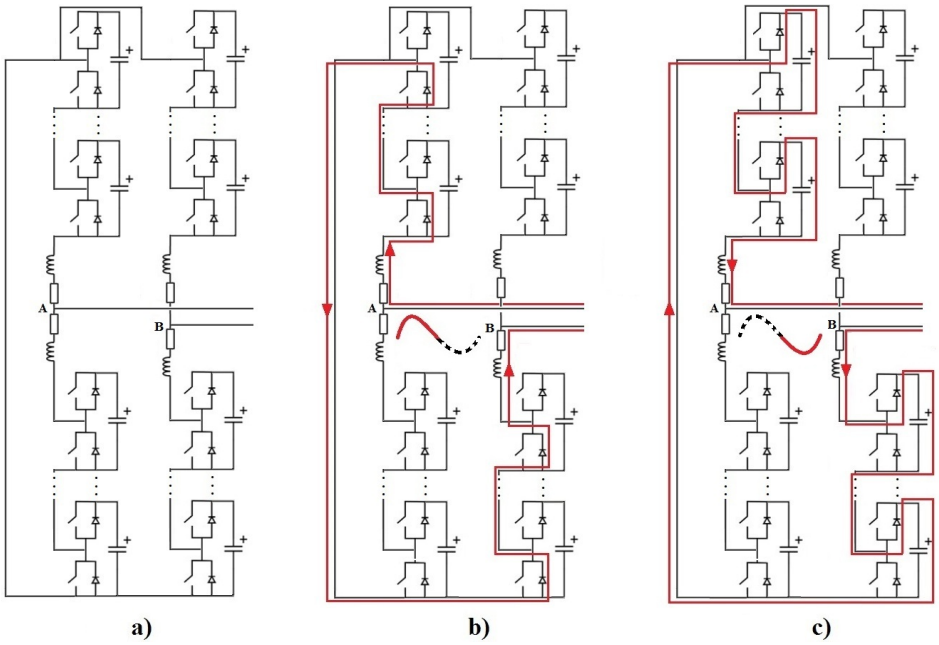


Figure 2.45: a) Half bridge short-circuit operation b) positive AC voltage c) negative AC voltage.

In conclusion the MMC topology based on half bridge cells can not be used as DC-CB since in the positive polarity of AC voltage the the short-circuit is not impeded.

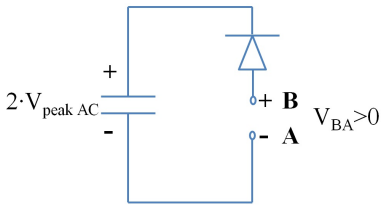


Figure 2.46: Negative AC voltage. Equivalent model.

**DC circuit breaker based on MMC topology with full bridge cells.**

Thanks to the inclusion of the full bridge instead of the half bridge, we can achieve that the capacitors do not let pass the short-circuit current for both AC voltage polarities, due to they are connected in series with a charge higher than the AC peak voltage.

In figure 2.47b the current behaviour is shown for the positive cycle. We can appreciate as the current direction is from AC source towards DC. In figure 2.47c the negative cycle is shown. We can observe as the current direction is from DC fault towards AC side.

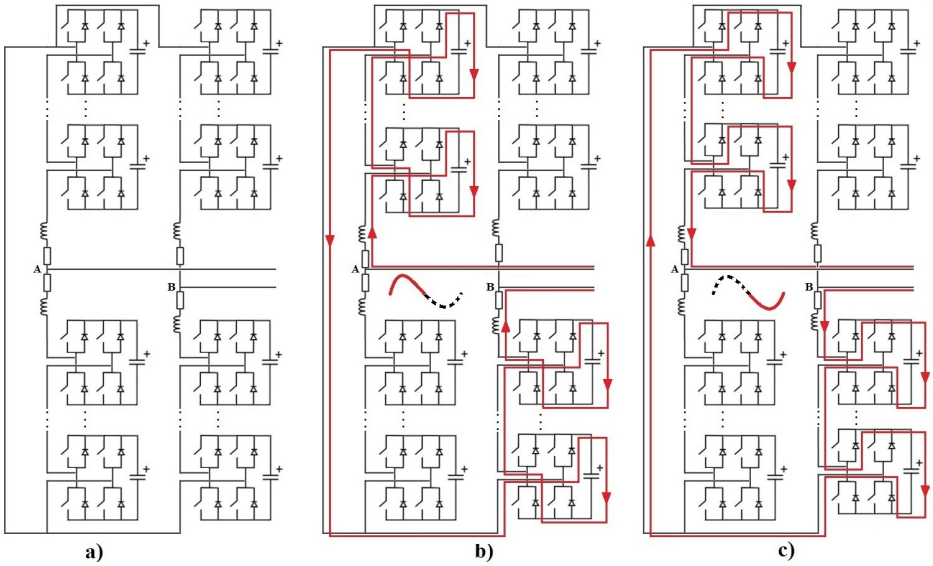


Figure 2.47: a) Full bridge short-circuit operation b) positive AC voltage c) negative AC voltage.

Due to the sum of the voltages of all capacitors in series is always twice the peak value of the AC voltage, it would be enough to put half of the modules full bridge and the other half with half bridge cells, in order to reduce the price of costs and the number of needed signals to control the IGBTs.

**Results (with full bridge cells).**

In order to show the phenomenon explained in section 2.6.3 a two phases MMC with full bridge sub-modules is tested in MATLAB-SIMULINKk® as figure 2.48 shows. The short-circuit at $t = 2\ s$ is simulated in DC side, and a DC line have been also considered (see parameters in table 2.16).

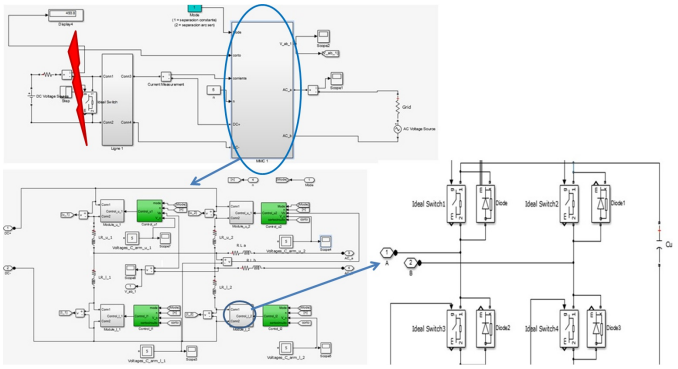

Figure 2.48: SIMULINK® file. Short-circuit in MMC with full bridge cells.

In figure 2.49a the AC current is shown. We can appreciate as when the short-circuit appears, the AC current keeps at 0 A, because the diodes do not let pass the short-circuit current, and consequently the AC side is isolated. We can identify much better this phenomenon in figure 2.49b.

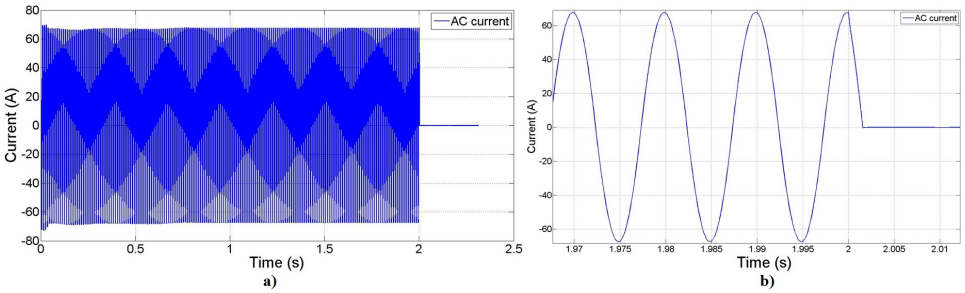


Figure 2.49: a) AC current. Short-circuit in MMC with full bridge cells. b) Zoom.

In figure 2.50 we observe as the DC current increases until 520 A due to short-circuit, and unfortunately the short-circuit is not mitigated in the DC side. However, if another MMC converter is implemented in the other side of the DC line, the problem only remains in this line, and then it will be isolated in a selective way and it will be dissipated by the resistances of the DC line.

In figure 2.51a the voltage of capacitor in the upper arm of phase 1 are shown. We observe as the after the fault they are in equilibrium close to 1 $kV$, and before they remain in a constant value, which is the value

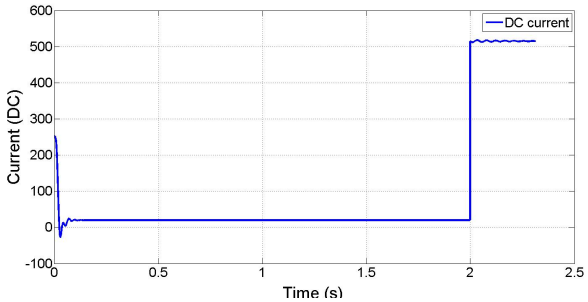


Figure 2.50: DC current. Short-circuit in MMC with full bridge cells.

explained in section 2.6.3 which is the peak value (divided by the total number of sub-modules per arm) of the AC voltage (1 $kV$). In figure 2.51b this phenomenon is shown with more detail.

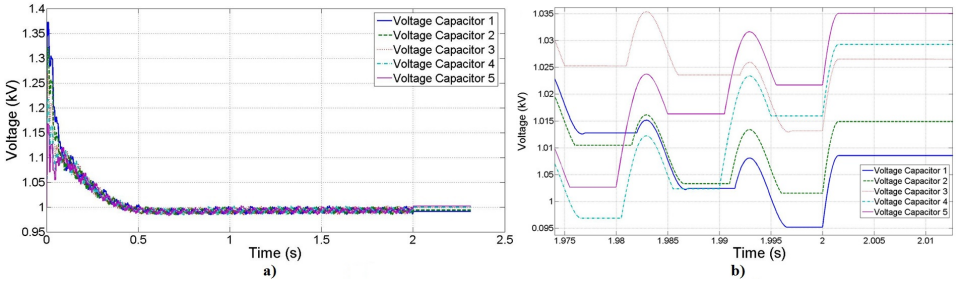


Figure 2.51: a) Capacitor voltage. Short-circuit in MMC with full bridge cells. b) Zoom.

Table 2.16: Two phases MMC converter. Simulation values when short-circuit appears.

| | | |
|---|---|---|
| $V_{DC,nom}$ | Nominal DC voltage | ±5 kV |
| $R_{line}$ | Resistance DC line | 0.01 Ω |
| $L_{line}$ | Inductance DC line | 0.001 $H$ |
| $C_{line}$ | Capacitance DC line | 0.1 $F$ |

## 2.7 Conclusions.

In this chapter three different topologies for DC/DC bidirectional converters suitable for MT-HVDC systems, as well as their different non-linear controls have been explained, detailed and verified by simulation for each of them.

The modelling and control of two phases DAB converter have been proposed. A discussion for different types of modulations is also addressed. A

non-linear robust control law is derived based on Lyapunov theory. The obtained control algorithm has been tested in closed-loop. Simulation results have been presented to highlight the good performances of the proposed control algorithm.

With respect to the three phases DAB; two viewpoints have been addressed and compared. Due to the intrinsic nature of this type of converters, the problem leads to a bilinear approach in a natural way, therefore a solution supported by bilinear theory has been presented. As the system is not completely actuated, a solution for the actuated subsystem has been developed. In a second step a non-linear control has been developed. A detailed stability analysis of the *zero dynamics* shows that our system is exponentially stable. Both control algorithms provide suitable results in simulations, so both will be considered for subsequent test bed experimentations.

A multi-terminal DC/DC converter with $k$ phases and $n$ terminals has been discussed using MMC technology. A mathematical proof based on switching systems theory is given in order to guarantee the stability of the system. Although the proof is valid for any values of DC voltages, in a real implementation the voltage relations between DC sides will most likely be small in order to keep small losses. Anyway, and thanks to the simulations we can conclude that the proposed control is valid for the use of these types of converters. In addition, a study on how to improve the harmonics in the generated signals for this topology is shown, and also a balancing philosophy is implemented in order to favour the use of capacitors in each module in a well-adjusted way.

Each one of the topologies studied in this chapter have advantages and inconvenients, as table 2.1 summarizes. The use, or not, of a topology is relative, and it depends on the application.

At first glance the converter which gives better performance and possibilities of operation is the topology based on MMC technology, because the resulting waveform has a very small harmonic content and it has reduced transient voltage stresses and hence lower high frequency noise [19]. Also it is able to operate at lower switching frequencies, it has the ability to continue its operation in unbalance conditions [20], and finally the internal transformer is avoided. But its control is much more difficult to implement, due to it uses much more semiconductors. For this reason, for simpler applications, it could be interesting to use topologies based on DAB converters.

As a complement, a new application for DC/DC bidirectional converters has been developed. It is the use of the converters as DC-CB due to its internal AC step. Different control philosophies have been addressed under unbalanced conditions, in order to show their behaviour. It is a new concept which can achieve that MT-HVDC networks will be safer and it could be capital for the implementation of MT-HVDC networks.

Chapter 3

# Primary control

## 3.1 Chapter introduction.

All electrical system, DC or AC, requires the implantation of a control in order to ensure its proper operation. As we have explained in section 1.1, a possible solution for MT-HVDC systems could be an hierarchical control strategy in resemblance to classic hierarchical AC control [15], which includes local, primary, secondary and tertiary control, each one with different time scales. Inside this hierarchical classification, it is clear that the primary control must be able to generate the appropriate reference signals for the local controllers and it has to follow the references that the secondary control imposes him.

In this chapter the primary control of a MT-HVDC is addressed. When an AC network is disturbed by imbalances between load and generation or when a line problem appears (shorts-circuits for example), the frequency, which is the global variable of the system, changes homogeneously throughout the circuit, responding to a power and/or voltage variation in the nodes. When that occurs, the primary control try to stabilize the frequency of each node in a local actuation way. Otherwise, in DC systems there is no frequency, not even a global variable already acknowledged, but we can also define the basic functions that our primary controller must be able to carry out when a disturbance appears.

From the point of view of safety and reliability of operation, the correct operation of a MT-HVDC system requires a proper coordination of voltage-power or voltage-current regulations. On this basis, in MT-HVDC systems the primary control operates in a time range of seconds [24].

In this chapter we have studied several control philosophies: master/slave, voltage margin control and droop control [25] in order to regulate the voltage-power or voltage-current relations. Finally we have choose to use droop control philosophy, among other reasons, because the communication between nodes is not required. Such primary control mechanism is often implemented through the droop control. Other authors, as [87, 88], consider that in the droop control there exists communication between nodes, and consequently some advantages could be achieve: as operate in optimal points. This is a different point of view, however in this thesis, we consider that the communication only exists in the next level, the secondary control.

Even though this is a standard strategy in AC systems, this is still an

open problem to DC networks. In this chapter we try to formalize the droop control. With this purpose two different approaches have been studied for the droop control. Firstly, we have considered that dynamics of converters (AC/DC) are negligible and thus we considered it as ideal current sources. Subsequently, we have studied the dynamics of converter and droop control together, and thanks to *singular perturbation* theory, see [38, 89, 90], we could establish under which conditions we can separate both dynamics. For the sake of simplicity, the converters used have been the VSC [91, 17], although if we chose MMC technology (see section 2.5), the reasoning will be similar.

## 3.2 DC voltage control strategies.

In this section, three different strategies proposed in the literature will be discussed: master/slave, voltage margin control and droop control.

### Master/slave control.

The operation of this type of strategy is well defined by its name. There is one node responsible for maintaining the voltage level of the entire network (master), while the others are responsible for controlling the absorption or insertion of power, by means of adapt its DC voltage values (slaves). The master node must be able to absorb or provide sufficient active power to achieve a power balance in the DC system [26]. Consequently, it adapts the output power in order to compensate all the losses in the system. This node has to be connected to a strong node in the AC system and must have sufficient DC power rating. In addition, an outage of this converter cannot be tolerated because it will entail the losing the DC voltage control, which is a great drawback. Other important inconvenient is that, suboptimal operation points could be achieved with this strategy [27].

In figure 3.1 a DC power/DC voltage characteristic for the master node is shown.

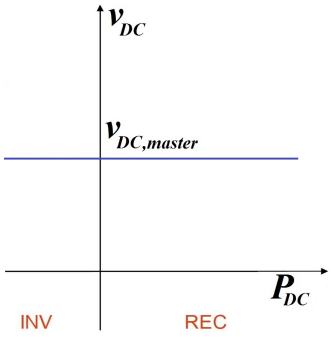


Figure 3.1: Power/voltage characteristic for the master node in master/slave.

In figures 3.2a and 3.2b the DC power/DC voltage characteristic for the slave nodes, absorbing and injection mode respectively, are shown.

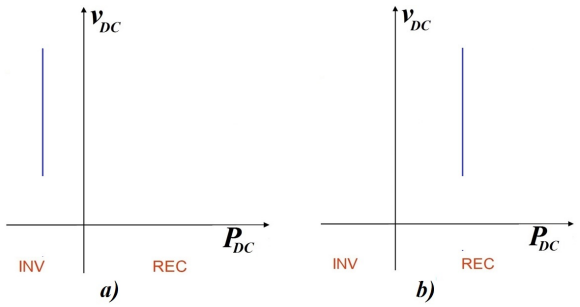


Figure 3.2: Power/voltage characteristic for the slave nodes.

If instead we operate with the DC current/DC voltage pair, the equivalent of figures 3.2a and 3.2b will be figures 3.3a and 3.3b for absorbing and injection mode respectively, where we can observe clearly that they follow a hyperbola, due to the current voltage products, which is the power in the figures 3.2a and 3.2b, must to be constant.

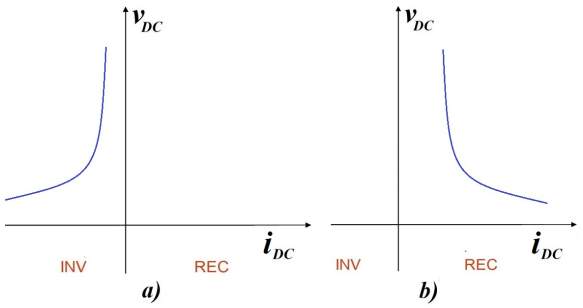


Figure 3.3: Current/voltage characteristic for the slave nodes.

**Voltage margin control.**

This philosophy can be summarized in that it is the same as previous but the master node is changing along the time when it reaches its limits. Consequently, it passes the responsibility to maintaining the voltage of the grid to other terminal.

As in the previous case, their characteristics could be expressed in terms of DC power/DC voltage (figure 3.4) or DC current/DC voltage (figure 3.5)

The drawbacks of this method are several. Firstly, only one converter is responsible to control the DC voltage at a given time. Otherwise, in a MT-HVDC network with a high number of nodes, the DC voltage is limited by $\pm 10\%$ of the nominal voltage, limiting the amount of converter that could

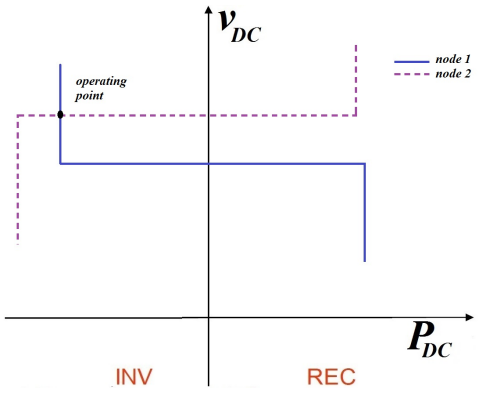


Figure 3.4: Power/voltage characteristic for the voltage margin control.

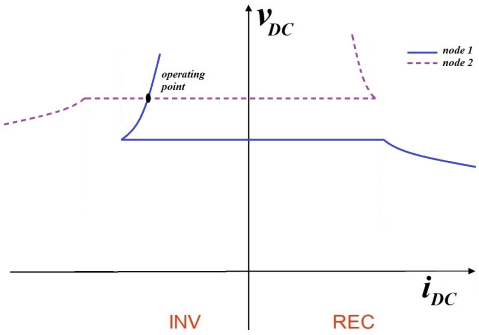


Figure 3.5: Current/voltage characteristic for the voltage margin control.

participate in this distributed DC voltage control strategy. And finally, suboptimal operation points could be achieved also with this strategy [87].

**Droop control.**

The philosophy of droop control technique is that several network nodes share out the responsibility to maintain the DC voltage of the grid at the same time.

Droop control is distributed and decentralized, and it employs the droop mechanism to regulate the DC voltage adapting the power injections or absorptions in nodes. Droop control reacts to a power imbalance, and it can be explained as follows. When there is a power variation in the grid, the nodes will adjust the amount of power via droop control who will adjust their voltages, see figure 3.6.

This control is a set of local proportional controllers with gain $k$, called *droop gain*. This local $k$ value is also the slope of the line in figure 3.6. This value in general depends on the size of each node's reserve, and it gives an idea of how much power provides each node when a variation occurs, in

function of its capabilities.

It is not necessary that droop control will be implemented in all nodes of the network, indeed, it is often implemented in nodes where exist energy reserves. A very important characteristic is that as it is a robust decentralized controller, communication is not necessary between nodes in MT-HVDC applications. From the point of view of control, droop control can be seen as a state feedback limited to local measurements, and it will give the DC voltage reference for the local controller. Each $k$ will be designed in a global way, such as to attain stability of the whole system, but will act in a local way.

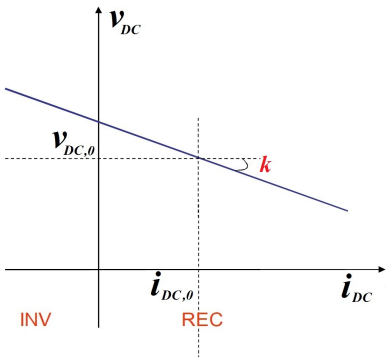


Figure 3.6: Droop control.

Each droop controller is simply expressed as:

$$i_{DC,0} = i_{DC} + k \cdot (v_{DC} - v_{DC,0}) \tag{3.1}$$

where $i_{DC,0}$ and $v_{DC,0}$ are initial points given by the power flow done in the secondary control (see chapter 4), $i_{DC}$ is the local current measurement, $v_{DC}$ is the DC voltage reference for the local controllers and $k > 0$ is the droop gain.

## 3.3 Droop control with VSC as current sources.

In this section, we will study the droop control without taking into account the dynamics of the local controllers, in an analogous form as [92, 93]. If we consider that the dynamics of current converter are much faster than the voltage, then equation (3.1) could be simply expressed as:

$$i_{DC,0} = k \cdot (v_{DC} - v_{DC,0}) \tag{3.2}$$

### 3.3.1 Multi-Terminal HVDC grid

Before to study in depth the droop control, we must define the state variables involved in the model. According to [93], a MT-HVDC network can

be represented as the interconnection of nodes and branches. The nodes come in three different forms: injection nodes (or power-input nodes), consumption nodes (or power-output nodes) and interconnection nodes. As we have neglected the internal dynamics of the converters, consequently the external grids (AC or DC) are modelled as current sources. Furthermore, the internal branches are modelled by $\pi$-equivalent circuits. Therefore, a general configuration of a MT-HVDC is shown in figure 3.7

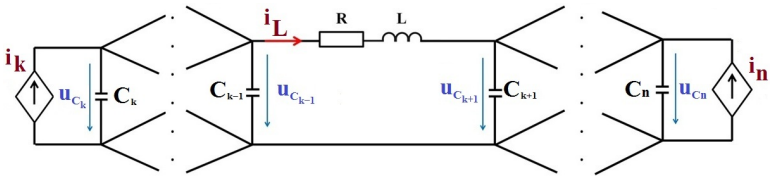


Figure 3.7: General configuration of a MT-HVDC network.

With this configuration adopted, the behaviour of any MT- HVDC grid can be described only in terms of capacitors, inductances, resistances and current sources. Thus it is possible to find a linear state-space representation, where the state variables are the voltages in the capacitors and the currents through the inductances, and the inputs are the currents on the sources.

As we have already mentioned, droop control is not applied in all nodes, it is usually implemented in nodes which have spare energy (usually called primary reserve). For example, if an external grid is a large AC network, then it can inject or absorb power with less restrictions, and it is more natural to implement the droop there. Even more if other nodes are connected to grids with high variability, as for example renewable energy nodes.

After all the aforesaid, the inputs could be divided in two sets. In the first set $u$ are the variables that can be used to control the system (nodes where there is droop control), and in the other set, $w$, there are the variables that are not possible to manipulate (nodes where there is no droop control). These last variables could also be treated as external disturbances. In the same way we split the output in two sets. One set contains the variables that can be used in the control ($v$), and the other contains the variables that are not employed by the controller ($y$).

If the system has $i$ injection nodes, $j$ consumption nodes, $p$ interconnection nodes and $l$ branches, the state-space is defined as:

$$\begin{cases} \dot{x} = Ax + B_u u + B_w w \\ v = C_v x \\ y = C_y x \end{cases} \tag{3.3}$$

where:

$$\begin{aligned} &x = [u_{C_1}, \cdots, u_{C_{i+j+p}}, i_{L_1}, \cdots, i_{L_l}]^T \\ &A \in \mathbb{R}^{(i+j+p+l)\times(i+j+p+l)} \\ &B_u \in \mathbb{R}^{(i+j+p+l)\times i} \\ &B_w \in \mathbb{R}^{(i+j+p+l)\times j} \\ &C_v \in \mathbb{R}^{i\times(i+j+p+l)} \\ &C_y \in \mathbb{R}^{j\times(i+j+p+l)} \end{aligned} \tag{3.4}$$

where $u_{C1}, \cdots, u_{C_{i+j+p}}$ are the voltages in the capacitors, and $i_{L_1}, \cdots, i_{L_l}$ are the currents through the inductances.

It should be noted that the size of matrix $B_u$, $B_w$, $C_v$ and $C_y$ could be changed if the droop controllers are applied in other nodes than injection nodes. But the most common case is the proposed one.

As our state variables are the currents through the lines (inductances) and the voltages in the nodes (capacitors), the matrix $A$ has always, whatever the topology, a special configuration which gives us important properties in order to study the stability. With $x$ defined in 3.4, matrix A in open loop has the form shown in equation 3.5:

$$A = \begin{bmatrix} D & -C^{-1} \cdot H^T \\ L^{-1} \cdot H & -L^{-1} \cdot R \end{bmatrix} \tag{3.5}$$

where matrices $R = diag(R_1, .., R_l)$, $L = diag(L_1, .., L_l)$ with $R_i$ and $L_i$ $\forall i \in \{1, .., l\}$ the resistance and inductance respectively in each branch, and matrix $C = diag(C_1, ..., C_n)$ with $C_j$ $\forall j \in \{1, .., n\}$ the capacitors in each node respectively (note that $n = i + j + p$). As all values are positive then $R, L$, and $C$ are positive definite matrices. On the other hand, if we are in open loop, it is always true that $D$ is a zero square matrix of order $n$ (this is easy to verify applying Kirchhoff's circuit laws).

$H \in \mathbb{R}^{l\times n}$ has the special form explained as follows. As two nodes are connected by a line, then in each row of $H$ appears only two non zero elements, which have opposite signs, 1 or -1 depending on the direction chosen for the current. Also if the line connects nodes $k$ and $r$, these non-zero elements appear in the columns $k$ and $r$ of this row. Consequently, it is clear that $H$ has as many rows as electric lines. On the other hand, we see that due to the duality of electrical systems, there is also a special form in the anti-diagonal of $A$. This means that the lower side is composed by the term $L^{-1}H$ and in the upper by $-C^{-1}H^T$.Therefore, in the upper side appears the opposite of the transpose of $H$.

We must note that the matrix $H$ is not exactly the incidence matrix of graph theory [94], because although both matrices have the same structure, that means, the non zero elements appear in the same position for both matrices, the incidence matrix has only positive (one) or zero elements, and matrix $H$ has also negative (minus one) elements. But obviously, matrix $H$ contains the information about the topology of the MT-HVDC grid.

### 3.3.2 Stability of droop control neglecting VSC dynamic

Taking into account above explanations and system equations 3.3, we can implement a particular state feedback. If we take:

$$u = K \cdot (v - v^*) \tag{3.6}$$

in system 3.3, we obtain a closed loop matrix $A_{cl} = A + B_u \cdot K \cdot C_v$, where $K \in \mathbb{R}^{i \times i}$, is the droop control matrix (diagonal) composed by $k_i$, the local droop gains, in its diagonal. To ensure the stability of the whole system, all eigenvalues of $A_{cl}$ must have negative real part. From equation 3.1, it is clear that matrix $K$ has dimensions of admittance, so in each node the droop control can be interpreted as a passive admittance. For this reason, to apply a droop control is similar to add energy dissipation to the system and, therefore, the whole system will be always stable for $K$ positive semi-definite, or in other words, if some elements $k_i$ of $K$ is positive ($K$ is always diagonal) the whole system will be always stable .

Since the *droop matrix* is a diagonal matrix, feedback acts only on the diagonal elements of the sub-matrix D defined in 3.5. So the closed-loop matrix $A_{cl}$ can be defined as:

$$A_{cl} = \begin{bmatrix} D_{cl} & -C^{-1} \cdot H^T \\ L^{-1} \cdot H & -L^{-1} \cdot R \end{bmatrix} \tag{3.7}$$

where $D_{cl} = diag(\delta_1, .., \delta_n)$ with $\delta_i = -k_i \leq 0 \ \forall i = 1, .., n$ with at least one smaller then zero (where the droop exists). With all of these premises we can study the stability of the system.

***Lemma* 4** *Let $n, l \in \mathbb{N}^*$, $D \in \mathbb{C}^{n \times n}$, $P \in \mathbb{C}^{l \times l}$, $H \in \mathbb{C}^{l \times n}$, $M \in \mathbb{C}^{n \times l}$ and*

$$A = \begin{bmatrix} D & M \\ H & P \end{bmatrix} \in \mathbb{C}^{n+l \times n+l},$$

*it holds that:*

$$if \ \exists \ P^{-1}, then \ |A| = |P| \cdot |D - M \cdot P^{-1} \cdot H|$$
$$if \ \exists \ D^{-1}, then \ |A| = |D| \cdot |P - H \cdot D^{-1} \cdot M|$$

***Proof.-***
Let A be equals to:

$$A = \begin{bmatrix} D & M \\ H & P \end{bmatrix} = \begin{bmatrix} D - MP^{-1}H & M \\ 0 & P \end{bmatrix} \cdot \begin{bmatrix} I & 0 \\ P^{-1}H & I \end{bmatrix} =$$
$$= \begin{bmatrix} D & 0 \\ H & P - HD^{-1}M \end{bmatrix} \cdot \begin{bmatrix} I & D^{-1}M \\ 0 & I \end{bmatrix} \ \square$$

***Lemma* 5** *Let $n, l \in \mathbb{N}$ such that $n \geq 2$ and $l \geq n-1$, $P \in \mathbb{R}^{l\times l}$ positive definite, $D = diag(\delta_1, ..., \delta_n) \in \mathbb{R}^{n\times n}$, $D_k = diag(0, ..0, \delta_k, 0.., 0) \in \mathbb{R}^{n\times n}$, $H = [H_1|...|H_n] \in \mathbb{R}^{l\times n}$, such that $H_1, ..., H_n$ are linearly dependent, and $\exists k \in \{1, .., n\}$ such that $H_1, ..., H_{k-1}, H_{k+1}, ...H_n$ are linearly independent, it holds that:*

*a) $H^TPH$ is positive semi-definitive of rank $n-1$.*

*b) If $\delta_k > 0$, then $D_k + H^TPH$ is positive definite and consequently $|D_k + H^TPH| > 0$.*

*c) If $\delta_k > 0$, and $\forall j \in \{1, .., n\}$ $\delta_j \geq 0$, then matrix $D + H^TPH$ is positive definite and $|D + H^TPH| > 0$.*

***Proof.-***

The matrix $H^TPH = G(H_1, ..., H_n) \in \mathbb{R}^{n\times n}$ is the Gram matrix of columns of H with the dot product defined by P, so it is at least positive semi-definite with rank: $rank(G(H_1, ..., H_n)) = rank(H) = n-1$.

As $H_1, .., H_{k-1}, H_{k+1}, H_n$ are linearly independent, then it is true that $G(H_1, ..., H_{k-1}, H_{k+1}, H_n)$ is positive definite.

Moreover if $j \in \mathbb{N}$, with $1 \leq j \leq n-1$ and $i_1, i_2, ..., i_j \in \mathbb{N}$ such that $1 \leq i_1 < i_2 < ... < i_j \leq n-1$, then all the matrix composed by the rows $i_1, i_2, ..., i_j$ and the columns $i_1, i_2, ..., i_j$ of $G(H_1, ..., H_{k-1}, H_{k+1}, ...H_n)$ are the Gram matrix of columns $H_{i_1}, H_{i_2}, ..., H_{i_j}$ and therefore they are positive definite and their determinants are positive.

If $\delta_k > 0$

$$D_k + H^TPH = \begin{bmatrix} g_{1,1} & \cdots & g_{1,k-1} & g_{1,k} & g_{1,k+1} & \cdots & g_{1,n} \\ \vdots & & \vdots & \vdots & \vdots & & \vdots \\ g_{k,1} & \cdots & g_{k,k-1} & g_{k,k}+\delta_k & g_{k,k+1} & \cdots & g_{k,n} \\ \vdots & & \vdots & \vdots & \vdots & & \vdots \\ g_{n,1} & \cdots & g_{n,k-1} & g_{n,k} & g_{n,k+1} & \cdots & g_{n,n} \end{bmatrix} \tag{3.8}$$

all its principal minors are positive since if $m \in \mathbb{N}$ it holds that:

1) if $1 \leq m < k$

$$\Delta_m = \begin{vmatrix} g_{1,1} & \cdots & g_{1,m} \\ \vdots & \ddots & \vdots \\ g_{m,1} & \cdots & g_{m,m} \end{vmatrix} = |G(H_1, \ldots, H_m)| > 0 \tag{3.9}$$

2) if $k \leq m \leq n$

$$\Delta_m = \begin{vmatrix} g_{1,1} & \cdots & g_{1,k} & \cdots & g_{1,m} \\ \vdots & & \vdots & & \vdots \\ g_{k,1} & \cdots & g_{k,k}+\delta_k & \cdots & g_{k,m} \\ \vdots & & \vdots & & \vdots \\ g_{m,1} & \cdots & g_{m,k} & \cdots & g_{m,m} \end{vmatrix} =$$

$$= |G(H_1, \ldots, H_m)| + \delta_k \cdot |G(H_1, \ldots, H_{k-1}, H_{k+1}, \ldots, H_m)| \tag{3.10}$$

as both determinants are positive then $\Delta_m > 0$. Therefore, as $D_k + H^T PH$ is a positive definite matrix, it is true that $|D_k + H^T PH| > 0$.

Let be $D'_k = diag(\delta_1, \ldots, \delta_{k-1}, 0, \delta_{k+1}, \ldots, \delta_n)$, that is $D = D_k + D'_k$, if $\delta_k > 0$, and $\forall j \in \{1, .., n\}$ $\delta_j \geq 0$, then $D_k + H^T PH$ is positive definite and $D'_k$ is positive semi-definite, therefore $D + H^T PH = D'_k + [D_k + H^T PH]$ is positive definite and $|D + H^T PH| > 0$. □

***Lemma* 6** *If $A, B \in \mathbb{R}^{n\times n}$ are symmetric, and if $A$ is positive definite, then $A + i \cdot B \in \mathbb{C}^{n\times n}$ is invertible.*

***Proof.-***

If A is positive definite, then $\exists$ $P_1 \in \mathbb{R}^{n\times n}$ which is invertible, such that $\tilde{A} = P_1^T A P_1 = I$.

If B is symmetric $\Rightarrow$ $\tilde{B} = P_1^T B P_1$ is symmetric, consequently $\exists$ $P_2 \in \mathbb{R}^{n\times n}$ which is orthogonal such that $\bar{B} = P_2^{-1}\tilde{B}P_2 = diag(\beta_1, \ldots, \beta_n)$, with $\beta_i \in \mathbb{R}$. Calling $P = P_1 P_2$, $P$ is invertible and $\bar{B} = P^T B P$.

Moreover $\bar{A} = P^T A P = P_2^T P_1^T A P_1 P_2 = P_2^T I P_2 = P_2^{-1} P_2 = I$, that means, $\bar{A} = P^T A P = I$ and $\bar{B} = diag(\beta_1, \ldots, \beta_n)$, and consequently:

$$\left.\begin{array}{c} \bar{A} + i \cdot \bar{B} = P^T (A + iB) P \\ \bar{A} + i \cdot \bar{B} = diag(1 + i\beta_1, .., 1 + i\beta_n) \Rightarrow |\bar{A} + i \cdot \bar{B}| \neq 0 \end{array}\right\} \Rightarrow |A + i \cdot B| \neq 0$$

□

***Theorem* 5** *Let $n, l \in \mathbb{N}$ such that $n \geq 2$ and $l \geq n - 1$,*

*$R = diag(R_1, ..., R_l) \in \mathbb{R}^{l\times l}$ positive definitive,*

*$L = diag(L_1, ..., L_l) \in \mathbb{R}^{l\times l}$ positive definitive,*

*$C = diag(C_1, ..., C_n) \in \mathbb{R}^{n\times n}$ positive definitive,*

*$D = diag(d_1, ..., d_n) \in \mathbb{R}^{n\times n}$ such that $\forall j \in \{1, ..., n\}$ $d_j \leq 0$,*

*$H = [H_1|...|H_n] \in \mathbb{R}^{l\times n}$ such that rank(H)=n-1, that means $H_1, ..., H_n$ are linearly dependent, and $\exists k \in \{1, ..., n\}$ such that $H_1, ..., H_{k-1}, H_{k+1}, ..., H_n$ are linearly independent,*

*And let $A$ be equals to*

$$A = \begin{bmatrix} D & -C^{-1} \cdot H^T \\ L^{-1} \cdot H & -L^{-1} \cdot R \end{bmatrix}, \tag{3.11}$$

*it holds that:*

*1) If D=0, then $|A|$=0 and 0 is a eigenvalue of $A$.*

*2) If $d_k < 0$, then all eigenvalues of $A$ have negative real part.*

***Proof.-***

If $D = 0$, the first $n$ columns of $A$ are linearly dependent, therefore $|A| = 0$ and consequently 0 is an eigenvalue of $A$.

The second part of the proof is as follows, let:

$$\chi_A(\lambda) = |\lambda I - A| = \begin{vmatrix} \lambda I - D & C^{-1}H^T \\ -L^{-1}H & \lambda I + L^{-1}R \end{vmatrix} \tag{3.12}$$

If $\lambda = \alpha + i\beta \in \mathbb{C}$ such that $\alpha = Re(\lambda) \geq 0$ and $\beta = Im(\lambda)$ it holds that:

$$\lambda I + L^{-1}R = diag(\frac{R_1}{L_1} + \alpha + i\beta, ..., \frac{R_l}{L_l} + \alpha + i\beta) = diag(\frac{R_1}{L_1} + \alpha, ..., \frac{R_l}{L_l} + \alpha) + i\beta I \tag{3.13}$$

and due to matrix $diag(\frac{R_1}{L_1} + \alpha, ..., \frac{R_l}{L_l} + \alpha)$ is positive definitive and $\beta I$ is symmetric then using Lemma 6, it is true that $\exists\ (\lambda I + L^{-1}R)^{-1}$, and $|\lambda I + L^{-1}R| \neq 0$, so using Lemma 4:

$$\chi_A(\lambda) = |\lambda I + L^{-1}R| \cdot |\lambda I - D + C^{-1}H^T(\lambda I + L^{-1}R)^{-1}L^{-1}H| \tag{3.14}$$

and, as it is true that:

$$\lambda I - D + C^{-1}H^T(\lambda I + L^{-1}R)^{-1}L^{-1}H = C^{-1}[\lambda C - CD + H^T(\lambda L + R)^{-1}H] \tag{3.15}$$

On the other hand, if we write $\lambda C - CD = \Gamma_1 + i \cdot \Gamma_2$, where:

$$\begin{aligned} \Gamma_1 &= diag((\alpha - d_1)C_1, ..., (\alpha - d_n)C_n) \\ \Gamma_2 &= diag(\beta C_1, ..., \beta C_n) \end{aligned} \tag{3.16}$$

As,

$$(\lambda L + R) = diag(\alpha L_1 + R_1 + i\beta L_1, .., \alpha L_l + R_l + i\beta L_l) \tag{3.17}$$

and consequently,

$$(\lambda L + R)^{-1} = \Lambda_1 + i\Lambda_2, \tag{3.18}$$

where,

$$\begin{cases} \Lambda_1 = diag\left(\frac{R_1 + \alpha L_1}{(R_1 + \alpha L_1)^2 + (\beta L_1)^2}, \ldots, \frac{R_l + \alpha L_l}{(R_l + \alpha L_l)^2 + (\beta L_l)^2}\right) \\ \Lambda_2 = diag\left(\frac{-\beta L_1}{(R_1 + \alpha L_1)^2 + (\beta L_1)^2}, \ldots, \frac{-\beta L_l}{(R_l + \alpha L_l)^2 + (\beta L_l)^2}\right) \end{cases} \tag{3.19}$$

It holds that $\Gamma_1$ is diagonal at least positive semi-definitive, $\Lambda_1$ is positive definitive, and $\Gamma_2$ and $\Lambda_2$ are symmetric, so we can write that:

$$\lambda C - CD + H^T(\lambda L + R)^{-1}H = [\Gamma_1 + H^T\Lambda_1 H] + i \cdot [\Gamma_2 + H^T\Lambda_2 H] \tag{3.20}$$

As $d_k < 0$ and $\forall j \in \{1, ..., n\}\ d_j \leq 0$, it holds that $(\alpha - d_k)c_k > 0$ and also that $\forall j \in \{1, ..., n\}\ (\alpha - d_j)c_j \geq 0$. Moreover $\Lambda_1$ is positive definite, so by Lemma 5, it is true that $\Gamma_1 + H^T\Lambda_1 H$ is positive definite.

On the other hand, $\Gamma_2$ and $H^T\Lambda_2 H$ are symmetric, so $\Gamma_2 + H^T\Lambda_2 H$ is symmetric, and applying Lemma 6 we can conclude that:

$[\Gamma_1 + H^T\Lambda_1 H] + i \cdot [\Gamma_2 + H^T\Lambda_2 H]$ is invertible, and therefore:

$|\lambda I - D + C^{-1}H^T(\lambda I + L^{-1}R)^{-1}L^{-1}H| \neq 0$, that means that if $Re(\lambda) \geq 0$, $\lambda$ is not an eigenvalue of $A$, which is equivalent to affirm that if $\lambda$ is an eigenvalue of $A$, then $Re(\lambda) < 0$. $\square$

**Calculation of K with LQR technique.**

Theorem 5 shows that the system is asymptotically stable if we apply droop control in at least one node. However, it says nothing about the size of $k_i$, the droop gain of node $i$. These gain values can be obtained with LQR methods, because as the droop control can be seen as a state feedback limited to local measurements. They can be optimized by means of optimal control techniques as linear-quadratic regulator (LQR) [95]. LQR strategy has as main advantages its robustness and the possibility to weight different variables of the control inputs and the state vector. This means that the controller will place less or more emphasis on stabilizing a desired variable following physical considerations of the system. This algorithm optimizes the control with respect to a *cost function*, $J$. This function is quadratic, and it is often defined as a sum of the deviations of key measurements from their desired values, and assures a minimum energy consumption to reach the equilibrium point.

Considering the variation respect to equilibrium point in system (3.3) ($x = x^* + \tilde{x}$ and $u = u^* + \tilde{u}$), we obtain:

$$\dot{\tilde{x}} = A\tilde{x} + B_u\tilde{u} \tag{3.21}$$

For an infinite-horizon continuous-time linear system its expression is given by (3.22).

$$J = \int_0^\infty \left(\tilde{x}^T Q\tilde{x} + \tilde{u}^T \mathcal{R}\tilde{u}\right) dt \tag{3.22}$$

where $Q$ is, at least, positive-semidefinite and $\mathcal{R}$ is positive definite.

Therefore, the feedback control that minimizes the value of the cost, function (3.22), is:

$$\tilde{u} = -F\tilde{x} \tag{3.23}$$

where $F$ is given by equation (3.24):

$$F = \mathcal{R}^{-1}B_u^T P \tag{3.24}$$

and $P$ is found by solving the continuous time algebraic *Riccati* equation,

$$A^T P + PA - PB_u\mathcal{R}^{-1}B_u^T P + Q = 0 \tag{3.25}$$

Also it holds that $\lim_{t\to\infty} \tilde{x}(t) = 0$ and $\lim_{t\to\infty} \tilde{u}(t) = 0$, and since,

$$\left.\begin{array}{r} v = C_v x \\ v_{ref} = C_v x^* \end{array}\right\} \Rightarrow v - v_{ref} = C_v(x - x^*) = C_v\tilde{x} \tag{3.26}$$

Taking $u = K(v - v^*)$, then:

$$u = KC_V\tilde{x} \tag{3.27}$$

and therefore $\lim_{t\to\infty} u(t) = 0$, so $u^* = 0$, and consequently $u = \tilde{u}$. Afterwards, from (3.23) we obtain:

$$u = -F\tilde{x} \tag{3.28}$$

and as this two conditions (3.27) and (3.28) hold $\forall\tilde{x}$, then $F = -KC_v$, and from equation (3.24) the droop matrix $K$ holds that:

$$KC_v = -\mathcal{R}^{-1}B_u^T P \tag{3.29}$$

Equation (3.29) shows that, if matrix $K$ is diagonal, then the droop value at each node depends on the value of the node capacitor, this is consistent with the idea expressed in [96].

### 3.3.3 Simulations.

#### Benchmark simulations.

In order to study the implementation of the control scheme neglecting the converter dynamics, a four terminal grid is tested. The model illustrated in figure 4.2 presents its behaviour.

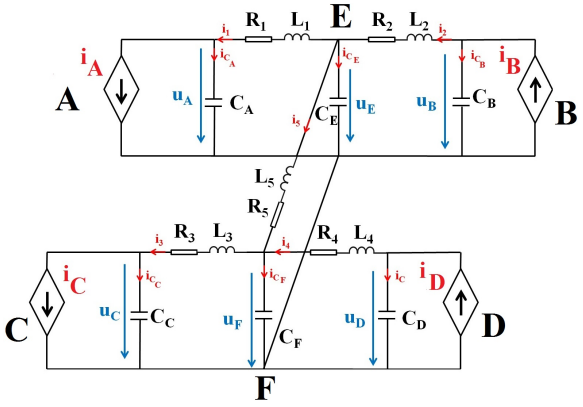


Figure 3.8: General benchmark.

In this model there are two consumptions nodes (A and C), where each one has a droop control, and two injections nodes (B and D) without droop. There are also two interconnection nodes (E and F) and five lines. As explained above, we have considered that the dynamics of converters are much faster than primary control, so external grids are modeled as current sources. Consequently, for this model we can obtain the state-space model shown in 3.3, where:

$$x = [u_A, u_B, u_C, u_D, u_E, u_F, i_1, i_2, i_3, i_4, i_5] \tag{3.30}$$

where $u_A, ..., u_F$ are the DC node's voltage and $i_1, ..., i_5$ are the branch's currents, and:

$$A = \begin{bmatrix} D & -C^{-1} \cdot H^T \\ L^{-1} \cdot H & -L^{-1} \cdot R \end{bmatrix}, \tag{3.31}$$

where $D = \mathbf{0}$,

$$-C^{-1} \cdot H^T = \begin{bmatrix} \frac{1}{C_A} & 0 & 0 & 0 & 0 \\ 0 & -\frac{1}{C_B} & 0 & 0 & 0 \\ 0 & 0 & \frac{1}{C_C} & 0 & 0 \\ 0 & 0 & 0 & -\frac{1}{C_D} & 0 \\ -\frac{1}{C_E} & \frac{1}{C_E} & 0 & 0 & -\frac{1}{C_E} \\ 0 & 0 & -\frac{1}{C_F} & \frac{1}{C_F} & \frac{1}{C_F} \end{bmatrix} \tag{3.32}$$

$$L^{-1} \cdot H = \begin{bmatrix} -\frac{1}{L_1} & 0 & 0 & 0 & \frac{1}{L_1} & 0 \\ 0 & \frac{1}{L_2} & 0 & 0 & -\frac{1}{L_2} & 0 \\ 0 & 0 & -\frac{1}{L_3} & 0 & 0 & \frac{1}{L_3} \\ 0 & 0 & 0 & \frac{1}{L_4} & 0 & -\frac{1}{L_4} \\ 0 & 0 & 0 & 0 & \frac{1}{L_5} & -\frac{1}{L_5} \end{bmatrix} \tag{3.33}$$

and

$$-L^{-1} \cdot R = \begin{bmatrix} -\frac{R_1}{L_1} & 0 & 0 & 0 & 0 \\ 0 & -\frac{R_2}{L_2} & 0 & 0 & 0 \\ 0 & 0 & -\frac{R_3}{L_3} & 0 & 0 \\ 0 & 0 & 0 & -\frac{R_4}{L_4} & 0 \\ 0 & 0 & 0 & 0 & -\frac{R_5}{L_5} \end{bmatrix} \tag{3.34}$$

$$y = \begin{bmatrix} v_B \\ v_D \end{bmatrix}, v = \begin{bmatrix} v_A \\ v_C \end{bmatrix}, u = \begin{bmatrix} i_A \\ i_C \end{bmatrix}, and \;\; w = \begin{bmatrix} i_B \\ i_D \end{bmatrix} \tag{3.35}$$

Where the cost function $J$ is:

$$J = \int_0^\infty \left( \tilde{u}_A^2 + \tilde{u}_C^2 + \tilde{i}_A^2 + \tilde{i}_C^2 \right) dt \tag{3.36}$$

And matrix $K$ has the form:

$$K = \begin{bmatrix} k_A & 0 \\ 0 & k_C \end{bmatrix} \tag{3.37}$$

**Simulations.**

Simulations will be carried out in MATLAB SIMULINK®. It is important to remark also that all simulations have included cable $\pi$ models.

**Assumptions.**

-The system configuration is shown in figure 4.2, in which nodes B and D are producers, and thus they provide power to the nodes A and C, which are consumers. We have assumed that there were enough energy reserves in the system.

- The control droop is carried out in nodes A and C, and there is no droop in production nodes (B ans D).

-The rated power of each node is 3 MW.

-In these simulations we have considered the cables' dynamics.

-Voltage references of primary control have been obtained by secondary level (see chapter 4).

**Network topology.**

The network parameters of system shown in figure 4.2 are summarized in table 3.1:

Table 3.1: Parameters Values.

| | R | L | C |
|---|---|---|---|
| Line 1 | 5.4 Ω | 0.9 H | 1800 $\mu$ F |
| Line 2 | 0.6 Ω | 0.1 H | 1800 $\mu$ F |
| Line 3 | 5.4 Ω | 0.9 H | 1800 $\mu$ F |
| Line 4 | 0.6 Ω | 0.1 H | 1800 $\mu$ F |
| Line 5 | 1.2 Ω | 0.2 H | 1800 $\mu$ F |
| Droop gain | | | |
| $k_A$ | | 0.2 | |
| $k_C$ | | 0.2 | |

**Results.**

In figures 3.9 and 3.10 the voltages and the power in each node are shown respectively. We have assumed that the system was in equilibrium for the initial time. If suddenly, there is a disturbance at node B (t=0.3 s), and supplied power goes from 730 kW to 0, the primary control acts, and it controls the voltages at nodes A and C. This primary control is responsible to stabilize and to keep as close as possible to their references the voltage in nodes A and C while the disturbance occurs, coming from a steady state (a) to (b), that becomes a new equilibrium point. We observe that, by varying the power at node B, the voltage changes in all nodes, and the power of nodes A and C has been adapted to the new situation, reducing their consumption (this is obviously the correct action since there is less power in the network). This adaptation of the voltage levels and power levels has been carried out by the droop control, only based on local measurements.

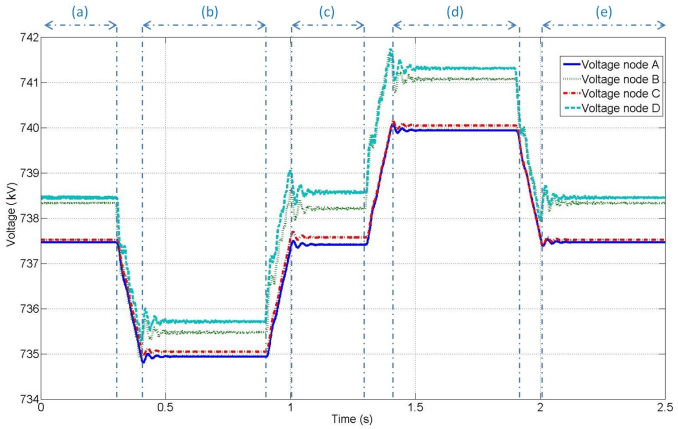


Figure 3.9: Voltage results. Droop control neglecting VSC dynamics.

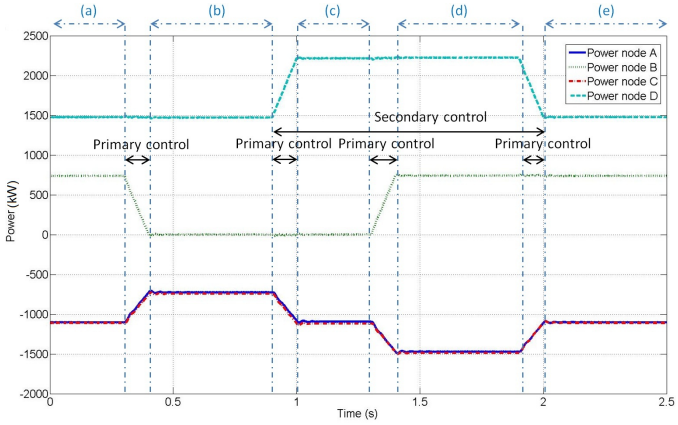


Figure 3.10: Power results. Droop control neglecting VSC dynamics.

It is in this point where secondary control comes into play, which will be explained in chapter 4, but a brief summary is addressed now. This control has a global vision of what is happening in the system. Since it uses communication, it has information about the voltages and powers at all nodes, as well as the state of energy reserves, forecast production and consumption, etc... The objective of this secondary control is to process all this information, and obtain the voltage values, by means of a power flow, which can keep the system stable. These values will serve as references to the droop controllers.

Before the calculations carried out by the secondary, the new voltage references to nodes A and C are 730.5 kV, and we obtained the new equilibrium point, state (c). We can observe that, by varying the voltage references the power are changed in all nodes, except where the perturbation exists (node B). This adaptation of the voltage levels and power levels, as in the previous

case, has been made by the droop control.

We can observe as in state (c) the power at the nodes A and C are very similar to state (a), but not exactly the same with respect to the initial power (before the disturbance). Something similar happens with the voltages in all nodes. The next step is once we have solved the problem at node B, and it can again provide the same initial power (730 kW). Secondary control analyses the situation, and it gives the signal to node B that it can supply the initial power (730 kW). But now, node D is still supplying more power than it did in initial time. With this values we obtain a new steady state (d).

Now node D reverts to its initial production, so we reach the new equilibrium point, state (e) thanks to the secondary control. We can observe from figures 3.9 and 3.16 that the initial and the final states are the same, so our control philosophy has a correct behaviour.

We could also mention that consumed powers in nodes A and C are very similar at any instant, and this is because the droop gains $k_A$ and $k_C$ are the same (calculate with LQR technique, see equation 3.29), and this it because both nodes have the same capacitance value.

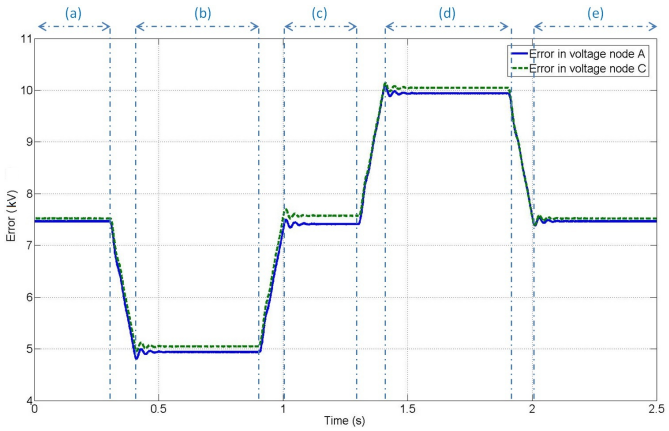


Figure 3.11: Error.

However, as figure 3.11 shows, the error between the reference value and the actual value is not zero, although it is provided next to him. This is because the droop control is a proportional control, and it does not reach zero error in steady state.

## 3.4 Droop control and VSC dynamics together.

This section focuses on the interaction between local and primary controllers for a MT-HVDC network connected to AC grids.

In AC/DC terminal nodes, VSC are implemented in order to carry out

the AC/DC conversion. The dynamic of VSC and its controller will be studied as well as their interaction with the primary control (droop control) which is distributed and regulates the voltage on the DC grid. As the references for the local controllers depend on primary control, two different dynamics could be distinguished.

In order to show the stability of the whole system, a methodology based on *singular perturbation* theory is carried out (see [38]), which provide us the mathematical tool necessary to separate both time scales. Otherwise, if we study both dynamics together, a non-linear system must be considered, where the local control variables (VSC) are time-variant, as well as the reference given by the primary control. In this complete case it is very difficult to establish a control law that guarantees the asymptotic stability of the overall system. Moreover, as these dynamics are very different in reality, this assumption is not far-fetched. Indeed, this fact is consistent with reality, because the local controller operates in a time range of milliseconds, see [91, 17], and the primary control operates in the range of seconds.

On the other hand, two possible control philosophies could be carried out depending on each node operation. There will be VSC nodes where the DC voltage and reactive AC power will be controlled, and other nodes where the local control is responsible to regulate the active and reactive power.

**VSC terminal model.**

A simplified configuration of a VSC terminal node connected to AC grid is depicted in figure 3.12. Where $R_i$ and $L_i$ represents the AC phase reactor in node $i$, and $C_i$ is the DC capacitor. $R_{b,j}$ and $L_{b,j}$ are the resistance and inductance respectively of the DC branch $j$.

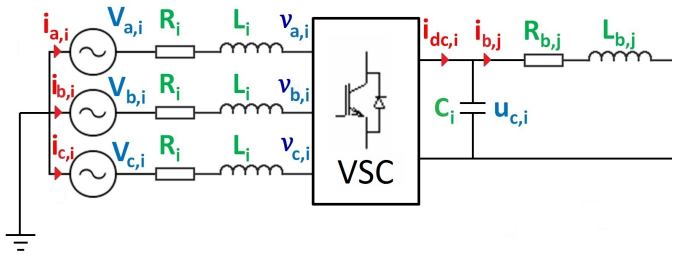


Figure 3.12: Configuration of a VSC terminal node.

Applying Kirchoff's laws in the left side of the figure 3.12, we obtain:

$$\begin{bmatrix} V_{a,i} \\ V_{b,i} \\ V_{c,i} \end{bmatrix} - \begin{bmatrix} v_{a,i} \\ v_{b,i} \\ v_{c,i} \end{bmatrix} - \mathcal{R}_i \begin{bmatrix} i_{a,i} \\ i_{b,i} \\ i_{c,i} \end{bmatrix} = \mathcal{L}_i \begin{bmatrix} \frac{di_{a,i}}{dt} \\ \frac{di_{b,i}}{dt} \\ \frac{di_{c,i}}{dt} \end{bmatrix} \tag{3.38}$$

where $\mathcal{R}_i$ and $\mathcal{L}_i$ are diagonal matrices with $R_i$ and $L_i$ elements respectively. $V_{a,i} = V_i sin(\omega_i t + \delta_i)$ is the AC voltage of the phase $a$, where $\omega_i \in \mathbb{R}$ is the pulsation of AC grid $i$, and $V_i$, $\delta_i \in \mathbb{R}$ are the voltage module and voltage phase respectively of the AC grid connected to node $i$.

Thanks to the well known technique Pulse Width Modulation (PWM), it is possible to obtain a relation between AC and DC voltages in the converter [97, 91]. This relation is:

$$v_{a,i} = c_i M_i \; u_{C,i} sin(\omega_i t + \phi_i) \tag{3.39}$$

where $u_{C,i}$ is the average value of the DC capacitor voltage in the node $i$, $c_i \in \mathbb{R}$ such that $0 < c_i \leq 1$, $\forall i \in \{1, ..., k\}$ is a coefficient of the AC/DC conversion (usually $c_i = 0.5$, [97]), and $M_i, \phi_i \in \mathbb{R}$ are respectively the module ($0 < M_i < 1$) and phase of the converter variable control coming from PWM.

In order to work in the *dq* synchronous frame, Park transformation shown in equation (3.40) is used to change from *abc* frame to *dq* frame[63].

$$\begin{bmatrix} x_a \\ x_b \\ x_c \end{bmatrix} = \sqrt{\frac{2}{3}} \begin{bmatrix} cos(\omega t) & -sin(\omega t) & 1/\sqrt{2} \\ cos(\omega t - 2\pi/3) & -sin(\omega t - 2\pi/3) & 1/\sqrt{2} \\ cos(\omega t + 2\pi/3) & -sin(\omega t + 2\pi/3) & 1/\sqrt{2} \end{bmatrix} \begin{bmatrix} x_d \\ x_q \\ x_0 \end{bmatrix} \tag{3.40}$$

The system (3.38) could be rewritten as:

$$\begin{bmatrix} V_{d,i} \\ V_{q,i} \\ V_{0,i} \end{bmatrix} - \begin{bmatrix} v_{d,i} \\ v_{q,i} \\ v_{0,i} \end{bmatrix} - \begin{bmatrix} R_i & -\omega_i L_i & 0 \\ \omega_i L_i & R_i & 0 \\ 0 & 0 & R_i \end{bmatrix} \begin{bmatrix} i_d \\ i_q \\ i_0 \end{bmatrix} = \mathfrak{L}_\mathfrak{i} \begin{bmatrix} \frac{di_d}{dt} \\ \frac{di_q}{dt} \\ \frac{di_0}{dt} \end{bmatrix} \tag{3.41}$$

where

$$\begin{bmatrix} v_{d,i} \\ v_{q,i} \\ v_{0,i} \end{bmatrix} = \begin{bmatrix} c_i M_i \; u_{C,i} sin(\phi_i) \\ -c_i M_i \; u_{C,i} cos(\phi_i) \\ 0 \end{bmatrix} \tag{3.42}$$

On the other hand, the instantaneous active and reactive power are given by:

$$P_i = v_{d,i} \cdot i_{d,i} + v_{q,i} \cdot i_{q,i} \tag{3.43}$$

$$Q_i = v_{q,i} \cdot i_{d,i} - v_{d,i} \cdot i_{q,i} \tag{3.44}$$

Finally, considering the power equality on both sides of VSC we obtain:

$$u_{c,i} \cdot i_{dc,i} = v_{d,i} \cdot i_{d,i} + v_{q,i} \cdot i_{q,i} \tag{3.45}$$

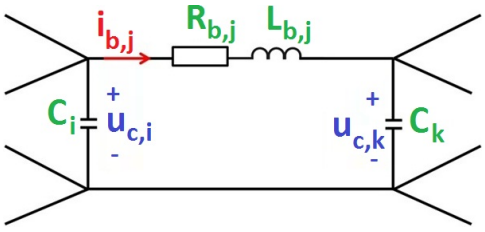


Figure 3.13: $\pi$-equivalent line circuit.

**HVDC line model.**

The branches of the DC side are modeled by $\pi$-equivalent circuits which is shown in figure 3.13.

We have considered that when a line $j$ is connected to terminal node $i$, the capacitor of this side of the line and the output capacitor of the VSC are the same. It should be pointed out that several lines could come up from a terminal node, in this case the capacitor will be common.

**VSC MT-HVDC grid model.**

From the above explanations, the behaviour of any VSC MT-HVDC grid connected to AC networks can be described in terms of capacitors, inductances, resistances and voltage sources. Thus, it is possible to find a non-linear state-space representation in open loop, where the state variables are the voltages in the capacitors and the currents through the inductances, and the inputs are the voltages on the sources in the AC side.

Proceeding in a similar way as [92], if we consider that there exist $n \in \mathbb{N}^*$ nodes in the DC grid, in which there are $k \in \mathbb{N}^*$ terminal nodes, and $d \in \mathbb{N}^*$ terminal nodes where exists droop control ($n \geq k \geq d$). Also, there will be $l \in \mathbb{N}$ lines, $n-1 \leq l \leq \sum_{i=1}^{n}(i-1)$ (if there is no more than one line between two nodes). On the other hand, it is clear that there will be $n-k$ interconnection nodes. With all these premises, we can write the whole open loop non-linear system in the following form:

$$\dot{x} = f(x,u) = A(u)x + B \tag{3.46}$$

where the states are:

$$x = [u_{C1}, \ldots, u_{Ck}, \ldots, u_{Cn}, i_{b,1}, \ldots, i_{b,l}, i_{d,1}, i_{q,1}, \ldots, i_{d,k}, i_{q,k}]^T \tag{3.47}$$

in $u$ are the control variables such that:

$$u = [M_1, \phi_1, \ldots, M_k, \phi_k] = [M_{d1}, M_{q1}, .., M_{dk}, M_{qk}] \tag{3.48}$$

where $M_{di} = M_i sin(\phi_i)$ and $M_{qi} = M_i cos(\phi_i)$.

In $B$ are the external variables:

$$B = [0, \ldots, 0, V_{d,1}/L_1, V_{q,1}/L_1, \ldots, V_{d,k}/L_k, V_{q,k}/L_k]^T \tag{3.49}$$

and finally:

$$A(u) = \begin{bmatrix} \mathbf{0} & A_{12} & A_{13}(u) \\ A_{21} & A_{22} & \mathbf{0} \\ A_{31}(u) & \mathbf{0} & A_{33} \end{bmatrix} \in \mathbb{R}^{(n+l+2k)\times(n+l+2k)} \tag{3.50}$$

where:

$$A_{22} = -\mathcal{L}_b^{-1} \cdot \mathcal{R}_b \tag{3.51}$$

with $\mathcal{R}_b = diag(R_{b,1}, ..., R_{b,l})$ and $\mathcal{L}_b = diag(L_{b,1}, ..., L_{b,l})$ with $R_{b,j}$ and $L_{b,j}$ the resistance and the inductance of the DC branch $j$ respectively.

Matrix $A_{33}$ is defined as:

$$A_{33} = \begin{bmatrix} -\frac{R_1}{L_1} & \omega_1 & 0 & 0 & \ldots & \ldots & 0 & 0 \\ -\omega_1 & -\frac{R_1}{L_1} & 0 & 0 & \ldots & \ldots & 0 & 0 \\ 0 & 0 & -\frac{R_2}{L_2} & \omega_2 & \ldots & \ldots & 0 & 0 \\ 0 & 0 & -\omega_2 & -\frac{R_2}{L_2} & \ldots & \ldots & 0 & 0 \\ \vdots & \vdots & \ldots & \ldots & \ddots & \ddots & \vdots & \vdots \\ 0 & 0 & \ldots & \ldots & \ldots & \ldots & -\frac{R_k}{L_k} & \omega_k \\ 0 & 0 & \ldots & \ldots & \ldots & \ldots & -\omega_k & -\frac{R_k}{L_k} \end{bmatrix} \in \mathbb{R}^{2k\times 2k} \tag{3.52}$$

where $R_i$ and $L_i$ represents the phase reactor in terminal node $i$, and $\omega_i$ is the pulsation of AC grid $i$.

Matrix $A_{21}$ is defined as:

$$A_{21} = \mathcal{L}_b^{-1} \cdot H \tag{3.53}$$

where matrix $H \in \mathbb{R}^{l\times n}$ has the special form explained as follows. As two nodes are connected by a line, then in each row of $H$ appears only two non-zero elements, which have opposite signs. Their values will be 1 or -1 depending on the direction chosen for the current. Also if the line connects nodes $s$ and $r$, these non-zero elements appear in the columns $s$ and $r$ of this row. Consequently, it is clear that $H$ has as many rows as electric lines. On the other hand, we see that due to the duality of electrical systems, in $A_{12}$ appears the opposite of the transpose of $H$, which is defined as:

$$A_{12} = -\mathcal{C}^{-1} \cdot H^T \tag{3.54}$$

where matrix $\mathcal{C} = diag(C_1, ..., C_n)$, with $C_i$ the DC capacitor of node $i$.

Matrix $A_{13}(u)$ is defined as:

$$A_{13}(u) = \mathcal{L}^{-1} \cdot \mathcal{H}(u) \tag{3.55}$$

with $\mathcal{L} = diag(L_1, L_1, ..., L_k, L_k) \in \mathbb{R}^{2k \times 2k}$ with $L_i$ the inductance phase reactor in terminal node $i$.

Finally, $A_{31}(u)$ is defined as:

$$A_{13}(u) = \mathcal{C}^{-1} \cdot \mathcal{H}^T(u) \tag{3.56}$$

As we can observe, the same phenomenon as before appears in matrix $\mathcal{H}(u)$, where in $A_{31}(u)$ arises the opposite of the transpose of $A_{13}(u)$. It must be pointed out that in this matrix $\mathcal{H}(u)$ the control of VSC terminals appears.

$$\mathcal{H}(u) = \begin{bmatrix} \mathfrak{h}_{11} & 0 & \dots & 0 & 0 & \dots & 0 \\ \mathfrak{h}_{21} & 0 & \dots & 0 & 0 & \dots & 0 \\ 0 & \mathfrak{h}_{32} & \dots & 0 & 0 & \dots & 0 \\ 0 & \mathfrak{h}_{42} & \dots & 0 & 0 & \dots & 0 \\ \vdots & & \ddots & \vdots & & & \vdots \\ \vdots & \dots & \ddots & \vdots & \dots & \dots & \vdots \\ 0 & \dots & \dots & \mathfrak{h}_{2k-1,k} & 0 & \dots & 0 \\ 0 & \dots & \dots & \mathfrak{h}_{2k,k} & 0 & \dots & 0 \end{bmatrix} \in \mathbb{R}^{2k \times n} \tag{3.57}$$

where the variables are:

$\mathfrak{h}_{11} = c_1 M_{d1}$, $\mathfrak{h}_{12} = -c_1 M_{q1}$, $\mathfrak{h}_{23} = c_2 M_2 M_{d2}$, $\mathfrak{h}_{24} = -c_2 M_{q2}$ until the row $k$. It is important to stress that $\forall\ i, j\ -1 \leq \mathfrak{h}_{ij} \leq 1$. The other parameters $c_i, M_{di}$ and $M_{qi}$ have been defined in above sections.

### 3.4.1 Singular perturbation. Brief explanation.

The essence of the *singular perturbation* theory is that if we study a whole system in separate time scales, we can avoid the discontinuity of solutions caused by these singular, and small, perturbations. The so-called *standard singular perturbation model* has the following form:

$$\begin{cases} \dot{x} = f(t, x, z, \epsilon) \\ \epsilon \dot{z} = g(t, x, z, \epsilon) \end{cases} \tag{3.58}$$

where $\epsilon$ is a small parameter, and if we sets $\epsilon = 0$, it causes an abrupt change in the dynamic properties of the whole system. Proceeding in this way in equation (3.58), we achieve:

$$0 = g(t, x, z, 0) \Rightarrow z = h(t, x) \tag{3.59}$$

and consequently,

$$\dot{x} = f(t, x, h(t, x), 0) \tag{3.60}$$

which is called the *quasi-steady-state model* or *slow model*, because $z$, whose velocity is $\dot{z} = g/\epsilon$ can be large when $\epsilon$ is small ($g \neq 0$).

### 3.4.2 Whole control

There exists two possible ways in order to control a VSC, either we control the DC voltage, $u_C$, and reactive power $Q$ (thanks to $i_q$) or we can control the active ($i_d$) and reactive powers [91, 17].

It is clear that the droop control acts in the DC voltage, therefore in the nodes where droop is implemented, the first option ($u_C$ and $Q$) will be considered. On the other hand, in the converters with no droop, the local controller will act on $P$ and $Q$. It is supposed that the references are given by the secondary level control, which is explained in chapter 4.

Therefore, if the droop control is implemented (we control $u_C$ and $Q$), the references given by the primary become:

$$\begin{cases} i^*_{d,i} = i^\circ_{d,i} - k_i(u_{C,i} - u^\circ_{C,i}) \\ i^*_{q,i} = q^\circ_i \end{cases} \tag{3.61}$$

and if there is no droop control implemented, then:

$$\begin{cases} i^*_{d,j} = i^\circ_{d,j} \\ i^*_{q,j} = q^\circ_j \end{cases} \tag{3.62}$$

where $i^\circ_{d,i}$, $u^\circ_{C,i}$ are given by the power flow carried out in the secondary control level (see chapter 4). Finally $q^\circ_i$ is usually equals to zero in each node.

### 3.4.3 System stability

Considering the *singular perturbation* explanation theory carried out in section 3.4.1, and if we rewrite the state vector $x$ shown in (3.47) in the form:

$$x = [x_1 \ z]^T \tag{3.63}$$

with,

$$x_1 = [u_{C1}, \ldots, u_{Ck}, .., u_{Cn}, i_{b,1}, \ldots, i_{b,l}]^T \in \mathbb{R}^{n+l} \tag{3.64}$$

$$z = [i_{d,1}, i_{q,1}, \ldots, i_{d,k}, i_{q,k}]^T \in \mathbb{R}^{2k} \tag{3.65}$$

then the system (3.46) could be rewritten as:

$$\begin{cases} \dot{x_1} = f_1(x_1) + f_2(z, \phi(x_1, z)) \\ \epsilon \dot{z} = g(x_1, z, \phi(x_1, z)) \end{cases} \tag{3.66}$$

where $\phi(x_1, z)$ is a function which depends on local control variables shown in equation (3.48). Consequently, we achieve that:

$$\begin{cases} M_{d1} = \phi_{d1}(i_{d1}, i_{q1}, k_1, u_{C1}) \\ \qquad\qquad \vdots \\ M_{qk} = \phi_{qk}(i_{dk}, i_{qk}, k_k, u_{Ck}) \end{cases} \tag{3.67}$$

Therefore, the standard practical assumption that the errors go to zero quickly in alternating currents $i_{d,i}$ and $i_{q,i}$ (variables $z$) compared to the DC voltage, can be summarized as the assumption that the control variables $\phi_i$ can obtain that (at least inside an operation region):

$$\epsilon \dot{z} = -cte(z - z^*) \tag{3.68}$$

where $z^*$ is given in equations (3.61) and (3.62), and $1/\epsilon$ is the velocity of convergence.

Thereby, the *quasi-steady-state model* becomes:

$$\begin{cases} \dot{u}_{C1} = -\frac{1}{C_1} ib_1 + \frac{M^*_{d1}}{C_1}(i^\circ_{d,1} - k_i(u_{C,1} - u^\circ_{C,1})) - \frac{M^*_{q1}}{C_1} \\ \vdots \\ \dot{u}_{Ck} = -\frac{1}{C_k} ib_k + \frac{M^*_{dk}}{C_k}(i^\circ_{d,k} - k_i(u_{C,k} - u^\circ_{C,k})) - \frac{M^*_{qk}}{C_k} \\ u_{Ck+1} = \frac{1}{C_{k+1}} ib_i + \frac{1}{C_{k+1}} ib_j \\ \vdots \\ \dot{u}_{Cn} = \frac{1}{Cn} ib_h + \frac{1}{Cn} ib_l \\ \dot{i}_{b1} = \frac{1}{L_{b1}} u_{C1} - \frac{1}{L_{b1}} u_{Cj} - \frac{R_{b1}}{L_{b1}} i_{b1} \\ \vdots \\ \dot{i}_{bl} = \frac{1}{L_{bl}} u_{Ch} - \frac{1}{L_{bl}} u_{Cn} - \frac{R_{bl}}{L_{bl}} i_{bl} \end{cases} \tag{3.69}$$

which has the same form as the model study in section 3.3, and therefore the same reasoning to prove the asymptotically stability of this quasi-steady-state model could be carried out.

Besides, some remarks and lemmas are laid out in other to clarify the explanation.

***Remark* 2** *All the elements of submatrices $L^{-1} \cdot \mathcal{H}(u)$ and $-\mathcal{C}^{-1} \cdot \mathcal{H}^T(u)$ are bounded.*

***Remark* 3** *Matrix $H$ has rank($H$)=$n-1$, so the columns of $H$ are linearly dependent.*

***Remark* 4** *Matrix $\mathcal{H} \in \mathbb{R}^{2k \times n}$ has rank($\mathcal{H}$)=$k$.*

***Remark* 5** *Matrix $A_{22}$ has $l$ eigenvalues with negative real part. These $l$ eigenvalues have the form $\lambda_i = -\frac{R_{b,i}}{L_{b,i}} \ \ \forall i = 1, ..., l$.*

***Remark* 6** *Matrix $A_{33}$ has $2k$ eigenvalues with negative real part. These firs $2k$ eigenvalues have the form $\lambda_j = -\frac{R_j}{L_j} \pm \omega_j \ \ \forall j = 1, ..., k$.*

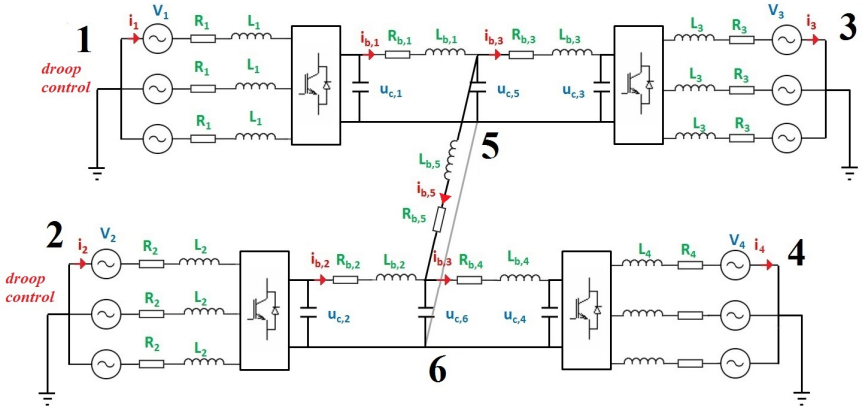


Figure 3.14: Simulation system

### 3.4.4 Simulations.

In order to apply the proposed control philosophy explained in the above sections, a four terminal VSC grid is proposed as shows figure 3.14 . It is composed by four VSC nodes, in which droop control is only applied in 1 and 2, two interconnection nodes and five lines.

The values of the parameters are shown in tables 3.2 and 3.3.

Table 3.2: Simulation parameter values. AC side.

| | Nominal voltage | Phase | Frequency | Resistance | Inductance |
|---|---|---|---|---|---|
| Grid 1 | 100 kV | 0 rad | 50 Hz | 1 Ω | 0.01 H |
| Grid 2 | 140 kV | 30 rad | 60 Hz | 1 Ω | 0.01 H |
| Grid 3 | 500 kV | 60 rad | 55 Hz | 1 Ω | 0.01 H |
| Grid 4 | 250 kV | 90 rad | 45 Hz | 1 Ω | 0.01 H |

Table 3.3: Simulation parameter values. DC side.

| | Resistance | Indutance |
|---|---|---|
| Branch 1 | 1.2 Ω | 0.12 H |
| Branch 2 | 2.4 Ω | 0.24 H |
| Branch 3 | 0.6 Ω | 0.06 H |
| Branch 4 | 0.6 Ω | 0.06 H |
| Branch 5 | 1.2 Ω | 0.12 H |

| Nominal DC voltage |
|---|
| ±600 kV |

| | $C_1$ | $C_2$ | $C_3$ | $C_4$ | $C_5$ | $C_6$ |
|---|---|---|---|---|---|---|
| Capacitance | 0.01 F | 0.01 F | 0.01 F | 0.01 F | 0.01 F | 0.01 F |

We have considered that each 60 seconds the higher level control gives

references to each node, either DC voltage and reactive power for nodes where droop control exists or active and reactive power for the others.

In figure 3.15 we observe the voltages in terminal nodes, and in figure 3.16 we observe the active power transfer between AC and DC side in terminal nodes. In these figures we notice that the equilibrium is reached for zero initial conditions and for given references. At $t = 35s$ a disturbance occurs on the AC side of node 3, which causes that the droop control acts to keep the equilibrium. We see in both figures as the values of voltage and power are different from the reference (from $t = 35s$), and in $t = 60s$ is when the secondary control gives new references according to the new state produced by the disturbance.

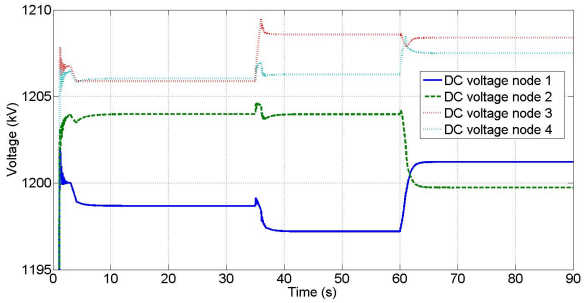


Figure 3.15: Terminal node voltages.

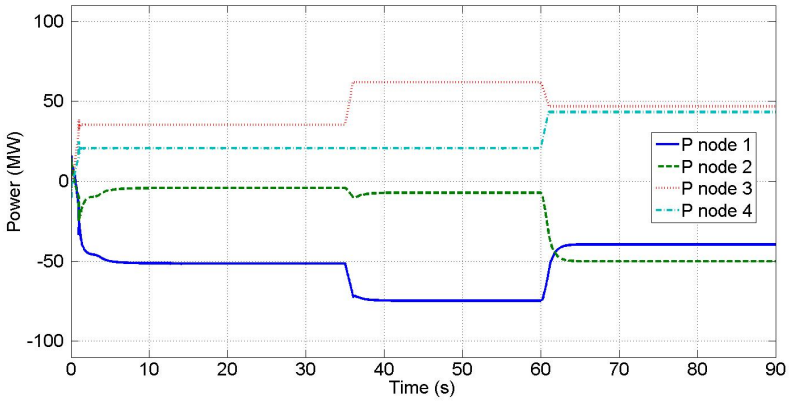


Figure 3.16: Active power in terminal nodes.

In figure 3.17 we observe as the variables $i_{q1}$ and $i_{q2}$ track their references at any time in a proper way.

In figure 3.18 we observe as the variables $i_{d3}$, $i_{q3}$, $i_{d4}$ and $i_{q4}$ track their references at any time in a proper way.

It could be notice that for these simulations we have chosen as *control*

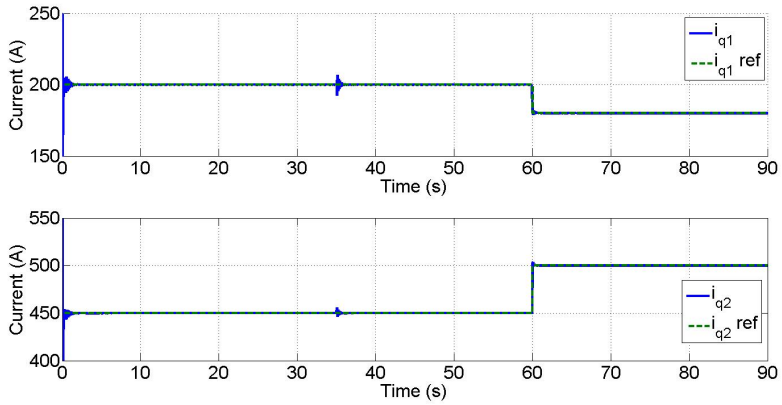


Figure 3.17: $i_{q1}$ and $i_{q2}$ currents.

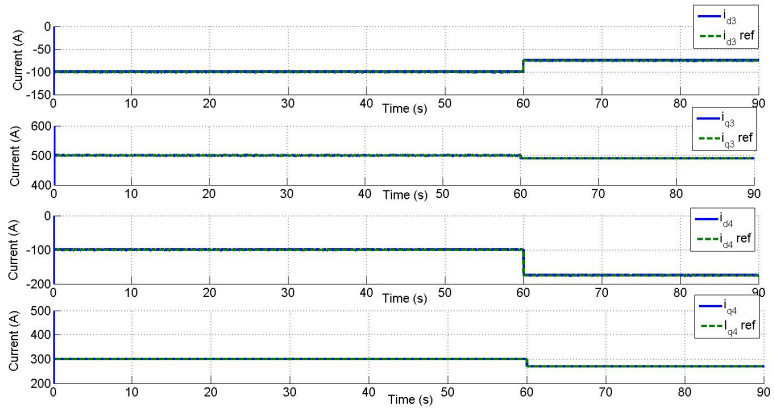


Figure 3.18: $i_{d3}$, $i_{q3}$, $i_{d4}$ and $i_{q4}$ currents.

*droop gains* $k_1 = -0.05$ and $k_2 = -0.05$. These values have been found in a similar way explained in [92]. It is important also to remark that due to the philosophy detailed here, it is possible to link AC areas with different frequencies via HVDC.

## 3.5 Conclusions

The goal of the present chapter is to develop and illustrate by simulations a primary distributed control philosophy for a MT-HVDC grid which regulates the DC voltage in the grid. Three philosophies have been discussed: master/slave, voltage margin control and droop control, among the last one has been chosen, because it does not require communication between nodes and it distributes the efforts between the nodes when a disturbance occurs.

In order to study the droop control. Two different approaches have been considered. In the first one, we have neglected the VSC and local control dynamics considering them as ideal current sources. A proof is included in order to guarantee the stability of the system. The control algorithms are developed based on LQR techniques. In the second one, the *singular perturbation* theory provides us the limits of neglecting the droop control philosophy together with VSC controllers, and gives the theoretical background to justify such practice.

The simulations shows that this control philosophy is suitable for MT-HVDC grids.

Chapter 4

# Secondary control

## 4.1 Chapter introduction.

The secondary control for a MT-HVDC network is addressed in this chapter. It is the first control level where data of several nodes is known by the controller. The main task of secondary control will be to schedule power transfer between the network nodes providing voltage and power references to local and primary controllers. In order to carry out this task, communication between nodes and secondary controller must exist. The sample time for this control is in the range of few minutes.

The references for lower controllers will be the result of periodic power flows, which are key elements for the proper functioning of the system. The main goal of a power flow study is to obtain voltage and power informations for each bus in the grid in steady state. However it may perform other types of analysis, such as short-circuit fault analysis, stability studies, unit commitment or economic dispatch.

In AC power systems, the optimal power flow (OPF) problem is defined by non-linear equations. In HVDC systems where there is no reactive power involved, the power flow problem is less complex but still retains its non-linear characteristic. There are several methods to solve non-linear system of equations. The most popular for the power flow problem is the well known Newton-Raphson (NR) method [15]. With this method the solutions can be easily obtained trough the equations' linearization. An important disadvantage is that the convergence of the method is not always guaranteed. In power systems applications, a slack bus is usually considered (master/slave strategy explained in section 3.2). This fact entails risks for the proper modelling of the system, such as the loss of the slack bus (for example a communication lost), that would cause the loss of the reference and consequently the abandon of the equilibrium because the method is not applicable.

More recently, some authors have proposed other solutions to solve the problem. For example in [28] a multi-terminal DC power flow with a conventional AC power flow has been proposed. Or in [29] a steady-state multiterminal DC model for power flow programs has been developed which allows to include converter limits as well as different converter topologies. However, both methods are based on the iterative resolution of the NR method until to find a solution which is smaller than a given error. Others authors

have solved the problem applying new techniques as in [30] where the problem is solved by genetic algorithm that is an evolutionary-based heuristic algorithm.

In section 4.2 we use a new approach to solve the power flow problem based on the contraction mapping theorem [79]. The contraction mapping theorem is also known as Banach fixed-point theorem [31]. This new method gives the possibility to use more than one bus for the power balance (slack bus), and consequently share the responsibilities between many actors. The method guarantees the unique existence of solution when some feasible constraints are fulfilled. Also, a complete study of the effects on the unknown variables with respect to the variations in the known variables is carried out, by means of the Jacobian Matrix.

On the other hand, in practical applications of variable energy power sources, as renewable energies for example, it is interesting considering storage devices in order to improve the stability and the efficiency of the whole system [34]. Due to the sample time for this level of control is up to the order of minutes, if we considered that some kind of forecast could be included, we can achieve more control objectives, such as manage storage reserves, very important for renewable energy integration for example. If we operate in these terms, including weather forecasts to optimally manage of storage systems, we were stated under the model predictive control approach, MPC. Minimize transmission losses or even avoid power network congestions could be also accomplished in this control level. In section 4.3 an optimal power flow problem for HVDC systems with predictive control tools is shown [32].

## 4.2 DC power flow.

A new power flow for DC grids is presented in this section. This new method gives the possibility of using more than one bus for the power balance and consequently share the responsibilities between many actors. A mathematical proof for this new power flow algorithm, which guarantees the unique existence of solution when voltages are close to nominal value. This new algorithm has in addition the advantage of being easily adapted for AC systems (see annex A). Besides, a detailed study of the effects on power and voltages when variables change is shown in this section.

### 4.2.1 Definitions and basic relations.

We have considered a passive network with $n$ nodes ($n \geq 2$). This grid is connected because any two nodes of the network are connected by at least one path formed by branches of the network. The lines are bipolar since they have two phases (+ and -) as shows figure 4.1.

***Def* 1** $\forall j,k \in \{1,2,..,n\}, j \neq k$, $g_{j,k}$ *is the conductance of the branch which*

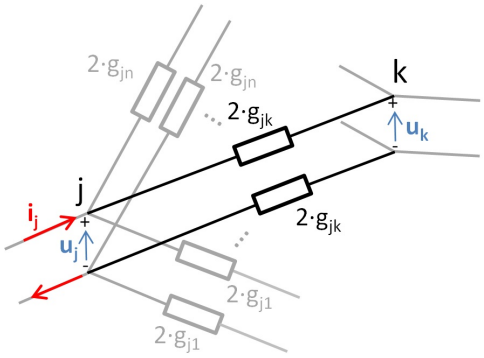


Figure 4.1: Bipolar line.

*connects node $j$ with node $k$. It corresponds with the two conductors (positive and negative). When the branch exits then $g_{j,k} > 0$, whereas if there is no branch $g_{j,k} = 0$. It holds that $g_{j,k} = g_{k,j}$.*

***Def* 2** *$\forall j \in \{1, 2, .., n\}$, $g_{j,j}$ is the sum of the conductances of the branches which converge at node $j$.*

$$g_{j,j} = \sum_{k=1(k\neq j)}^{n} g_{j,k} \tag{4.1}$$

***Def* 3** *$\forall j \in \{1, 2, .., n\}$, $u_j$ is the voltage between positive and negative terminals of node $j$.*

***Def* 4** *$\forall j \in \{1, 2, .., n\}$, $i_j$ is the current which comes into the network through the positive terminal of node $j$. (Its value is negative when the current leaves the grid).*

***Def* 5** *$\forall j \in \{1, 2, .., n\}$, $P_j$ is the power which comes into the network at node $j$. (Its value is negative when the power leaves the grid).*

In steady state, the system of equations shown in (4.2) are satisfied:

$$\begin{cases} g_{1,1} \cdot u_1 - g_{1,2} \cdot u_2 - g_{1,3} \cdot u_3 - \ldots - g_{1,n} \cdot u_n = i_1 \\ -g_{1,2} \cdot u_1 + g_{2,2} \cdot u_2 - g_{2,3} \cdot u_3 - \ldots - g_{2,n} \cdot u_n = i_2 \\ \vdots \\ -g_{1,n} \cdot u_1 - g_{2,n} \cdot u_2 - g_{3,n} \cdot u_3 - \ldots + g_{n,n} \cdot u_n = i_n \end{cases} \tag{4.2}$$

Moreover:

$$P_1 = u_1 \cdot i_1 \ , \ P_2 = u_2 \cdot i_2 \ , \ \ldots \ , P_n = u_n \cdot i_n \tag{4.3}$$

and consequently,

$$\begin{cases} g_{1,1}\cdot u_1^2 - g_{1,2}\cdot u_1\cdot u_2 - g_{1,3}\cdot u_1\cdot u_3 - .. - g_{1,n}\cdot u_1\cdot u_n = P_1 \\ -g_{1,2}\cdot u_1\cdot u_2 + g_{2,2}\cdot u_2^2 - g_{2,3}\cdot u_2\cdot u_3 - .. - g_{2,n}\cdot u_2\cdot u_n = P_2 \\ \vdots \\ -g_{1,n}\cdot u_1\cdot u_n - g_{2,n}\cdot u_2\cdot u_n - g_{3,n}\cdot u_3\cdot u_n - .. + g_{n,n}\cdot u_n^2 = P_n \end{cases} \tag{4.4}$$

In matrix form:

$$\mathbf{G}\cdot\mathbf{u} = \mathbf{i} \tag{4.5}$$

$$\mathbf{u}^T\cdot\mathbf{G}_j^*\cdot\mathbf{u} = \mathbf{P}_j \quad \forall j\in\{1,2,\ldots,n\} \tag{4.6}$$

$$\mathbf{u}^T\cdot\mathbf{G}\cdot\mathbf{u} = \sum_{j=1}^{n}\mathbf{P}_j \tag{4.7}$$

with $\mathbf{i}$=$[i_1, i_2, \ldots, i_n]^T$, $\mathbf{u}$=$[u_1, u_2, \ldots, u_n]^T$, $\mathbf{P}$=$[P_1, P_2, \ldots, P_n]^T$, and $\mathbf{G}$ is the conductance matrix defined in (4.8):

$$\mathbf{G} = \begin{bmatrix} g_{1,1} & -g_{1,2} & \cdots & -g_{1,n} \\ -g_{1,2} & g_{2,2} & \cdots & -g_{2,n} \\ \vdots & \vdots & \ddots & \vdots \\ -g_{1,n} & -g_{2,n} & \cdots & g_{n,n} \end{bmatrix} \tag{4.8}$$

and $\forall j\in\{1,2,..,n\}$, $\mathbf{G}_j^*$ has the form:

$$\mathbf{G}_j^* = \begin{bmatrix} 0 & \ldots & 0 & -\frac{g_{1,j}}{2} & 0 & \ldots & 0 \\ \vdots & \ddots & \vdots & \vdots & \ldots & \vdots & \vdots \\ 0 & \ldots & 0 & -\frac{g_{j-1,j}}{2} & 0 & \ldots & 0 \\ -\frac{g_{1,j}}{2} & \ldots & -\frac{g_{j-1,j}}{2} & g_{j,j} & -\frac{g_{j,j+1}}{2} & \vdots & -\frac{g_{j,n}}{2} \\ 0 & \ldots & 0 & -\frac{g_{j,j+1}}{2} & 0 & \ldots & 0 \\ \vdots & \vdots & \vdots & \vdots & \ldots & \ddots & \vdots \\ 0 & \ldots & 0 & -\frac{g_{j,n}}{2} & 0 & \ldots & 0 \end{bmatrix} \tag{4.9}$$

### 4.2.2 Basic properties.

Next some basic properties are explained and detailed.

***Basic property* 1** *If we know the voltages on all nodes, we can find all currents and powers.*

***Basic property* 2** *Since $i_1 + i_2 + \ldots + i_n = 0$, then if we know the input currents in $n-1$ nodes, it is possible to establish the input current in the remaining node.*

***Basic property* 3** *$P_1+P_2+\ldots+P_n \geq 0$ ($P_1+P_2+\ldots+P_n$ is the dissipated power in the network)*

*If $u_1 = u_2 = \ldots = u_n$, then $i_1 = \ldots = i_n = 0$ and $P_1+P_2+\ldots+P_n = 0$.*

*If $\exists\ j,k \in \{1,2,\ldots,n\}$ such that $u_j \neq u_k$ then $P_1 + P_2 + .. + P_n > 0$.*

***Basic property* 4** *The matrix $\boldsymbol{G}$ is positive semi-definite of rank $n-1$.*

*$\forall j \in \{1,2,\ldots,n\}$ the matrix of order $n-1$ that results to remove row $j$ and column $j$ of $\boldsymbol{G}$ is positive definite.*

*$\forall k \in \{1,2,\ldots,n-1\}$ matrix $\boldsymbol{G}_k$, formed by the elements of the first $k$ rows and first $k$ columns of $\boldsymbol{G}$, and matrix $\Lambda_{n-k}$ formed by the elements of the last $n-k$ rows and last $n-k$ columns of $\boldsymbol{G}$, are definite positive. And matrix -$\Gamma_k$ formed by the elements of the first $k$ rows and $n-k$ last columns of $\boldsymbol{G}$ is not null.*

$$\boldsymbol{G}_k = \begin{bmatrix} g_{1,1} & \cdots & -g_{1,k} \\ -g_{1,2} & \cdots & -g_{2,k} \\ \vdots & \ddots & \vdots \\ -g_{1,k} & \cdots & g_{k,k} \end{bmatrix} \in \mathbb{R}^{k\times k} \tag{4.10}$$

$$\Gamma_k = \begin{bmatrix} g_{1,k+1} & \cdots & g_{1,n} \\ g_{2,k+1} & \cdots & g_{2,n} \\ \vdots & \cdots & \vdots \\ g_{k,k+1} & \cdots & g_{k,n} \end{bmatrix} \in \mathbb{R}^{k\times(n-k)} \tag{4.11}$$

$$\Lambda_{n-k} = \begin{bmatrix} g_{k+1,k+1} & \cdots & -g_{k+1,n} \\ -g_{k+1,k+2} & \cdots & -g_{k+2,n} \\ \vdots & \ddots & \vdots \\ -g_{k+1,n} & \cdots & g_{n,n} \end{bmatrix} \in \mathbb{R}^{(n-k)\times(n-k)} \tag{4.12}$$

***Basic property* 5** *$\forall j \in \{1,2,\ldots,n\}$ matrix $\boldsymbol{G}_j^*$ is indefinite of rank 2. That means, $\boldsymbol{G}_j^*$ has a positive eigenvalue, other negative, and the remaining $n-2$ are null.*

***Basic property* 6** *If we know the input currents in $k$ nodes and the voltages in the other $n-k$ nodes, with $0 < k < n$, the voltages in all nodes are uniquely determined, and hence also the currents and powers. For known $i_1,\ldots,i_k,u_{k+1},\ldots,u_n$, the values of $u_1,\ldots,u_k$ are solutions of the linear system (4.13) whose coefficient matrix $\boldsymbol{G}_k$ is invertible.*

$$\begin{cases} g_{1,1}\cdot u_1 - g_{1,2}\cdot u_2 - .. - g_{1,k}\cdot u_k = i_1 + g_{1,k+1}\cdot u_{k+1} + .. + g_{1,n}\cdot u_n \\ -g_{1,2}\cdot u_1 + g_{2,2}\cdot u_2 - .. - g_{2,k}\cdot u_k = i_2 + g_{2,k+1}\cdot u_{k+1} + .. + g_{2,n}\cdot u_n \\ \vdots \\ -g_{1,k}\cdot u_1 - g_{2,k}\cdot u_2 - .. + g_{k,k}u_k = i_k + g_{k,k+1}\cdot u_{k+1} + .. + g_{k,n}\cdot u_n \end{cases} \tag{4.13}$$

***Basic property 7*** *If we know the input power in $k$ nodes, $0 < k < n$, and the voltages in the other $n-k$ nodes, for sufficiently high voltage values, we can find the remaining voltages, and therefore also the currents and powers in all nodes. In addition, if the known voltage values $u_{k+1}, ..., u_n$ are close to nominal voltage value $U_n$ of the network, and this is sufficiently high, the unknown voltage values $u_1, \ldots, u_k$ are also close to $U_n$, and they will be unique.*

In effect, if we know $P_1, \ldots, P_k, u_{k+1}, \ldots, u_n$, the values of $u_1, \ldots, u_k$ are the solution of the following system:

$$\begin{cases} g_{1,1} \cdot u_1 - g_{1,2} \cdot u_2 - .. - g_{1,k} u_k = \frac{P_1}{u_1} + g_{1,k+1} \cdot u_{k+1} + .. + g_{1,n} \cdot u_n \\ -g_{1,2} \cdot u_1 + g_{2,2} \cdot u_2 - .. - g_{2,k} \cdot u_k = \frac{P_2}{u_2} + g_{2,k+1} \cdot u_{k+1} + .. + g_{2,n} \cdot u_n \\ \vdots \\ -g_{1,k} \cdot u_1 - g_{2,k} \cdot u_2 - .. + g_{k,k} \cdot u_k = \frac{P_k}{u_k} + g_{k,k+1} \cdot u_{k+1} + .. + g_{k,n} \cdot u_n \end{cases} \tag{4.14}$$

and applying the following Property 1 the results in this Basic property 7 are obtained.

### 4.2.3 Main properties.

In this section the main results of this chapter are formulated and proved.

***Property* 1**

- *Let $k \in \mathbb{N}$ be such that $0 < k < n$.*
- *Let $\boldsymbol{G} \in \mathbb{R}^{n \times n}$ be the conductance matrix defined in (4.8) such that:*

$$\boldsymbol{G} = \begin{bmatrix} \boldsymbol{G}_k & -\Gamma_k \\ -\Gamma_k^T & \Lambda_{n-k} \end{bmatrix} \tag{4.15}$$

  *where $\boldsymbol{G}_k$, $\Lambda_{n-k}$ and $\Gamma_k$ are defined in (4.10) and (4.12).*

- *Let $P_1 \ldots, P_k$ be the input power in the first $k$ nodes, and let $P$ be $P = max\{|P_j| \quad / \quad 1 \leq j \leq k\}$.*
- *Let $c, \rho, \epsilon, \delta \in \mathbb{R}$ be such that: $0< c <1$, $0< \rho <1$, $0< \epsilon$ and $0 < \delta \leq \frac{\rho \cdot \epsilon}{\left\| \boldsymbol{G}_k^{-1} \cdot \Gamma_k \right\|_\infty}$.*
- *Let $u_0, u_N \in \mathbb{R}$ be such that: $u_0 \geq max \left\{ \frac{P \cdot \left\| \boldsymbol{G}_k^{-1} \right\|_\infty}{(1-\rho) \cdot \epsilon}, \sqrt{\frac{P \cdot \left\| \boldsymbol{G}_k^{-1} \right\|_\infty}{c}} \right\}$, with $u_0 > 0$ and $u_N > u_0 + \epsilon > u_0$.*
- *Let $D$ be defined as $D = \left\{ (u_1, \ldots, u_k)^T \in \mathbb{R}^k : u_1 \geq u_0, \ldots, u_k \geq u_0 \right\}$*
- *Let $\Psi : D \to \mathbb{R}^k$ be the function defined by: $\Psi \left( (u_1, .., u_k)^T \right) = (\frac{P_1}{u_1}, .., \frac{P_k}{u_k})^T$*

- *Let $V_N$, $W_N$ be such that:*

$$V_N = (u_N, ..., u_N)^T \in \mathbb{R}^k \tag{4.16}$$
$$W_N = (u_N, ..., u_N)^T \in \mathbb{R}^{n-k} \tag{4.17}$$

*With these conditions is true that for any $W = (w_{k+1}, .., w_n)^T \in \bar{B}_\infty(W_N, \delta)$[1] there exists a unique $V = (v_1, .., v_k)^T \in D$ such that:*

***1.-***

$$\begin{cases} g_{1,1} \cdot v_1 - g_{1,2} \cdot v_2 - .. - g_{1,k} \cdot v_k = \frac{P_1}{v_1} + g_{1,k+1} \cdot w_{k+1} + .. + g_{1,n} \cdot w_n \\ -g_{1,2} \cdot v_1 + g_{2,2} \cdot v_2 - .. - g_{2,k} \cdot v_k = \frac{P_2}{v_2} + g_{2,k+1} \cdot w_{k+1} + .. + g_{2,n} \cdot w_n \\ \vdots \\ -g_{1,k} \cdot v_1 - g_{2,k} \cdot v_2 - .. + g_{k,k} \cdot v_k = \frac{P_k}{v_k} + g_{k,k+1} \cdot w_{k+1} + .. + g_{k,n} \cdot w_n \end{cases} \tag{4.18}$$

***2.-*** $V \in \bar{B}_\infty(V_N, \epsilon)$
***3.-*** *If $(s_j)_{j \in \mathbb{N}}$ is a sequence defined by:*
$s_0 \in D$ *and* $s_{j+1} = G_k^{-1} \cdot \Psi(s_j) + G_k^{-1} \cdot \Gamma_k \cdot W \ \forall j \in \mathbb{N}$, *it holds that:*
***3.1.*** $V = \lim_{j \to \infty} s_j$
***3.2.*** $\|s_j - V\|_\infty \leq \|s_2 - s_1\|_\infty \cdot \frac{c^{j-1}}{1-c} \leq 2 \cdot \epsilon \cdot \frac{c^{j-1}}{1-c} \quad \forall j \in \mathbb{N}^*$

***Proof.-***
**1.-** If $v = (u_1, \ldots, u_k)^T \in D$, and $g : D \to D$ is the mapping such that $\forall v \in D, \quad g(v) = \mathbf{G}_k^{-1} \cdot \Psi(v) + \mathbf{G}_k^{-1} \cdot \Gamma_k \cdot W$, then when the voltages $u_{k+1} = w_{k+1}, \ldots, u_n = w_n$ are known. The system shown in (4.18) is equivalent to:

$$\mathbf{G}_k \cdot v = \Psi(v) + \Gamma_k \cdot W \tag{4.19}$$

which is equivalent to:

$$v = \mathbf{G}_k^{-1} \cdot \Psi(v) + \mathbf{G}_k^{-1} \cdot \Gamma_k \cdot W \tag{4.20}$$

and this is equivalent to:

$$v = g(v) \tag{4.21}$$

so $v$ is a solution of (4.19) if and only if it is a fixed point of the mapping $g$.

Let us check that $g$ is a contractive application in D. First we verify that $\forall v \in D$, $g(v) \in D$, as

$$g(v) = \mathbf{G}_k^{-1} \cdot \Psi(v) + \mathbf{G}_k^{-1} \cdot \Gamma_k \cdot W \tag{4.22}$$

from (4.2) is easy to show that it fulfills:

$$\mathbf{G}_k \cdot V_N = \Gamma_k \cdot W_N \tag{4.23}$$

[1] See annex B.

and consequently:

$$V_N = \mathbf{G}_k^{-1} \cdot \Gamma_k \cdot W_N \tag{4.24}$$

from (4.22) and (4.24) we obtain:

$$g(v) - V_N = \mathbf{G}_k^{-1} \cdot \Psi(v) + \mathbf{G}_k^{-1} \cdot \Gamma_k \cdot (W - W_N) \tag{4.25}$$

and consequently:

$$\|g(v) - V_N\|_\infty \leq \left\|\mathbf{G}_k^{-1}\right\|_\infty \cdot \|\Psi(v)\|_\infty + \left\|\mathbf{G}_k^{-1} \cdot \Gamma_k\right\|_\infty \cdot \|W - W_N\|_\infty \tag{4.26}$$

from (4.26), and taking into account that:

$$\|\Psi(v)\|_\infty = max\left\{\frac{|P_j|}{u_j} : 1 \leq j \leq k\right\} \leq \frac{P}{u_0} \leq \frac{(1-\rho)\cdot\epsilon}{\left\|\mathbf{G}_k^{-1}\right\|_\infty} \tag{4.27}$$

and also that:

$$\|W - W_N\|_\infty \leq \delta \leq \frac{\rho \cdot \epsilon}{\left\|\mathbf{G}_k^{-1} \cdot \Gamma_k\right\|_\infty} \tag{4.28}$$

we may deduce that

$$\|g(v) - V_N\|_\infty \leq (1-\rho)\cdot\epsilon + \rho\cdot\epsilon = \epsilon \tag{4.29}$$

which is equivalent to:

$$g(v) \in \bar{B}_\infty(V_N, \epsilon) \tag{4.30}$$

and taking into account that:

$$\bar{B}_\infty(V_N, \epsilon) \subset D \tag{4.31}$$

it is true that:

$$g(v) \in D \tag{4.32}$$

Secondly, $\forall x, y \in D$ it is clear that $\|g(x) - g(y)\|_\infty \leq c \cdot \|x - y\|_\infty$ due to:

$$g(x) = \mathbf{G}_k^{-1} \cdot \Psi(x) + \mathbf{G}_k^{-1} \cdot \Gamma_k \cdot W \tag{4.33}$$
$$g(y) = \mathbf{G}_k^{-1} \cdot \Psi(y) + \mathbf{G}_k^{-1} \cdot \Gamma_k \cdot W \tag{4.34}$$

and therefore:

$$\|g(x) - g(y)\|_\infty = \left\|\mathbf{G}_k^{-1}\left(\Psi(x) - \Psi(y)\right)\right\|_\infty \leq \left\|\mathbf{G}_k^{-1}\right\|_\infty \|\Psi(x) - \Psi(y)\|_\infty \tag{4.35}$$

besides,

$$\Psi(x)-\Psi(y)=\begin{bmatrix}\frac{P_1\cdot(y_1-x_1)}{x_1\cdot y_1}\\ \vdots \\ \frac{P_k\cdot(y_k-x_k)}{x_k\cdot y_k}\end{bmatrix}\Rightarrow\|\Psi(x)-\Psi(y)\|_\infty\leq\frac{P}{u_0^2}\cdot\|x-y\|_\infty \quad (4.36)$$

therefore $\forall x,y\in D$:

$$\|g(x)-g(y)\|_\infty\leq\left\|\mathbf{G}_k^{-1}\right\|_\infty\cdot\frac{P}{u_0^2}\cdot\|x-y\|_\infty\leq c\cdot\|x-y\|_\infty \quad (4.37)$$

and as $0<c<1$ it holds that $g$ is a contractive mapping in $D$.

As $D$ is a closed set, the fixed-point theorem ensures that, for a contractive mapping, there exists a single point $V=(v_1,...,v_k)^T\in D$ such that $g(V)=V$, that means, $V$ is a fixed point of $g$, and by the above explanation this is the unique solution vector from equation (4.19) and system (4.18).

**2.-**

Result 2 of property 1 is satisfied because $V=g(V)\in D$ and also $g(V)\in\bar{B}_\infty(V_N,\epsilon)$ according to (4.30).

**3.-**

The fixed-point theorem of contractive application also ensures that if $(s_j)_{j\in\mathbb{N}}$ is a sequence defined by: $s_0\in D$ and $s_{j+1}=g(s_j)\quad\forall j\in\mathbb{N}$, the only fixed point V holds:

a) $\mathrm{V}=\lim_{j\to\infty}s_j$

b) $\|s_j-V\|_\infty\leq\|s_2-s_1\|_\infty\cdot\frac{c^{j-1}}{1-c}\quad\forall j\in\mathbb{N}^*$

Due to $s_1=g(s_0)\in\bar{B}_\infty(V_N,\epsilon)$ and also $s_2=g(s_1)\in\bar{B}_\infty(V_N,\epsilon)$, we verify that:

$$\|s_2-s_1\|_\infty\leq 2\cdot\epsilon \quad (4.38)$$

so it is true that:

$$\|s_j-V\|_\infty\leq\|s_2-s_1\|_\infty\frac{c^{j-1}}{1-c}\leq 2\cdot\epsilon\cdot\frac{c^{j-1}}{1-c}\quad\forall j\in\mathbb{N}^* \quad (4.39)$$

□

**Note:** If the maximum voltage variation, with respect to nominal voltage $u_N$, of the known voltages $w_{k+1},..,w_n$ is lesser or equal than $\delta$, then the maximum voltage variation with respect to $u_N$ of the initially unknown variables $v_1,..,v_k$ is lesser or equal than $\epsilon$.

**Algorithm:**

With the definitions indicated in the statement of property 1, if the conductance matrix $\mathbf{G}$, the nominal voltage of the grid $u_N$, the powers $P_1,...,P_k$ and the voltages $\omega_{k+1},...,\omega_n$ are known, we proceed as follows:

1.- We obtain $\mathbf{G}_k$ and $\Gamma_k$.

2.- We calculate P.

3.- We consider $c, \rho, \epsilon$ and $\delta$ taking into account that $c$ and $\rho$ are auxiliary constants, while $\epsilon$ and $\delta$ are the bounds indicates before for the voltage variations with respect to the nominal value.

4.- We determine $u_0$.

5.- We verify that $u_N > u_0 + \epsilon$ and $|\omega_{k+1} - u_N| \leq \delta, ..., |\omega_n - u_N| \leq \delta$. If it is not fulfil come back to step 3.

6.- We consider the sequence $(s_j)_{j\in\mathbb{N}}$ such that:

6.1.- The $k$ components of $s_0$ are greater or equal than $u_0$, (we can choose $s_0 = [u_N, ..., u_N]^T \in \mathbb{R}^k$).

6.2.- $\forall\ j \in \mathbb{N} \quad s_{j+1} = G_k^{-1} \cdot \Psi(s_j) + G_k^{-1} \cdot \Gamma_k \cdot W$.

7.- We calculate V$= \lim_{j\to\infty} s_j$, which components are the voltages $v_1, ..., v_k$.

8.- As we know all voltages $v_1, ..., v_k, \omega_{k+1}, ..., \omega_n$ we can determine all currents and all powers.

***Property 2*** *If $P_1, P_2, \ldots, P_k$ remain constant, calling $\Pi = (P_{k+1}, \ldots, P_n)^T$,*

$$\frac{\partial V}{\partial W} = \begin{bmatrix} \frac{\partial v_1}{\partial w_{k+1}} & \frac{\partial v_1}{\partial w_{k+2}} & \cdots & \frac{\partial v_1}{\partial w_n} \\ \frac{\partial v_2}{\partial w_{k+1}} & \frac{\partial v_2}{\partial w_{k+2}} & \cdots & \frac{\partial v_2}{\partial w_n} \\ \vdots & \vdots & \ddots & \vdots \\ \frac{\partial v_k}{\partial w_{k+1}} & \frac{\partial v_k}{\partial w_{k+2}} & \cdots & \frac{\partial v_k}{\partial w_n} \end{bmatrix}, \frac{\partial \Pi}{\partial W} = \begin{bmatrix} \frac{\partial P_{k+1}}{\partial w_{k+1}} & \frac{\partial P_{k+1}}{\partial w_{k+2}} & \cdots & \frac{\partial P_{k+1}}{\partial w_n} \\ \frac{\partial P_{k+2}}{\partial w_{k+1}} & \frac{\partial P_{k+2}}{\partial w_{k+2}} & \cdots & \frac{\partial P_{k+2}}{\partial w_n} \\ \vdots & \vdots & \ddots & \vdots \\ \frac{\partial P_n}{\partial w_{k+1}} & \frac{\partial P_n}{\partial w_{k+2}} & \cdots & \frac{\partial P_n}{\partial w_n} \end{bmatrix} \quad (4.40)$$

*(considering the applications from $W$ to $V$ and from $W$ to $\Pi$), it is also true that:*

- *The jacobian matrix $\frac{\partial V}{\partial W}$ fulfils the following relation:*

$$\left[\boldsymbol{G}_k - \Psi'(V)\right] \cdot \frac{\partial V}{\partial W} = \Gamma_k \quad (4.41)$$

*where*

$$\Psi'(V) = \frac{\partial \Psi}{\partial V} = \begin{bmatrix} -\frac{P_1}{v_1^2} & 0 & \ldots & 0 \\ 0 & -\frac{P_2}{v_2^2} & \ldots & 0 \\ \vdots & \vdots & \ddots & \vdots \\ 0 & 0 & \ldots & -\frac{P_k}{v_k^2} \end{bmatrix} \quad (4.42)$$

*is the Jacobian matrix of $\Psi$ with respect to $V$.*

*Besides, if $[\boldsymbol{G}_k - \Psi'(V)]$ is invertible, then:*

$$\frac{\partial V}{\partial W} = \left[\boldsymbol{G}_k - \Psi'(V)\right]^{-1} \cdot \Gamma_k \quad (4.43)$$

- *The jacobian matrix* $\frac{\partial \Pi}{\partial W}$ *is determined by the following expression:*

$$\frac{\partial \Pi}{\partial W} = [\Phi] + [W] \cdot \left[ \Lambda_{n-k} - \Gamma_k^T \cdot \frac{\partial V}{\partial W} \right] \tag{4.44}$$

*where* $[\Phi]$=$diag\left(\frac{P_{k+1}}{w_{k+1}}, \frac{P_{k+2}}{w_{k+2}}, \ldots, \frac{P_n}{w_n}\right)$ *and* $[W] = diag\,(w_{k+1}, \ldots, w_n)$.
*If* $[\boldsymbol{G}_k - \Psi'(V)]$ *is invertible then:*

$$\frac{\partial \Pi}{\partial W} = [\Phi] + [W] \cdot \left[ \Lambda_{n-k} - \Gamma_k^T \cdot \left[ \boldsymbol{G}_k - \Psi'(V) \right]^{-1} \cdot \Gamma_k \right] \tag{4.45}$$

***Proof.-***
The system (4.18) is equivalent to:

$$\mathbf{G}_k \cdot V = \Psi(V) + \Gamma_k \cdot W \tag{4.46}$$

and if $\Psi'(V) = \frac{\partial \Psi}{\partial V}$ is the jacobian matrix of $\Psi$, it holds that:

$$\mathbf{G}_k \cdot \frac{\partial V}{\partial W} = \Psi'(V) \cdot \frac{\partial V}{\partial W} + \Gamma_k \tag{4.47}$$

which is equivalent to equation (4.41), and if in addition $[\mathbf{G}_k - \Psi'(V)]$ is invertible, then equation (4.43) is verified.

When $u_1 = v_1, \ldots, u_k = v_k, u_{k+1} = w_{k+1}, \ldots, u_n = w_n$, from system (4.4) and due to $w_{k+1} > 0, \ldots, w_n > 0$, we obtain:

$$\begin{cases} -g_{1,k+1} \cdot v_1 - .. - g_{k,k+1} \cdot v_k + g_{k+1,k+1} \cdot w_{k+1} - .. - g_{k+1,n} \cdot w_n = \frac{P_{k+1}}{w_{k+1}} \\ \vdots \\ -g_{1,n} \cdot v_1 - .. - g_{k,n} \cdot v_k - g_{k+1,n} \cdot w_{k+1} - .. + g_{n,n} \cdot w_n = \frac{P_n}{w_n} \end{cases} \tag{4.48}$$

and writing (4.48) in matrix form, we obtain:

$$-\Gamma_k^T \cdot V + \Lambda_{n-k} \cdot W = \Phi(W) \tag{4.49}$$

where

$$\Phi(W) = \Phi((w_{k+1}, w_{k+2}, \ldots, w_n)^T) = \left( \frac{P_{k+1}}{w_{k+1}}, \frac{P_{k+2}}{w_{k+2}}, \ldots, \frac{P_n}{w_n} \right)^T \tag{4.50}$$

At this point, it should be pointed out that $P_{k+i}$ are function of $W$, and consequently $\Phi(W) = \left( \frac{P_{k+1}(W)}{w_{k+1}}, \ldots, \frac{P_n(W)}{w_n} \right)^T$.

From expression (4.49), we deduce:

$$-\Gamma_k^T \cdot \frac{\partial V}{\partial W} + \Lambda_{n-k} = \Phi'(W) = \frac{\partial \Phi}{\partial W} \tag{4.51}$$

where

$$\Phi'(W) = \begin{bmatrix} \frac{1}{w_{k+1}}\frac{\partial P_{k+1}}{\partial w_{k+1}} - \frac{P_{k+1}}{w_{k+1}^2} & \frac{1}{w_{k+1}}\frac{\partial P_{k+1}}{\partial w_{k+2}} & \cdots & \frac{1}{w_{k+1}}\frac{\partial P_{k+1}}{\partial w_n} \\ \frac{1}{w_{k+2}}\frac{\partial P_{k+2}}{\partial w_{k+1}} & \frac{1}{w_{k+2}}\frac{\partial P_{k+2}}{\partial w_{k+2}} - \frac{P_{k+2}}{w_{k+2}^2} & \cdots & \frac{1}{w_{k+2}}\frac{\partial P_{k+2}}{\partial w_n} \\ \vdots & \vdots & \ddots & \vdots \\ \frac{1}{w_n}\frac{\partial P_n}{\partial w_{k+1}} & \frac{1}{w_n}\frac{\partial P_n}{\partial w_{k+2}} & \cdots & \frac{1}{w_n}\frac{\partial P_n}{\partial w_n} - \frac{P_n}{w_n^2} \end{bmatrix} \quad (4.52)$$

and consequently:

$$[W]\cdot\Phi'(W) = \begin{bmatrix} \frac{\partial P_{k+1}}{\partial w_{k+1}} - \frac{P_{k+1}}{w_{k+1}} & \frac{\partial P_{k+1}}{\partial w_{k+2}} & \cdots & \frac{\partial P_{k+1}}{\partial w_n} \\ \frac{\partial P_{k+2}}{\partial w_{k+1}} & \frac{\partial P_{k+2}}{\partial w_{k+2}} - \frac{P_{k+2}}{w_{k+2}} & \cdots & \frac{\partial P_{k+2}}{\partial w_n} \\ \vdots & \vdots & \ddots & \vdots \\ \frac{\partial P_n}{\partial w_{k+1}} & \frac{\partial P_n}{\partial w_{k+2}} & \cdots & \frac{\partial P_n}{\partial w_n} - \frac{P_n}{w_n} \end{bmatrix} \quad (4.53)$$

and therefore:

$$[W]\cdot\Phi'(W) + [\Phi] = \begin{bmatrix} \frac{\partial P_{k+1}}{\partial w_{k+1}} & \frac{\partial P_{k+1}}{\partial w_{k+2}} & \cdots & \frac{\partial P_{k+1}}{\partial w_n} \\ \frac{\partial P_{k+2}}{\partial w_{k+1}} & \frac{\partial P_{k+2}}{\partial w_{k+2}} & \cdots & \frac{\partial P_{k+2}}{\partial w_n} \\ \vdots & \vdots & \ddots & \vdots \\ \frac{\partial P_n}{\partial w_{k+1}} & \frac{\partial P_n}{\partial w_{k+2}} & \cdots & \frac{\partial P_n}{\partial w_n} \end{bmatrix} = \frac{\partial \Pi}{\partial W} \quad (4.54)$$

From equations (4.51) and (4.54), we deduce the expression (4.44), and if $[\mathbf{G}_k - \Phi'(V)]$ is invertible, then equation (4.45) is verified.

□

***Property* 3** *If $w_{k+1}, \ldots, w_n$ remain constant, defining $\mathcal{P} = (P_1, \ldots, P_k)^T$,*

$$\frac{\partial V}{\partial \mathcal{P}} = \begin{bmatrix} \frac{\partial v_1}{\partial P_1} & \frac{\partial v_1}{\partial P_2} & \cdots & \frac{\partial v_1}{\partial P_k} \\ \frac{\partial v_2}{\partial P_1} & \frac{\partial v_2}{\partial P_2} & \cdots & \frac{\partial v_2}{\partial P_k} \\ \vdots & \vdots & \ddots & \vdots \\ \frac{\partial v_k}{\partial P_1} & \frac{\partial v_k}{\partial P_2} & \cdots & \frac{\partial v_k}{\partial P_k} \end{bmatrix}, \quad \frac{\partial \Pi}{\partial \mathcal{P}} = \begin{bmatrix} \frac{\partial P_{k+1}}{\partial P_1} & \frac{\partial P_{k+1}}{\partial P_2} & \cdots & \frac{\partial P_{k+1}}{\partial P_k} \\ \frac{\partial P_{k+2}}{\partial P_1} & \frac{\partial P_{k+2}}{\partial P_2} & \cdots & \frac{\partial P_{k+2}}{\partial P_k} \\ \vdots & \vdots & \ddots & \vdots \\ \frac{\partial P_n}{\partial P_1} & \frac{\partial P_n}{\partial P_2} & \cdots & \frac{\partial P_n}{\partial P_k} \end{bmatrix} \quad (4.55)$$

*(considering the applications from $\mathcal{P}$ to $V$ and from $\mathcal{P}$ to $\Pi$), it is also true that:*

- *The Jacobian matrix $\frac{\partial V}{\partial \mathcal{P}}$ fulfils the following relation:*

$$\left[\boldsymbol{G}_k - \Psi'(V)\right]\cdot\frac{\partial V}{\partial \mathcal{P}} = [V]^{-1} \quad (4.56)$$

*where $\Psi'(V) = \frac{\partial \Psi}{\partial V}$ is the Jacobian matrix of $\Psi$ with respect to $V$ shown in (4.42), and $[V] = diag(v_1, v_2, ..., v_k)$. Besides, if $[\boldsymbol{G}_k - \Psi'(V)]$ is invertible, then:*

$$\frac{\partial V}{\partial \mathcal{P}} = \left[\boldsymbol{G}_k - \Psi'(V)\right]^{-1}\cdot[V]^{-1} \quad (4.57)$$

- *The jacobian matrix* $\frac{\partial \Pi}{\partial \mathcal{P}}$ *is determined by the following expression:*

$$\frac{\partial \Pi}{\partial \mathcal{P}} = -[W] \cdot \Gamma_k^T \cdot \frac{\partial V}{\partial \mathcal{P}} \tag{4.58}$$

*where* $[W] = diag\,(w_{k+1}, w_{k+2}, \ldots, w_n)$*, so if* $[\boldsymbol{G}_k - \Psi'(V)]$ *is invertible then:*

$$\frac{\partial \Pi}{\partial \mathcal{P}} = -[W] \cdot \Gamma_k^T \cdot \left[\boldsymbol{G}_k - \Psi'(V)\right]^{-1} \cdot [V]^{-1} \tag{4.59}$$

***Proof.-***
The system (4.18) is equivalent to:

$$\mathbf{G}_k \cdot V = \Psi(V) + \Gamma_k \cdot W \tag{4.60}$$

where $\Psi(V) = \left(\frac{P_1}{v_1}, ..., \frac{P_k}{v_k}\right)^T$ and $\Gamma_k \cdot W$ is constant, so:

$$\mathbf{G}_k \cdot \frac{\partial V}{\partial \mathcal{P}} = \begin{bmatrix} \frac{1}{v_1} - \frac{P_1}{v_1^2} \cdot \frac{\partial v_1}{\partial P_1} & -\frac{P_1}{v_1^2} \cdot \frac{\partial v_1}{\partial P_2} & \cdots & -\frac{P_1}{v_1^2} \cdot \frac{\partial v_1}{\partial P_k} \\ -\frac{P_2}{v_2^2} \cdot \frac{\partial v_2}{\partial P_1} & \frac{1}{v_2} - \frac{P_2}{v_2^2} \cdot \frac{\partial v_2}{\partial P_2} & \cdots & -\frac{P_2}{v_2^2} \cdot \frac{\partial v_2}{\partial P_k} \\ \vdots & \vdots & \ddots & \vdots \\ -\frac{P_k}{v_k^2} \cdot \frac{\partial v_k}{\partial P_1} & -\frac{P_k}{v_k^2} \cdot \frac{\partial v_k}{\partial P_2} & \cdots & \frac{1}{v_k} - \frac{P_k}{v_k^2} \cdot \frac{\partial v_k}{\partial P_k} \end{bmatrix} \tag{4.61}$$

which is equivalent to equation (4.56), and if in addition $[\mathbf{G}_k - \Psi'(V)]$ is invertible, then equation (4.57) is verified.

From expressions (4.49) and (4.50), and as $\Lambda_{n-k} \cdot W$ is constant, we deduce that:

$$-\Gamma_k^T \cdot \frac{\partial V}{\partial \mathcal{P}} = \begin{bmatrix} \frac{1}{w_{k+1}} \cdot \frac{\partial P_{k+1}}{\partial P_1} & \frac{1}{w_{k+1}} \cdot \frac{\partial P_{k+1}}{\partial P_2} & \cdots & \frac{1}{w_{k+1}} \cdot \frac{\partial P_{k+1}}{\partial P_k} \\ \frac{1}{w_{k+2}} \cdot \frac{\partial P_{k+2}}{\partial P_1} & \frac{1}{w_{k+2}} \cdot \frac{\partial P_{k+2}}{\partial P_2} & \cdots & \frac{1}{w_{k+2}} \cdot \frac{\partial P_{k+2}}{\partial P_k} \\ \vdots & \vdots & \ddots & \vdots \\ \frac{1}{w_n} \cdot \frac{\partial P_n}{\partial P_1} & \frac{1}{w_n} \cdot \frac{\partial P_n}{\partial P_2} & \cdots & \frac{1}{w_n} \cdot \frac{\partial P_n}{\partial P_k} \end{bmatrix} \tag{4.62}$$

and consequently,

$$-\Gamma_k^T \cdot \frac{\partial V}{\partial \mathcal{P}} = diag(\frac{1}{w_{k+1}}, \frac{1}{w_{k+2}}, ..., \frac{1}{w_n}) \cdot \frac{\partial \Pi}{\partial \mathcal{P}} \tag{4.63}$$

and therefore,

$$\frac{\partial \Pi}{\partial \mathcal{P}} = -[W] \cdot \Gamma_k^T \cdot \frac{\partial V}{\partial \mathcal{P}}$$

which is the equation (4.58), and if $[\mathbf{G}_k - \Psi'(V)]$ is invertible, then equation (4.59) is verified. □

***Property* 4** *Let $f : \mathbb{R}^n \to \mathbb{R}^n$ be the mapping from the known variables $(P_1, ..., P_k, w_{k+1}, ..., w_n)$ to the unknown variables $(v_1, ..., v_k, P_{k+1}, ..., P_n)$ such that system 4.4 and the hypothesis of property 1 hold. Then:*

$$f(P_1, ..., P_k, w_{k+1}, ..., w_n) = (v_1, ..., v_k, P_{k+1}, ..., P_n) \tag{4.64}$$

*and $f'$, the Jacobian Matrix of $f$, is:*

$$f' = \begin{bmatrix} \frac{\partial V}{\partial \mathcal{P}} & \frac{\partial V}{\partial W} \\ \\ \frac{\partial \Pi}{\partial \mathcal{P}} & \frac{\partial \Pi}{\partial W} \end{bmatrix} \tag{4.65}$$

*If $[\boldsymbol{G}_k - \Psi'(V)]$ is invertible, then it holds that:*

$$\begin{aligned} \tfrac{\partial V}{\partial \mathcal{P}} &= [\boldsymbol{G}_k - \Psi'(V)]^{-1} \cdot [V]^{-1} \\ \tfrac{\partial V}{\partial W} &= [\boldsymbol{G}_k - \Psi'(V)]^{-1} \cdot \Gamma_k \\ \tfrac{\partial \Pi}{\partial \mathcal{P}} &= -[W] \cdot {\Gamma_k}^t \cdot [\boldsymbol{G}_k - \Psi'(V)]^{-1} \cdot [V]^{-1} \\ \tfrac{\partial \Pi}{\partial W} &= [\Phi] + [W] \cdot (\Lambda_{n-k} - {\Gamma_k}^t \cdot [\boldsymbol{G}_k - \Psi'(V)]^{-1} \cdot \Gamma_k) \end{aligned}$$

***Proof.-***
It is a direct consequence of properties 2 and 3. □

### 4.2.4 Application example. Six nodes system.

In order to illustrate how the proposed algorithm operates, a multi-terminal HVDC grid model shown in figure 4.2 is presented.

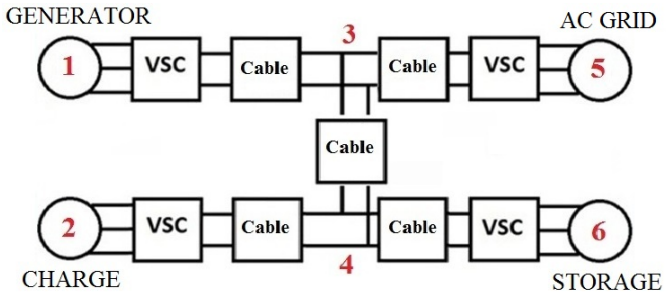


Figure 4.2: General benchmark.

In this model there are one producer node (1), one consumptions node (2), a node connected to an AC grid (5) which can supply or absorb power, and a storage in the node 6 which can supply or absorb energy. There are also two interconnection nodes (3 and 4), where no power is injected or consumed. Table 4.1 lists the parameters values of this model.

Table 4.1: Simulation values.

| | | |
|---|---|---|
| $u_N$ | Nominal voltage | 400 kV |
| $P_{nom-1}$ | Nominal power generator node 1 | 200 MW |
| $R_{cable}$ | Cable resistance | 0.0121 Ω/km |
| $L_{13}$ | Length line 1-3 | 2×90 km |
| $L_{24}$ | Length line 2-4 | 2×100 km |
| $L_{34}$ | Length line 3-4 | 2×75 km |
| $L_{35}$ | Length line 3-5 | 2×50 km |
| $L_{46}$ | Length line 4-6 | 2×35 km |

For this set of data, the conductance matrix $\mathbf{G}$ of the network is:

$$\mathbf{G} = \begin{bmatrix} 0.46 & 0 & -0.46 & 0 & 0 & 0 \\ 0 & 0.41 & 0 & -0.41 & 0 & 0 \\ -0.46 & 0 & 1.84 & -0.55 & -0.83 & 0 \\ 0 & -0.41 & -0.55 & 2.14 & 0 & -1.18 \\ 0 & 0 & -0.83 & 0 & 0.83 & 0 \\ 0 & 0 & 0 & -1.18 & 0 & 1.18 \end{bmatrix} (\Omega^{-1}) \qquad (4.66)$$

We select nodes 5 and 6 as nodes where the voltage is known, and consequently we suppose known the power in the remaining. It could be remarked that the power in interconnection nodes will always be zero as explained above. So according with the formulation explained, $k = 4$, and matrices $\mathbf{G}_4$ and $\Gamma_4$ are:

$$\mathbf{G}_4 = \begin{bmatrix} 0.46 & 0 & -0.46 & 0 \\ 0 & 0.41 & 0 & -0.41 \\ -0.46 & 0 & 1.84 & -0.55 \\ 0 & -0.41 & -0.55 & 2.14 \end{bmatrix} \qquad \Gamma_4 = \begin{bmatrix} 0 & 0 \\ 0 & 0 \\ 0.83 & 0 \\ 0 & 1.18 \end{bmatrix} \qquad (4.67)$$

In the next examples the values of the constants used in the proof of Property 1 are: $c = 0.5$, $\rho = 0.4$, $\epsilon = 4$ kV (1% of $u_N$), $\delta = 1.5$ kV and $u_N = 400$ kV. With these constants an unique solution is guarantee.

**Property 1. Examples.**

Example 1.

If node 1 produces 200 MW, the charge in node 2 consumes 120 MW, the voltage at node 5 is 400 kV, and the voltage at node 6 is 399 kV, then the minimum value of $u_0$ is 364.26 kV. This means that from any initial point which components are greater than $u_0$ the sequence converges to the unique solution. We have selected in this case the initial point as $s_0 = [400, 400, 400, 400]^T$. The result of our algorithm is shown in table 4.2.

The results of table 4.2 show that AC grid in node 5 absorbs 7.46 MW and the storage absorbs 71.33 MW. We observe also that voltages in nodes

Table 4.2: Power flow result. Example 1.

| Algorithm inputs | | | | | |
|---|---|---|---|---|---|
| $P_1$ | $P_2$ | $P_3$ | $P_4$ | $u_5$ | $u_6$ |
| 200 MW | -120 MW | 0 MW | 0 MW | 400 kV | 399 kV |
| Results | | | | | |
| $u_1$ | $u_2$ | $u_3$ | $u_4$ | $P_5$ | $P_6$ |
| 401.11 kV | 398.42 kV | 400.02 kV | 399.15 kV | -7.46 MW | -71.33 MW |

1, 2, 3 and 4 are close to the nominal value of the grid (400 kV). In this case the power losses in the grid due to cable resistances are 1.21 MW.

Example 2.

If now, only the voltage at node 6 varies ($u_6 = 398,9$ kV), we obtain:

Table 4.3: Power flow result. Example 2.

| Algorithm inputs | | | | | |
|---|---|---|---|---|---|
| $P_1$ | $P_2$ | $P_3$ | $P_4$ | $u_5$ | $u_6$ |
| 200 MW | -120 MW | 0 MW | 0 MW | 400 kV | 398.9 kV |
| Results | | | | | |
| $u_1$ | $u_2$ | $u_3$ | $u_4$ | $P_5$ | $P_6$ |
| 401.08 kV | 398.34 kV | 399.99 kV | 399.07 kV | 2.86 MW | -81.60 MW |

The results of table 4.3 show now as the AC grid in node 5 supplies only 2.86 MW and the storage absorbs 81.60 MW. We observe that the voltages in nodes 1, 2, 3 and 4 are close to the nominal value of the grid (400 kV). In this case the power losses in the grid due to cable resistances are 1.26 MW.

Example 3.

If now node 1 does not produce power and the load remains with the same consumption, for a voltage value of 400 kV and 399 kV at nodes 5 and 6 respectively we obtain that the minimum value of $u_0$ is 218.6 kV, and the result of the algorithm is:

Table 4.4: Power flow result. Example 3.

| Algorithm inputs | | | | | |
|---|---|---|---|---|---|
| $P_1$ | $P_2$ | $P_3$ | $P_4$ | $u_5$ | $u_6$ |
| 0 MW | -120 MW | 0 MW | 0 MW | 400 kV | 399 kV |
| Results | | | | | |
| $u_1$ | $u_2$ | $u_3$ | $u_4$ | $P_5$ | $P_6$ |
| 399.61 kV | 398.29 kV | 399.61 kV | 399.02 kV | 129.67 MW | -9.13 MW |

The results of table 4.4 show that AC grid in node 5 supplies 129.67 MW and the storage absorbs 9.13 MW. We also remark that voltages in nodes 1, 2, 3 and 4 are close to the nominal value of the grid (400 kV). In this case the power losses in the grid due to cable resistances are 0.54 MW.

Example 4.

If now, the node 1 does not produce power and the load remains with the same consumption, for a voltage value of 400 kV and 399.1 kV at nodes 5 and 6 respectively, we obtain table 4.5. The results of table 4.5 that AC grid in node 5 supplies 119.33 MW and the storage supplies 1.16 MW. We also remark that voltages in nodes 1, 2, 3 and 4 are close to the nominal value of the grid (400 kV). In this case the power losses in the grid due to cable resistances are 0.49 MW.

Table 4.5: Power flow result. Example 4.

| Algorithm inputs | | | | | |
|---|---|---|---|---|---|
| $P_1$ | $P_2$ | $P_3$ | $P_4$ | $u_5$ | $u_6$ |
| 0 MW | -120 MW | 0 MW | 0 MW | 400 kV | 399.1 kV |
| Results | | | | | |
| $u_1$ | $u_2$ | $u_3$ | $u_4$ | $P_5$ | $P_6$ |
| 399.64 kV | 398.37 kV | 399.64 kV | 399.10 kV | 119.33 MW | 1.16 MW |

**Property 2. Example.**

Property 2 gives us information about how the unknown variables will change if we vary the known voltages ($u_5$ and $u_6$). For example, if we know the result of the previous example 1 and we want to know what happens if we reduce the voltage at node 6 by 0.1 kV, we can achieve approximately the same result from the previous example 2, without the need to use the iterative method, and by using the Jacobian Matrix.

For this example 1, applying (4.43), the Jacobian Matrix $\partial V/\partial W$ is:

$$\frac{\partial V}{\partial W} = \begin{bmatrix} \frac{\partial u_1}{\partial u_5} & \frac{\partial u_1}{\partial u_6} \\ \frac{\partial u_2}{\partial u_5} & \frac{\partial u_2}{\partial u_6} \\ \frac{\partial u_3}{\partial u_5} & \frac{\partial u_3}{\partial u_6} \\ \frac{\partial u_4}{\partial u_5} & \frac{\partial u_4}{\partial u_6} \end{bmatrix} = \begin{bmatrix} 0.68 & 0.31 \\ 0.22 & 0.78 \\ 0.69 & 0.31 \\ 0.22 & 0.78 \end{bmatrix} \tag{4.68}$$

and applying (4.44), the Jacobian Matrix $\partial \Pi/\partial W$ is:

$$\frac{\partial \Pi}{\partial W} = \begin{bmatrix} \frac{\partial P_5}{\partial u_5} & \frac{\partial P_5}{\partial u_6} \\ \frac{\partial P_5}{\partial u_5} & \frac{\partial P_6}{\partial u_6} \end{bmatrix} = \begin{bmatrix} 103.51 & -103.25 \\ -102.99 & 102.73 \end{bmatrix} \tag{4.69}$$

Taking into account that:
$\Delta V \approx \frac{\partial V}{\partial \mathcal{P}} \cdot \Delta \mathcal{P} + \frac{\partial V}{\partial W} \cdot \Delta W$ and also that $\Delta \Pi \approx \frac{\partial \Pi}{\partial \mathcal{P}} \cdot \Delta \mathcal{P} + \frac{\partial \Pi}{\partial W} \cdot \Delta W$.
If $\Delta W = [0, -0.1]^T$ and $\Delta \mathcal{P} = 0$ then:

$$\Delta V = \begin{bmatrix} -0.03 \\ -0.08 \\ -0.03 \\ -0.08 \end{bmatrix} kV \Rightarrow V = \begin{bmatrix} 401.07 \\ 398.34 \\ 399.99 \\ 399.07 \end{bmatrix} kV \tag{4.70}$$

which are approximately the same voltages as in example 2, and

$$\Delta \Pi = \begin{bmatrix} 10.33 \\ -10.27 \end{bmatrix} MW \Rightarrow \Pi = \begin{bmatrix} 2.86 \\ -81.61 \end{bmatrix} MW \tag{4.71}$$

which are approximately the same powers as in example 2.

**Property 3. Example.**

Property 3 gives us information about how the unknown variables will change if we vary the known power ($P_1$, $P_2$, $P_3$ and $P_6$). For example, if we know the result of the previous example 1 and we want to know what happens if we vary the power at node 1 by -200 MW, we can achieve approximately the same result from previous example 3, without the need to use the iterative method, and by using the Jacobian matrix. In this example 1, applying (4.57), the Jacobian Matrix $\partial V / \partial \mathcal{P}$ is:

$$\frac{\partial V}{\partial \mathcal{P}} = \begin{bmatrix} \frac{\partial u_1}{\partial P_1} & \frac{\partial u_1}{\partial P_2} & \frac{\partial u_1}{\partial P_3} & \frac{\partial u_1}{\partial P_4} \\ \frac{\partial u_1}{\partial P_1} & \frac{\partial u_2}{\partial P_2} & \frac{\partial u_2}{\partial P_3} & \frac{\partial u_2}{\partial P_4} \\ \frac{\partial u_3}{\partial P_1} & \frac{\partial u_3}{\partial P_2} & \frac{\partial u_3}{\partial P_3} & \frac{\partial u_3}{\partial P_4} \\ \frac{\partial u_4}{\partial P_1} & \frac{\partial u_4}{\partial P_2} & \frac{\partial u_4}{\partial P_3} & \frac{\partial u_4}{\partial P_4} \end{bmatrix} = \begin{bmatrix} 0.00748 & 0.00066 & 0.00207 & 0.00066 \\ 0.00066 & 0.00775 & 0.00066 & 0.00166 \\ 0.00207 & 0.00067 & 0.00208 & 0.00066 \\ 0.00066 & 0.00166 & 0.00066 & 0.00166 \end{bmatrix} \tag{4.72}$$

and applying (4.58) the Jacobian Matrix $\partial \Pi / \partial \mathcal{P}$ is:

$$\frac{\partial \Pi}{\partial \mathcal{P}} = \begin{bmatrix} \frac{\partial P_5}{\partial P_1} & \frac{\partial P_5}{\partial P_2} & \frac{\partial P_5}{\partial P_3} & \frac{\partial P_5}{\partial P_4} \\ \frac{\partial P_6}{\partial P_1} & \frac{\partial P_6}{\partial P_2} & \frac{\partial P_6}{\partial P_3} & \frac{\partial P_6}{\partial P_4} \end{bmatrix} = \begin{bmatrix} -0.68 & -0.22 & -0.69 & -0.22 \\ -0.31 & -0.78 & -0.31 & -0.78 \end{bmatrix} \tag{4.73}$$

Taking into account that:
$\Delta V \approx \frac{\partial V}{\partial \mathcal{P}} \cdot \Delta \mathcal{P} + \frac{\partial V}{\partial W} \cdot \Delta W$ and also that $\Delta \Pi \approx \frac{\partial \Pi}{\partial \mathcal{P}} \cdot \Delta \mathcal{P} + \frac{\partial \Pi}{\partial W} \cdot \Delta W$.
If $\Delta W = 0$ and $\Delta \mathcal{P} = [-200, 0, 0, 0]^T$ then:

$$\Delta V = \begin{bmatrix} -1.50 \\ -0.13 \\ -0.41 \\ -0.13 \end{bmatrix} kV \Rightarrow V = \begin{bmatrix} 399.61 \\ 398.29 \\ 399.61 \\ 399.02 \end{bmatrix} kV \tag{4.74}$$

which are approximately the same voltages as in example 3, and:

$$\Delta \Pi = \begin{bmatrix} 136.62 \\ 61.97 \end{bmatrix} MW \Rightarrow \Pi = \begin{bmatrix} 129.16 \\ -9.36 \end{bmatrix} MW \tag{4.75}$$

which are approximately the same powers as in example 3.

**Property 4. Example.**

Property 4 provides information about how all the unknown variables will change if we vary the known variables. For example, if we know the result of previous example 1, and we want to evaluate the effects of a variation on power at node 1 by -200 MW and the voltage in node 5 by 0.1 kV, we can achieve approximately the same result that on previous example 4 without needing to use the iterative method, and by using the Jacobian matrix. The Jacobian Matrix $f'$ shown in (4.65) is composed by matrices: $\frac{\partial V}{\partial W}$, $\frac{\partial \Pi}{\partial W}$, $\frac{\partial V}{\partial \mathcal{P}}$ and $\frac{\partial \Pi}{\partial \mathcal{P}}$ which are the same as previous sections: (4.68), (4.69), (4.72) and (4.73) respectively.

Taking into account that:
$\Delta V \approx \frac{\partial V}{\partial \mathcal{P}} \cdot \Delta \mathcal{P} + \frac{\partial V}{\partial W} \cdot \Delta W$ and also that $\Delta \Pi \approx \frac{\partial \Pi}{\partial \mathcal{P}} \cdot \Delta \mathcal{P} + \frac{\partial \Pi}{\partial W} \cdot \Delta W$.
If $\Delta W = [0, 0.1]^T$ and $\Delta \mathcal{P} = [-200, 0, 0, 0]^T$ then:

$$\Delta V = \begin{bmatrix} -1.46 \\ -0.05 \\ -0.38 \\ -0.05 \end{bmatrix} kV \Rightarrow V = \begin{bmatrix} 399.64 \\ 398.37 \\ 399.64 \\ 399.10 \end{bmatrix} kV \tag{4.76}$$

which are approximately the same voltages as in example 4, and:

$$\Delta \Pi = \begin{bmatrix} 126.29 \\ 72.24 \end{bmatrix} MW \Rightarrow \Pi = \begin{bmatrix} 118.83 \\ 0.91 \end{bmatrix} MW \tag{4.77}$$

which are approximately the same powers as in example 4.

## 4.3 Secondary control with MPC.

As have been explained in section 4.1, if we consider that some type of predictions can be available, and if we include some storage devices in order

to operate the grid in a more secure way if renewable energies are considered, the use of MPC is particularly interesting, since it is able to manipulate effectively systems with constraints [98].

This section presents a short summary of MPC strategy, and then we will explain a power flow strategy for multi-terminal HVDC grids, where energy is mainly generated via renewable energy sources and there are nodes in the network with the possibility to store energy. This energy is generated taking into account real weather conditions in order to make the best scheduling of the system in a realistic approach. An optimization scheme through a prediction horizon, $N_p$, is proposed due to it is possible to possess reliable wind and consumption forecasts in which all these elements are included as well as real operation constraints, as for example: maximum and minimum value for the DC voltage or the maximum injected or supplied power in each node. Distribution losses are minimized for the whole network. This gives as a result a control strategy being able to deal with the whole system and its inherent constraints giving the framework for a multi-objective optimization control.

### 4.3.1 Model predictive control strategy.

The development of predictive control has always been driven by advances in industrial application, rather than rigorous mathematical derivation. To solve different types of industry problems, several control algorithms based on heuristic ideas have been developed, among which could be addressed: MPHC (Model Predictive Heuristic Control), DMC (Dynamic Matrix Control), QDMC (Quadratic Dynamic Matrix Control) and GPC (Generalized Predictive Control) [98], [99]. In this section we choose GPC for application.

The predictive control integrates optimal control, control of processes with dead time, multi variable processes and uses the future reference when they are available. Using a strategy with finite control horizon, it allows for consideration of constraints and non-linear processes. The main features of this control are the explicit use of a model to predict the process output at future time points (up to a certain prediction horizon), the calculation of control signals minimizing a certain objective function and a sliding strategy so that at each instant the horizon is moving toward the future, which involves applying the first control signal at each instant and reject the rest, repeating the calculation in each sample. As the optimization problem is solved by computer involved and that the receding horizon technique is applied to the solution, it is more natural to consider discrete models.

All controllers belonging to the family of MPC can be explained with the help of Figure 4.3.

For a given $N_p$, future output are predicted at time $t$ based on a process model. These predicted outputs, depend on the variable values known at time $t$ (the past inputs and the outputs) and the future control signals.

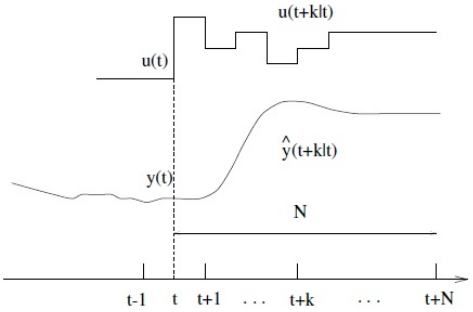


Figure 4.3: MPC strategy. Source

The set of future control signals is calculated by optimizing an objective function according to a given criterion, which aims to make the process output follow as closely as possible the reference trajectory.

The basic elements of predictive control are: the prediction model, the objective function, and the control law.

**Prediction Model.**

It is the mathematical prediction model that describes the expected system behaviour. This model can be linear or non-linear, continuous time or discrete time, expressed in terms of state-space variables or input-output signals.

One of the disadvantages of predictive control is the urgent need for an appropriate model of the dynamical system, since the control algorithm is based on it. As the behaviour obtained depends on the discrepancies between the real process and the model used. In our application we need to know with a certain precision the weather and the consumption forecast all will be explained in section 4.4.

**Cost function.**

The cost function is the one that indicates the criteria to optimize. It must be a positive definite function. The cost is expressed in the form of a particular evolution of the system along the prediction horizon $N_p$. In general, future output on the horizon considered follows a reference signal, while the control effort required for achieving it may be penalized.

**Control law.**

The values of future control are obtained by minimizing the cost function . To do this, we will calculate the predicted output values as a function of past values of inputs, outputs and future control signals, using the model that has been chosen (in this case the GPC) and appears in the cost function.

### 4.3.2 HVDC network.

We consider a general MT-HVDC network connecting wind farms, storage devices and AC grids (see figure 4.4). As the wind is an intermittent energy source, not only does it provide the primary energy to be transformed into electrical form but it also constitutes a source of disturbances both in terms of quality of the energy produced and in the overall stability of the system. Consequently and as we mentioned above, storage devices will be placed strategically in order to cope with possible peaks of energy demand or low energy availability in the production nodes.

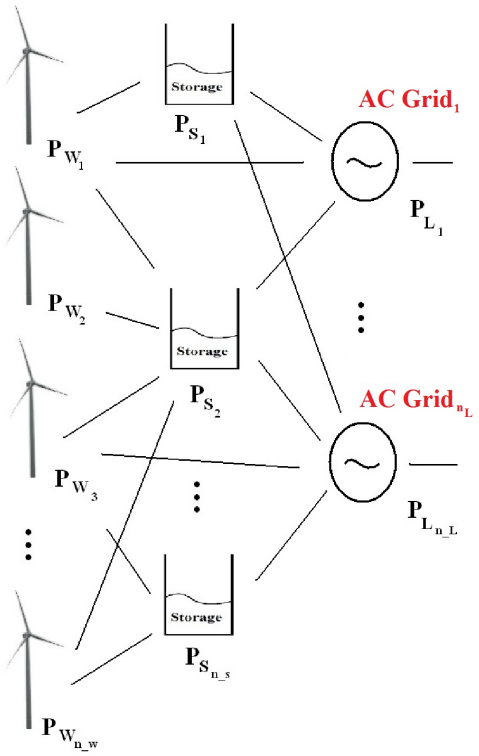


Figure 4.4: MT-HVDC Grid with wind farms and storage devices.

We will consider a scenario in which the AC networks connected to the grid will demand variable power, either because the load is variable or because market negotiation leads to that operating point. Wind farms together with the storage devices must be able to supply the consumed power via a MT-HVDC grid. To tackle this problem, our work has used real wind measures [100] and we have considered weather forecasting [101, 102]. In this way the control scheme only has to deal with the prediction error instead of dealing with the full amount of variability.

Finally, as the sample time used is in the order of minutes, we can neglect the dynamics of cables, and we can use resistive models.

### 4.3.3 Formulation of the problem.

As it has been shown in equation (4.6), in DC grids, the active power in the node $i$ could be rewritten as:

$$P_i = u_i \sum_{j=1}^{n} g_{i,j} \cdot u_j \tag{4.78}$$

where elements $g_{i,j}$, are the elements of conductance matrix shown in (4.8).

If we see the whole DC grid in terms of power, there will be nodes that inject power into the system, there will be nodes that absorb power from the system and there will be nodes that neither supply nor absorb power, these last nodes are the internal interconnection nodes (they are inside the grid). The algebraic sum of all these powers must be equal to the losses in the system (transmission losses in the lines). Using this idea we can define a losses function, $F_{Losses}$, which depends on voltages of each node.

$$F_{Losses}(u_1, \cdots, u_n) = \sum_{k=1}^{n} P_i = [u]^T \cdot [G] \cdot [u] \tag{4.79}$$

where $[u] = [u_1, \cdots, u_n] \in \mathbb{R}^n$, and $u_i$ is the voltage in node $i$.

Our purpose is to minimize the transmission losses in the system, or equivalently we want to find a set of voltage values which minimize our function shown in equation (4.79). Obviously, not any set of voltages will be valid, because several constraints must be guaranteed. However, DC systems present other advantages compared to AC, where a significant deviation with respect to the nominal state produces irreparable damage to rotative elements, because a deviation of the nominal voltage and/or power causes a variation in the frequency (or vice versa), which is critical for the proper operation of the system. In DC systems, the nominal voltage will not have as severe restrictions as in the AC systems, so we can talk of a "nominal strip" instead of a nominal value, in concordance with chapter 3. In this zone, any value for the voltage guarantees the proper functioning of the system. It is in this context where we can find the optimal set for all voltages, which minimizes the losses.

The "nominal strip" will have to be subject to numerous restrictions (they will be explained below), and for this reason, the use of MPC is particularly interesting, since it is able to manipulate effectively systems with constraints [98].

In addition, it is possible to carry out the minimization through a longer horizon if we possess reliable wind and consumption forecasts since the MPC handles in a natural way these types of problems with prediction horizon, $N_p$. Fortunately this is possible because current forecasts provide a very high reliability [101, 102]. So we can carry out an optimization along $N_p$,

and the result will be improved compared to making it at each instant in a single state way.

Furthermore, as renewable (variable) energies are used in this work, it is interesting to include in the grid storage devices, to store energy when there is an excess and to supply energy when there exits a shortage in the system. Also, and thanks to the use of MPC, it is possible to include the dynamics of these storages, with their efficiencies $\mu_i$, which, in general, will be different when they are charging or discharging. In equation (4.80), $E_s^k$ represents the energy at instant $k$ in the storage $s$, and $T$ is the sample time (we will consider that all sampling periods have the same duration).

$$E_s^{k+1} = E_s^k - T \cdot \mu_i \cdot P_s \qquad \forall s \in S \tag{4.80}$$

On the other hand and in concordance with definitions made in chapter 3, in our overall system, there will exist four types of nodes, the production nodes, $W$, (in this case wind farms), consumption nodes, $L$, storage nodes, $S$, and internal interconnection nodes, $IC$. It must be stressed that in $IC$ nodes there is no power production or consumption. Our objective function will minimize the subject to a number of constraints over a prediction horizon $N_p$. These restrictions are:

- The production and load power must be equal to forecast values (4.82a).
- The voltages at the nodes must be only in the "nominal strip" described above (4.82b).
- The current lines can not exceed certain values (maximum admissible current through the cables), (4.82c).
- The storage devices can absorb or supply power until a maximum value (4.82d).
- Also we have taken into account that a storage can not provide (absorb) power if it is empty (full) (4.82e).
- The balance of power has to be complied at all moments (4.82f).

With all this, our control variables will be the power supplied or absorbed by storage devices. However, as the restrictions of the system are formulated in terms of voltage our problem consists in finding the best combination of voltages which minimize $F_{Losses}$. These founded values will be the references to a lower control.

With the aforementioned considerations and taking the transmission losses equation as described in (4.79) the optimization problem can be formulated as follows:

$$J = min(F_{Losses}(u_1^k, \cdots, u_n^{k+N_p})) = min(\sum_{k=1}^{N_p} [\mathbf{u}^k]^T \cdot [\mathbf{G}] \cdot [\mathbf{u}^k]) \tag{4.81}$$

subject to:

$$\begin{aligned}
&\text{a) } j \in W \cup L \ / \ P_j = [\mathbf{u}^k]^T \cdot [G_j^*] \cdot [\mathbf{u}^k] \ \forall j, \text{ and } \forall k \\
&\text{b) } u_{i,min}^k \leq u_i^k \leq u_{i,max}^k \ \forall i, \text{ and } \forall k \\
&\text{c) } \left| \frac{u_i^k - u_j^k}{R_{i,j}} \right| \leq I_{max,line_{ij}} \forall i, j, k \\
&\text{d) } P_{s,min} \leq P_s^k \leq P_{s,max} \ \forall s \in S \text{ and } \forall k \\
&\text{e) } [E]_{s,min}^k \leq [E]_s^k \leq [E]_{s,max}^k \forall s \in S \text{ and } \forall k \\
&\text{f) } \sum P_{W_i}^k - \sum P_{L_i}^k = \sum P_{S_i}^k - \sum P_{Loss}^k \ \forall k
\end{aligned} \tag{4.82}$$

where $[\mathbf{u}^k] = [u_1^k, \cdots, u_n^k] \in \mathbb{R}^n$, and $u_i^k$ is the voltage in node i at instant $k$.

### 4.3.4 Advantages.

One of the biggest advantages of this method is that the losses are minimized with respect to a "classic" power flow as for example NR, and this is particularly important since we increase the number of nodes. Other benefits must be pointed out, and one of the most significant is that there does not exist a balance node, so there is no dependence on such nodes, something crucial in methods that use node balance. Other advantage that can be obtained, is that, thanks to the implantation of the MPC, we can anticipate problems in the grid such as: over-voltages, over-currents, emptying or filling of storage devices, etc...

Also the storage models used are closer to reality as they include performance in charge and discharge (in general different).

### 4.3.5 Existence of solutions.

The first question that we should ask is whether the proposed problem has a solution, and if there is solution we should also ask whether it is unique. In this section we will expose the demonstration that there are many possible solutions, but there is only one that gives the minimum value for $F_{Losses}$. For simplicity, firstly we carry out for the case of $\mathbb{R}^3$ (3 nodes) and then we will generalize to the case of $\mathbb{R}^n$ (n nodes).

### 4.3.6 Existence of solutions in $\mathbb{R}^3$.

Our problem is to minimize a function subject to some restrictions. We are going to analyse the properties of these constraints to ensure that there will be a region in the space that fulfills all the constraints. In this explanation

we will assume that $N_p$=1. This fact does not diminish the generality of the proof, it is only to make the calculations clearer.

**Constraints type a)**

According to our definitions made before, the first constraints are the type $j \in W \cup L \ / \ P_j = [\mathbf{u}]^T \cdot [G_j^*] \cdot [\mathbf{u}]$, and if we assume that we know the power in nodes 1 and 3:

$$[u_1\ u_2\ u_3] \cdot \begin{bmatrix} g_{1,1} & -\frac{g_{1,2}}{2} & -\frac{g_{1,3}}{2} \\ -\frac{g_{1,2}}{2} & 0 & 0 \\ -\frac{g_{1,3}}{2} & 0 & 0 \end{bmatrix} \cdot \begin{bmatrix} u_1 \\ u_2 \\ u_3 \end{bmatrix} = P_1 \tag{4.83}$$

$$[u_1\ u_2\ u_3] \cdot \begin{bmatrix} 0 & 0 & -\frac{g_{1,3}}{2} \\ 0 & 0 & -\frac{g_{2,3}}{2} \\ -\frac{g_{1,3}}{2} & -\frac{g_{2,3}}{2} & g_{3,3} \end{bmatrix} \cdot \begin{bmatrix} u_1 \\ u_2 \\ u_3 \end{bmatrix} = P_3 \tag{4.84}$$

These restrictions are clearly shaped in a quadric. We are going to analyse the quadric of equation (4.83), noting that the development is analogous to the other equation (4.84).

Firstly we want to know the nature of its center $\mathbf{c} = [x_0,y_0,z_0]$ .

$$\begin{bmatrix} g_{1,1} & -\frac{g_{1,2}}{2} & -\frac{g_{1,3}}{2} \\ -\frac{g_{1,2}}{2} & 0 & 0 \\ -\frac{g_{1,3}}{2} & 0 & 0 \end{bmatrix} \cdot \begin{bmatrix} x_0 \\ y_0 \\ z_0 \end{bmatrix} = 0 \Rightarrow \mathbf{c} = \begin{bmatrix} 0 \\ -\frac{g_{1,3}}{g_{1,2}} \cdot a \\ a \end{bmatrix} \tag{4.85}$$

As the system of equation (4.85) is an under-determinate compatible system, there are infinite centers that are on the line $\mathbf{r} \equiv u_2 = \text{-}\frac{g_{1,3}}{g_{1,2}} \cdot u_3$ (in the plane $u_1 = 0$).

Since matrix $G$ is symmetric, by the theorem of Schur there exists an orthogonal matrix $P$ such that $D = P^t G^* P$, where $D = diag(\lambda_1, \lambda_2, \lambda_3)$ and $\lambda_i \ \forall \ i = 1, 2, 3$ are the eigenvalues of $G^*$.

In general, the eigenvalues of $G^*$ has the form:

$$|\lambda \cdot I - G^*| = 0 \Longleftrightarrow \begin{cases} \lambda_1 = 0 \\ \lambda_2 = \frac{g_{1,1} + \sqrt{g_{1,1}^2 + g_{1,2}^2 + g_{1,3}^2}}{2} \triangleq \frac{\theta_2}{2} \\ \lambda_3 = \frac{g_{1,1} - \sqrt{g_{1,1}^2 + g_{1,2}^2 + g_{1,3}^2}}{2} \triangleq \frac{\theta_3}{2} \end{cases} \tag{4.86}$$

By definition, it is always true that $G_{i,i} \geq \sum_{j=1, j \neq i}^{N} g_{i,j}$ in the conductance matrix $G$. By other way it is also true that: $\sqrt{g_{1,1}^2 + g_{1,2}^2 + g_{1,3}^2} > g_{1,1}$, and for this reason $\lambda_2 > 0$ and $\lambda_3 < 0$. Therefore, matrix $G^*$ has zero, positive and negative eigenvalues (see basic property 5 of section 4.2.2). This fact makes power constraints of this kind non-convex restrictions.

An orthonormal base, $\mathfrak{B}_1$, made up by eigenvectors associated to each eigenvalue is $\mathfrak{B}_1 = \{\mathbf{v}_1|\mathbf{v}_2|\mathbf{v}_3\}$, where:

$$\mathbf{v}_1 = \frac{1}{\sqrt{g_{1,2}^2 + g_{1,3}^2}} \begin{bmatrix} 0 \\ -g_{1,3} \\ g_{1,2} \end{bmatrix}, \mathbf{v}_2 = \frac{1}{\sqrt{\theta_2^2 + g_{1,2}^2 + g_{1,3}^2}} \begin{bmatrix} \theta_2 \\ -g_{1,2} \\ g_{1,3} \end{bmatrix}$$

$$\mathbf{v}_3 = \frac{1}{\sqrt{\theta_3^2 + g_{1,2}^2 + g_{1,3}^2}} \begin{bmatrix} -\theta_3 \\ g_{1,2} \\ g_{1,2} \end{bmatrix} \tag{4.87}$$

Thus making a change of variables of the form:

$$\begin{bmatrix} u_1 \\ u_2 \\ u_3 \end{bmatrix} = [P] \begin{bmatrix} \mathrm{x}_1 \\ \mathrm{y}_1 \\ \mathrm{z}_1 \end{bmatrix} + \mathbf{c} \tag{4.88}$$

we obtain the reduced form of quadric $S_1$ shown in (4.83):

$$S_1 \equiv \alpha \mathrm{y}_1^2 + \beta \mathrm{z}_1^2 = P_1$$

$$\begin{aligned} \alpha &= \frac{g_{1,1}\theta_2^2 + g_{1,2}^2\theta_2 + g_{1,3}\theta_2^2}{\theta_2^2 + g_{1,2}^2 + g_{1,3}^2} > 0 \\ \beta &= \frac{g_{1,1}\theta_3^2 + g_{1,2}^2\theta_3 + g_{1,3}\theta_3^2}{\theta_3^2 + g_{1,2}^2 + g_{1,3}^2} < 0 \end{aligned} \tag{4.89}$$

also if we simplify the operations, we obtain that $\alpha = \lambda_2$ and $\beta = \lambda_3$ so:

$$S_1 \equiv \lambda_2 \mathrm{y}_1^2 + \lambda_3 \mathrm{z}_1^2 = P_1 \tag{4.90}$$

therefore the quadric is a hyperbolic cylinder as figure 4.5 shows.

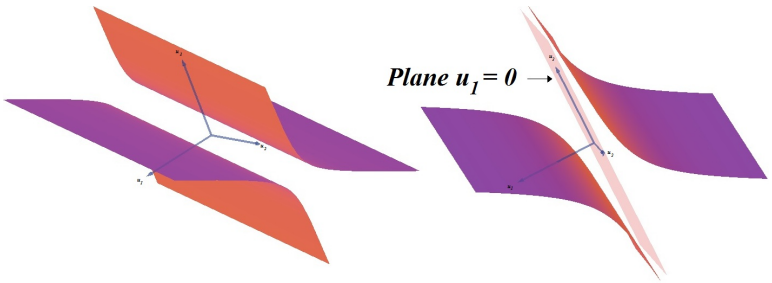


Figure 4.5: Hyperbolic cylinder $S_1$.

If we proceed in an analogous manner at node 3, we obtain the reduced form of the quadric $S_3$ shown in (4.84):

$$S_3 \equiv \lambda_1' \mathrm{x}_3^2 + \lambda_2' \mathrm{y}_3^2 = P_3 \tag{4.91}$$

where $\lambda_1'$ and $\lambda_2'$ are the eigenvalues of the matrix of system (4.84). It can now be noted, that the hyperbolic cylinder is symmetric with respect to the plane $u_3 = 0$, and also the axes $\mathrm{x}_3, \mathrm{y}_3, \mathrm{z}_3$ are different to $\mathrm{x}_1, \mathrm{y}_1, \mathrm{z}_1$.

The intersection of two quadric, figure 4.6, gives a curve, $\mathfrak{C}$, which can be parametrized, and it contains all the values of $u_1$, $u_2$ and $u_3$ in that our function objective must be minimized. $\mathfrak{C}$ can be defined as:

$$\mathfrak{C} \equiv \{(u_1, u_2, u_3) \in \mathbb{R}s / S_1 \cap S_3\} \tag{4.92}$$

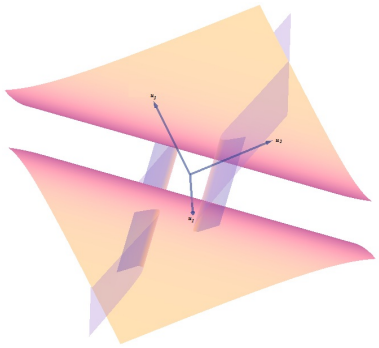

Figure 4.6: Intersection of hyperbolic cylinders.

### Constraints type b)

The second type of restrictions is related to the "nominal strip" values for the voltages at each node. Graphically, these constraints form a cuboid whose side lengths are the lengths of the intervals for each voltage at each node.

### Constraints type c)

This type of constraints is related to the maximum transmission capacity of the lines (maximum current through the lines). They are of the type $\left|\frac{u_i - u_j}{R_{i,j}}\right| \leq I_{max\ line}$. In $\mathbb{R}^3$ these restrictions are easy to plot, they have the form shown in figure 4.7, and the set of correct values is the space within the intersection of all these planes (and remember that only the octant of the space where the variables are positive has a physical interpretation).

### Other constraints.

The other kinds of restrictions (type $d, e$ and $f$) are not geometrically significant, because they have no a direct relation with the voltage values.

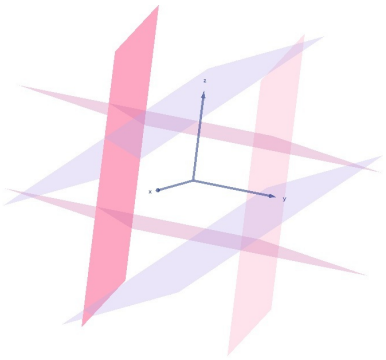

Figure 4.7: Current lines constraints.

**Region of solutions in this case.**

The curve $\mathfrak{C}$, given by equation (4.92), is always within the bounds stated by constraints 4.3.6 and 4.3.6. Besides, in all cases, the curve $\mathfrak{C}$ will exist because it is by definition the intersection between two hyperbolic cylinders, and these quadrics are each symmetric with respect to a perpendicular plane (in this case $u_1 = 0$ and $u_3 = 0$). So, in general, the curve $\mathfrak{C}$ is in a non null region in $\mathbb{R}^3$ where the optimum point lies.

### 4.3.7 Existence of solutions in $\mathbb{R}^n$.

If we proceed in analogous form of $\mathbb{R}^3$ we can achieve a set of values in $\mathbb{R}^n$ where all restrictions are satisfied.

**Constraints type a)**

Now, we assume that there are $n = n_w + n_S + n_L$ nodes, where $n_w$ is the number of production nodes, and they form a subspace with dimension $n_w$, and something similar for $n_L$ (number of load nodes). Once again, we have $j \in W \cup L \ / P_j = [u]^t \cdot [G_j^*] \cdot [u]$, where $[G_j^*]$ is shown in equation (4.9). It is again a quadric in non reduced form, and therefore we can obtain a change of variable to obtain the reduced form of the quadric. If we calculate the eigenvalue of these matrices, they are:

$$|\lambda \cdot I - G^*| = 0 \Longleftrightarrow \begin{cases} \lambda_1 = 0 \\ \vdots \\ \lambda_{n-2} = 0 \\ \lambda_{n-1} = \frac{g_{i,i} + \sqrt{\sum_{k=1}^{n} g_{i,k}^2}}{2} \\ \lambda_n = \frac{g_{i,i} - \sqrt{\sum_{k=1}^{n} g_{i,k}^2}}{2} \end{cases} \tag{4.93}$$

and as $g_{i,i} < \sqrt{\sum_{k=1}^{n} g_{i,k}^2}$ is always true, we obtain for all the cases that these matrices $G^*$ have one positive eigenvalue, one negative eigenvalues and the rest of them are zero (in concordance with 5 of section 4.2.2). So the quadric have the form of hyperbolic cylinders in the space $\mathbb{R}^n$, which also are intersected because each of them is centred in the corresponding plane whose variable is equal to zero $u_i = 0$. That is, they are perpendicular to each other.

**Constraints type b)**

In $\mathbb{R}^n$, these restrictions form hypercubes bounding maximum and minimum values of voltages.

**Constraints type c)**

In the case of $\mathbb{R}^n$, the restrictions about the maximum transmission capacity are planes of order 2, and the intersection of all of them form a region of space $\mathbb{R}^n$. In this case we only work in the region of space where all the variables are positive.

## 4.4 Application case: a six-terminal system.

The simulations for the proposed method will be carried out in the system shown in figure 4.8, where there are two wind farms, two storage systems and two AC networks, in which there are different consumptions. Note also, that geographically and by proximity, the whole system could be divided into two subsystems, each one with a wind farm, a load and a storage device. This does not mean that they work separately, but if it is true that from the energetic point of view, it will be more reasonable to supply power from node 1 to nodes of its subsystem, rather than to the other subsystem. Although, there will be cases, included in the simulations, where this does not happen.

Observing the model shown in equation (4.81), we have to minimize a nonlinear function subject to both linear and nonlinear constraints. To solve this problem we have used a tool called Opti Toolbox and simulations have been carried out in the MATLAB © environment.

Table 4.6 lists the parameter values and constraints used for the model of the whole system. We have supposed that when we are at instant $k$, we have a forecast for the next 2 hours. And, as our sampling time is 15 min, then $N_p = 8$.

According to table 4.6, we have considered that the "nominal voltage strip" is $\pm 10\%$ with respect to 100 kV. Also, we have taken into account that the efficiency of each storage is different, and the nominal power too. It shows how all possible cases are easily executable thanks the formulation of the problem. With respect to HVDC transmission cables, we have chosen

Table 4.6: Simulation parameter values.

| | | |
|---|---|---|
| Prediction Horizon | $N_p$ | 2 hours |
| Sampling Time | $T$ | 15 min |
| Nominal power of wind farm 1 | $P_{nom-wf-1}$ | 400 MW |
| Nominal power of wind farm 2 | $P_{nom-wf-2}$ | 300 MW |
| Nominal voltage of DC grid | $u_{nom}$ | 100 kV |
| Nominal power of DC grid | $P_{nom}$ | 100 MW |
| Minumum voltage in all nodes | $u_{i,min}$ | 0.9 p.u |
| Maximum voltage in all nodes | $u_{i,max}$ | 1.1 p.u |
| Maximum current per line 12 | $i_{max-line12}$ | 1 p.u. |
| Maximum current per line 13 | $i_{max-line13}$ | 1 p.u. |
| Maximum current per line 15 | $i_{max-line15}$ | 1 p.u. |
| Maximum current per line 23 | $i_{max-line23}$ | 1 p.u. |
| Maximum current per line 24 | $i_{max-line24}$ | 1 p.u. |
| Maximum current per line 36 | $i_{max-line36}$ | 1 p.u. |
| Maximum current per line 45 | $i_{max-line45}$ | 1 p.u. |
| Maximum current per line 46 | $i_{max-line46}$ | 1 p.u. |
| Maximum current per line 56 | $i_{max-line56}$ | 1 p.u. |
| Resitance cables | $R_{cable}$ | 0.121 Ω/km |
| Length line 12 | | 50 km |
| Length line 13 | | 180 km |
| Length line 15 | | 1000 km |
| Length line 23 | | 180 km |
| Length line 24 | | 1200 km |
| Length line 36 | | 1000 km |
| Length line 45 | | 40 km |
| Length line 46 | | 200 km |
| Length line 56 | | 150 km |
| | Storage 1 | Storage2 |
| Energy at initial time | 3.6 GWh (60%) | 1.5 GWh (50%) |
| Maximun power charging | 350 MW | 220 MW |
| Maximun power discharging | 300 MW | 200 MW |
| Charge efficiency $\eta_{c1}$ | 0.8 | |
| Discharge efficiency $\eta_{d1}$ | 0.8 | |
| Charge efficiency $\eta_{c2}$ | | 0.85 |
| Discharge efficiency $\eta_{d2}$ | | 0.85 |

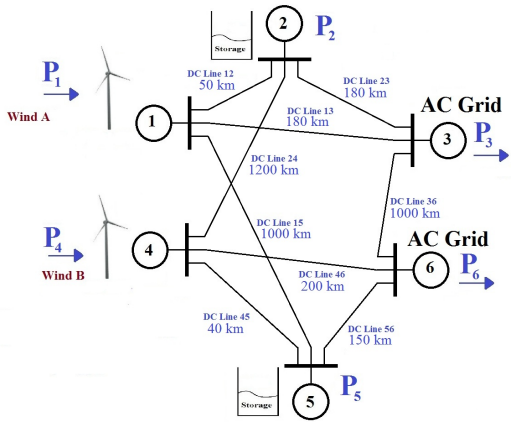


Figure 4.8: Six-terminal simulation grid.

typical values for them. As explained above, we will only consider resistive models, due to the selected sample time, thereby ignoring the dynamics of cables.

With these data and constraints we have carried out simulations for a typical week. We have used real measures of wind [100] as we observe in figure 4.9.

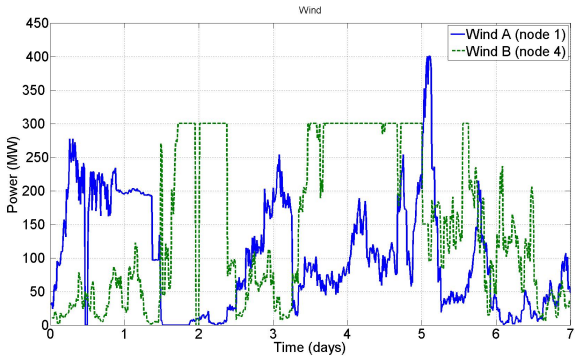


Figure 4.9: Wind power in production nodes for a typical week.

In figure 4.10, real demand predictions are shown for a week, for two different areas [36]. We have selected the criterion that a negative power means that the concern node absorbs energy from the system.

With these two premises and starting from initial conditions in the energy levels of the storage devices, as shown in table 4.6, we operate the system with a view to minimizing losses with a prediction sliding horizon of 2 h. The results that we have obtained are as follows.

If we look closely at figures 4.9, 4.10 and 4.11, we can point out many interesting moments which occurred throughout the week.

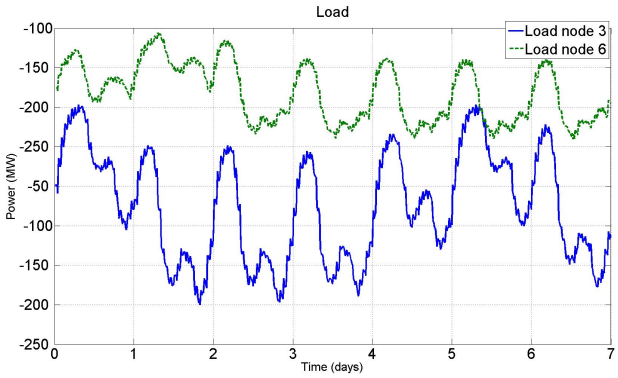


Figure 4.10: Consumption power for a typical week.

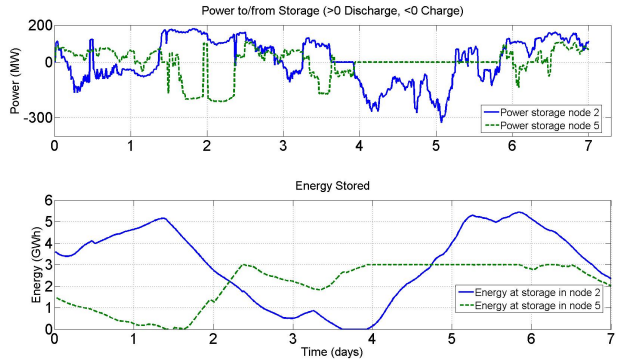


Figure 4.11: a) Power storage b) Energy storage.

On the first day, in the subsystem 1 there was more wind than consumption, so the storage in node 2 was charged. With respect to subsystem 2, there was less wind than load so that the storage in node 5 was discharged. Between the end of the second day and the beginning of the third, it is clearly shown that the trend was in reverse, so the storage at node 5 was charged and the other was discharged. But perhaps the most interesting moment occurs when the storage at node 5 is filled (at the end of the fourth day), we observe that from this moment, although there was more wind than load in subsystem 2, the energy went to the storage device of the other subsystem, and this storage device is charging in spite of the fact that there was more consumption than generation in this subsystem. It is an unequivocal evidence that our control is working properly.

Another positive sign is that all constraints are satisfied. In effect, if we see figure 4.11a, we can confirm that any storage device was suppling (or consuming) power beyond their limits (see table 4.6). Something similar occurs if we observe figure 4.11b, we can validate that when one storage is

full, it does not absorb more power, and when it is empty, it does not supply power.

In figure 4.12 we see that all the voltages are always in the "nominal strip", so these restrictions are satisfied too. We can also point out that the voltages are nearer than 1.1 p.u, this is a fact that it should not surprise us, because to minimize losses it is clear that high voltage levels favor it. Moreover, it has to be stressed that when the storage at node 2 is full (on the fifth day) we can observe that the voltage regimes of subsystem 1 (the subsystem of this storage) are decreased, but they are always within the limits.

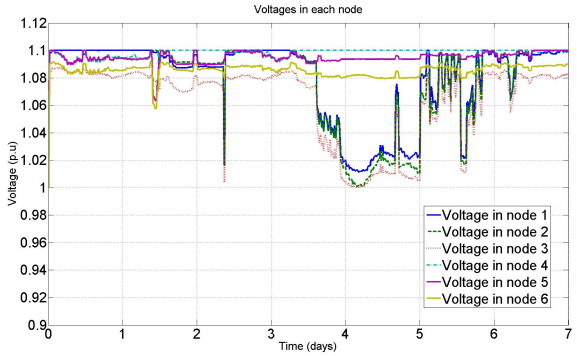


Figure 4.12: Voltages in each node.

In figure 4.13 we notice how all the currents through the lines do not exceed the maximum current that they can tolerate (the positive or negative values only indicate the power direction with respect to the reference).

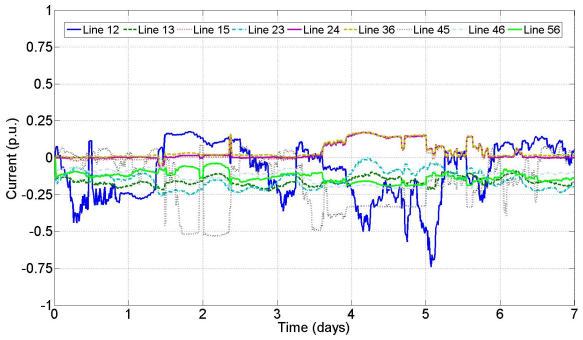


Figure 4.13: Currents thought the lines.

### 4.4.1 Losses comparative.

To appreciate more precisely the power of our optimal control, we are now going to compare the losses obtained with those that we would obtain if we carried out a classic NR method (explained in section 2) with the slack bus always in node 2. This comparison is shown in figure 4.14, and it is clear that with our proposed optimal controller the efficiency of the system is improved. In addition, if we compute the total losses in this week, we obtain that for the MPC the losses are 78.6 GWh and for the NR method they are 194.3 GWh, that is, a 60% reduction in losses with the optimal control (see table 4.7).

Table 4.7: Losses comparative.

| | Total Losses |
|---|---|
| NR method | 194.3 GWh |
| MPC method | 78.6 GWh |

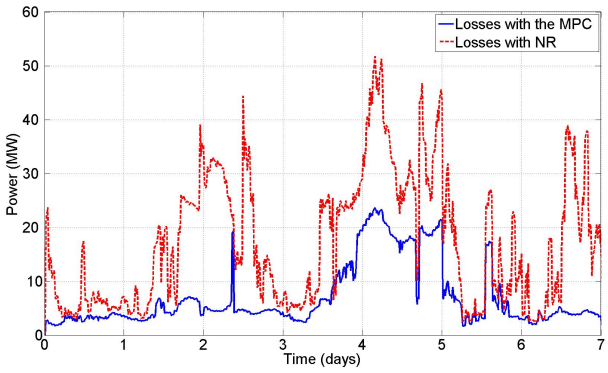


Figure 4.14: Losses comparison.

## 4.5 Conclusions.

In this chapter, the secondary control is addressed. A new method to solve the power flow problem (nonlinear system of equations) in DC grids is exhibited in this chapter. The main difference with classical methods is that there is not any more needed that an unique node have an arbitrary voltage (slack bus), and it will allow a safer grid, because the voltages will be assured by several nodes instead of only one. The method is based on recurrent sequences which always converges to the solution. The results shown in this work will in the future generalized for AC systems, where the reactive power appears, proceeding in analogous form with the same philosophy.

Another important result shown in this chapter is a complete study on the effects of the variation of some key variables on the remaining ones, which is a very valuable information to understand the behaviour of our system. Some examples are also presented in order to illustrate the advantages of the presented method.

On the other hand, a secondary control strategy, for a MT-HVDC network is explained in this chapter based on MPC approach. The control strategy includes weather forecasts and load predictions, and it optimizes the power flows in the network in order to: minimize transmission losses, and with the possibility to avoid power network congestions.

These goals are obtained by calculating the best set of voltages for each terminal, taking into account several restrictions (see section 4.3.3). A new formulation is proposed in this chapter, which will help us to better handle the restrictions in order to optimize the problem. One of the key elements will be the storage devices, and they will allow us to manipulate the system optimally.

As we have used forecast in order to optimize the transmission losses in the system, the employ of MPC has some drawbacks concerning the reliability of these data. Because, a difference, even if it is small, will appear and it will produce errors. For this reason, it is necessary to rely on a lower level controller (see chapters 3), which must keep the system stable between secondary sample times.

It is also noteworthy to remark that we have chosen the criterion to minimize losses in the system, but there may be moments that for security this is not the most advisable. Also, and thanks to the proposed formulation, it is possible to operate the system with secondary criterion such as maintaining the energy of the storage devices in an pre-established interval, or maintaining the voltages in a range more suitable for us.

Chapter 5

# Tertiary control

## 5.1 Chapter introduction.

As we have discussed in the introduction of this thesis, the MT-HVDC system could be controlled in an hierarchical way in resemblance as AC classic networks. In previous chapters, we have discussed and analysed from local to more global controllers, but always from the point of view of electrical stability of the system. However, in this chapter the economic point of view prevails with respect to electrical stability.

The tertiary control layer is located on the top of the hierarchical whole control philosophy, and it is the link with electrical market. The main task of this controller is to manage the load flow of the whole MT-HVDC grid in order to achieve economical optimization, especially relevant with the presence of storage devices. With the proposed control, we will be able to maximize the economic profits of the MT-HVDC grid, where storage devices will play a key role in the optimization [103].

We will consider a general MT-HVDC network, with variable renewable energy sources, storage devices and AC grids. We will take into account that AC main networks absorb all the power that the wind farms and the storage devices are able to supply via the MT-HVDC grid. Technical restrictions such as maximum allowed power through the lines, or maximum supplied/absorbed power by the storage devices will be considered. This means that all generated power will be remunerated by distribution system operators, which are located in the AC networks. This is in line with current legislation which imposes preference to renewable sources [104, 105].

The strategy to follow is explained in the following sections, but the main idea is to store as much power as possible when the price is low, and sell as much power as possible when the price is high while all constraints are respected.

Tertiary control provides power references to secondary control for a specific period of time (the sampling time of the tertiary is usually around 15 minutes). These references are based on load, weather and energy prices forecasts, and thanks to the use of MPC, which includes an sliding prediction horizon, the predictions will be updated progressively. However, although these refreshed predictions are more reliable than the old ones, there will always exist an error, even if small, with respect to the reality. This error is not a problem, because it is mitigated by the lower controllers (local,

primary and secondary) by setting theirs parameters. The tertiary control only gives the guidelines to the lower levels view from a economic point of vew. Besides, and thanks to the use of MPC and forecasts, power network congestions will be predicted and avoided.

To tackle this problem, real measures of wind [100] and electric market price [36] have been used in this chapter, as well as real weather forecasts.

In this chapter two different formulations for the same problem are presented. The first one is in terms of power, where some constraints are included as for example: maximum supplied/absorbed power by storage devices, or maximum and minimum of energy level of them, or maximum supplied/absorbed power by AC areas. The second applied formulation is in terms of voltages. Thanks to it, we can considerer additional constraints as power losses in the lines, maximum power thought them or maximum/minimum voltage level in the nodes (nominal strip defined in section 4.3).

## 5.2 Tertiary control. MPC Power formulation.

In this section we use the MPC techniques, which have been explained in section 4.3. As we consider predictions for load, wind and price, the use of MPC is particularly interesting, since it is able to manipulate successfully systems with constraints [98].

### 5.2.1 Optimization context.

In concordance with definitions of section 3.3.1, we will consider three different types of nodes for the MT-HVDC grid: injection, consumption, and interconnection nodes.

Besides, we will consider the wind as variable renewable energy source. In consequence, we will also take into account storage reserves in order to achieve a MT-HVDC network more reliable, due to presence of renewable energies, which are inherently variable, and they can cause network problems from the point of electrical stability if they are the only sources in the system.

If we suppose a MT-HVDC grid with $n$ terminal nodes nodes (injection plus consumption nodes), then we can define: $n_W$, as the number of wind production nodes, $n_S$, like the number of nodes where storage devices exist and, $n_L$, as the number of AC external grids connect to our DC grid. At this point, it is easy to realise that $n = n_W + n_S + n_L$.

The objective in this section is to maximize the profit of the installation, considering that there are $n_L$ different prices (as many as AC zones exist). The main idea, is to sell as much energy as possible during the periods of peak price given priority at zones with higher prices. We assume that each AC zone will buy all the energy that MT-HVDC grid can supply,

excluding technical constraints. This restrictions are: the maximum supplied/absorbed power by the storage devices, including their performances, the maximum and minimum storage device energy capacity and the maximum supplied/absorbed power by AC areas, see constraints shown in (5.4).

In order to formulate the problem, the following variables are define:

Let $P^k_{W,i}$ be the power supplied by the wind farm $i$ at instant $k$, with $i \in \{1, .., n_W\}$ and $k \in \mathbb{N}^*$. We must remark that $P^k_{W,i} \geq 0$, $\forall\ i, k$.

Let $P^k_{S,i}$ be the power absorbed/supplied by the storage $i$ at instant $k$, with $i \in \{1, .., n_S\}$, where $P^k_{S,i} > 0$ when the power flows to the storage (and consequently it is charging) and $P^k_{S,i} < 0$ when power flows from the storage to the MT-HVDC network (and consequently it is discharging).

Finally, let $P^k_{L,i}$ be the total power delivered to the AC grid $i$ at instant $k$, with $i \in \{1, .., n_L\}$, where $P^k_{L,i} \geq 0$ all the time.

Therefore, with the defined signs and without taking into account losses, the power balance at instant $k$ could be defined as:

$$\sum_{i=1}^{n_L} P^k_{L,i} = \sum_{i=1}^{n_W} P^k_{W,i} - \sum_{i=1}^{n_S} P^k_{S,i} \quad \forall k \tag{5.1}$$

The objective function in this case takes the following form:

$$\sum_{k=1}^{N_p} \left( \left( \sum_{i=1}^{n_W} P^k_{W,i} \cdot p^k_{max} \cdot T \right) - \left( \sum_{i=1}^{n_S} P^k_{S,i} \cdot p^k_{max} \cdot T \right) \right) \tag{5.2}$$

where $p^k_{max}$ is the maximum price of offered prices at instant $k$, and is therefore the price at which we want to sell all the possible energy at instant $k$ (except power constraints in lines, etc...). $N_p$ is the prediction horizon in the optimization, or in other words, the number of intervals until forecast are available. Finally, $T$ is the sampling time.

In expression (5.2), we can only act on $P^k_{S,i}$ which are our decision variables. We are interested in maximizing the profit, or in other words, to maximize the function (5.2). With all these considerations taken into account, the function to optimize becomes:

$$J = \max \sum_{k=1}^{N_p} \left( \left( \sum_{i=1}^{n_W} P^k_{W,i} \right) - \left( \sum_{i=1}^{n_S} P^k_{S,i} \right) \cdot p^k_{max} \cdot T \right) \tag{5.3}$$

$$\text{subject to} \begin{cases} E_{\min,i} & \leq E^k_i & \leq E_{\max,i} & (a) \\ P^k_{S,i} & \leq P^k_{W,i} & & (b) \\ -P_{w\ nom,i} & \leq P^k_{S,i} & & (c) \\ P_{min\ L,i} & \leq P^k_{L,i} & \leq P_{max\ L,i} & (e) \end{cases} \tag{5.4}$$

where $P_{w\ nom,i}$ is the rated power of each wind farm. $P_{max\ L,i}$ / $P_{min\ L,i}$ are the maximum/minimum power supplied to each AC node. In addition,

$E_i^k$ is the energy stored in storage $i$ at instant $k$, which is defined by:

$$E_i^{k+1} = E_i^k + \eta_{S,i}^* \cdot P_{S,i}^k \cdot T \quad \forall k \tag{5.5}$$

where $\eta_{S,i}^*$ is the charge ($\eta_{cS,i}$) or discharge ($\eta_{dS,i}$) in each storage $i$, and they are defined in (5.6).

$$\begin{cases} \eta_{S,i}^* = \eta_{cS,i} & \forall k, i \quad / \quad P_{S,i}(k) \geq 0 \\ \eta_{S,i}^* = 1/\eta_{cd,i} & \forall k, i \quad / \quad P_{S,i}(k) < 0 \end{cases} \tag{5.6}$$

The prediction equation for the storage device $i$ can be expressed as:

$$\begin{bmatrix} E_i^{k+1} \\ E_i^{k+2} \\ \vdots \\ E_i^{k+N_p} \end{bmatrix} = \eta_{S,i}^* \cdot \begin{bmatrix} T & 0 & \cdots & 0 \\ T & T & \cdots & 0 \\ \vdots & \vdots & \ddots & 0 \\ T & T & T & \end{bmatrix} \cdot \begin{bmatrix} P_{S,i}^k \\ P_{S,i}^{k+1} \\ \vdots \\ P_{S,i}^{k+N_p-1} \end{bmatrix} + \begin{bmatrix} E_i^k \\ E_i^k \\ \vdots \\ E_i^k \end{bmatrix} \tag{5.7}$$

### 5.2.2 Simulations for a seven-terminal system.

The simulations for this method, formulated in power terms, will be carried out in the system shown in figure 5.1 for a typical week.

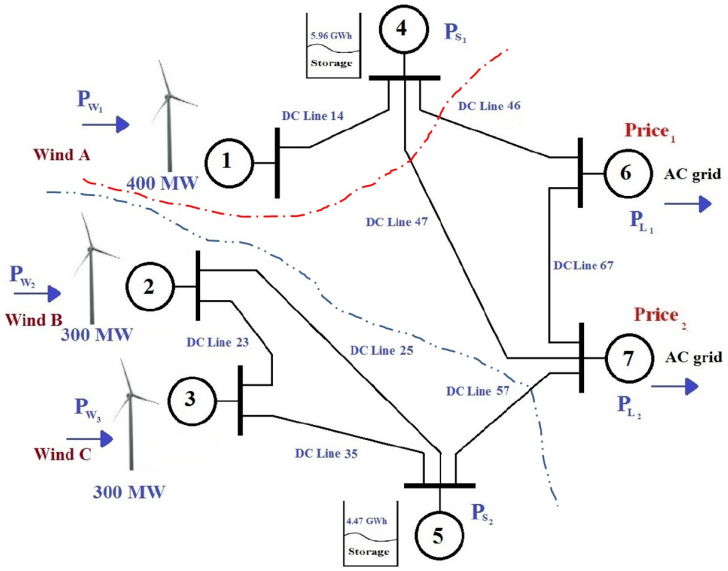


Figure 5.1: Seven-terminal simulation grid.

In the system shown in figure 5.1, there are three wind farms (with three different winds) in nodes 1, 2 and 3. There are also two storage devices (nodes 4 and 5) and two AC networks (nodes 6 and 7), in which there are two different prices. Due to their geographical proximity (see table 5.2), we

can consider two subsystems, the first one includes nodes 1 and 4 which are near to AC node 6, and the second subsystem which includes nodes 2 and 3. These last nodes are close the AC node 7.

In figure 5.2, prices for each AC zone are shown (see [36, 106]).

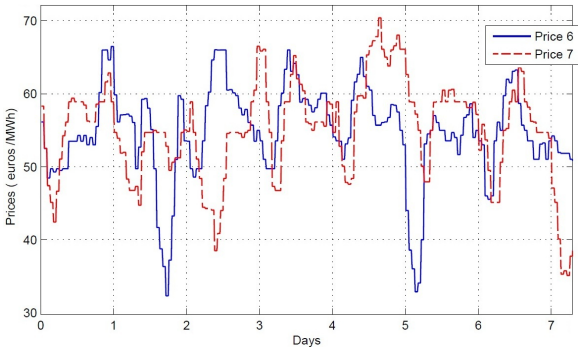


Figure 5.2: Energy prices.

The following tables 5.1 and 5.2 list the parameter values used for the model of the network.

Table 5.1: Simulation parameters. Power formulation.

| | | |
|---|---|---|
| Prediction Horizon | $N_p$ | 2 hours |
| Maximum Power AC node 6 | $P_{max-node-AC,6}$ | 600 MW |
| Maximum Power AC node 7 | $P_{max-node-AC,7}$ | 600 MW |
| Sampling Time | $T$ | 15 min |
| Nominal power of wind farm 1 | $P_{nom-wind-farm-1}$ | 400 MW |
| Nominal power of wind farm 2 | $P_{nom-wind-farm-2}$ | 300 MW |
| Nominal power of wind farm 3 | $P_{nom-wind-farm-2}$ | 300 MW |
| Wind turbine nominal power | $P_{nom-aero}$ | 6.25 MW |
| | Storage 1 | Storage2 |
| Maximum Energy | 5.96 GWh | 4.47 GWh |
| Minimum Energy | 0 GWh | 0 GWh |
| Energy at initial time | 1.92 GWh (32%) | 1.2 MWh (37%) |
| Charge efficiency $\eta_{c1}$ | 0.8 | |
| Discharge efficiency $\eta_{d1}$ | 0.8 | |
| Charge efficiency $\eta_{c2}$ | | 0.85 |
| Discharge efficiency $\eta_{d2}$ | | 0.85 |

The results for this simulation are shown in figures 5.3, 5.4 and 5.5. We must note that power levels at each storage device, $P_S$, always remain within the limits delimited by their constraints. They also show that power absorbed by AC grid of node 6 (figure 5.5) never reaches the power limits for the proper functioning of the network. Also, as expected, we observe

Table 5.2: Line distances.

| | Subsystem 1 | | | | Subsystem 2 | | | |
|---|---|---|---|---|---|---|---|---|
| Line | 14 | 46 | 47 | 67 | 23 | 25 | 35 | 57 |
| km | 50 | 30 | 500 | 480 | 25 | 60 | 40 | 30 |

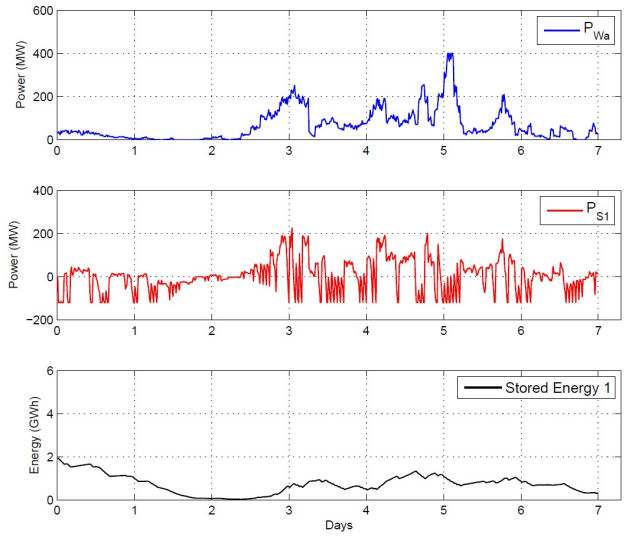


Figure 5.3: Simulations results. Power formulation. Sub-system 1.

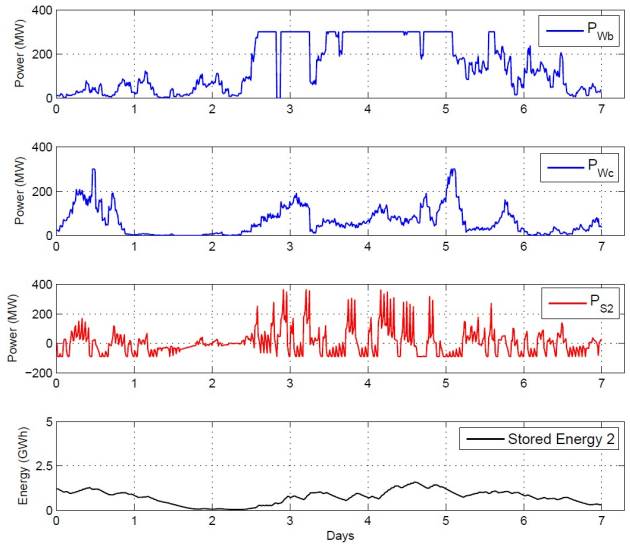


Figure 5.4: Simulations results. Power formulation. Sub-system 1.

that this power increases with price. A similar remark can be made for the supplied power to AC side in node 7 (figure 5.5).

With these simulations, and taking into account the power delivered at

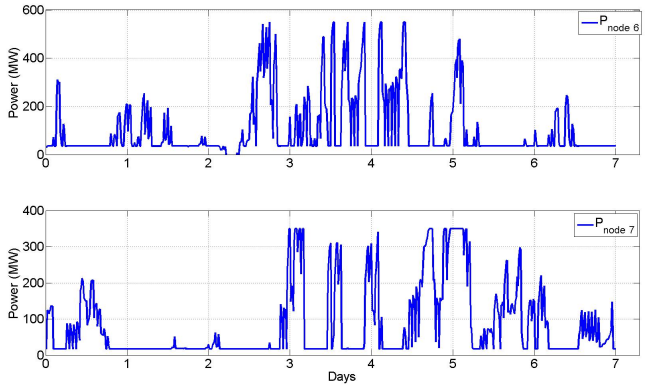


Figure 5.5: Simulations results. Power formulation. Consumed power by AC grids.

Table 5.3: Incomes.

| | Incomes/week (with planning) | Incomes/week (without storage) |
|---|---|---|
| Grid 1 | 3.83 M€/ week | 2.37 M€/ week |
| Grid 2 | 6.71 M€/ week | 6.94 M€/ week |
| Total | 10.55 M€/ week | 9.41 M€/ week |

each instant to each network, and their corresponding prices, the following incomes, shown in table 5.3, are obtained. We can observe in this table 5.3 that the overall income is 11% higher with planning than without planning. We can note that "without storage" means that there are no storage devices and all production from wind farm 1 goes to AC grid 6 and all production of wind farms 2 and 3 goes to AC grid 7. It can also be remarked that "without storage" there are higher profits for sub-network 2, mainly due to the fact that the instants of higher prices coincide with higher production, but if we consider the overall system the revenues are lower.

## 5.3 Tertiary control. MPC Volatge formulation.

The methodology proposed in section 5.2 is valid for some type of problems, however it could be improved because it only cover few constraints. When we formulate the problem in terms of power, we can not include restrictions as the maximum current thought the lines, and consequentially the maximum allowed powers through them are not considered. If we express the problem in terms of voltage, then additional constraints could be included as the maximum and minimum voltage in a node, or the maximum allowed current through the lines. Thanks to this formulation, the losses in the system are inherently considered. In this section, we will formulate the problem in a

similar way than section 4.3, but with a different goal, which will not be other than to maximize incomes.

As it has been shown in equation (4.6), in DC grids, the active power in the node $i$ could be rewritten as:

$$P_i = u_i \sum_{j=1}^{n} g_{i,j} \cdot u_j \tag{5.8}$$

where elements $g_{i,j}$, are the elements of conductance matrix defined in (4.8), and $u_i$ is the voltage of the node $i$.

In concordance with definitions exposed in the before chapter 5.2, we can define:

The power supplied by the wind farm $i$ at instant $k$ as:

$$P_{W,i}^k = [\mathbf{u}^k]^T \cdot [G_{W,i}^*] \cdot [\mathbf{u}^k] \qquad i \in \{1, .., n_W\} \tag{5.9}$$

where matrix $[G_{W,j}^*]$ was defined in (4.9), and $P_{W,i}^k > 0 \ \forall k$.

The power absorbed/supplied by the storage $i$ at instant $k$ as:

$$P_{S,i}^k = [\mathbf{u}^k]^T \cdot [G_{S,i}^*] \cdot [\mathbf{u}^k] \qquad i \in \{1, .., n_S\} \tag{5.10}$$

with matrix $[G_{S,i}^*]$ defined in (4.9). It is important to remark that $P_{S,i}^k > 0$ when the power flows from the storage to the MT-HVDC grid, and consequently it is discharging. And $P_{S,i}^k < 0$ when power flows from MT-HVDC grid to the storage device, and consequently it is charging (opposite criteria sign with respect to section 5.2).

Finally, we can define the delivered power to AC grid $i$ at instant $k$ as:

$$P_{L,i}^k = [\mathbf{u}^k]^T \cdot [G_{L,i}^*] \cdot [\mathbf{u}^k] \qquad i \in \{1, .., n_L\} \tag{5.11}$$

where matrix $[G^*]_{L,i}$ was defined in (4.9). It is important to remark that $P_{L,i}^k \geq 0$ all the time.

As our purpose is to maximize costs, the objective function will be defined as follows:

$$F_{max\ costs}(u_1^k, \cdots, u_n^k) = \sum_{i=1}^{n_L} P_{L,i}^k \cdot p_i^k = p_i^k \cdot [u^k]^T \cdot [G_{L,i}^*] \cdot [u^k] \tag{5.12}$$

where $[u^k] = [u_1^k, \cdots, u_n^k] \in \mathbb{R}^n$, and $u_i^k$ is the voltage in node $i$ at instant $k$, and $p_i^k$is the price of the AC market in node $i$ at instant $k$.

Our objective function will be optimized subject to a number of constraints over a prediction horizon $N_p$. These restrictions are:

- The wind production for power must be equal to forecast values (5.14a).
- The voltages at the nodes must be within their limits (5.14b).

- The current lines can not exceed certain values (maximum admissible current through the cables), (5.14c).
- The storage devices can absorb or supply power until a maximum value (5.14d).
- Also we have taken into account that a storage can not provide (absorb) power if it is empty (full) (5.14e).

With all this, our control variables will be the power supplied or absorbed by AC sides. However, as the restrictions of the system are formulated in terms of voltage our problem consists in finding the best combination of voltages which maximize $F_{max\ costs}$ shows in (5.12). The founded power for AC systems will be the references to the secondary control, and also the founded voltages values give an idea of how they should be.

With the aforementioned considerations, the optimization problem can be formulated as follows:

$$J = min\left(F_{max\ costs}(u_1^k, \cdots, u_n^k)\right) = \left(\sum_{k=1}^{N_p}\left(\sum_{i=1}^{n_L} p_i^k \cdot [u^k]^T \cdot [G_{L,i}^*] \cdot [u^k]\right) \cdot T\right) \tag{5.13}$$

subject to:

$$\begin{aligned}
&a)\ P_{W,i}^k = [\mathbf{u}^k]^T \cdot [G_i^*] \cdot [\mathbf{u}^k] \quad \forall i \in \{1, .., n_W\}, \quad \forall k. \\
&b)\ u_{i,min}^k \leq u_i^k \leq u_{i,max}^k \quad \forall i,\ \forall k \\
&c)\ \left|\frac{u_i^k - u_j^k}{R_{i,j}}\right| \leq I_{max,line_{ij}} \quad \forall i, j, k \\
&d)\ P_{s,min} \leq P_s^k \leq P_{s,max} \quad \forall s \in \{1, .., n_S\}, \quad \forall k \\
&e)\ E_{s,min}^k \leq E_s^k \leq E_{s,max}^k \quad \forall s \in \{1, .., n_S\}, \quad \forall k
\end{aligned} \tag{5.14}$$

where $[\mathbf{u}^k] = [u_1^k, \cdots, u_n^k] \in \mathbb{R}^n$, and $u_i^k$ is the voltage in node i at instant $k$.

### 5.3.1 Simulations.

In order to implement the proposed philosophy the same system as before, see figure 5.1, has been considered. The lengths for the lines are addressed in table 5.2. The same prices as before have been considered for the AC grids (see 5.2).

The following tables 5.4 list the additional parameter values used with respect to before simulations.

Table 5.4: Simulation parameters. Power formulation.

| | | |
|---|---|---|
| Prediction Horizon | $N_p$ | 2 hours |
| Nominal voltage | $V_{nom}$ | 100 kV |
| Nominal power of DC grid | $P_{nom}$ | 400 MW |
| Maximum Power per line 14 | $P_{max-line14}$ | 400 MW |
| Maximum Power per line 23 | $P_{max-line23}$ | 60 MW |
| Maximum Power per line 25 | $P_{max-line25}$ | 250 MW |
| Maximum Power per line 35 | $P_{max-line35}$ | 400 MW |
| Maximum Power per line 46 | $P_{max-line46}$ | 300 MW |
| Maximum Power per line 47 | $P_{max-line47}$ | 200 MW |
| Maximum Power per line 57 | $P_{max-line57}$ | 550 MW |
| Maximum Power per line 67 | $P_{max-line67}$ | 400 MW |

In figure 5.6, we can observe the results of the optimization for the voltage values for each node. We can remark as the constraints for maximum/minimum voltage values are respected.

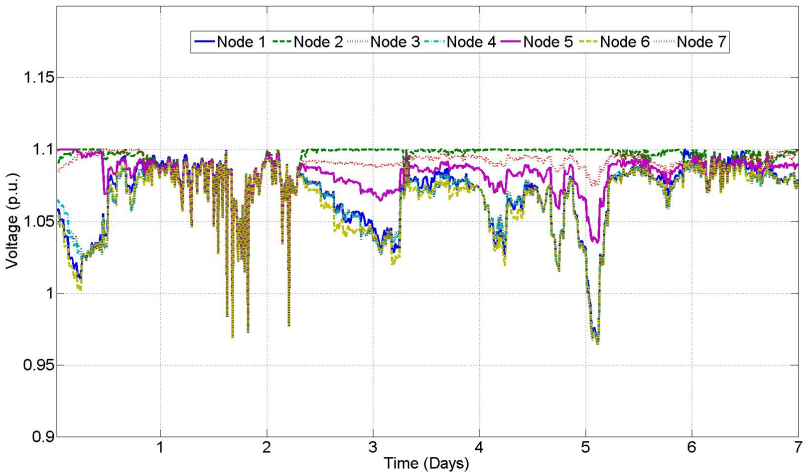


Figure 5.6: Simulations results. Voltage formulation. DC voltage.

In figure 5.7, we can observe the power delivered to AC grids.

Finally in figures 5.8 and 5.9 the power through the lines are presented. We can see as their limits are not reached.

In table 5.5 we can appreciate the incomes with both formulations. They are very similar, as we expected. The discrepancy is due to the different formulation.

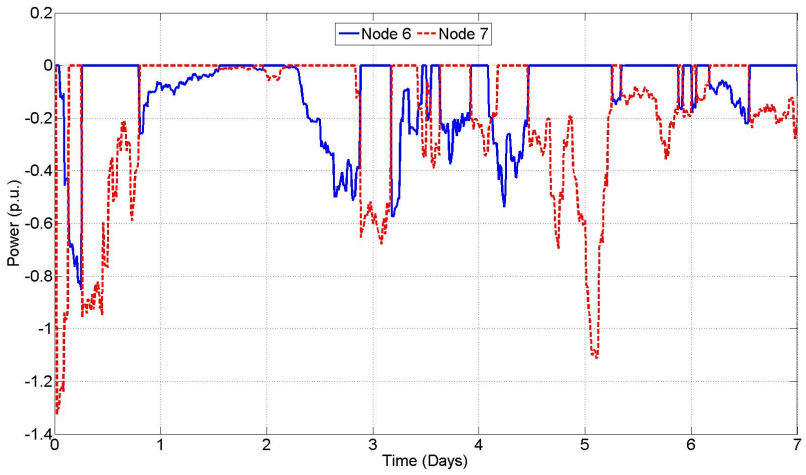


Figure 5.7: Simulations results. Voltage formulation. AC power.

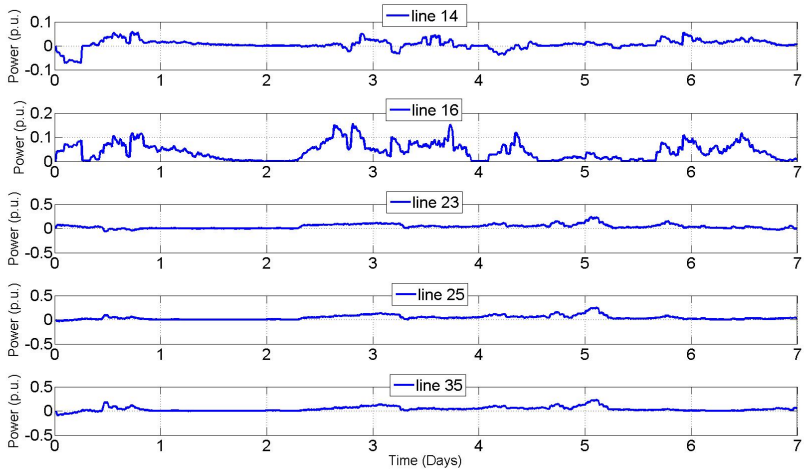


Figure 5.8: Simulations results. Voltage formulation. Power lines.

Table 5.5: Incomes.

| | Incomes/week Formulation 1 | Incomes/week Formulation 2 |
|---|---|---|
| Grid 1 | 3.83 M€/ week | 3.96 M€/ week |
| Grid 2 | 6.71 M€/ week | 6.67 M€/ week |
| Total | 10.55 M€/ week | 10.63 M€/ week |

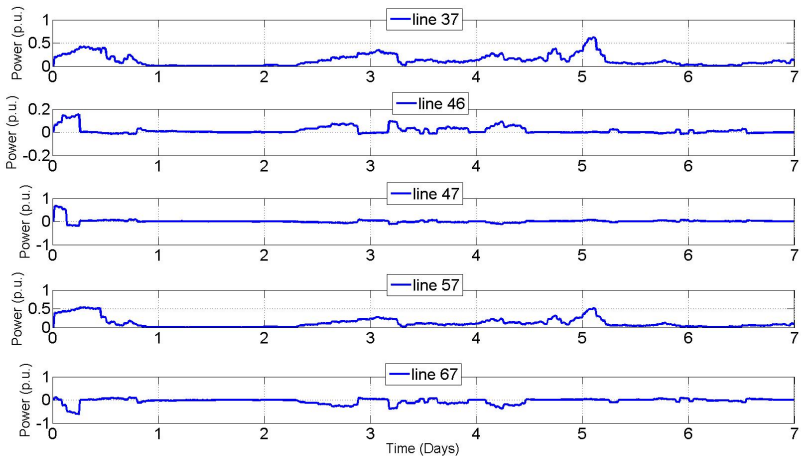


Figure 5.9: Simulations results. Voltage formulation. Power lines.

## 5.4 Conclusions.

This chapter has developed a control economic strategy, to be included in a hierarchical scheme, for a MT-HVDC network. The control strategies include weather, load and price predictions, and optimize the power flows in the network in order to: maximize total profit and avoid power network congestions via MPC approach. These goals are obtained by defining the power input/output of each terminal, there including the storage unities.

Two different formulations have been proposed. In the first one, we operate in terms of power ans some constraints have been considered. However, this strategy does not permit manage all restrictions which can be appear in the real grids. For this reason, the second terminology is used, which depends on the node voltages. It allows us to operate the systems considering more constraints.

Several conclusions can be drawn from this chapter. The first is that the application of the optimization algorithm has some drawbacks, as for example, it is very sensible with respect the weather forecasts. For this reason, it is necessary to rely on a lower levels controllers (chapters 2, 3 and 4) that must keep the system stable between tertiary sample times.

In the same way, the optimization allows a significant improvement of profit. Often, renewable sources produce power when it is not necessary, and as consequence, when its price is low. With the storage, the energy becomes available in the mostly needed moments, which means higher prices. This increase on the profits make easier to construct financially sustainable renewable energy based on power plants.

Chapter 6

# Experimental test bench

## 6.1 Chapter introduction.

With the aim of implementing the hierarchical control philosophy and the theoretical results of previous chapters, we have build an experimental test bench in the facilities of the Department of Power & Energy Systems of Supélec (École supérieure d'électricité, Gif-surYvette, France) with the support of EDF (Electricité de France) and ALSTOM GRID as industrial partners and LSS (Laboratory of signals and systems) and Supélec as academic ones.

A practical implementation is always important in order to check the theoretical results, as well as it always helps us to better understand the problem, providing new ideas to improve the control techniques. This results have been very beneficial to transmit the main ideas of this thesis, and for better comprehension. It is important to remark that this chapter was not originally planned in the thesis, and although the time of construction of the platform has not been negligible, but it was very productive.

Thanks to the results shown in this chapter, we can assert that the control philosophy proposed in this thesis for a MT-HVDC network could be a suitable solution to manage DC meshed grids, since the whole control proposed has a satisfactory behaviour in operation mode, even when disturbances appear, as we will see in section 6.3.

This implementation ranges from the local control of converters (VSC) to secondary control of the grid. The local VSC converters are controlled each one by a dSPACE® software package. Also, in this network a supervisor PC (secondary controller) is included, which communicates with each dSPACE® through a National Instruments CompactRIO® programmable automation controller hardware, which combines embedded real-time and FPGA technology, through a local area network (internet). All these aspects will be explained and detailed in section 6.2.

## 6.2 Test bench explanation.

The test bed is composed by 4 terminal nodes as figure 6.1 and 6.2 show, which can work at a maximum of 400 V DC, and with a maximum allowed current of 15 A. The HVDC lines are simulated by variable resistors, therefore we have the ability to vary the length of the represented lines. Each

terminal node is connected to an AC grid of 127 V (rms phase to phase) and 50 Hz. Afterwards, the AC voltage is decreased to 50 V (rms phase to phase) by means to a $\Delta/d$ step-down transformer (see table 6.1 for parameters).

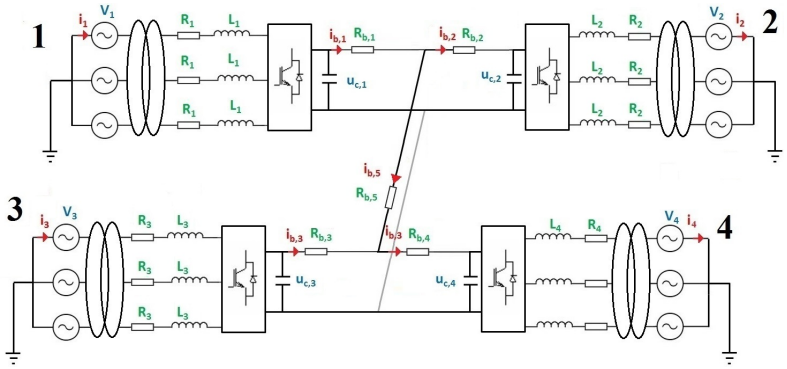


Figure 6.1: Test bench network scheme.

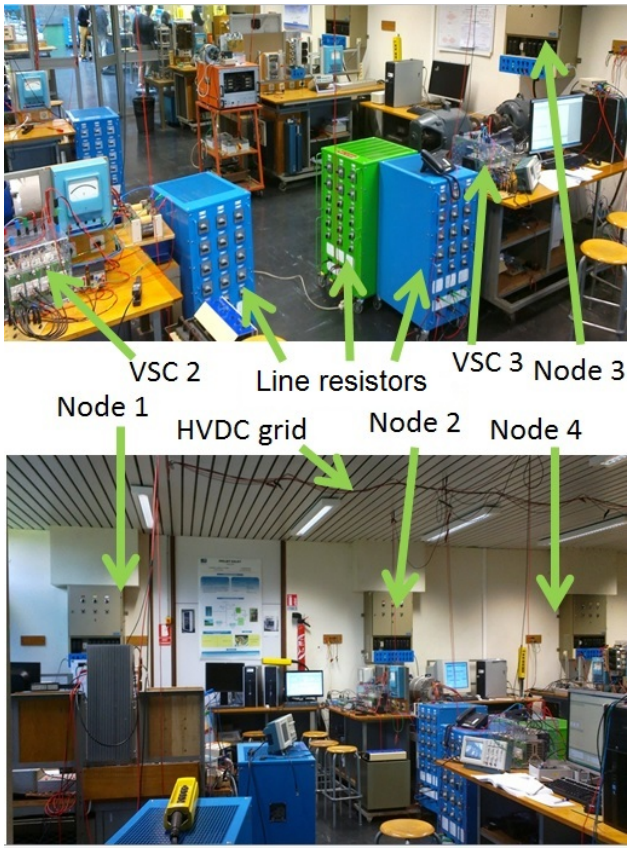


Figure 6.2: Test bench network.

The VSCs make the AC/DC transformation. The converters are able to operate in both current senses, and they are controlled by means of dSPACE® software package, by the interface of MATLAB SIMULINK® files in real time, thanks to the ControlDesk® software.

With the aim of implementing the secondary controller, a supervisor PC is included in the test bench, which receives periodically every voltage and power measures of each terminal node by means of National Instruments CompactRIO® programmable automation controller hardware. These measures are sent with a sample time of 20 seconds. This value was chosen in function of the characteristics of the test bench, and also in order to illustrate the experiments, since the number of data that can be stored in memory is limited, and if we chose a higher value, we can not include all data. Also, this value is chosen, because it is a suitable value between the dynamics of primary control (order of a few seconds) with respect to the level of memory. In fact, this value could be reduced because the available hardware with respect to the test bench size allows it. However we have decided to operate with $20s$ in order to be within values consistent with real applications for the secondary control.

### 6.2.1 Transformer.

A $\Delta/d$ step-down transformer is used to reduce the AC voltage in order to achieve the ideal value for the proper operation point of the VSC converters. Besides, it is employed to provide electric galvanic isolation to the system, as figure 6.3 shows. Its parameters, shown in table 6.1, were obtained after the short-circuit and open-circuit tests.

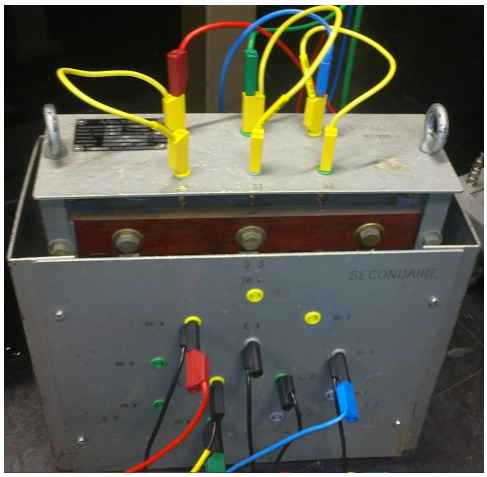


Figure 6.3: Transformer $\Delta/d$.

Table 6.1: Test bench parameters.

| Transformer $\Delta/d$ | | |
|---|---|---|
| Transformer ratio | $n$ | 127/50 |
| Primary voltage | $V_p$ | 127 |
| Secondary voltage | $V_p$ | 50 |
| Apparent nominal power | $S_n$ | 3500 VA |
| Foucault Losses | $R_f$ | 222.05 Ω |
| Magnetizing inductance | $L\omega$ | 41.36 Ω |
| Short-circuit voltage | $U_{sc}$ | 5.7 V (4% $U_n$) |

### 6.2.2 Current Sensor.

The current sensors (see figure 6.4) have been produced manually in Supélec. Their characteristics are shown in table 6.2. They are able to measure the current with a sampling time in the order of 100 $\mu s$ and with reliable accuracy.

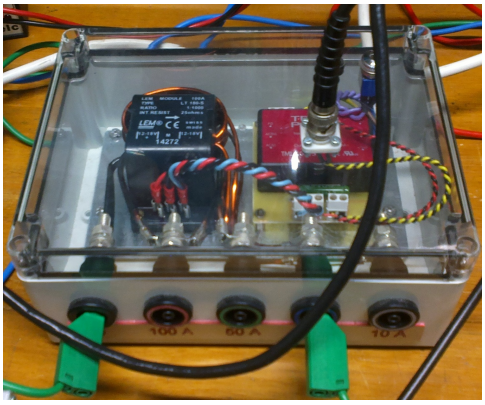


Figure 6.4: Current Sensor.

### 6.2.3 VSC

In each terminal node of the grid there is a VSC, which is a two-level, three phases converter as figure 6.5a shows. In each leg there is a commercial IGBT module (see figure 6.5b). The module is made of 2 IGBTs with an anti-parallel diode, connected in series, of which the middle point is at terminal 1. The IGBT used here is a commercial device: SEMITEACH-IGBT, SKM 50 GB 123D-SKD 51-P3/250F [107].

In figure 6.6 the real configuration of a VSC converter is shown in the test bench. We can remark the capacitors, the IGBTs, the inductances (in the AC side) and the current sensors.

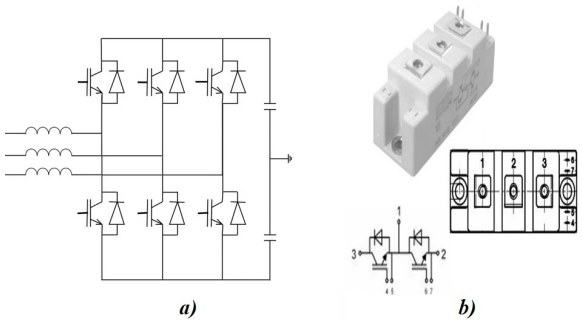


Figure 6.5: a) VSC scheme b) IGBT module. Source

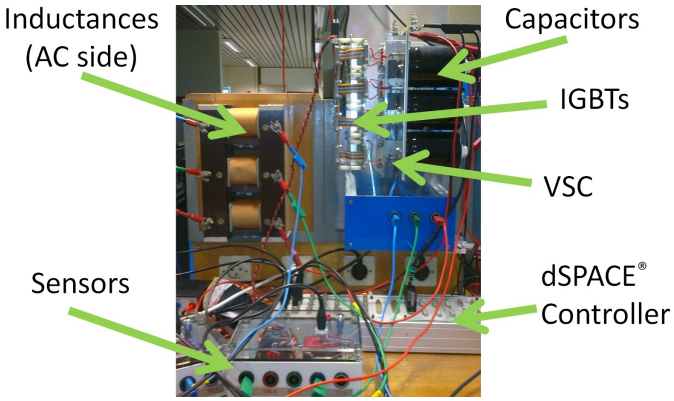


Figure 6.6: VSC. Real converter.

### 6.2.4 dSPACE® software and hardware.

We have used DS1104 R&D controller card (figure 6.7) in order to implement the real-time control on the VSC converters, where analogue signals from sensors are converted in digital signals for their processing in the PC, and after signal processing on the computer, these digital signals are sent to the controller card for its conversion in analogue signals to implement PWM technique. This card makes our PC a powerful development system for rapid prototyping of control laws. The Real-Time Interface includes SIMULINK® blocks for graphic configuration of input and output by means of ControlDesk® software (see figure 6.8).

ControlDesk® is the dSPACE® experiment software for a smooth development of the computer. It performs all the necessary tasks and offers only the beginning of the working environment at the end of the experiment. It includes rapid prototyping of control laws (fullpass, bypass), simulation hardware-in-the-Loop, measurement calculator and access to bus systems. These characteristics allows us to apply local and primary controllers in real time.

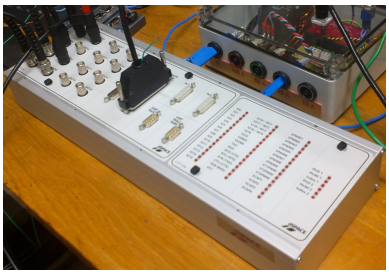

Figure 6.7: dSPACE 1104 controller card.

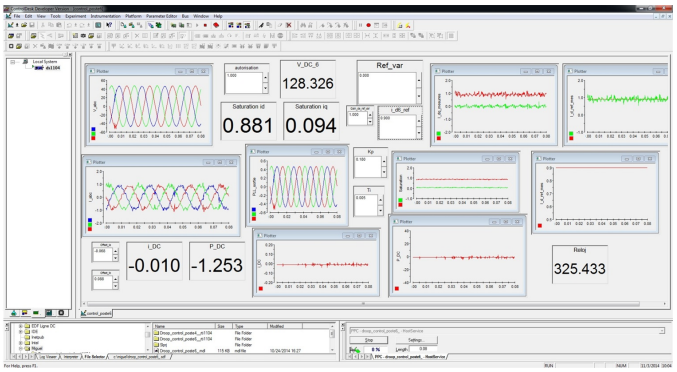


Figure 6.8: ControlDesk software file.

### 6.2.5 Local Controller.

The local VSC controllers have been carried out in section 3.4, however, a brief explanation with the implemented controllers in the test bench is addressed here. The local controller is responsible to control the VSC converters, see [91, 17]. It operates in a time range of milliseconds. Two possible control philosophies could be carried out depending on node operation. There will be VSC nodes where the DC voltage and AC reactive power will be controlled, and other nodes where the local controller is responsible to regulate the active and reactive power.

If we desire to control the pair DC voltage and reactive power, the local controller is composed by the so-called *inner* and *outer controllers* [108]. The first one is responsible to control the currents in the VSC, which have a dynamic much faster than the DC voltage, which is regulated by the *outer controller*. This second controller gives the references to the *inner controller*. On the contrary, if we want to handle the active and reactive power, the local controller of VSC is only composed by the *inner controller*.

**Inner controller.**

The *inner controller* is responsible to control the active and reactive power thanks to the control of the current. If the control is implemented in the $dq$ frame, we will control the active power controlling the current $i_d$, and we will control the reactive power controlling $i_q$. The simplest control loop consists of two PI controllers, respectively for $d$ and $q$ axis current control, as figure 6.9 shows.

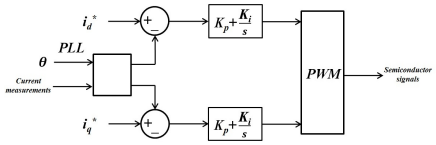


Figure 6.9: *Inner controller*

In order to apply the $dq$ transformation, it is necessary to know the value of the angle of the AC voltage for all instants. This value is computed by using the well-known phase lock loop (PLL) synchronization technique.

The corresponding signals to the switches are generated by means of Pulse Width Modulation (PWM) technique.

**Outer controller.**

The DC voltage has a dynamic much slower than the current. The control consists of one PI controller, as figure 6.10 shows. This controller is responsible for the DC voltage tracks its reference given by the primary controller.

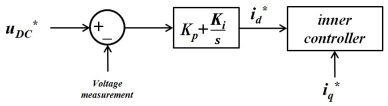


Figure 6.10: *Outer controller*

### 6.2.6 Primary Controller.

As have been explained in chapter 3 the primary controller will be the droop control. It operates in a time range of seconds. It is only implemented in nodes 1 and 2 of figure 6.1, in concordance with the explanation of chapter 3.2 which explains that droop control is not necessarily implemented in all nodes of the network. Indeed, it is often implemented in nodes where exist energy reserves. As in our test bend each terminal is connected to the AC main grid, we can suppose that in all nodes there will be available energy reserves.

### 6.2.7 Secondary controller.

In chapter 4 the secondary controller have been studied. The main task of secondary control will be to schedule power transfer between the network nodes providing voltage and power references to local and primary controllers. In order to carry out this task communication between nodes and supervisor PC must exist.

The references for lower controllers will be the result of periodic power flows, which are key elements for the proper functioning of the system. The main goal of a power flow study is to obtain voltage and power informations for each bus in the grid in steady state. However it may perform other types of analysis, such as short-circuit fault analysis, stability studies, unit commitment or economic dispatch.

We will use the new approach shown in section 4.2 to solve the power flow problem based on the contraction mapping theorem. This new method gives the possibility to use more than one bus for the power balance (slack bus), and consequently share the responsibilities between many actors. The method guarantees the unique existence of solution when some feasible constraints are fulfilled. It is studied in deep in section 4.2. Basically the method could be slightly explained as follows:

For a DC grid with $n$ terminals, if we know the conductance matrix $\mathbf{G}$, the nominal voltage of the grid $u_N$, the powers $P_1, ..., P_k$ $(1 \leq k \leq n)$ and the voltages in the remaining nodes $u_{DC,k+1}, ..., u_{DC,n}$ for a given instant, we can create a vector sequence $V$ for the unknown voltages, where thanks to the contraction mapping theorem, each component converges to an unique value, which is close to the nominal value of the grid. Then as we know all voltages in the grid we can determine all powers. This method is easily applied for AC systems, see A. Thanks to it, the references for reactive power in each AC side of the converter could be obtained.

### 6.2.8 cRIO® hardware.

The secondary controller is carried out by means of a supervisor PC, which calculates periodic power flows based on the philosophy explained in section 4. In this PC the LabVIEW® National Instruments (NI) real time software is implemented, which acts as the link with the hardware.

The hardware equipment is the system control and data acquisition CompactRIO® (shown in figure 6.11), which is formed by an embedded real-time processor for reliable autonomous operation and FPGA device that provides flexibility, high performance and reliability. Each data acquisition cRIO is connected to the PC via Ethernet. Figure 6.11 shows a photo of CompactRIO® 9074 model, which is the used hardware.

The explained method is implemented in LabVIEW® in order to solve the power flow problem as figure 6.12 shows. Thanks to this file, the sec-

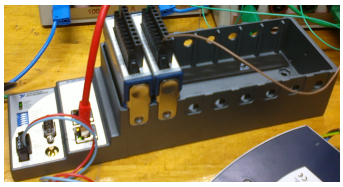

Figure 6.11: cRIO®

ondary control is updating periodically the data, which come from each of the nodes via internet, and it calculates the respective references, and it sends them to the respective nodes. It is important to emphasize that, due to computing power, the time to carry out these calculus is in the order of $\mu s$.

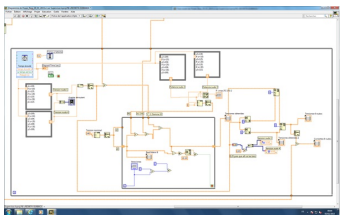

Figure 6.12: LabView power flow file.

### 6.2.9 Hierarchical control.

The whole control proposed in this paper is shown in figure 6.13. As it has been explained before the primary controller (droop control) is not implemented in all nodes, and also it only acts if there is a perturbation in the system, if not, the references for the local controller is given directly by the secondary controller.

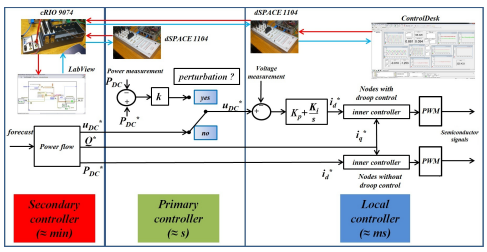


Figure 6.13: Whole hierarchical control.

## 6.3 Results.

In this section the main experimental results will be presented. In order to increase their understanding, firstly the results for single node with variable charge will be shown, and where only local control will be implemented. Subsequently the results for a three nodes system with master/slave philosophy will be presented. And finally, the results for a four nodes grid, with droop control philosophy as primary controller with a supervisor will be exhibited.

In table 6.2 all the parameters for the four nodes are summarized, where the node numeration is associated with figure 6.1.

Table 6.2: Test bench parameters.

| | | Node 1 | Node 2 | Node 3 | Node 4 |
|---|---|---|---|---|---|
| AC source | Maximum Power | 4000 $W$ | 4000 $W$ | 4000 $W$ | 4000 $W$ |
| | Voltage (line to line, RMS) | 127 V | 127 V | 127 V | 127 V |
| | Frequency | 50 $Hz$ | 50 $Hz$ | 50 $Hz$ | 50 $Hz$ |
| AC reactor | Inductance | 2.1 $mH$ | 2.1 $mH$ | 2.1 $mH$ | 3.34 $mH$ |
| | Resistance | 0.142 Ω | 0.142 Ω | 0.142 Ω | 0.165 Ω |
| VSC converter | Switch frequency | 20 $kHz$ | 20 $kHz$ | 20 $kHz$ | 20 $kHz$ |
| | PWM carrier freq. | 10 $kHz$ | 10 $kHz$ | 15 $kHz$ | 15 $kHz$ |
| DC side | DC capacitor | 9.9 $mF$ | 9.9 $mF$ | 9.9 $mF$ | 9.9 $mF$ |
| | Nominal voltage | 150$V$ | 150$V$ | 150$V$ | 150$V$ |
| Sensors (Sample time) | AC current | 100 $\mu s$ | 100 $\mu s$ | 100 $\mu s$ | 100 $\mu s$ |
| | DC current | 100 $\mu s$ | 100 $\mu s$ | 100 $\mu s$ | 100 $\mu s$ |
| | AC voltage | 100 $\mu s$ | 100 $\mu s$ | 100 $\mu s$ | 100 $\mu s$ |
| | DC voltage | 100 $\mu s$ | 100 $\mu s$ | 100 $\mu s$ | 100 $\mu s$ |
| Local controller | Gain Kp AC current | 0.003 | 0.18 | 0.21 | 0.008 |
| | Gain Ki AC current | 1100 | 200 | 200 | 715 |
| | Gain Kp DC voltage | 0.002 | – | – | 0.012 |
| | Gain Ki DC voltage | 1250 | – | – | 100 |
| Primary controller | Droop gain, $k_1$ | 10 $V/A$ | – | – | – |
| | Droop gain, $k_4$ | – | – | – | 10 $V/A$ |
| | | (Voltage control) | (Power control) | (Power control) | (Voltage control) |

### 6.3.1 Voltage control of a node with variable load.

Firstly, the results for a single node are shown, where the goal is to keep the reference voltage in the presence of a variable load, see figure . As the

node is responsible to maintain the voltage, the applied control is the one exhibited in section 6.2.5.

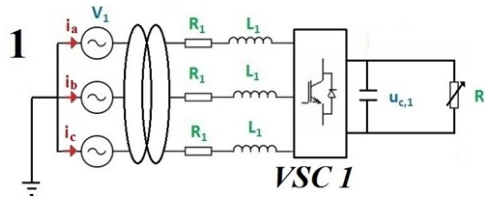


Figure 6.14: A node with variable load.

In figure 6.15 we can observe the voltage of the node, where the reference value is 120 V. At $t = 5\ s$ the charge increases, and although the current varies (see figure 6.16), the control keeps the voltage in 120 V.

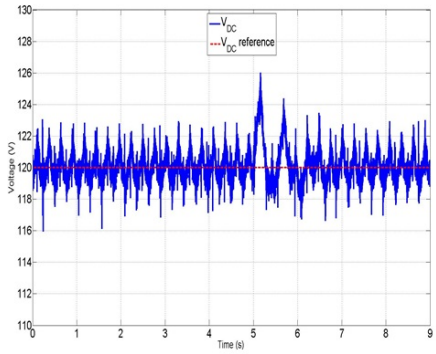


Figure 6.15: DC Voltage result. Experimental test bench. Variable load.

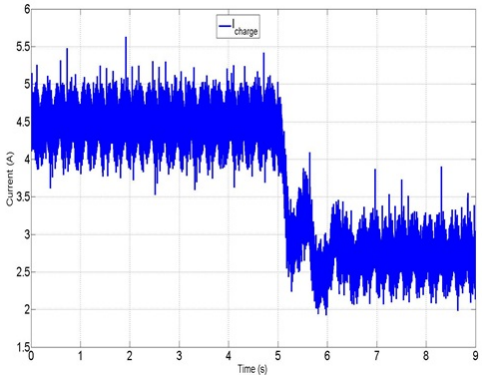


Figure 6.16: DC Current result. Experimental test bench. Variable load.

In figure 6.17, the measured AC voltage of the grid is shown. We can remark that almost no disturbance appears.

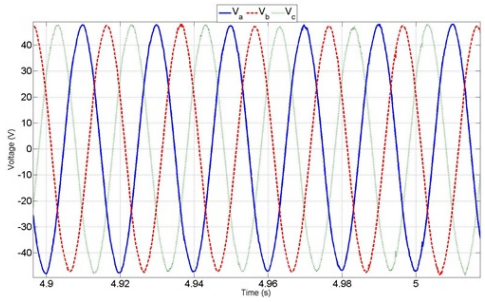


Figure 6.17: AC voltage result. Experimental test bench. Variable load.

In figure 6.18, the measured AC current of the grid is shown. We can remark that due to the change in the load, the AC current changes. These values are not purely sinusoidal because of commutation of IGBTs, however they achieve acceptable values.

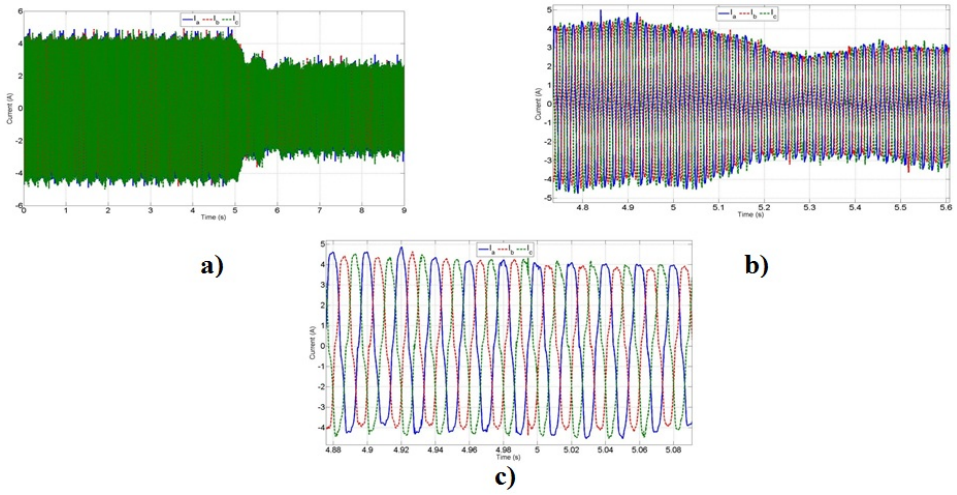


Figure 6.18: AC current result. Experimental test bench. Variable load.

### 6.3.2 Three nodes grid. Experimental results with master/slave philosophy.

The results for a three nodes system with master/slave philosophy are presented in this section. In figure 6.19 the system is shown, where node 1 operates as master, which is responsible to control the DC voltage grid, and nodes 2 and 3 control the injection power in the grid, adapting their voltage values (slaves). This philosophy was explained in section 3.2. The secondary control is also implemented, and it gives references for each node every 20 $s$.

In figure 6.20 we observe as the DC voltage in node 1 tracks always

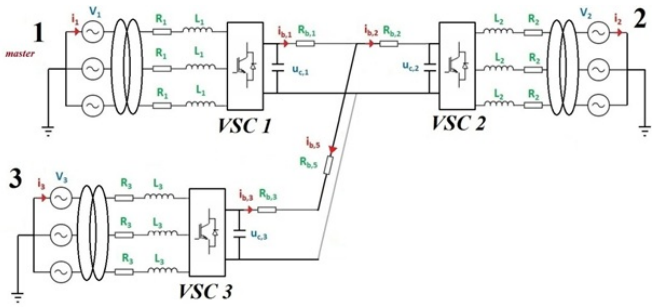


Figure 6.19: Three nodes grid. Master/slave philosophy.

the references given by the secondary controller. In figures 6.21 and 6.22 we can appreciate as the currents follow their references in nodes 2 and 3 respectively. At $t = 5\ s$, node 2 demand increases from 0 to 1.7 A, and node 3 changes from 1.2 A to 0.5 A, but in total, they require more current to node 1, and consequently in node 1 the voltage drops initially in $t = 5\ s$, as figure 6.20 shows.

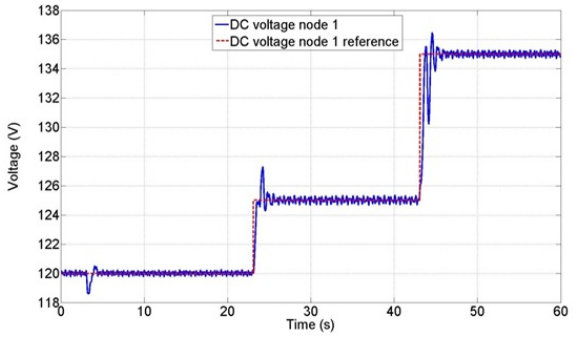


Figure 6.20: DC voltage node 1. Master/slave philosophy.

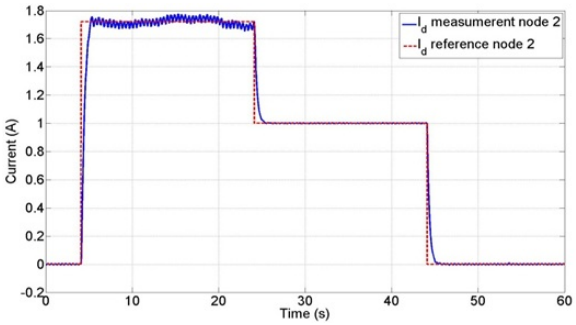


Figure 6.21: DC current node 2. Master/slave philosophy.

In figures 6.23 and 6.24 we can discern, since the voltage values of these

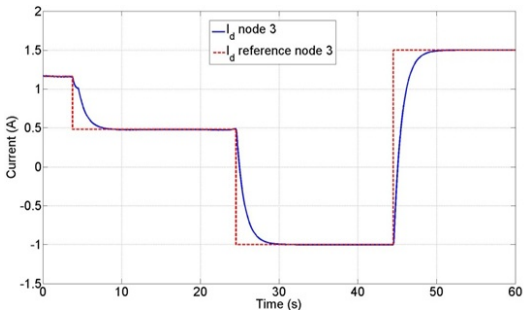


Figure 6.22: DC current node 3. Master/slave philosophy.

nodes change every $20s$, when the secondary change their references. The reached values in these nodes depend on the conditions that exist in this instant in the network and obviously, they depend on the value of the voltage at node 1 (master). It is also important to stress that the voltage values vary much more than in node 1. This is because these nodes are not supposed to control the voltage and also to the existing noise in the measuring equipment.

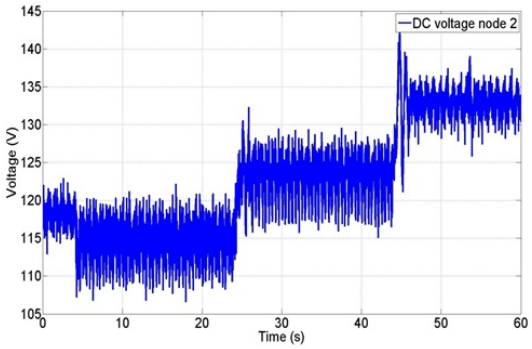


Figure 6.23: DC voltage node 2. Master/slave philosophy.

### 6.3.3 Four node grid. Experimental results with droop control philosophy.

In this section the experimental results with droop control philosophy are presented. The grid is shown in figure 6.25. In this network, there are two nodes responsible to maintain the voltage of the grid (1 and 4), and two nodes responsible to the power injections (2 and 3). When a perturbation appears, the nodes 1 and 4 adjust their voltage reference following their respective droop laws. The secondary is also implemented in order to bring the system to the correct operation point given by the power flow solve by the secondary.

Figures 6.26 and 6.27 illustrate several things. Firstly, before to instant

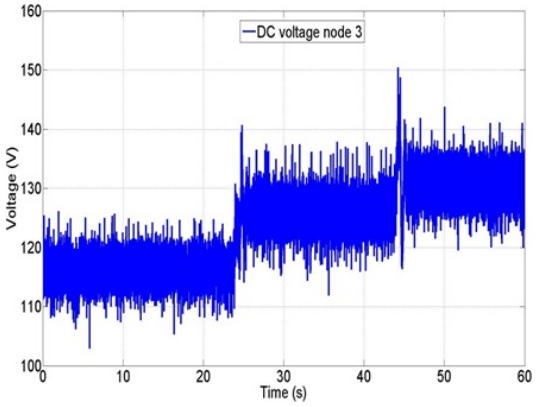


Figure 6.24: DC voltage node 3. Master/slave philosophy.

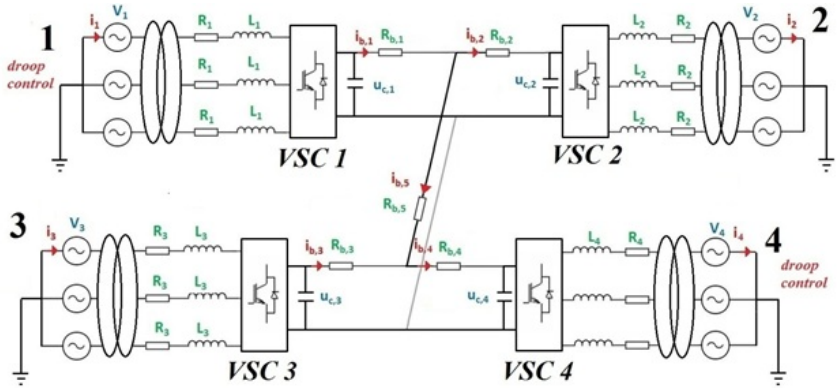


Figure 6.25: Four nodes grid. Droop control philosophy.

$t = 1\ s$, the system is in equilibrium, and in this instant the secondary changes the references and consequently the operation point. It is around $t = 5\ s$ when the steady state is attained.

Later, around $t = 11\ s$, a disturbance at node 2 makes this node to absorb zero current, or zero power, as figure 6.27 shows. This disturbance makes that the voltage at nodes 2 (see figure 6.26) varies instantly. However it is necessary a few seconds, in order to the primary controllers act and vary their voltage references as figure 6.26 shows, this time is exactly the droop control dynamic. We can observe in figures 6.26 and 6.27 as nodes 1 and 4 adapt they current whilst the voltage varies.

Once the droop acts, we can observe as all nodes achieve the voltage equilibrium (around $t = 15\ s$). It is important to empathise that node 3 remain absorbing the same power in this interval. This state, which is not optimal, is send to the supervisor (secondary), which makes its calculations (power flow), and it send the new references to each node ($t = 21\ s$).

Around $t = 35\ s$, the problem disappears at node 2, and it begins to

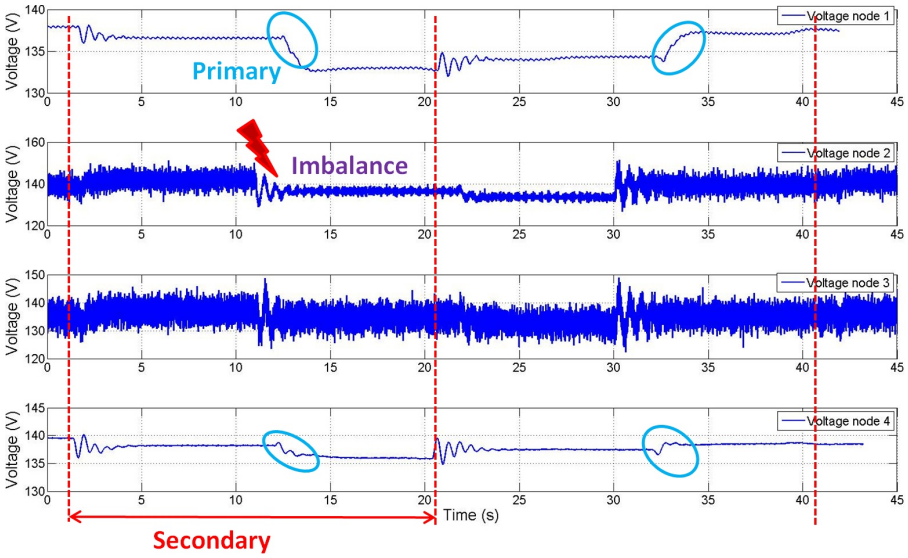


Figure 6.26: Voltage results. Experimental test bench.

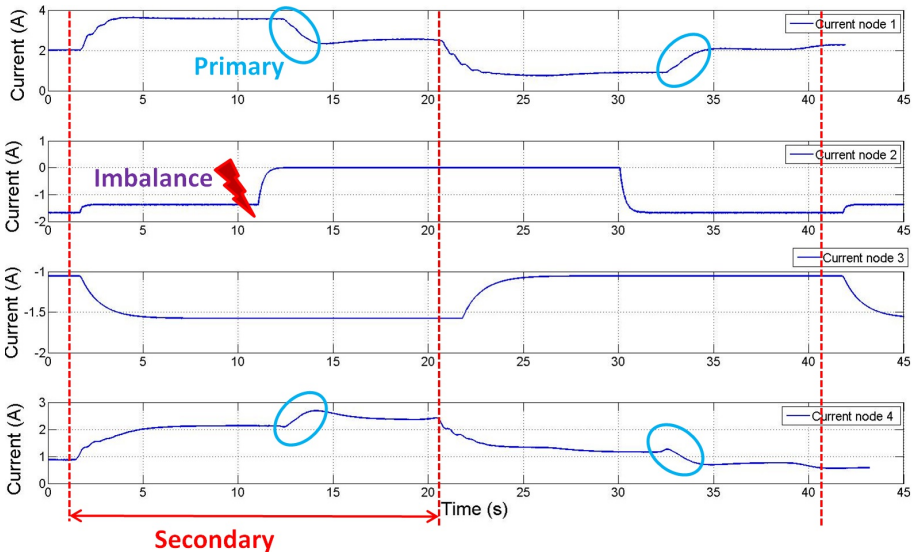


Figure 6.27: Current results. Experimental test bench.

absorb the same power than before. This change could be seen as a perturbation from existent equilibrium state. A similar reasoning can be applied as previously.

## 6.4 Conclusions.

In this chapter the practical experimentation of a hierarchical control for MT-HVDC network is shown, explained and detailed. The control is composed for three level: local, primary and secondary, which have been explained in this thesis.

The tertiary level was not implemented because a too long time scale, and because it would need the inclusion of an energy market and weather forecast. In practice these are not necessary to be done in a hardware in the loop test bed

The test bench has 4 terminals interconnected via a DC grid, and connected to the main AC grid through VSC power converters. Each one of the real components: transformers, sensors, converters, controller board, software, etc .. are explained.

Different control strategies have been tested on a real test bench. Principally, a master/slave and droop control philosophy. Droop control strategy provides better performances than master/slave strategy when a disturbance appears, because the responsibility of keeping the voltage level is divided among several players. It is important to remark also that no communication is needed when a disturbance appears, because each node adapts itself to the new situation. However it is interesting to implement a superior control than droop, secondary control, in order to give new reference operating points, which have been calculate solving periodic power flows. For this task, it is clear that communication is necessary.

In the exhibited simulations, it is shown as we can satisfactorily control a MT-HVDC network with the hierarchical monitoring proposed in this thesis, even when disturbances appear.

Chapter 7

# Conclusions and further work

## 7.1 Conclusions.

This thesis covers all controllers, with their different time scales, of MT-HVDC grids. The proposed solution is a hierarchical control, which includes: local controllers of converters (AC/DC and DC/DC), primary control (droop control philosophy), secondary control (optimal power flow) and tertiary control.

From the point of view of DC/DC converters, three different topologies have been studied in **chapter 2**: two phases DAB, three phases DAB and MMC. Different non-linear control techniques have been implemented: Lyapunov theory, bilinear control, zero dynamics or switching theory, which provides asymptotic stability for each topology respectively.

The use of a topology depends on the application. Therefore, in general, the DAB topology can be interesting for low power applications, and MMC for high power applications. Besides the topology based on MMC technology can be used for link several DC grids with different voltage values, where a balancing philosophy is implemented and a study on how improve the harmonics is explained.

On the other hand, a new use for DC/DC converters has been studied in depth in **section 2.6**. It is the use of them as DC-CB, which may facilitate the development and implementation of DC networks. Different cases and philosophies have been explained for each one of the topologies studied, obtaining interesting results, especially in topology based on MMC technology with full bridge cells.

With respect to AC/DC converters, they have been studied together with their interaction with the primary control (see **section 3.4**). Although must be emphasized that, the control techniques applied to the DC/DC converters, in reality (DC/AC/DC), are easily adaptable for AC/DC topologies.

Concerning the primary controls: three different philosophies have been studied in **chapter 3**: master/slave, voltage margin control and droop control philosophy. We have opted for the latter, because thanks to it, when a perturbation appears on the network, the converters adapt their voltage and power value in function of a law (droop gain), which we choose, and consequentially the problem is shared out in the desired terms defined for

their gains. Besides, and not less important, the local controllers act without need of communication between them.

A study of the problem of the interaction between local and primary control has been approached from the perspective of the singular perturbation (see **section 3.4**), which allows us to obtain a notion until where both dynamics can be considered negligible. Afterwards, a study based on matrix properties of electrical systems is carried out in order to show the asymptotic stability of the controllers.

Even though when a perturbation appears in the system, the droop control will bring the system towards an stable operation point, but not optimal. For these reason the system requires a periodic power flow.

In **chapter 4** we have proposed a new method to solve the power flow problem (non-linear equations) in DC grids (see **section 4.2**), and also for AC grids (see **appendix A**). Thanks to it, we can establish several slack bus with different voltage references. This fact implies that the responsibility for maintaining the voltage level of the whole grid is shared between these nodes, in concordance with the droop control philosophy, and consequently the risks decrease.

Furthermore, we have also proposed an optimal power flow in order to minimize the losses in the transmission line, and with the possibility to avoid power network congestions. The control strategy includes weather forecasts and load predictions. These goals are obtained by calculating the best set of voltages for each terminal, taking into account several restrictions (maximum allowed current through the lines, or maximum/minimum DC voltage level in each node among others, see **section 4.3**). It is also noteworthy to remark that we have chosen the criterion to minimize losses in the system, but there may be moments that for security this is not the most advisable. Also, and thanks to the proposed formulation, it is possible to operate the system with secondary criterion such as maintaining the energy of the storage devices in a pre-established interval, or maintaining the voltages in a range better suited for us.

With respect to tertiary control, which is explained in **chapter 5**, we have proposed two new formulations in order to maximize the profits of a MT-HVDC network, where it has been assumed renewable generation (wind farms), storage devices and different markets. Both formulations have been carried out by MPC procedures, where restrictions have also been taken into account. The objective of this tertiary control is to provide power references to secondary level power under the optics of maximize incomes.

Finally, thanks to the real implementation on a test bench (see **chapter 6**), two important conclusions can be drawn: the first one is that MT-HVDC networks are technically feasible and the second is that the control philosophy and the methods developed in this thesis are perfectly valid in order to operate these MT-HVDC grids.

## 7.2 Main results.

The main results of this thesis can be summarized in:

- Modulation study, an average model proposed, and a control law which assures global asymptotically stability (based on Lyapunov theory) for the two phases DAB.
- Bilinear and non-linear control algorithms based on Lyapunov theory (with the study of the *zero dynamics* of the system) for the three phases DAB with PWM, which assures exponentially stability.
- A control law, based in switching theory, which assures globally exponentially stability for a new topology of DC/DC converters based in MMC technology. This converter is able to link $n$ DC grids with different voltages, and with $k$ internal phases.
- A new service for a DC/DC converter. Its use as DC-CB. Several strategies have been explained with this purpose.
- A study based on matrix properties of electrical systems is carried out in order to show the asymptotic stability of the droop control.
- A new methodology to solve the power flow problem in DC and AC systems.
- An optimal power flow to minimize the losses in a MT-HVDC network subject several constraints and taking into account storage devices via MPC.
- An optimal power flow to maximize the profit of a MT-HVDC grid taking into account several spot markets via MPC.
- A real MT-HVDC test bench with four terminal nodes, which includes local, primary and secondary controllers.

## 7.3 Further work.

Since this thesis covers many scopes, from local control to tertiary control, where many fields have been treated, namely: power electronics, electrical engineering and automatic control, therefore the range of future work is very broad.

If we start with the DC/DC converters, certainly an investigation line will be the improvement of MMC technology, which entails the study of new electronic devices, new topologies, etc.. Undoubtedly, other research line will be the study of these topologies as DC-CB, since these devices will be a key element to the development of DC meshed networks.

Relative to the primary control, a future research line would be the study of another control law for the droop control philosophy. That means, hitherto, it has always been considered that the relationship between power and voltage (or between current/voltage) in this philosophy follows a straight line, but there may be other relationships, such as hyperboles, or in general quadratics, which carry out the control in a more efficient way when a disturbance appears in the system.

Also, and more specifically, it could be interesting to perform an analogous study as carried out in section 3.4, but this time taking into account MMC technology instead of VSC, with respect to the interaction between local control and primary. At this point, and because the references of local control depends on the primary, clearly shows that there is a distinction in the dynamics, which have been study in this thesis with the theory of singular perturbations in order to separete both dynamics, but other theories could be interesting to apply as the the small gain theorem, or to work in the frequency domain.

Concerning secondary and tertiary control, as they are based on forecasts in order to optimize their respective objectives, it is clear that the reliability of these data will be a fundamental factor. Our secondary controller works with a sample time in the order of tens of seconds or even minute, the so-called *very short space of time forecast*. Recent studies show that it is possible to use Markov methods to carry out it [101, 102]. Therefore another line of research may be this one.

With respect to the experimental test bench, in the future is expected to include a framework for economic aspect. Also, with the material available at this time, we can connect a maximum of four terminal nodes, however the facilities of Department of Power & Energy Systems of Supélec allow the connection of more nodes, and thus create a mesh DC network, the only impediment is economical.

# List of publications

## Journals:

**-Published:**

M. Jiménez Carrizosa, F. Dorado Navas, G. Damm , A. Benchaib and F. Lamnabhi-Lagarrigue, *Optimal power flow in multi-terminal HVDC grids with offshore wind farms and storage devices.* International Journal of Electrical Power and Energy Systems. Volume 65, February 2015, Pages 291-298.

**-Submitted:**

M. Jiménez Carrizosa, G. Bergna, A. Benchaib, P. Alou, A. Arzandé, G. Damm, and F. Lamnabhi-Lagarrigue, *Stability of DC/DC multi-terminal converter using Modular Multilevel Converters for HVDC systems.* IEEE Transactions on Power Electronics.

M. Jiménez Carrizosa, A. Arzandé, A. Benchaib, G. Damm, E. Berne, P. Egrot, J.C. Vannier and F. Lamnabhi-Lagarrigue, *Hierarchical control of a Multi-terminal HVDC grid in an experimental set-up.* IEEE Transactions on Power Systems.

E. Jiménez, M. Jiménez Carrizosa, A. Benchaib, G. Damm and F. Lamnabhi-Lagarrigue, *A new generalized power flow method for multi connected DC grids.* International Journal of Electrical Power and Energy Systems.

Y. Chen, M. Jiménez Carrizosa, G. Damm, A. Benchaib and F. Lamnabhi-Lagarrigue, *Nonlinear Control of Multi-Terminal VSC-HVDC Systems Based on Control Induced Time-Scale Separation with "Plug and Play Property".* IFAC journal.

## Conferences:

**-Published:**

M. Jiménez Carrizosa, A. Benchaib, P. Alou and G. Damm, *DC transformer for DC/DC connection in HVDC network.* $15^{th}$ European Conference on Power Electronics and Applications September 2013, Lille, France.

M. Jiménez Carrizosa, J. Cortés, A. Benchaib, P. Alou, G. Damm, J. A. Cobos and F. Lamnabhi-Lagarrigue, *DC / DC converters as DC circuit-breakers in HVDC networks operation.* $16^{th}$European Conference on Power Electronics and Applications, August 2014, Lappeenranta, Finland.

M. Jiménez Carrizosa, G. Damm, A. Benchaib, P. Alou, M. Netto and F. Lamnabhi-Lagarrigue, *Bilinear and nonlinear control algorithms for a DC/DC converter for multi-terminal HVDC networks*, $19^{th}$ World Congress of the International Federation of Automatic Control .August 2014, Cape Town, South Africa.

M. Jiménez Carrizosa, Y. Chen, G. Damm, A. Benchaib and F. Lamnabhi-Lagarrigue, *Multi-Terminal High Voltage Direct Current networks for renewable energy sources*, ERCIM, European Research Consortium for Informatics and Mathematics, number 97. April 2014.

M. Jiménez Carrizosa, F. Dorado Navas, G. Damm , A. Benchaib and F. Lamnabhi-Lagarrigue, *Optimal power flow operation of a multi-terminal HVDC system with renewable sources and storages.* $12^{th}$ IEEE International conference on Industrial informatics - INDIN 2014 Porto Alegre, Brazil July 27-30 2014.

M. Jiménez Carrizosa, A. Arzandé, A. Benchaib, G. Damm, E. Berne, P. Egrot, J.C. Vannier and F. Lamnabhi-Lagarrigue, *Local and primary controls of a Multi-terminal HVDC grid in an experimental setup*, $17^{th}$ Conference on Power Electronics and Applications, EPE'15-ECCE Europe, Geneva, Switzerland, 8-10 September 2015.

M. Jiménez Carrizosa, G. Bergna, A. Arzandé, G. Damm, P. Alou, A. Benchaib and F. Lamnabhi-Lagarrigue, *Stability of DC/DC three terminals converter using Modular Multilevel Converters for HVDC systems.* $17^{th}$ Conference on Power Electronics and Applications, EPE'15-ECCE Europe, Geneva, Switzerland, 8-10 September 2015.

**-Submitted:**

M. Jiménez Carrizosa, G. Damm , A. Benchaib and F. Lamnabhi-Lagarrigue, *Distributed primary droop control in Multi Terminal High Voltage Direct Current networks.* $24^{th}$ IEEE lnternational Symposium on Industrial Electronics, Rio de Janeiro, Brazil June 3-5, 2015.

Chapter 8

# French summary

Cette thèse traite de la commande hiérarchique de réseaux à courant continu (Direct current) multi-terminaux à haute tension (HVDC-MT) intégrant des sources d'énergie renouvelables à grande échelle. Le schéma de contrôle proposé est composé de quatre 'couches' : i) le contrôle local, le plus bas, où se trouvent les convertisseurs de puissance, avec une échelle de temps de l'ordre de la milliseconde ; ii) le contrôle primaire qui est décentralisé et appliqué à plusieurs terminaux avec une échelle du temps de l'ordre de la seconde ; puis iii) un niveau de commande où la communication est prise en compte et où l'approche de Modèle du Commande Prédictive 'Model Predictive Control' (MPC) assure la planification de la tension et de la puissance à leur état d'équilibre, pour l'ensemble du système - cette commande est aussi capable de gérer le stockage à grande échelle en prenant en compte les prévisions météo; enfin, iv) le contrôleur de niveau supérieur, qui est principalement basé sur les techniques d'optimisation, où les aspects économiques sont pris en compte en même temps que les prévisions météo (il s' agit du réglage dit tertiaire).

Au niveau des convertisseurs, un accent particulier est mis sur les convertisseurs bidirectionnels DC/DC. La tâche principale de ces dispositifs est de relier plusieurs réseaux DC possédant des tensions différentes, sous une forme analogue à celle de l'utilisation de transformateurs pour les réseaux AC. Dans cette thèse, trois topologies différentes sont étudiées en profondeur: 1) deux phases Dual Active Bridge (DAB), 2) trois phases DAB, et 3) utilisation de la technologie Modular Multilevel converter (MMC) comme convertisseur DC/DC. Pour chaque topologie, une commande non-linéaire spécifique est présentée et discutée. Ainsi, une commande non-linéaire, basée sur la théorie de Lyapunov, est appliquée aux deux phases DAB (voir [38, 39, 40]). Pour les trois phases DAB, un contrôle basé sur la théorie des systèmes bilinéaires est développé (voir [41, 42, 43, 44]), ainsi qu'un contrôle basé sur la théorie de Lyapunov, où la dynamique des zéros du système a été étudiée avec précision [45]. Enfin, pour le convertisseur DC/DC utilisant la technologie de commande MMC, la théorie du contrôle des systèmes à commutations a été appliquée [46]. D'autre part, toujours pour cette première couche, une nouvelle fonction pour le convertisseur DC/DC est introduite. Il s'agit de son utilisation comme disjoncteur à courant continu ' Direct-Current Circuit-Breaker' (DC-CB), qui est un dispositif très important pour le développement des futurs réseaux MT-HVDC. Ceci est

rendu possible car les convertisseurs DC/DC étudiés ici comprennent un état AC : il existe donc des instants pour lesquels le courant passe par zéro, et par conséquent nous pouvons ouvrir les commutateurs en cas de défaut. Plusieurs stratégies d'exploitation pour ces topologies utilisées comme DC-CB sont alors étudiées.

En ce qui concerne le contrôle primaire, qui permet de maintenir le niveau de tension continue dans le réseau, nous avons étudié trois philosophies de contrôle: i) celle de maître/esclave, ii) celui du contrôle de la marge de tension (voltage margin control) et iii) celle de la commande du statisme (droop control). Enfin, nous avons choisi d'utiliser le droop control, entre autres, parce que la communication entre les noeuds n'est pas nécessaire. Deux approches différentes ont été étudiées pour le droop control. Tout d'abord, nous avons considéré que la dynamique des convertisseurs (AC/DC) sont négligeables (trop rapide par rapport au réseau), et dans une seconde étape, sur la base de ces résultats, nous avons étudié la dynamique du droop control couplée à la dynamique des convertisseurs AC/DC. Dans cette approche les convertisseurs de source de tension (VSC) sont utilisés comme convertisseurs AC/DC.

Concernant la commande secondaire, son principal objectif est de planifier le transfert de puissance entre les noeuds du réseau, qui fournissent la tension et la puissance de référence, et les contrôleurs locaux et primaires, et ce, même lorsque des perturbations apparaissent. De plus, le contrôle secondaire pourra gérer le stockage de la puissance. Dans cette partie, nous avons proposé une nouvelle approche pour résoudre les problèmes de flux de puissance (équations non-linéaires) basée sur le théorème du point fixe de l' application contractive. Ceci permet d'utiliser plus d'un slack bus (noeud bilan à puissance infinie) pour équilibrer la puissance, contrairement à l'approche classique basée sur la méthode de Newton-Raphson (NR). En outre, avec la méthode proposée dans cette thèse, l'existence unique de solution est garantie lorsque certaines contraintes sont remplies. Ces contraintes s'avèrent réalistes. Par ailleurs, le réglage secondaire joue un rôle très important dans les applications pratiques, en particulier lorsque les sources d'énergie sont variables dans le temps, ce qui est bien sûr le cas des énergies renouvelables. Dans de tels cas, il est intéressant de considérer des dispositifs de stockage afin d'améliorer la stabilité et l'efficacité de tout le système. En raison du temps du réglage secondaire, la période d'échantillonnage est de l'ordre de quelques minutes. Il est également possible d'envisager différents types de prévisions (météo, charge, ..) pour atteindre des objectifs de contrôle supplémentaires, basées sur la gestion des réserves de stockage. Toutes ces caractéristiques ont suggéré, là aussi, l'utilisation d'une approche MPC. Dans ce contexte, plusieurs critères d'optimisation ont été considérés, en particulier la minimisation des pertes de transmission ou des congestions dans le réseau.

La tâche principale de réglage tertiaire est de gérer le flux de l'ensemble

de la grille de charge HVDC afin d'atteindre l'optimisation économique, particulièrement pertinent avec la présence de dispositifs de stockage. Ce niveau de contrôle fournit des références de puissance au contrôleur secondaire. Dans cette thèse, nous avons pu maximiser le profit économique du système en agissant sur le marché réel, et en optimisant l'utilisation des périphériques de stockage. Dans ce niveau, l'approche MPC a été à nouveau utilisé, mais cette fois, en agissant sur une échelle de temps plus élevée, et de manière complémentaire aux objectifs de la couche secondaire.

Dans le but de mettre en oeuvre la philosophie de contrôle hiérarchique présentée dans cette thèse, nous avons construit un banc d'essai expérimental. Cette plate-forme dispose de quatre terminaux reliés entre eux par l'intermédiaire d'un réseau à courant continu, et connectés au réseau principal de courant alternatif à travers des convertisseurs de puissance VSC. Ce réseau DC peut fonctionner à un maximum de 400 V, et avec une courant maximal de 15 A. Les convertisseurs VSC locaux sont contrôlés par le logiciel dSPACE. Aussi, dans ce réseau, un superviseur PC (contrôleur secondaire) est inclus, qui communique avec chaque logiciel dSPACE de chaque VSC par un contrôleur CompactRIO de National Instruments, à travers l'internet.

**Contrôleurs locaux.**

Dans un réseau MT-HVDC connecté aux réseaux alternatifs externes, c'est clair que les convertisseurs AC/DC bidirectionnels sont les éléments clés pour transmettre la puissance dans les deux directions. Cependant, l'étude des convertisseurs DC/DC bidirectionnels est aussi intéressante, parce qu'ils peuvent s'appliquer au MT-HVDC pour relier différents réseaux DC avec différentes valeurs de tension. Dans cette thèse, un chapitre est totalement consacré à étudier les convertisseurs DC/DC (chapitre 2), tandis que l'étude des convertisseurs AC/DC est étudiée en complément d'autres tâches, voir les chapitres 3 et 6. De plus, les techniques du contrôle appliquées pour les convertisseurs DC/DC peuvent être valables, en les adaptant, à celles des convertisseurs AC/DC, parce que le convertisseur DC/DC est un dispositif avec des étapes DC/AC/DC.

**Convertisseurs bidirectionnels AC/DC.**

Jusqu'au développement du VSC [1, 16, 17], les CSC (current source converters) ont été utilisés comme onduleurs et redresseurs dans les systèmes HVDC. Les convertisseurs VSC utilisent IGBT tandis que les CSC utilisent des thyristors. Les systèmes VSC-HVDC présentent de nombreux avantages par rapport aux systèmes CSC-HVDC, par exemple : la surveillance simultanée de la puissance active et réactive ; la possibilité de créer n' importe quel angle de phase ou amplitude de tension (dans certaines limites toutefois) ; il n'y a pas de changement de polarité de la tension lorsque la direction de puissance est modifiée. Il faut aussi des systèmes de communication entre les convertisseurs CSC alors que ce n'est pas nécessaire avec les systèmes VSC [16]. Cependant, plus récemment, une nouvelle topologie prévaut, le MMC [18].

Les avantages d'utiliser MMC par rapport à la technologie VSC sont nombreux: la forme d'onde résultante a un très faible contenu harmonique ; il réduit les contraintes de tension transitoires et le bruit à haute fréquence inférieure [19] ; il est fiable pour fonctionner à des fréquences de commutation plus faibles ; et enfin, il a la capacité de continuer à fonctionner en conditions de déséquilibre [20].

**Convertisseurs DC/DC bidirectionnel.**

Un élément clé pour le développement des réseaux MT-HVDC est le convertisseur DC/DC bidirectionnel, l'équivalent au transformateur pour les réseaux à courant alternatif, dont la mission principale est de relier les réseaux de tensions différentes. En outre, le convertisseur DC/DC peut fournir d'autres services tels que : l'utilisation de lui-même comme DC-CB, et également la régulation du flux de puissance dans le réseau [9].

Une ligne de recherche pour les convertisseurs DC/DC bidirectionnels appropriée pour MT-HVDC a été discutée dans les sections 2.2 et 2.4, qui sont fondées sur la topologie Dual Active Bridge (DAB). Cependant, et bien que la topologie DAB ait des performances optimales et des avantages sur les autres topologies, notamment par rapport à SRC (Series Resonant Converter) et à DHB (Dual Half Bridge), son principal inconvénient est qu'elle utilise un transformateur interne à haute fréquence [21, 22] qui augmente considérablement le coût du dispositif. D'autres auteurs proposent de relier deux MMC par le côté AC pour connecter deux réseaux avec différentes tensions continues, comme l'a proposé [23]. Cette structure offre est intéressante car elle évite l' utilisation du transformateur, et par conséquent, les coûts sont réduits. Elle offre aussi tous les avantages fournis par l'utilisation de la technologie du MMC qui a été expliquée auparavant.

**Contrôleurs primaires.**

Le fonctionnement correct d'un système MT-HVDC nécessite une bonne coordination du réglage entre la tension et la puissance (ou entre la tension et le courant). Le contrôle primaire fonctionne dans un intervalle de temps de quelques secondes. Il est responsable du maintien de la tension du réseau. Dans les systèmes à courant continu, il y a certains candidats appropriés pour le contrôle primaire: maître / esclave, 'voltage margin control' et le 'droop control' [24, 25].

Pour la stratégie maître/esclave, il y a un noeud responsable du maintien du niveau de l'ensemble du réseau (maître) de tension, tandis que les autres noeuds sont responsables de la commande de l'absorption de puissance ou l'insertion, en adaptant ses valeurs de tension DC (esclaves). Le noeud maître doit être capable d'absorber ou de fournir suffisamment de puissance active pour parvenir à un équilibre dans le système [26]. Une panne de ce convertisseur ne peut être tolérée car elle entraînera la perte du contrôle de la tension continue, ce qui est un grand inconvénient. Un autre important inconvénient est que des points de fonctionnement sous-optimaux peuvent être obtenus avec cette stratégie [27].

La philosophie de contrôle 'voltage margin control' est à peu près la même que la précédente, sauf qu' ici, le noeud maître change au cours du temps quand il atteint ses limites [25]. En conséquence, il passe' la responsabilité du maintien de la tension du réseau à autre noeud. Bien que cette stratégie soit plus sure que la précédente, elle comporte aussi des risques car, pour un instant donné, il n'y a qu'un seul noeud qui est responsable du maintien de la tension du réseau. D'autre part, des points de fonctionnement sous-optimaux peuvent aussi être obtenus avec cette stratégie [27].

Enfin, le droop control est décentralisé, et est employé pour réguler la tension continue en s'adaptant aux injections de puissance ou aux absorptions dans les noeuds. Dans cette stratégie, il existe plusieurs noeuds responsables de la tension du réseau au même instant. Pour cette raison, nous avons choisi d'utiliser la philosophie du 'droop control' qui, de plus, ne nécessite pas la communication entre les noeuds.

**Contrôleurs secondaires.**

Dans les réseaux électriques avec charge et production réelles, la tâche principale du niveau secondaire est de réaliser le power flow (le flux de puissance), qui est crucial pour le bon le fonctionnement du système. L'objectif principal du 'power flow' est d'obtenir les informations de la tension et de la puissance pour chaque bus dans le réseau, en régime permanent. Cependant, il peut effectuer d'autres types d'analyse, tels que l'analyse des défauts court-circuit, ou des études de stabilité. Dans les systèmes AC, le problème du 'power flow' est composé d'équations non-linéaires quadratiques. Dans les systèmes HVDC, où il n'y a pas de puissance réactive, le système power flow est moins complexe, mais conserve toujours son caractère non linéaire. Il y a plusieurs méthodes pour résoudre des systèmes d'équations non linéaires. La plus populaire est la méthode de Newton-Rhapson (NR) [15]. Avec cette méthode, les solutions sont facilement approchées en linéarisant les équations. Un autre inconvénient important est que la convergence de la méthode n'est pas toujours garantie. En outre, dans le cas de systèmes électriques, un unique bus qui donne la tension (slack bus), est généralement considéré. Ce fait entraîne des risques pour le bon fonctionnement du système, tels que la perte de ce bus (par exemple, une perte de communication), qui pourrait entraîner la perte de la référence et par conséquent l'abandon de l'équilibre parce que la méthode n'est alors plus applicable. Dans cette thèse, il est proposé un nouvel algorithme pour résoudre le 'power flow', où ce risque disparaît, car plus d'un noeud peut être utilisé comme référence de tension.

Plus récemment, certains auteurs ont proposé d'autres solutions pour résoudre le problème. Par exemple dans [28] plusieurs noeuds a été proposé. Dans [29], où un régime permanent pour un modèle de réseaux multi-terminaux à courant continu a été développé, les limites de conversion ainsi que différentes topologies pour les convertisseurs ont été prises en compte. Cependant, les deux méthodes sont basées sur la résolution de

la méthode itérative NR. D'autres auteurs ont résolu le problème en appliquant de nouvelles techniques comme dans [30] en utilisant un algorithme génétique heuristique évolutif.

La nouvelle méthode proposée dans cette thèse pour résoudre le problème du 'power flow' est basée sur le célèbre théorème du point fixe pour les applications contractives. Il est également connu comme le théorème de point de Banach [31]. Pour un réseau de $n$ noeuds, si nous connaissons la puissance dans $k$ noeuds ($0 < k < n$) et les tensions dans les autres $n < k$ noeuds, le système d'équations peut avoir plusieurs solutions, mais n'en n'a qu' une seule pour laquelle les tensions de tous les noeuds sont proches de la valeur de la tension nominale du réseau, lorsque celle-ci est suffisamment élevée. La méthode exposée ici conduit toujours à cette solution, et seulement quelques itérations sont nécessaires pour y parvenir.

D'autre part, si la capacité de stocker de l'énergie entre en jeu, cette puissance pourrait être optimisée. Dans [32] un problème optimal de power flow pour MT-HVDC avec des outils de commande prédictive est présenté. Il utilise des techniques géométriques afin de garantir l'existence de solutions. D'autres auteurs comme [33], ont proposé un ' power flow' optimal afin de minimiser les pertes dans un réseau multi-terminaux à courant continu. Ils ont considéré l'état du réseau à chaque temps d' échantillonnage pour lequel ils ont formulé un problème d'optimisation concernant les pertes de transmission.

Cependant, dans les applications pratiques des sources de production d'énergie variables, il est intéressant de tenir compte des dispositifs de stockage afin d'améliorer la stabilité et l'efficacité de l'ensemble du système [34]. Dans [35] une solution à un problème de répartition pour un réseau intelligent composé i) de multiples sources de production (conventionnelles et renouvelables), ii) de noeuds consommateurs et iii) de systèmes de stockage, est proposée en utilisant la formulation centrée sur l'énergie. Leur formulation, prenant en compte les prévisions météorologiques pour exploiter de façon optimale les stockages dans les systèmes, a été abordée avec l'approche de commande prédictive, MPC, résultant ainsi en un problème d'optimisation quadratique.

Cette thèse présente aussi une stratégie de 'power flow' pour les systèmes MT-HVDC où les pertes de transmission sont réduites au minimum (voir section 4.3 ). Le problème d'optimisation donne une solution, où les valeurs de tension aux noeuds du réseau minimisent les pertes de transport et tiennent compte également de toutes les contraintes prises en considération (section 4.3.3). Cette formulation conduit à une fonction d'objectif quadratique convexe mais avec des contraintes non convexes. L'existence de la solution à ce problème est également abordée dans les sections 4.3.5 et 4.3.7. Les pertes de distribution sont minimisées pour l'ensemble du réseau. On obtient ensuite une stratégie de contrôle qui est en mesure de faire face à l'ensemble du système et de ses contraintes inhérentes donnant le cadre

d'un contrôle d'optimisation multi-objectif. L'énergie est principalement générée par des sources d'énergie renouvelables et des noeuds sont présents dans le réseau, avec la possibilité de stocker de l'énergie. Cette énergie est générée en tenant compte des conditions météorologiques réelles afin de faire le meilleur ordonnancement du système dans une approche réaliste. Un schéma d'optimisation est proposé dans lequel tous ces éléments sont inclus ainsi que des contraintes de fonctionnement réel.

**Contrôleurs tertiaires.**

Le réglage tertiaire est responsable de l'organisation de la planification de l'énergie électrique du point de vue économique. Le marché de l'électricité est basé sur une série de négociations entre les producteurs et les opérateurs afin d'obtenir un prix final pour le produit énergie. Il est discuté dans le marché de la veille (D-1 jour) et dans le marché du jour actuel (jour D) [36]. Le marché D-1 est un marché marginal où le prix pour chaque heure est le résultat de l' équilibre entre l'offre et la demande. Chaque jour, les opérateurs reçoivent des offres des producteurs pour le prix de l'électricité de la journée suivante. Par la suite, l'opérateur communique les prix de l'énergie (achat et vente) dans une plate-forme publique pour le lendemain (jour D-1). Au jour D, plusieurs marchés intra-jour sont effectués dans le but de permettre aux acheteurs et vendeurs pour d'ajuster leurs offres en fonction des prévisions nouvelles disponibles. Dans cette thèse, nous avons utilisé le prix final (jour D) provenant de toutes les négociations à procéder à la programmation de puissance par des techniques MPC.

**Explication du banc d' essai.**

Pour mettre en oeuvre la philosophie de contrôle hiérarchique et les résultats théoriques proposés dans cette thèse, nous avons développé un banc d' essai expérimental dans les installations du département d' énergie de CentraleSupelec (Gif-surYvette, France) avec le soutien d'EDF (Electricité de France) et Alstom Grid en tant que partenaires industriels et le L2S (Laboratoire des Signaux et Systèmes) et CentraleSupelec comme partenaires académiques.

Une mise en oeuvre pratique est toujours importante afin de vérifier les résultats théoriques. Elle permet également de mieux comprendre la problématique et de fournir de nouvelles idées pour améliorer les techniques de contrôle. Il est important de remarquer que ce chapitre n' était pas initialement prévu dans la thèse, et bien que le temps de la construction de la plate-forme n'ait pas été négligeable, ce travail a été, in fine, extrêmement productif.

Grâce aux résultats présentés dans ce chapitre, nous pouvons affirmer que la philosophie de contrôle proposé dans cette thèse pour un réseau MT-HVDC pourrait être une solution appropriée pour gérer des réseaux DC, puisque les contrôle appliqués ont un comportement satisfaisant en mode de fonctionnement, même lorsque des perturbations apparaissent, voir section 6.3.

**Principaux résultats de la thèse.**
Les principaux résultats de cette thèse peuvent se résumer en:

- Pour les deux phases DAB, une étude de modulation a été faite, un modèle moyen non linéaire a été proposé, et une loi de commande qui assure la stabilité asymptotique (basée sur la théorie de Lyapunov) a été conçue.

- Des algorithmes de contrôle, bilinéaires et non linéaires, basés sur la théorie de Lyapunov (avec l'étude des dynamique zéro du système) pour les trois phases DAB ont été développés. La stabilité exponentielle a été assurée grâce à l'utilisation de la technique PWM.

- Une loi de commande de convertisseur DC/DC, utilisant la technologie MMC, basée sur la théorie de la commutation, qui assure la stabilité global et exponentielle pour une nouvelle topologie, a été proposée. Ce convertisseur est en mesure de relier n DC avec plusieurs réseaux avec différentes valeurs de tensions, et avec, en général, $k$ phases internes.

- Une nouvelle fonctionnalité du convertisseur DC/DC a été introduite. Son utilisation comme DC-CB a été suggérée. Plusieurs stratégies ont été expliquées dans ce but.

- Une étude basée sur les propriétés de la matrice des systèmes électriques est réalisée afin de montrer la stabilité asymptotique du droop control.

- Une nouvelle méthodologie pour résoudre le problème du 'power flow' aussi bien en DC qu' en AC a été introduite.

- Un 'power flow' optimal pour minimiser les pertes dans un réseau MT-HVDC, soumis à plusieurs contraintes et tenant compte des dispositifs de stockage, a été également introduit en utilisant le MPC.

- Un 'power flow' optimal pour maximiser le bénéfice d'un réseau MT-HVDC en tenant compte de plusieurs marchés réels a été également obtenu par le MPC.

- Un banc d'essai MT-HVDC réel avec quatre noeuds terminaux, qui comprend des contrôleurs locaux, primaires et secondaires, a été mis en place et testé avec succès.

**La poursuite des travaux.**
Comme cette thèse couvre de nombreux champs d'application, du contrôle local au réglage tertiaire, où de nombreux champs ont été traités, à savoir: l'électronique de puissance, ingénierie électrique et l' automatique, donc une gamme des travaux futurs est large.

Tout d' abord, pour les convertisseurs DC/DC, une ligne de direction de recherche sera certainement l'amélioration de la technologie du MMC, ce qui implique l'étude de nouveaux appareils, de nouvelles topologies, etc ...

Sans aucun doute, une autre ligne de recherche sera l'étude des topologies DC-CB, puisque ces dispositifs constituent un élément clé pour le développement des réseaux maillés DC.

Par rapport à la commande primaire, une future ligne de recherche sera l'étude d'une autre loi de commande pour la philosophie 'droop control'. Jusqu'à présent, il a toujours été considéré que la relation entre la puissance et la tension (ou entre courant et tension) était linéaire, mais il peut y avoir d'autres relations, comme des hyperboles, ou en général des équations du second ordre, qui permettent un contrôle plus efficace quand une perturbation apparaît dans le système.

En ce qui concerne l'interaction entre le contrôle local et le contrôle primaire, il pourrait être intéressant d'effectuer une étude analogue à celle effectuée dans la section 3.4, mais en prenant cette fois en compte la technologie du MMC à la place du VSC. Dans cette thèse nous avons montré comment séparer les deux dynamiques locale et primaire en utilisant les perturbations singulières. Cependant, d'autres méthodes pourraient être utilisées comme le théorème du petit gain. On pourrait aussi travailler dans le domaine fréquentiel.

En ce qui concerne les contrôles secondaire et tertiaire, qui sont fondées sur des prévisions afin d'optimiser leurs objectifs respectifs, il est clair que la fiabilité de ces données sera un facteur fondamental. Nos travaux de contrôleur secondaire, avec un temps d'échantillonnage de l'ordre de dizaines de secondes ou de minutes pourraient être améliorés, car ces échantillonnages sont très courts pour ce type de prévisions. Des études récentes montrent qu' il est possible d'utiliser des méthodes de Markov pour mener à bien cette problématique [101, 102].

En ce qui concerne le banc d'essai expérimental, il devrait inclure à l'avenir, un cadre pour l'aspect économique. En outre, avec le matériel disponible à ce moment, nous pouvons nous connecter un maximum de quatre noeuds terminaux, alors que les installations du département d'énergie du CentraleSupélec permettraient la connexion de plusieurs noeuds, et de créer ainsi un réseau DC plus maillé.

Appendix A

# New AC power flow

A new power flow for AC (single phase) grids is presented in this annex based on the contraction mapping theorem, in concordance with the method presented in section 4.2. This new method gives the possibility of using more than one node as slack bus, and consequently the responsibilities are shared between many actors [80].

The most general and complex case is when we are working with AC systems, because the variables are complex numbers (phasors). Note that the other cases could be seen as particular cases of this one. In AC systems, the main information obtained from the *power flow* is the magnitude and phase angle of the voltage in each bus, and the active and reactive power flowing through the lines.

Throughout history, the NR method has been one of the most used methods to solve this type of quadratic equations [15]. Other methods derived from it that can be highlighted are the so-called quasi-Newton-Rapshon methods (QNR). They are an alternative to NR method when the Jacobian is unavailable or too expensive to compute at every iteration. Among these methods, it can be emphasized the Fast Decoupled Newton Rapshon Method (FDNR) [15]. However, all of these algorithms have some problems: basically, they are not always convergent and also they can lead us to a not physically feasible solution.

## A.1 Definitions and basic relations.

We have considered a single phase passive AC network with $n$ nodes ($n \geq 2$) in steady state. This grid is connected because any two nodes of the network are connected by at least one path formed by branches of the network. The lines are bipolar since they have two phases (+ and -) as shows figure A.1.

***Def* 6** $\forall j,k \in \{1,2,..,n\}, j \neq k,\ y_{j,k} = G_{j,k} + \boldsymbol{i} \cdot B_{j,k}$ *is the complex admittance of the branch which connects node* $j$ *with node* $k$*. It corresponds with the two conductors (positive and negative). When the branch leaves a node then* $G_{j,k} > 0$*, whereas if there is no branch* $y_{j,k} = 0$*. It holds that* $y_{j,k} = y_{k,j}$*.*

***Def* 7** $\forall j \in \{1,2,..,n\},\ y_{j,j}$ *is the sum of the admittances of the network*

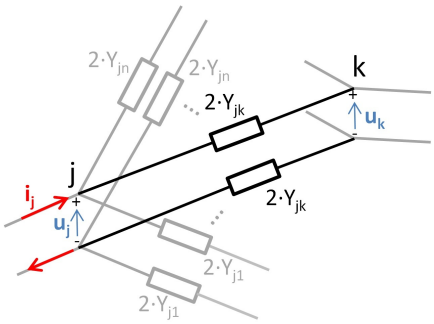


Figure A.1: Bipolar line.

*which converge at node $j$.*

$$y_{j,j} = \sum_{\substack{k=1 \\ k \neq j}}^{n} y_{j,k} \tag{A.1}$$

***Def* 8** *$\forall j \in \{1, 2, .., n\}$, $u_j$ is the voltage (complex) between positive and negative terminals of node $j$.*

***Def* 9** *$\forall j \in \{1, 2, .., n\}$, $i_j$ is the current (complex) which comes into the network through the positive terminal of node $j$.*

***Def* 10** *$\forall j \in \{1, 2, .., n\}$, $S_j = u_j \cdot \bar{i_j} = P_j + \boldsymbol{i} \cdot Q_j$ is the apparent power which comes into the network at node $j$. ($\bar{i_j}$ is the conjugate of $i_j$)*

***Def* 11** *$\forall j \in \{1, 2, .., n\}$, $P_j$ is the active power which comes into the grid at node $j$ (its value is negative when the power leaves the grid).*

***Def* 12** *$\forall j \in \{1, 2, .., n\}$, $Q_j$ is the reactive power which comes in the grid at node $j$.*

In steady state, the system of equations shown in (A.2) are satisfied:

$$\begin{cases} y_{1,2}(u_1 - u_2) + y_{1,3}(u_1 - u_3) + .. + y_{1,n}(u_1 - u_n) = i_1 \\ y_{1,2}(u_2 - u_1) + y_{2,3}(u_2 - u_3) + .. + y_{2,n}(u_2 - u_n) = i_2 \\ \vdots \\ y_{1,n}(u_n - u_1) + y_{2,n}(u_n - u_2) + .. + y_{n-1,n}(u_n - u_{n-1}) = i_n \end{cases} \tag{A.2}$$

which is equivalent to system shown in (A.3):

$$\begin{cases} y_{1,1} \cdot u_1 - y_{1,2} \cdot u_2 - y_{1,3} \cdot u_3 - \ldots - y_{1,n} \cdot u_n = i_1 \\ -y_{1,2} \cdot u_1 + y_{2,2} \cdot u_2 - y_{2,3} \cdot u_3 - \ldots - y_{2,n} \cdot u_n = i_2 \\ \vdots \\ -y_{1,n} \cdot u_1 + y_{2,n} \cdot u_2 - y_{3,n} \cdot u_3 - \ldots + y_{n,n} \cdot u_n = i_n \end{cases} \tag{A.3}$$

Moreover:

$$S_1 = u_1 \cdot \overline{i_1}\ ,\ S_2 = u_2 \cdot \overline{i_2}\ ,\ \ldots\ , S_n = u_n \cdot \overline{i_n} \tag{A.4}$$

and consequently,

$$\begin{cases} u_1 \cdot \overline{y_{1,1}} \cdot \overline{u_1} - u_1 \cdot \overline{y_{1,2}} \cdot \overline{u_2} - \ldots - u_1 \cdot \overline{y_{1,n}} \cdot \overline{u_n} = S_1 \\ -u_2 \cdot \overline{y_{1,2}} \cdot \overline{u_1} + u_2 \cdot \overline{y_{2,2}} \cdot \overline{u_2} - \ldots - u_2 \cdot \overline{y_{2,n}} \cdot \overline{u_n} = S_2 \\ \vdots \\ -u_n \cdot \overline{y_{1,n}} \cdot \overline{u_1} - u_n \cdot \overline{y_{2,n}} \cdot \overline{u_2} - \ldots + u_n \cdot \overline{y_{n,n}} \cdot \overline{u_n} = S_n \end{cases} \tag{A.5}$$

as $u_j \neq 0\ \forall j \in \{1, 2, .., n\}$ then (A.5) is equivalent to:

$$\begin{cases} +y_{1,1} \cdot u_1 - y_{1,2} \cdot u_2 - \ldots - y_{1,n} \cdot u_n = \overline{\left[\frac{S_1}{u_1}\right]} \\ -y_{1,2} \cdot u_1 + y_{2,2} \cdot u_2 - \ldots - y_{2,n} \cdot u_n = \overline{\left[\frac{S_2}{u_2}\right]} \\ \vdots \\ -y_{1,n} \cdot u_1 - y_{2,n} \cdot u_2 - \ldots + y_{n,n} \cdot u_n = \overline{\left[\frac{S_n}{u_n}\right]} \end{cases} \tag{A.6}$$

In matrix form, and calling:

$$i = \begin{bmatrix} i_1 \\ i_2 \\ \vdots \\ i_n \end{bmatrix},\ u = \begin{bmatrix} u_1 \\ u_2 \\ \vdots \\ u_n \end{bmatrix},\ P = \begin{bmatrix} P_1 \\ P_2 \\ \vdots \\ P_n \end{bmatrix},\ Q = \begin{bmatrix} Q_1 \\ Q_2 \\ \vdots \\ Q_n \end{bmatrix},\ S = \begin{bmatrix} S_1 \\ S_2 \\ \vdots \\ S_n \end{bmatrix} \tag{A.7}$$

$$Y = \begin{bmatrix} y_{1,1} & -y_{1,2} & \ldots & -y_{1,n} \\ -y_{1,2} & y_{2,2} & \ldots & -y_{2,n} \\ \vdots & \vdots & \ddots & \vdots \\ -y_{1,n} & -y_{2,n} & \ldots & y_{n,n} \end{bmatrix} = G + \mathtt{i} \cdot B =$$

$$= \begin{bmatrix} G_{1,1} + \mathtt{i} \cdot B_{1,1} & -G_{1,2} - \mathtt{i} \cdot B_{1,2} & \ldots & -G_{1,n} - \mathtt{i} \cdot B_{1,n} \\ -G_{1,2} - \mathtt{i} \cdot B_{1,2} & G_{2,2} + \mathtt{i} \cdot B_{2,2} & \ldots & -G_{2,n} - \mathtt{i} \cdot B_{2,n} \\ \vdots & \vdots & \ddots & \vdots \\ -G_{1,n} - \mathtt{i} \cdot B_{1,n} & -G_{2,n} - \mathtt{i} \cdot B_{2,n} & \ldots & G_{n,n} + \mathtt{i} \cdot B_{n,n} \end{bmatrix} \tag{A.8}$$

where $G$ and $B$ are respectively the conductance and susceptance matrices which are real and symmetric.

$$G = \begin{bmatrix} G_{1,1} & -G_{1,2} & \ldots & -G_{1,n} \\ -G_{1,2} & G_{2,2} & \ldots & -G_{2,n} \\ \vdots & \vdots & \ddots & \vdots \\ -G_{1,n} & -G_{2,n} & \ldots & G_{n,n} \end{bmatrix}, \quad B = \begin{bmatrix} B_{1,1} & -B_{1,2} & \ldots & -B_{1,n} \\ -B_{1,2} & B_{2,2} & \ldots & -B_{2,n} \\ \vdots & \vdots & \ddots & \vdots \\ -B_{1,n} & -B_{2,n} & \ldots & B_{n,n} \end{bmatrix} \tag{A.9}$$

and defining $A_j = H_j + Y_j^*$, where:

$$A_j = \begin{bmatrix} 0 & \dots & 0 & 0 & 0 & \dots & 0 \\ \vdots & \ddots & \vdots & \vdots & \vdots & \vdots & \vdots \\ 0 & \dots & 0 & 0 & 0 & \dots & 0 \\ -\overline{y_{1,j}} & \dots & -\overline{y_{j-1,j}} & \overline{y_{j,j}} & -\overline{y_{j,j+1}} & \dots & -\overline{y_{j,n}} \\ 0 & \dots & 0 & 0 & 0 & \dots & 0 \\ \vdots & \vdots & \vdots & \vdots & \vdots & \ddots & \vdots \\ 0 & \dots & 0 & 0 & 0 & \dots & 0 \end{bmatrix} \tag{A.10}$$

$$H_j = \begin{bmatrix} 0 & \dots & 0 & -\frac{y_{1,j}}{2} & 0 & \dots & 0 \\ \vdots & \ddots & \vdots & \vdots & \vdots & \vdots & \vdots \\ 0 & \dots & 0 & -\frac{y_{j-1,j}}{2} & 0 & \dots & 0 \\ -\frac{\overline{y_{1,j}}}{2} & \dots & -\frac{\overline{y_{j-1,j}}}{2} & G_{j,j} & -\frac{\overline{y_{j,j+1}}}{2} & \dots & -\frac{\overline{y_{j,n}}}{2} \\ 0 & \dots & 0 & -\frac{y_{j+1,j}}{2} & 0 & \dots & 0 \\ \vdots & \vdots & \vdots & \vdots & \vdots & \ddots & \vdots \\ 0 & \dots & 0 & -\frac{y_{n,j}}{2} & 0 & \dots & 0 \end{bmatrix} \tag{A.11}$$

$$Y_j^* = \begin{bmatrix} 0 & \dots & 0 & \frac{y_{1,j}}{2} & 0 & \dots & 0 \\ \vdots & \ddots & \vdots & \vdots & \vdots & \vdots & \vdots \\ 0 & \dots & 0 & \frac{y_{j-1,j}}{2} & 0 & \dots & 0 \\ -\frac{\overline{y_{1,j}}}{2} & \dots & -\frac{\overline{y_{j-1,j}}}{2} & -\mathtt{i} \cdot B_{j,j} & -\frac{\overline{y_{j,j+1}}}{2} & \dots & -\frac{\overline{y_{j,n}}}{2} \\ 0 & \dots & 0 & \frac{y_{j+1,j}}{2} & 0 & \dots & 0 \\ \vdots & \vdots & \vdots & \vdots & \vdots & \ddots & \vdots \\ 0 & \dots & 0 & \frac{y_{n,j}}{2} & 0 & \dots & 0 \end{bmatrix} \tag{A.12}$$

From (A.2) to (A.12) we can write in matrix form:

$$Y \cdot u = i \tag{A.13}$$

$$\forall j \in \{1, 2, .., n\} \quad \begin{cases} u^T \cdot A_j \cdot \bar{u} = S_j \\ u^T \cdot H_j \cdot \bar{u} = P_j \\ u^T \cdot Y_j^* \cdot \bar{u} = \mathtt{i} \cdot Q_j \end{cases} \tag{A.14}$$

$$\begin{cases} u^T \cdot \bar{Y} \cdot \bar{u} = \sum_{j=1}^{n} S_j \\ u^T \cdot G \cdot \bar{u} = \sum_{j=1}^{n} P_j \\ u^T \cdot (-B) \cdot \bar{u} = \sum_{j=1}^{n} Q_j \end{cases} \tag{A.15}$$

### A.1.1 Basic properties.

Next some basic properties are explained and detailed.

***Basic property* 8** *If we know the voltages on all nodes, we can find all currents and powers.*

***Basic property* 9** *Since $i_1 + i_2 + \ldots + i_n = 0$, then if we know the input currents in $n-1$ nodes, it is possible to establish the input current in the remaining node.*

***Basic property* 10** *$P_1 + P_2 + \ldots + P_n \geq 0$, so $P_1 + P_2 + \ldots + P_n$ is the dissipated power in the network.*

*If $u_1 = u_2 = \ldots = u_n$, then $i_1 = \ldots = i_n = 0$ and $P_1 + P_2 + \ldots + P_n = 0$.*

*If $\exists\ j, k \in \{1, 2, \ldots, n\}$ such that $u_j \neq u_k$ then $P_1 + P_2 + .. + P_n > 0$.*

***Basic property* 11** *The matrix $\boldsymbol{G}$ is positive semi-definite of rank $n-1$.*

*$\forall j \in \{1, 2, \ldots, n\}$ the matrix of order $n-1$ that results to remove row $j$ and column $j$ of $\boldsymbol{G}$ is positive definite.*

*$\forall k \in \{1, 2, \ldots, n-1\}$ matrix $\boldsymbol{G}_k$, formed by the elements of the first $k$ rows and first $k$ columns of $\boldsymbol{G}$, and matrix $\mathcal{G}_{\mathbf{n-k}}$ formed by the elements of the last $n-k$ rows and last $n-k$ columns of $\boldsymbol{G}$, are positive definite, and as $\boldsymbol{B}$ is symmetric, then matrix $\boldsymbol{Y}_k$ formed by the elements of the first $k$ rows and first $k$ columns of $\boldsymbol{Y}$, and matrix $\Lambda_{n-k}$ formed by the elements of the last $n-k$ rows and last $n-k$ columns of $\boldsymbol{Y}$, are invertible.*

*Matrix $-\Gamma_k$, formed by the elements of the first $k$ rows and last $n-k$ columns of $\boldsymbol{Y}$, are not null.*

$$\boldsymbol{Y}_k = \begin{bmatrix} y_{1,1} & -y_{1,2} & \cdots & -y_{1,k} \\ -y_{1,2} & y_{2,2} & \cdots & -y_{2,k} \\ \vdots & \vdots & \ddots & \vdots \\ -y_{1,k} & -y_{2,k} & \cdots & y_{k,k} \end{bmatrix} \in \mathbb{C}^{k \times k} \tag{A.16}$$

$$\Lambda_{n-k} = \begin{bmatrix} y_{k+1,k+1} & \cdots & -y_{k+1,n} \\ -y_{k+1,k+2} & \cdots & -y_{k+2,n} \\ \vdots & \ddots & \vdots \\ -y_{k+1,n} & \cdots & y_{n,n} \end{bmatrix} \in \mathbb{C}^{(n-k) \times (n-k)} \tag{A.17}$$

$$\Gamma_k = \begin{bmatrix} -y_{1,k+1} & -y_{1,k+2} & \cdots & -y_{1,n} \\ -y_{2,k+1} & -y_{2,k+2} & \cdots & -y_{2,n} \\ \vdots & \vdots & \ldots & \vdots \\ -y_{k,k+1} & -y_{k,k+2} & \cdots & -y_{k,n} \end{bmatrix} \in \mathbb{C}^{k \times (n-k)} \tag{A.18}$$

$$\boldsymbol{G}_k = \begin{bmatrix} G_{1,1} & -G_{1,2} & \dots & -G_{1,k} \\ -G_{1,2} & G_{2,2} & \dots & -G_{2,k} \\ \vdots & \vdots & \dots & \vdots \\ -G_{1,k} & -G_{2,k} & \dots & G_{k,k} \end{bmatrix} \in \mathbb{R}^{k\times k} \tag{A.19}$$

$$\mathcal{G}_{\mathbf{n-k}} = \begin{bmatrix} G_{k+1,k+1} & -G_{k+,k+2} & \dots & -G_{k+1,n} \\ -G_{k+1,k+2} & G_{k+2,k+2} & \dots & -G_{k+2,n} \\ \vdots & \vdots & \dots & \vdots \\ -G_{k+1,n} & -G_{k+2,n} & \dots & G_{n,n} \end{bmatrix} \in \mathbb{R}^{(\mathbf{n-k})\times(\mathbf{n-k})} \tag{A.20}$$

***Basic property* 12** *$\forall j \in \{1, 2, \dots, n\}$ matrix $\boldsymbol{H}_j$ is hermitian and indefinite of rank 2. That means, $\boldsymbol{H}_j$ has a positive eigenvalue, other negative, and the remaining $n-2$ are null.*

***Basic property* 13** *If we know the input currents in k nodes, with $0 < k < n$, and the voltages in the other $n-k$ nodes, the voltages in all nodes are uniquely determined, and hence also the currents and powers. For known $i_1, \dots, i_k, u_{k+1}, \dots, u_n$, the values of $u_1, \dots, u_k$ are solutions of the linear system (A.21) whose coefficient matrix $\boldsymbol{Y}_k$ is invertible.*

$$\begin{cases} y_{1,1}u_1 - y_{1,2}u_2 - .. - y_{1,k}u_k = i_1 + y_{1,k+1}u_{k+1} + .. + y_{1,n}u_n \\ -y_{1,2}u_1 + y_{2,2}u_2 - .. - y_{2,k}u_k = i_2 + y_{2,k+1}u_{k+1} + .. + y_{2,n}u_n \\ \vdots \\ -y_{1,k}u_1 - y_{2,k}u_2 - .. + y_{k,k}u_k = i_k + y_{k,k+1}u_{k+1} + .. + y_{k,n}u_n \end{cases} \tag{A.21}$$

***Basic property* 14** *If we know the input power in k nodes, $0 < k < n$, and the voltages in the other $n-k$ nodes, for sufficiently high voltage values, we can find the remaining voltages, and therefore also the currents and powers in all nodes. In addition, if the known voltage values $u_{k+1}, ..., u_n$ are close to value $u_N$, such that $|u_N|$ is the nominal value of the network, and this is sufficiently high, the unknown voltage values $u_1, \dots, u_k$ are also close to $u_N$, and they will be unique.*

In effect, if we know $S_1, \dots, S_k, u_{k+1}, \dots, u_n$, the values of $u_1, \dots, u_k$ are the solution of the following system:

$$\begin{cases} y_{1,1}u_1 - y_{1,2}u_2 - .. - y_{1,k}u_k = \overline{[\frac{S_1}{u_1}]} + y_{1,k+1}u_{k+1} + .. + y_{1,n}u_n \\ -y_{1,2}u_1 + y_{2,2}u_2 - .. - y_{2,k}u_k = \overline{[\frac{S_2}{u_2}]} + y_{2,k+1}u_{k+1} + .. + y_{2,n}u_n \\ \vdots \\ -y_{1,k}u_1 - y_{2,k}u_2 - .. + y_{k,k}u_k = \overline{[\frac{S_k}{u_k}]} + y_{k,k+1}u_{k+1} + .. + y_{k,n}u_n \end{cases} \tag{A.22}$$

and applying the following **Property 5** the results in this basic property 14 are obtained.

## A.2 Main property.

In this section the main results of this section are formulated and proved.

***Property* 5**

- *Let* $k \in \mathbb{N}$ *be such that* $0 < k < n$.
- *Let* $\boldsymbol{Y} \in \mathbb{C}^{n\times n}$ *be the admittance matrix defined in (A.8) such that:*

$$\boldsymbol{Y} = \begin{bmatrix} \boldsymbol{Y}_k & -\Gamma_k \\ -\Gamma_k^t & \Lambda_{n-k} \end{bmatrix} \tag{A.23}$$

  *where* $\boldsymbol{Y}_k$, $\Lambda_{n-k}$ *and* $\Gamma_k$ *are defined in (A.16), (A.17) and (A.18) respectively.*

- *Let* $S_1 \ldots, S_k$ *be the input apparent power in the first k nodes, and let* $S = max\{|S_j| : 1 \leq j \leq k\}$.
- *Let* $c, \rho, \epsilon, \delta \in \mathbb{R}$ *be such that:* $0< c <1$, $0< \rho <1$, $0< \epsilon$ *and* $0 < \delta \leq \frac{\rho\cdot\epsilon}{\|\boldsymbol{Y}_k^{-1}\cdot\Gamma_k\|_\infty}$.
- *Let* $U_0 \in \mathbb{R}$ *and* $u_N \in \mathbb{C}$ *be such that:* $U_0 \geq max\left\{\frac{S\cdot\|\boldsymbol{Y}_k^{-1}\|_\infty}{(1-\rho)\cdot\epsilon}, \sqrt{\frac{S\cdot\|\boldsymbol{Y}_k^{-1}\|_\infty}{c}}\right\}$, *with* $U_0 > 0$ *and* $|u_N| \geq U_0 + \epsilon > U_0$.
- $D=\left\{(u_1, \ldots, u_k)^T \in \mathbb{C}^k : |u_1| \geq U_0, \ldots, |u_k| \geq U_0\right\}$
- *Let* $\Psi : D \to \mathbb{C}^k$ *be the function defined by:* $\Psi\left((u_1, .., u_k)^T\right) = (\overline{[\frac{S_1}{u_1}]}, .., \overline{[\frac{S_k}{u_k}]})^T$
- *Let* $V_N$, $W_N$ *be such that:*

$$V_N = (u_N, ..., u_N)^T \in \mathbb{C}^k \tag{A.24}$$

$$W_N = (u_N, ..., u_N)^T \in \mathbb{C}^{n-k} \tag{A.25}$$

*With these conditions is true that for any* $W = (w_{k+1}, .., w_n)^T \in \bar{B}_\infty(W_N, \delta)$[1] *there exists a unique* $V = (v_1, .., v_k)^T \in D$ *such that:*

***1.-***

$$\begin{cases} y_{1,1}v_1 - y_{1,2}v_2 - .. - y_{1,k}v_k = \overline{[\frac{S_1}{u_1}]} + y_{1,k+1}w_{k+1} + .. + y_{1,n}w_n \\ -y_{1,2}v_1 + y_{2,2}v_2 - .. - y_{2,k}v_k = \overline{[\frac{S_2}{u_2}]} + y_{2,k+1}w_{k+1} + .. + y_{2,n}w_n \\ \vdots \\ -y_{1,k}v_1 - y_{2,k}v_2 - .. + y_{k,k}v_k = \overline{[\frac{S_k}{u_k}]} + y_{k,k+1}w_{k+1} + .. + y_{k,n}w_n \end{cases} \tag{A.26}$$

[1] See annex B.

***2.-*** $V \in \bar{B}_\infty(V_N, \epsilon)$
***3.-*** *If* $(s_j)_{j\in\mathbb{N}}$ *is a sequence defined by:*
$s_0 \in D$ *and* $\forall j \in \mathbb{N} \quad s_{j+1} = Y_k^{-1} \cdot \Psi(s_j) + Y_k^{-1} \cdot \Gamma_k \cdot W$, *it holds that:*
***3.1.-*** $V = \lim_{j\to\infty} s_j$
***3.2.-*** $\|s_j - V\|_\infty \leq \|s_2 - s_1\|_\infty \cdot \frac{c^{j-1}}{1-c} \leq 2 \cdot \epsilon \cdot \frac{c^{j-1}}{1-c}$, $\forall j \in \mathbb{N}^*$

***Proof.-***
**1.-** If the term $v = (u_1, \ldots, u_k)^T \in D$, and $g$ is the mapping such that $g : D \to D$, $g(v) = \mathbf{Y}_k^{-1} \cdot \Psi(v) + \mathbf{Y}_k^{-1} \cdot \Gamma_k \cdot W \quad \forall v \in D$, then when the voltages $u_{k+1} = w_{k+1}, \ldots, u_n = w_n$ are known, the system shown in (A.22) is equivalent to:

$$\mathbf{Y}_k \cdot v = \Psi(v) + \Gamma_k \cdot W \tag{A.27}$$

which is equivalent to

$$v = \mathbf{Y}_k^{-1} \cdot \Psi(v) + \mathbf{Y}_k^{-1} \cdot \Gamma_k \cdot W \tag{A.28}$$

and this is equivalent to

$$v = g(v) \tag{A.29}$$

so $v$ is a solution of (A.27) if and only if it is a fixed point of the mapping $g$.

Let us check that $g$ is a contractive application in D. First we verify that $\forall v \in D$, $g(v) \in D$, because

$$g(v) = \mathbf{Y}_k^{-1} \cdot \Psi(v) + \mathbf{Y}_k^{-1} \cdot \Gamma_k \cdot W \tag{A.30}$$

from (A.2) and (A.3) is easy to show that it fulfills:

$$\mathbf{Y}_k \cdot V_N = \Gamma_k \cdot W_N \tag{A.31}$$

and consequently:

$$V_N = \mathbf{Y}_k^{-1} \cdot \Gamma_k \cdot W_N \tag{A.32}$$

from (A.30) and (A.32) we obtain:

$$g(v) - V_N = \mathbf{Y}_k^{-1} \cdot \Psi(v) + \mathbf{Y}_k^{-1} \cdot \Gamma_k \cdot (W - W_N) \tag{A.33}$$

and consequently:

$$\|g(v) - V_N\|_\infty \leq \left\|\mathbf{Y}_k^{-1}\right\|_\infty \cdot \|\Psi(v)\|_\infty + \left\|\mathbf{Y}_k^{-1} \cdot \Gamma_k\right\|_\infty \cdot \|W - W_N\|_\infty \tag{A.34}$$

from (A.34), and taking into account that:

$$\|\Psi(v)\|_\infty = max\left\{\left|\frac{S_j}{u_j}\right| : 1 \leq j \leq k\right\} \leq \frac{S}{U_0} \leq \frac{(1-\rho)\cdot\epsilon}{\left\|\mathbf{Y}_k^{-1}\right\|_\infty} \tag{A.35}$$

and also that:

$$\|W - W_N\|_\infty \leq \delta \leq \frac{\rho \cdot \epsilon}{\left\|\mathbf{Y}_k^{-1} \cdot \Gamma_k\right\|_\infty} \tag{A.36}$$

we may deduce that

$$\|g(v) - V_N\|_\infty \leq (1-\rho) \cdot \epsilon + \rho \cdot \epsilon = \epsilon \tag{A.37}$$

which is equivalent to:

$$g(v) \in \bar{B}_\infty(V_N, \epsilon) \tag{A.38}$$

and taking into account that:

$$\bar{B}_\infty(V_N, \epsilon) \subset D \tag{A.39}$$

it is true that:

$$g(v) \in D \tag{A.40}$$

Secondly, $\forall x, y \in D$ it is clear that $\|g(x) - g(y)\|_\infty \leq c \cdot \|x - y\|_\infty$, due to:

$$g(x) = \mathbf{Y}_k^{-1} \cdot \Psi(x) + \mathbf{Y}_k^{-1} \cdot \Gamma_k \cdot W \tag{A.41}$$
$$g(y) = \mathbf{Y}_k^{-1} \cdot \Psi(y) + \mathbf{Y}_k^{-1} \cdot \Gamma_k \cdot W \tag{A.42}$$

and therefore:

$$\|g(x) - g(y)\|_\infty = \left\|\mathbf{Y}_k^{-1}\left(\Psi(x) - \Psi(y)\right)\right\|_\infty \leq \left\|\mathbf{Y}_k^{-1}\right\|_\infty \|\Psi(x) - \Psi(y)\|_\infty \tag{A.43}$$

besides

$$\Psi(x) - \Psi(y) = \begin{bmatrix} \frac{\overline{S}_1 \cdot (\overline{y_1} - \overline{x_1})}{\overline{x_1} \cdot \overline{y_1}} \\ \vdots \\ \frac{\overline{S}_k \cdot (\overline{y_k} - \overline{x_k})}{\overline{x_k} \cdot \overline{y_k}} \end{bmatrix} \Rightarrow \|\Psi(x) - \Psi(y)\|_\infty \leq \frac{S}{U_0^2} \cdot \|x - y\|_\infty \tag{A.44}$$

therefore $\forall x, y \in D$:

$\|g(x) - g(y)\|_\infty \leq \left\|\mathbf{Y}_k^{-1}\right\|_\infty \cdot \frac{S}{U_0^2} \cdot \|x - y\|_\infty \leq c \cdot \|x - y\|_\infty$ and as $0 < c < 1$ it holds that $g$ is a contractive mapping in $D$.

As $D$ is a closed set, the contraction mapping theorem ensures that there exists a single point $V = (v_1, ..., v_k)^T \in D$ such that $g(V) = V$, that means, $V$ is a fixed point of $g$, and by the above explanation this is the unique solution vector from equation (A.27) and system (A.22).

**2.-**

Due to $V = g(V) \in D$ and $g(V) \in \bar{B}_\infty(V_N, \epsilon)$ according to (A.38), then result 2 of **property 5** is satisfied .

**3.-**

The contraction mapping theorem also ensures that if $(s_j)_{j\in\mathbb{N}}$ is a sequence defined by: $s_0 \in D$ and $\forall j \in \mathbb{N}$, $s_{j+1} = g(s_j)$, the only fixed point V holds:

a) V=$\lim_{j\to 0} s_j$

b) $\|s_j - V\|_\infty \leq \|s_2 - s_1\|_\infty \cdot \frac{c^{j-1}}{1-c} \leq \|s_1 - s_0\|_\infty \cdot \frac{c^j}{1-c} \quad \forall j \in \mathbb{N}^*$

As $s_1 = g(s_0) \in \bar{B}_\infty(V_N, \epsilon)$ and $s_2 = g(s_1) \in \bar{B}_\infty(V_N, \epsilon)$, we verify that:

$$\|s_2 - s_1\|_\infty \leq 2 \cdot \epsilon \tag{A.45}$$

so it is true that:

$$\|s_j - V\|_\infty \leq \|s_2 - s_1\|_\infty \frac{c^{j-1}}{1-c} \leq 2 \cdot \epsilon \cdot \frac{c^{j-1}}{1-c} \quad \forall j \in \mathbb{N}^* \tag{A.46}$$

□

**Note:** If the maximum voltage variation, with respect to nominal voltage $u_N$, of the known voltages $w_{k+1}, .., w_n$ is lesser or equal than $\delta$, then the maximum voltage variation with respect to $u_N$ of the initially unknown variables $v_1, .., v_k$ is lesser or equal than $\epsilon$.

**Algorithm:**

With the definitions indicated in the statement of property 1, if the admittance matrix $\mathbf{Y}$, the nominal voltage of the grid, the powers $S_1, ..., S_k$, and the voltages $\omega_{k+1}, ..., \omega_n$ are known, we proceed as follows:

1.- We obtain $\mathbf{Y}_k$ and $\Gamma_k$.

2.- We calculate S.

3.- We consider $c$, $\rho$, $\epsilon$ and $\delta$ taking into account that $c$ and $\rho$ are auxiliary constants, while $\epsilon$ and $\delta$ are arbitrary bounds previously set for the voltage variations with respect to the nominal value.

4.- We determine $U_0$, and we chose $u_N$ such that $|u_N|$ is the nominal voltage of the grid.

5.- We verify that $|u_N| \geq U_0 + \epsilon$ and $|\omega_{k+1} - u_N| \leq \delta, ..., |\omega_n - u_N| \leq \delta$. If it is not, come back to step 3.

6.- We consider the sequence $(s_j)_{j\in\mathbb{N}}$ such that:

6.1.- The modules of the $k$ components of $s_0$ are higher or equal than $U_0$, (we can choose $s_0 = (u_N, ..., u_N)^T \in \mathbb{C}^k$).

6.2.- $\forall\ j \in \mathbb{N} \quad s_{j+1} = Y_k^{-1} \cdot \Psi(s_j) + Y_k^{-1} \cdot \Gamma_k \cdot W$.

7.- We calculate V= $\lim_{j\to\infty} s_j$, which components are the voltages $v_1, ..., v_k$.

8.- As we know all voltages $v_1, ..., v_k, \omega_{k+1}, ..., \omega_n$ we can determine all currents and all powers.

Appendix B

# Annex B

In concordance with [109].

- If $x = (x_1, x_2, \ldots, x_n) \in \mathbb{R}^n$

  $\|x\|_1 = |x_1| + |x_2| + \ldots + |x_n|$

  $\|x\|_2 = \sqrt{x_1^2 + x_2^2 + \ldots + x_n^2}$

  $\|x\|_\infty = max\{|x_1|, |x_2|, \ldots, |x_n|\}$

  $\|x\|_\infty \leq \|x\|_2 \leq \|x\|_1$

- If $a \in \mathbb{R}^n$ and $0 < r \in \mathbb{R}$ (with p=1,2 or $\infty$)

  $B_p(a, r) = \left\{x \in \mathbb{R}^n : \|x - a\|_p < r\right\}$

  $\bar{B}_p(a, r) = \left\{x \in \mathbb{R}^n : \|x - a\|_p \leq r\right\}$

  $B_1(a, r) \subset B_2(a, r) \subset B_\infty(a, r)$

  $\bar{B}_1(a, r) \subset \bar{B}_2(a, r) \subset \bar{B}_\infty(a, r)$

- If $A \in \mathbb{R}^{m,n}$ (with p=1,2 or $\infty$)

  $\|A\|_p = max_{x \neq 0} \frac{\|Ax\|_p}{\|x\|_p} = max_{\|x\|_p = 1} \|Ax\|_p$

  $\|A \cdot B\|_p \leq \|A\|_p \cdot \|B\|_p$ where $B \in \mathbb{R}^{n,l}$

  $\|A\|_1 = max\left\{\|A_1\|_1, \|A_2\|_1, \ldots, \|A_n\|_1\right\}$ (the maximum value of the one norm applied to the columns of A).

  $\|A\|_\infty = max\left\{\left\|A^1\right\|_1, \left\|A^2\right\|_1, \ldots, \|A^n\|_1\right\}$ (the maximum value of the one norm applied to the rows of A).

- $\Psi((v_1, v_2, \ldots, v_k)^T) = \left(\frac{P_1}{v_1}, \frac{P_2}{v_2}, \ldots, \frac{P_k}{v_k}\right)^T = (i_1, i_2, \ldots, i_k)^T$

# Bibliography


[1] J. Arrillaga, Y.H. Liu, and N.R. Watson. *Flexible Power Transmission. The HVDC Options.* John Wiley & Sons Ltd, 2007.

[2] G. Asplund. *Ultra high voltage transmission.* ABB review, February 2007.

[3] J. Kreuse. *The future is now.* ABB review, March 2008.

[4] D. Ravemark and B. Normark. *Light and invisible.* ABB review, March 2005.

[5] G. Beck, D. Povh, D. Retzmann, and E. Teltsch. *Global blackouts. lessons learned.* Siemens review, July 2011.

[6] O.A. Mousavi, L. Bizumic, and R. Cherkaoui. *Assessment of HVDC grid segmentation for reducing the risk of cascading outages and blackouts.* Bulk Power System Dynamics and Control - IX Optimization, Security and Control of the Emerging Power Grid (IREP), 2013 IREP Symposium.

[7] M. P. Bahrman. *HVDC transmission overview.* IEEE/PES Transmission and Distribution Conference and Exposition, April 2008.

[8] D. Jovcic, D. Van Hertem, K. Linden, J.-P. Taisne, and W. Grieshaber. *Feasibility of DC transmission networks.* Innovative Smart Grid Technologies (ISGT Europe), 2011 2nd IEEE PES International Conference and Exhibition on, Dec 2011.

[9] M. Jiménez Carrizosa, J. Cortés, A. Benchaib, P. Alou, G. Damm, J. A. Cobos, and F. Lamnabhi-Lagarrigue. V*DC/DC converters as DC circuit-breakers in HVDC networks operation.* Power Electronics and Applications (EPE), 2014 16th European Conference on, pages 1–10, August 2014.

[10] D. Jovcic and B. T. Ooi. *Tapping on hvdc lines using dc transformers.* Electric Power Systems Research, pages 561-569, 2011.

[11] V. Collet Billon, J.P. Taisne, V. Arcidiacono, and F. Mazzoldi. *The Corsican tapping: from design to commissioning tests of the third terminal of the Sardinia-Corsica-Italy HVDC link.* IEEE Transactions on Power Delivery, January 1989.

[12] J.A Donahuea, D.A. Fisher, B.D. Raling, and P.J. Tatro. *Performance testing of the Sandy Pond HVDC converter.* IEEE Transactions on Power Delivery, Volume 8, No. 1, pp: 422 - 428., Jan. 1993.

[13] W.F. Long, J. Reeve, J.R. McNichol, M.S. Holland, J.P. Taisne, J. LeMay, and D.J. Lorden. *Application aspects of multiterminal DC power transmission.* IEEE Transactions on Power Delivery, Volume 5, No. 4, pp: 2084 - 2098., Jan. 1993.

[14] T.M. Haileselassie, K. Uhlen, and T.Undenland. *Control and operation of MT-HVDC for market integrated offshore wind farms.* NTNU, 2010.

[15] P. Kundur. *Power systems stability and control.* Mc Graw Hill, first edition, 1993.

[16] S.G. Johansson, G. Asplund, E.Jansson, and R. Rudervall. *Power system stability. benefits with VSC-HVDC transmission systems.* CIGRE, 2007.

[17] Yijing Chen, Jing Dai, G. Damm, and F. Lamnabhi-Lagarrigue. *Nonlinear control design for a multi-terminal VSC-HVDC system.* European Control Conference (ECC), 2013, pages 3536–3541, July 2013.

[18] A. Lesnicar and R. Marquardt. *An innovative modular multilevel converter topology suitable for a wide power range.* Power Tech Conference Proceedings, 2003 IEEE Bologna, volume 3, pages 6 pp. Vol.3–, June 2003.

[19] U.N. Gnanarathna, A.M. Gole, and R.P. Jayasinghe. *Efficient modelling of modular multilevel HVDC converters (MMC) on electromagnetic transient simulation programs.* Power Delivery, IEEE Transactions on, pages 316–324, Jan 2011.

[20] G. Bergna, A. Garces, E. Berne, P. Egrot, A. Arzande, J.-C. Vannier, and M. Molinas. *A generalized power control approach in abc frame for modular multilevel converter HVDC links based on mathematical optimization.* Power Delivery, IEEE Transactions on, pages 386–394, Feb 2014.

[21] G.Ortiz, J. Biela, and JW Kolar. *Optimized design of medium frequency transformers with high isolation requirements.* $36^{th}$ Conference on IEEE Industrial Electronics Society, November 2010.

[22] H.Fan and H. Li. *igh frequency high efficiency bidirectional DC-Dc converter module design for 10 kVA solid state transformer.* Applied Power Electronics Conference and Exposition (APEC), 2010 Twenty-Fifth Annual IEEE, pages 210–215, February 2010.

[23] T. Lüth, M.M.C. Merlin, T.C. Green, C.D. Barker, F. Hassan, R.W. Critchley, R.W. Crookes, and K. Dyke. *Performance of a DC/AC/DC*

*VSC system to interconnect HVDC systems.* AC and DC Power Transmission (ACDC 2012), 10th IET International Conference on, pages 1–6, Dec 2012.

[24] R. Hassan, S. Shah, and J. Sun. *Review of control methods for HVDC transmission systems.* 2013.

[25] A. Benchaib. *Control and operation of power network: System of systems approach based on spatio-temporal scales.* Memory for authorization to conduct the research. STITS, December 2014.

[26] C.D. Barker and R. Whitehouse. *Autonomous converter control in a multi-terminal HVDC system.* $9^{th}$ International Conference on AC and DC Power Transmission, pages 1–5, Oct 2010.

[27] J. Beerten, D. Van Hertem, and R. Belmans. *VSC MTDC systems with a distributed DC voltage control - a power flow approach.* PowerTech, 2011 IEEE Trondheim, pages 1–6, June 2011.

[28] W. Wang and M. Barnes. *Power flow algorithms for multi-terminal VSC-HVDC with droop control.* Power Systems, IEEE Transactions on, pages 1721–1730, July 2014.

[29] J. Beerten, S. Cole, and R. Belmans. *Generalized steady-state VSC MTDC model for sequential AC/DC power flow algorithms.* Power and Energy Society General Meeting (PES), 2013 IEEE, pages 1–1, July 2013.

[30] U. Kiliç, K. Ayan, and U. Arifoğlu. *Optimizing reactive power flow of HVDC systems using genetic algorithm.* International Journal of Electrical Power & Energy Systems, pages:1–12, February 2014.

[31] D.G. Luenberger. *Optimization by vector space methods.* John Wiley & Sons, 1969.

[32] M. Jiménez Carrizosa, F. Dorado Navas, G.Damm, and F. Lamnabhi-Lagarrigue. *Optimal power flow in multi-terminal HVDC grids with offshore wind farms and storage devices.* International Journal of Electrical Power & Energy Systems, pages 291 – 298, February 2015.

[33] M. Aragüés-Penalba, A. Egea-Àlvarez, O. Gomis-Bellmunt, and A. Samper. *Optimum voltage control for loss minimization in HVDC multi-terminal transmission systems for large offshore wind farms.* Electric Power Systems Research, pages 54–63, March 2012.

[34] A. Chakraborty, S. K. Musunuri, A. K. Srivastava, and A. K. Kondabathini. *Integrating STATCOM and battery energy storage system for power system transient stability: A review and application.* Advances in Power Electronics. 2012.

[35] A.J. del Real, A. Arce, and C.Bordons. *Combined environmental and economic dispatch of smart grids using distributed model predictive control.* Electrical Power and Energy Systems, pages 65–76, 2014.

[36] `http://www.omie.es/inicio/informacion-de-agentesl`. OMIE. Operador del mercado ibérico de la energía.

[37] M. Jiménez Carrizosa, A. Benchaib, P. Alou, and G. Damm. *DC transformer for DC/DC connection in HVDC network.* 15th European Conference on Power Electronics and Applications, September 2013.

[38] H. Khalil. *Nonlinear systems.* Prentice Hall, 2002.

[39] J. Aracil and F. Gómez-Estern. *Notes of automatic regulation.* Dep. Ingeniería Electrónica, E.T.S.I.I. Universidad Politécnica Madrid. 2000.

[40] A. Castro Figueroa. *Some applications of Lyapunov functions for stability problems and existence of invariant manifolds.* Departamento de Matemáticas, Facultad de Ciencias, Universidad de los Andes, Mérida, Venezuela.

[41] R.R. Mohler. *Bilinear Control Processes.* Academic Press, 1973.

[42] R.R. Mohler. *Nonlinear systems. Applications to Bilinear Control.* Printence Hall, 1991.

[43] I.D. Landau. *On the optimal regulator problem and stabilization of bilinear systems.* Laboratoire d'Automatique (CNRS), 1979.

[44] D.L. Elliot. *Bilinear Control Systems.* Springer, 2009.

[45] A. Isidori. Nonlinear control systems. Springer Verlag, 1995.

[46] D. Liberzon. *Switching in systems and control.* Birkhauser, 2003.

[47] G. Ortiz, J. Biela, D. Bortis, and JW Kolar. *1 MW, 20 kHz, isolated, 1.2-12 kV bidirectional DC-DC renewable converter for energy applications.* IEEE International Power Electronics Conference, 2010.

[48] D. Aggeler, J. Biela, and J.W. Kolar. *Solid-state transformer based on SiC JFET for future energy distribution systems.* ETH Zurich, Power Electronic Systems Laboratory., 2009.

[49] J. Biela, D. Aggeler, D. Bortis, and J. W. Kolar. *5kV/200ns pulsed power switch based on a SiC-JFET super cascode.* IEEE Power Modulators and High Voltage Conference, pages 358–361, May 2008.

[50] P. Friedrichs, H. Mitlehner, R. Schorner, K. Donhke, R. Elpelt, and D. Stephani. *Stacked high voltage switch based on SiC JFETs.* ISPSD Cambridge, April 2003.

[51] R. Singhi. *Ultra high voltage sic bipolar devices for reduced power electronics complexity.* GeneSiC Semiconductor Inc, February 2011.

[52] J.W. Palmour. *High voltage silicon carbide power devices.* ARPA-E Power Technologies Workshop, CREE Inc, February 2010.

[53] H. Bai, C. Mi, C. Wang, and S. Gargies. *The dynamic model and hybrid phase-shift control of a dual-active-bridge converter.* Industrial Electronics. IECON 2008. 34th Annual Conference of IEEE, 26(4):2840–2845, November 2008.

[54] J.Sebastián, A.Rodríguez, D. G. Lamar, M. M. Hernando, and A. Vázquez. *An overall study of a dual active bridge for bidirectional DC/DC conversion.* Energy Conversion Congress and Exposition, pages 1129–1135, 2010.

[55] S. Bacha, I. Munteanu, and A. I. Bratcu. *Power electronic converters modeling and control.* Springer, 2014.

[56] John G. Kassakian, Martin F. Schlecht, and George C. Verghese. *Principles of power electronics.* Addison - Wesley Publishing Company, 1991.

[57] V.I. Utkin. *Sliding modes in control and optimization.* Springer-Verlag, 1992.

[58] G. Anderson, P. Kundur, and V. Vittal et al. *Definition and Classification of Power System Stability*, IEEE transactions on power systems, 2004.

[59] M. Jiménez Carrizosa, G. Damm, A. Benchaib, M. Netto, P. Alou, and F. Lamnabhi-Lagarrigue. *Bilinear and nonlinear control algorithms for a DC/DC converter for multi-terminal HVDC networks.* IFAC World Congress, pages 523–528, August 2014.

[60] D Grahame Holmes and Thomas A Lipo. *Pulse width modulation for power converters: principles and practice.* John Wiley & Sons, 2003.

[61] H. Sira-Ramirez, M. Garcia-Esteban, and A.S.I. Zinober. *Dynamical adaptive pulse-width-modulation control of DC-to-DC power converters: a backstepping approach.* Journal of control, pages 205–222, 1994.

[62] M.P. Kazmierkowski, R. Krishnan, and F. Blaabjerg. *Pulse width modulation for power converters: principles and practice.* San Diego: Academic Press, 2002.

[63] R.H. Park. *Two reaction theory of synchronous machines.* 1929.

[64] M. Barragán-Villarejo, G. Venkataramanan, F. Mancilla-David, J.M. Maza-Ortega, and A. Goómez-Expósito. *Dynamic modelling and control of a shunt-series power flow controller based on AC-link.* IET Generation, Transmission & Distribution, pages 792–802, 2012.

[65] S. Mendel, C. Vogel, and N. Da Dalt. *A Phase-Domain All-Digital Phase-Locked Loop Architecture Without Reference Clock Retiming* IEEE Transactions on Circuits and Systems II: Express Briefs, pages 860–864, November 2009.

[66] N. Kawasaki, H. Nomura, and M. Masuhiro. *A new control law of bilinear DC-DC converters developed by direct application of Lyapunov.* IEEE Transactions on Power Electronics, May 1995.

[67] D.E. Koditschek and K.S Narendra. *The controllability of planar bilinear systems.* IEEE Transactions on Automatic control, pages 87–89, January 1985.

[68] J.B. Barras, J.R. Goncalves, O. do Rocio, and L.A.B San Martín. Controllability of two-dimensional bilinear systems. *Proyeciones*, pages 111–139, 1996.

[69] V. Ayala, E. Cruz, and W. Kliemann. *Controllability of bilinear systems on the projective space.* Computer and Mathematics with Applications, 2009.

[70] D.E. Koditschek and K.S Narendra. *Stability of* $2^n d$ *order bilinear systems.* IEEE Transactions on Automatic control, January 1983.

[71] Y. Chen, J. Dai, G. Damm, and F. Lamnabhi-Lagarrigue. *Analysis of a control strategy for a multi-terminal VSC-HVDC system.* ECC, 2013.

[72] S. Nguefeu. *Réseaux à courant continu: Twenties, et aprés?* Soiré-Débat Club Sysèmes Electriques, $3^{rd}$ June 2014.

[73] J. Stevens and D. Rogers. *Control of multiple VSC-HVDC converters within an offshore AC-hub.* Energytech, 2013 IEEE, pages 1–5, May 2013.

[74] M. Geidl, G. Koeppel, P. Favre-Perrod, B. Klockl, G. Andersson and K. Frohlich. *Energy hubs for the future.* IEEE Power and Energy Magazine, Jan 2007.

[75] G.J. Kish, M. Ranjram, and P.W. Lehn. *A modular multilevel DC/DC converter with fault blocking capability for hvdc interconnects.* IEEE Transactions on Power Electronics, Jan 2015.

[76] L. Harnefors, A. Antonopoulos, S. Norrga, L. Angquist, and H.-P. Nee. *Dynamic analysis of modular multilevel converters.* IEEE Transactions on Industrial Electronics, pages 2526–2537, July 2013.

[77] A. Antonopoulos, L. Angquist, L. Harnefors, K. Ilves, and H.-P. Nee. *Global asymptotic stability of modular multilevel converters. Industrial Electronics, IEEE Transactions on*, 61(2):603–612, Feb 2014.

[78] A. Antonopoulos, L. Angquist, and H.P. Nee. *On dynamics and voltage control of the modular multilevel converter.* $13^{th}$ European Conference on Power Electronics and Applications, 2009. EPE '09, pages 1–10, Sept 2009.

[79] E. Jiménez, M. Jiménez Carrizosa, A. Benchaib, G. Damm, and F.Lamnabhi-Lagarrigue. *A new generalized power flow method for multi connected DC grids.* International Journal of Electrical Power and Energy Systems. *Submitted.*

[80] E. Jiménez, M. Jiménez Carrizosa, A. Benchaib, G. Damm, and F.Lamnabhi-Lagarrigue. *A new generalized power flow method for multi connected single phase AC grids.* International Journal of Electrical Power and Energy Systems. *Submitted.*

[81] P. Hu, D. Jiang, Y. Zhou, Y. Liang, J. Guo, and Z. Lin. *Energy-balancing control strategy for modular multilevel converters under submodule fault conditions.* IEEE Transactions on Power Electronics, pages 5021–5030, Sept 2014.

[82] C. Meyer. *Circuit breaker concepts for future high-power DC-applications.* Industry Applications Conference. Fourtieth IAS Annual Meeting, pages 860–866, October 2005.

[83] C.J. Greiner, T. Langeland, J. Solvik, and O. A.Rui. *Availability evaluation of multi-terminal DC networks with DC circuit breakers.* PowerTech, 2011 IEEE Trondheim, pages 1–8, June 2011.

[84] W. Grieshaber. *DC-breaker prototype: challenges and advances.* EWEA workshop. ALSTOM GRID, TWENTIES project, 2012.

[85] M. Ghandhari, D. Van Hertem, J.B. Curis, O. Despouys, and A. Marzin. *Protection requirements for a multi-terminal meshed DC grid.* CIGRE International Symposium. The electric power system of the future. Integrating supergrids and microgrids location, 2011.

[86] J. Descloux. *Protection contre les courts-circuits des réseaux à courant continu de forte puissance.* PhD thesis, Universite de Grenoble, 2003.

[87] M. Andreasson, M. Nazari, D. V. Dimarogonas, H. Sandberg, K. H. Johansson, and M. Ghandhar. *Distributed controllers for multi-terminal HVDC transmission systems.* IFAC, August 2014.

[88] M. Andreasson, D. V. Dimarogonas, H. Sandberg, and K. H. Johansson. *Distributed controllers for multi-terminal HVDC transmission systems.* IEEE Transactions on Automatic Control, November 2014.

[89] M.A. Pai, P.W. Sauer, and K. Khorasani. *Singular perturbations and large scale power system stability.* In the 23rd IEEE Conference on Decision and Control, Dec 1984.

[90] S. Ahmed-Zaid, P.W. Sauer, and J.R. Winkelman. *Higher order dynamic equivalents for power systems.* Automatica 1986.

[91] J.-L.Thomas, S. Poullain, and A.Benchaib. *Analysis of a robust DC-bus voltage control system for a VSC transmission scheme.* $7^{th}$ International Conference on AC-DC Power Transmission, pages 119–124, Nov 2001.

[92] M. Jiménez Carrizosa, G. Damm, A. Benchaib, and F. Lamnabhi-Lagarrigue. *Distributed primary droop control in multi terminal high voltage direct current networks.* $24^{th}$ IEEE International Symposium on Industrial Electronics, June 2015. *submitted*

[93] E. Prieto-Araujo, F.D. Bianchi A.Junyent-Ferré, and O. Gomis-Bellmunt. *Methodology for droop control dynamic analysis of multi-terminal VSC-HVDC grids for offshore wind farms.* IEEE Transactions on power delivery, pages 2479–2485, October 2011.

[94] W. T. Tutte. *Graph theory.* Cambridge Mathematical Library, 2001.

[95] B.D.O. Anderson and J.B. Moore. *Optimal control- linear quadratic methods.* Prentice Hall, 1989.

[96] P. Rault. *Dynamic modelling and control of multi-terminal HVDC grids.* Thesis, Lille University, 2014.

[97] J.M. Mauricio and A.G. Exposito. *Modeling and control of an hvdc-vsc transmission system.* IEEE/PES Latin America Transmission Distribution Conference and Exposition, pages 1–6, Aug 2006.

[98] E. F. Camacho and C. Bordons. *Model predictive control in the process industry.* Springer, 1995.

[99] D. Limón. *Predictive control in nonlinear systems with constraints: stability and robustness.* Thesis, September 2002.

[100] `http://www.metoffice.gov.uk/weather/marine/shipping_forecast.html#All~All` Government of UK.

[101] R. Langella, A. Tesa, and M. Giorgio. *Very short-term probabilistic wind power forecasting based on Markov chain models.* IEEE $11^{th}$ International Conference on Probabilistic Methods Applied to Power Systems (PMAPS), Singapore, June 2010.

[102] S.A. Pourmousavi-Kani and M.M. Ardehali. *Very short-term wind speed prediction: A new artificial neural network Markov chain model.* Energy Conversion and Management, pages 738–745, August 2010.

[103] M. Jiménez Carrizosa, F. Dorado Navas, G. Damm, A. Benchaib, and F. Lamnabhi-Lagarrigue. *Optimal power flow operation of a multi-terminal HVDC system with renewable sources and storages.* $12^{th}$ International Conference on Industrial Informatics, INDIN, July 2014.

[104] Regulación de la actividad de producción de energía eléctrica en régimen especial. Real decreto 661/2007. B.O.E. num. 126, 26 May 2007.

[105] Le service public de l'électricité. Loi 2000-108 du 10 février 2000. Ministère de l'Écologie, du Développement durable et de l'Énergie,10 February 2000.

[106] `http://www.ofgem.gov.uk/Pages/OfgemHome.aspx`. Office of the gas and electricity markets, Government of UK.

[107] `www.semikron.com` SEMIKRON. IGBT power electronics teaching system principle for sizing power converters. 2008.

[108] Chandra Bajracharya. *Control of VSC-HVDC for wind power.* Norwegian University of Science and Technology, June 2008.

[109] R. A. Horn and C. R. Johnson. *Matrix analysis.* Cambridge University Press, 1988.